1-1-2018

Tandem Mass Spectrometry And Computational Approaches To Elucidate Conformations And N-Glycosidic Bond Stabilities Of Dna And Rna Nucleosides And Mononucleotides

Yanlong Zhu
Wayne State University,

TANDEM MASS SPECTROMETRY AND COMPUTATIONAL APPROACHES TO ELUCIDATE CONFORMATIONS AND N-GLYCOSIDIC BOND STABILITIES OF DNA AND RNA NUCLEOSIDES AND MONONUCLEOTIDES

by

YANLONG ZHU

DISSERTATION

Submitted to the Graduate School

of Wayne State University,

Detroit, Michigan

in partial fulfillment of the requirements

for the degree of

DOCTOR OF PHILOSOPHY

2018

MAJOR: CHEMISTRY (Analytical)

Approved By:

_____

Advisor Date

_____

_____

_____

ACKNOWLEDGEMENTS

First and foremost, I would like to thank my advisor Professor Mary T. Rodgers. Because of her, I was able to learn and explore the great field of mass spectrometry. Professor Rodgers is a remarkable mentor in training and educating graduate students. I received a lot of informative advice on every manuscript I wrote and every presentation I prepared. She is also a role model for me because of her work ethic, intelligence, patience, and wide knowledge of science. Without her guidance and support, I wouldn't be able to complete this thesis work and become a confident and independent chemist.

I would also like to thank Dr. Cliff E. Frieler for his kind support for maintaining a computational lab, and the staff members of the WSU C&IT for facilitating the computational work in this thesis research. I would like to thank Dr. Jos Oomens and Dr. Giel Berden at the FELIX facility for their help on the IRMPD action spectroscopy experiments. My gratitude also goes to my committee members, Dr. Christine S. Chow, Dr. Colin F. Poole and Dr. Andre R. Venter. Special thanks to Dr. Peter B. Armentrout for his support and recommendation for my post-doc application.

I would like to thank all previous and current members of the Rodgers group for the excellent working environment. My special thanks go to Dr. Ranran Wu, Dr. Yuan-wei Nei, Dr. Bo Yang and Lucas A Hamlow for their help on the computational chemistry, data analysis and instrumentation. Thanks to all my good friends for their great friendship and kindness. I had a wonderful time at Wayne State University.

Most importantly, I would like to thank my parents, Mr. Bo Zhu and Mrs. Zhenrui Guo. They are the greatest father and mother in the world. They always support and encourage me in my entire life.

TABLE OF CONTENTS

LIST OF TABLES

LIST OF FIGURES

LIST OF ABBREVIATIONS

Adenine, Ade

Adenosine, Ado

Adenosine-5'-monophosphate, pAdo

Collision-induced dissociation, CID

Cytidine, Cyd

Cytosine, Cyt

2'-Deoxyadenosine, dAdo

2'-Deoxyadenosine-5'-monophosphate, pdAdo

2'-Deoxycytidine, dCyd

2'-Deoxyguanosine, dGuo

Deoxyribonucleic acid, DNA

2'-Deoxyuridine, dUrd

Electrospray ionization, ESI

Energy resolved collision-induced dissociation, ER-CID

Fourier transform ion cyclotron resonance mass spectrometer, FT-ICR MS

Free electron laser, FEL

Free electron laser for infrared experiments, FELIX

Guanine, Gua

Guanosine, Guo

Infrared multiple photon dissociation, IRMPD

5-Methyluridine, Thd

Nucleobase, Nue

Nucleoside, Nuo

Optical parametric oscillator/amplifier, OPO/OPA

Quadrupole ion trap mass spectrometer, QIT MS

rf Excitation amplitude, rf_{EA}

Ribonucleic acid, RNA

Threshold collision-induced dissociation, TCID

Thymidine, dThd

Thymine, Thy

Transfer RNA, tRNA

Uracil, Ura

Uridine, Urd

CHAPTER 1 INTRODUCTION

1.1 FUNDAMENTAL NUCLEIC ACID CHEMISTRY

Deoxyribonucleic acid (DNA) is a polymer that carries the genetic instructions used in the growth, development, functioning and reproduction of all known living organisms and many viruses.[1] Ribonucleic acid (RNA) is a polymer essential in various biological roles in coding, decoding, regulation, and expression of genes.[2-5] Nucleotides are the fundamental building blocks of nucleic acids, and each nucleotide comprises a phosphate group, nucleobase residue, and sugar moiety. Nucleosides are building blocks of the nucleotides that only comprise the nucleobase residue and sugar moiety. One of the main structural/chemical differences between DNA and RNA is that the sugar moiety of DNA is 2'-deoxyribose, whereas the sugar moiety of RNA is ribose. The biochemical properties and function of each nucleoside and nucleotide depend on the identity of the nucleobase. Adenine (Ade), cytosine (Cyt), guanine (Gua), and thymine (Thy) are naturally occurring nucleobases found in DNA, whereas Ade, Cyt, Gua and uracil (Ura) are naturally occurring nucleobases of RNA.

Although DNA and RNA exhibit chemical similarities, the secondary, tertiary and quaternary structures of DNA and RNA are generally quite different. To better understand the overall structures of DNA and RNA, determination of the nucleoside conformation is of fundamental importance. The nucleobase orientation and sugar puckering of the 2'-deoxyribose and ribose moieties are two of the major structural factors that influence the overall geometries of DNA and RNA. DNA is most often found as a B-form right-handed double helix with the nucleobases in an *anti* orientation and the 2′-deoxyribose sugar moieties exhibiting C2′-endo puckering, which is stabilized by

Watson-Crick base pairing and π-stacking interactions. However, DNA is highly polymorphic and can take on a variety of other double-stranded structures including the A and Z forms.[6,7] Additionally, triple[8] and quadruple[9]-stranded structures are achieved by altering the base pairing, π-stacking, sugar puckering, and the direction and periodicity of the helix. A change in sugar puckering to C3'-endo results in transition to the A-forms of DNA and RNA, which are generally observed in RNA-DNA and RNA-RNA complexes.[6] In the less common left-handed Z-form of double-stranded DNA, the Ade, Cyt and Thy nucleosides exhibit that same conformations as in B-form DNA, however, the nucleobase of the Gua nucleosides are in the *syn* orientation and their sugar moieties exhibit C3'-endo sugar puckering.[7] Clearly the structures of the nucleobases, nucleosides and nucleotides have significant impacts on the secondary, tertiary and quaternary structures of DNA and RNA.

1.2 NUCLEOSIDES AND NUCLEOTIDES

A variety of naturally occurring and chemically synthesized nucleosides have been widely studied because of their antiviral or antitumoral functions.[10-12] DNA and RNA nucleosides as ingredients play important roles in modified DNA and RNA nucleoside synthesis.[13] The four canonical DNA nucleosides are 2'-deoxyadenosine (dAdo), 2'-deoxyguanosine (dGuo), 2'-deoxycytidine (dCyd) and thymidine (dThd); whereas the four canonical RNA nucleosides are adenosine (Ado), guanosine (Guo), cytidine (Cyd) and uridine (Urd). These canonical DNA and RNA nucleosides as well as two common modified nucleosides, 2'-deoxyuridine (dUrd) and 5-methyluridine (Thd) have also been studied as these are common modifications and comparative studies help elucidate differences in DNA and RNA structure and function. **Figure 1.1** shows

the chemical structures of these 10 DNA and RNA nucleosides along with their names, three-letter abbreviations, and the numbering of each atom of the nucleobase and sugar ring. Phosphorylation of nucleosides by specific kinases in the cell produces nucleotides, the molecular building blocks of DNA and RNA.[14-18] In the present work, the adenine mononucleotides are also studied. **Figure 1.2** shows the chemical structures of 2'-deoxyadenosine-5'-monophosphate (pdAdo) and adenosine-5'-monophosphate (pAdo) along with the numbering of each atom of the adenine nucleobase, sugar moiety and phosphate group.

1.2.1 ADENINE NUCLEOSIDES AND MONONUCLEOTIDES

The adenine nucleosides and mononucleotides examined in this thesis work include: dAdo, Ado, pdAdo and pAdo. dAdo plays an important role in adenosine deaminase (ADA) deficiency, which causes severe combined immunodeficiency disease of infancy and childhood.[19,20] A low concentration of dAdo can lead to the selective lymphopenia observed in ADA deficient patients.[21,22] dAdo and pdAdo are also involved in protein synthesis, molecular recognition and cellular respiration.[23,24] Ado and pAdo play important roles in biochemical processes as the nucleoside and nucleotide of adenosine-5′-triphosphate (ATP) and adenosine-5′-diphospate (ADP), which act as energy carriers in cells, and of 3′,5′-cyclic adenosine monophosphate (cAMP), which serves as a secondary messenger of intracellular signal transduction.[25,26] Extracellular Ado is generated from the conversion of extracellular ATP[27,28] and extracellular cAMPs.[29,30] Adenosine is also an anti-inflammatory that is elevated by extracellular guanosine, which increases under conditions of cell injury.[31]

1.2.2 GUANINE NUCLEOSIDES

In addition to the important roles that dGuo and Guo play as constituents of DNA and RNA, they also serve as important targets for anti-cancer drugs.[32,33] The N7 atom of guanine has been found to be the major binding site of cisplatin and its derivatives,[34-38] whereas the O6 atom is a minor binding site for platinum.[39,40] The interactions between multi-nuclear platinum complexes and guanine in DNA have been found to induce irreversible conformational changes from B-form to A- or Z-form DNA.[41-43] Among the canonical nucleobases, Gua has the lowest oxidation potentials,[44,45] so that guanine nucleosides are susceptible to oxidative damage involving a variety of alkylating and oxidizing agents.[46-49] A unique ability of Gua is the formation of G-quartets, a square planar structure involving four guanine nucleobases hydrogen bonded via Hoogsteen base paring; two or more G-quartets can form a G-quadruplex structure by stacking on top of each other.[50-52] Synthetic analogues of dGuo and Guo are used as therapeutic and antiviral agents.[53,54]

1.2.3 CYTOSINE NUCLEOSIDES

Cyt is the most alkaline canonical nucleobase in aqueous solution.[55] Thus, protonated Cyt has been found to form various noncanonical nucleobase pairs, such as C^+•C mismatches,[56,57] and Hoogsteen C^+•G base pairing.[58-63] Additionally, protonated Cyt has also been found to stabilize DNA *i*-motif structures.[57,64,65] The tetrameric structure of the *i*-motif consists of two parallel duplexes combined in an antiparallel fashion by forming intercalated hemiprotonated Cyt-Cyt (C^+•C) base pairs.[64] The cytosine nucleotide, cytidine-5'-monophosphate (pCyd), induces conformational change to the enzyme sialytransferase that catalyzes the synthesis of sialic acid containing

oligosaccharides.[66] A variety of dCyd analogues play an important role in pharmacology. For example, apricitabine (4-amino-1-[(2R,4R)-2-(hydroxymethyl)-1,3-oxathiolan-4-yl]prymidine-2(1H)-one, ATC) is active against HIV.[67] 4'-Azido-2'-deoxycytidine analoges show dual antiviral activity against both HIV and hepatitis C (HCV).[68] Gemcitabine (2',2'-difluoro-2'-deoxycytidine) exhibits activity in solid tumors.[69,70]

1.2.4 URACIL NUCLEOSIDES

Urd is one of the naturally occurring pyrimidine nucleosides of RNA, comprised of a uracil nucleobase (Ura) and a ribose sugar moiety. (dUrd) is a naturally occurring modified form of Urd that parallels the DNA nucleosides in that it is comprised of Ura and a 2'-deoxyribose sugar moiety. However, dUrd is not one of the canonical DNA nucleosides. Previous studies have reported two major processes that lead to uracil incorporation into DNA, deamination of cytosine and misincorporation of 2'-deoxyuridine-5'-monophosphate (pdUrd) instead of thymidine-5'-monophosphate (pdThd) during replication.[71] Due to the chemical instability of cytosine in DNA, slow hydrolytic deamination occurs and leads to uracil: guanine (U:G) mismatches.[72] Additionally, the theoretical rate of cytosine deamination is about 60-500 per genome per day, and this process in single stranded DNA occurs faster than in ds DNA.[73,74] Enzymatic deamination and activation-induced deaminase are suggested as two mechanisms of cytosine deamination.[75-78] The incorporation of pdUrd into DNA usually produces uracil:adenine (U:A) mismatches, and has been reported both in bacteria and isolated mammalian nuclei.[79,80] Such U:G and U:A mismatches are recognized by uracil-DNA glycosylases (UDG) and repaired by the base excision repair (BER) pathway, which involves N-glycosidic bond cleavage.[81-83]

1.2.5 THYMINE NUCLEOSIDES

Thymine (Thy) is one of the naturally occurring pyrimidine nucleobases found in DNA. It is similar to uracil, but possesses a methyl substituent at the 5-position. Thymine has been well studied due to its slow dissipation of electronic energy upon optical excitation.[84,85] UV-induced carcinogenesis and mutagenesis may be caused by ultraviolet light absorption by Thy.[86,87] Thymine has been found to be involved in conventional *i*-motif structures containing protonated cytosine base pairs. The i-motif structures may incorporate T:T pairs to form various i-motif structures, such as $[d(TCCCCC)]_4$, $[d(TCC)]_4$, $[d(5mCCT)]_4$, $[d(T5mCC)]_4$, $[d(CCTCC)]_4$, or $[d(5mCCTCC)]_4$.[88] Thymine also participates in T:A:T triplets to form a DNA asymmetric triple helix via Hoogsteen hydrogen-bonding interactions.[89] Thymidine (dThd) comprised of a thymine nucleobase and 2'-deoxyribose sugar is a naturally occurring nucleoside of DNA. 5-Methyluridine (Thd) is the ribonucleoside counterpart of dThd, but is not a common RNA nucleoside. Thd is found as a natural modified nucleoside in transfer RNA (tRNA).[90,91] In addition, Thd is an important reagent for the synthesis of the anti-AIDS drugs AZT and D4T.[92,93]

1.3 TAUTOMERIZATION OF NUCLEOBASES

The aromatic ring structures along with the presence of several solvent-exchangeable protons enables the DNA and RNA nucleobases to form/exist in multiple tautomeric forms via keto-enol and amino-imino tautomerization.[94] Tautomeric forms of nucleobases play important roles in the formation of spontaneous mutations in DNA,[95,96] and facilitate many RNA enzymes and aptamers to execute their biological functions.[97-99] The hydrogen atoms of the 6-amino substituent of Ade can shift to the adjacent N1

and N7 imino groups to form amino-imino tautomers.[100] In previous studies, both theoretical calculations and experiments have suggested that the keto-enol tautomers of guanine and its derivatives are important in the gas phase.[101-103] For the isolated cytosine nucleobase, the N1 proton may engage in tautomerization. The keto-amino form is the canonical tautomeric form of cytosine found in DNA and RNA. X-ray diffraction (XRD) studies have found that this is the only tautomeric form present in cytosine crystals.[104,105] However, minor tautomers, such as enol-amino and keto-imino forms, have been observed experimentally.[106-108] Zhibo Yang, a former Ph.D. student from our goup, studied the gas-phase association of cytosine with an alkali metal cation.[109] He found that thermal vaporization of cytosine produces a mixture of cytosine tautomers, such that gas-phase association produces a mixture of tautomeric complexes. Later, Bo Yang, another former Ph.D. student from our group, re-examined alkali metal cation-cytosine binding and found that only the canonical keto-amino form of cytosine is generated when the ions are formed from solution using an electrospray ionization (ESI) source.[110] Tautomerization of uracil has been the subject of many theoretical[111-113] and experimental[114-116] investigations. The canonical uracil nucleobase exhibits the most stable 2,4-diketo form. Yuan-wei Nei, yet another former Ph.D. student from our group, studied protonated and sodium cationized uracil complexes via infrared multiple photon dissociation (IRMPD) action spectroscopy experiments.[117,118] The 2,4-dihydroxy tautomer of protonated uracil is dominantly populated in the experiments, whereas the 2,4-diketo tautomer of sodium cationized uracil is dominantly populated in the experiments. Further, Ranran Wu, also a former group member, reported that 2,4-dihydroxy and O4 protonated conformers of protonated uracil nucleosides coexist as a

mixture in the gas phase.[119] Similar to uracil, an interesting characteristic of thymine is tautomerization that may occur to the canonical 2,4-diketo structure, which may lead to point mutations and molecular based diseases resulting from nucleobase mismatches of tautomeric thymine.[95] The tautomerization of thymine has also been examined both experimentally and theoretically.[116,120-122] For the canonical form of thymine, sodium cations show a preference for binding to O4 over the O2 carbonyl.[123,124] However, a theoretical study found that tautomeric Thy with the O4 hydrogen atom pointed toward the 5-methyl substituent and sodium cation binding to the O2 and N3 atoms exhibits the largest total stabilization energy.[124] Ranran Wu also reported that 2,4-dihydroxy and O2 protonated conformers of protonated thymine nucleosides coexist as a mixture in the gas phase.[125] Therefore, investigations of sodium cation binding to DNA and RNA nucleosides performed in this thesis work must also explicitly examine the canonical and minor tautomeric forms of the nucleobase to definitively examine their importance in these nucleosides, nucleotides and nucleic acids.

1.4 MODIFICATIONS OF NUCLEOSIDES

DNA and RNA modifications alter their structures and can therefore influence their function. Modifications have been found to influence the stability of DNA and RNA strands, hydrogen bonding, and the rigidity of nucleotide bonds.[126] There are currently over 144 naturally occurring modifications in RNA.[127] Of the 144 naturally occurring modifications currently known, 80 involve methylation. Methylation is a common modification that can occur at the nucleobase, sugar, or at the base and sugar moieties. More specifically, C5-methylation of cytosine residues is also a known tRNA stabilizing modification.[126,128] Certain modifications are only found at very specific locations of

tRNA.[129] For example, modifications of purine nucleobases with a bulky moiety are found at position 37 of tRNA, but never found at other positions.[130] Additionally, methylation can occur at the sugar. Methylation at the 2'-hydroxyl substituent of the sugar is known to block sugar edge interactions and stabilize against hydrolysis.[131] Nucleoside analogues play a major role as anti-cancer and antiviral drugs. For example, 2',3'-dideoxynucleoside analogues have been used for AIDS treatment.[132] Fluoropyrimidine, thymidine and purine derivatives have been used in cancer therapy.[133] In addition, cytarabine (arabinosylcytosine, araCyd) is one of the most effective drugs used in hematopoietic malignancies.[134] The effects of modifications to DNA and RNA have been elucidated in limited cases, but many questions related to the influence of modifications on the structures, stabilities and functions remain unanswered.

1.5 NONCOVALENT INTERACTIONS

Noncovalent interactions differ from covalent bonds in that the highly localized sharing of electrons between atoms is not involved. In contrast to covalent bonds, noncovalent interactions involve more dispersed variations of electromagnetic interactions, and are observed in almost all biological processes. For example, noncovalent interactions are important for maintaining the structures of large biomolecules such as proteins and nucleic acids via both intermolecular and intramolecular interactions.[135] Generally, noncovalent interactions are weaker than covalent interactions, because the sharing of electrons is less localized. However, multiple noncovalent interactions can be achieved to provide greater overall stabilization to structures. There are four types of noncovalent interactions: electrostatic, π-interactions, van der Waals forces, and hydrophobic effects.[136] Noncovalent interactions

play important roles in drug design, self-assembly materials design and crystallinity, organic synthesis, and all biological systems.[137-139]

1.5.1 METAL CATION-LIGAND INTERACTIONS

Metal cations, as electrophiles carry positive charges and are able to form electrostatic interactions or covalent bonds with other atoms.[140] Typically, alkali and alkaline earth metal cations prefer noncovalent interations with electronegative atoms, because these metal cations already have complete shell electron configurations. Numerous studies in the literature have found that sodium cations preferentially bind via multiple chelation interactions to hetero atoms,[141-151] and in particular, oxygen atoms and π-systems of organic and biologically relevant ligands.[145,146,152-158] The size of the alkali metal cation significantly affects the strength of binding. Generally, the bond dissociation energies (BDEs) of alkali metal cation-ligand complexes decrease as the size of alkali metal cation increases from Li^+ to Cs^+.[110,123,143,159-161]

1.5.2 METAL CATION-NUCLEIC ACID INTERACTIONS

Na^+ and K^+ are the most abundant metal cations and participate in biological processes via noncovalent interactions with DNA and RNA nucleic acids.[162,163] At low concentrations of sodium, preferential binding to the deprotonated phosphate moieties along the polyanionic backbone is observed due to their strong Coulombic attraction to the negative charges.[164] At higher concentrations, sodium cations may also interact with the nucleobases or sugar moieties and potentially disrupt hydrogen bond base pairing, and thus influence the structural integrity of the nucleic acid polymer. Free sodium cations and protein-bound forms of sodium affect synthesis, replication, and cleavage of DNA and RNA.[165] The B-form of DNA and G-quadruplex structures are stabilized by

alkali metal cations, particularly Na^+ and K^+.[166-170] Sodium cations have been found to affect the synthesis, replication, and cleavage of DNA and RNA.[171] High Na^+ concentrations stabilize the Z-form of DNA, because the Na^+ cations reduce the electrostatic repulsion along the negatively charged phosphate backbone.[172] Although high concentrations of alkali metal cations have been demonstrated to stabilize DNA and RNA, alkali metal cations also show negative effects on their overall stability. For example, a high concentration of Na^+ could cause oxidative damage to the nucleobases of DNA and unzipping of DNA helical structures.[173] Thus, the effects of metal cation-nucleic acid interactions on the structure and function of DNA and RNA and its nucleoside and nucleotide building blocks are of great interest.

1.6 N-GLYCOSIDIC BOND STABILITY

The N-glycosidic bond, which is the covalent bond that links the nucleobase residue and sugar moiety, is important to the overall stability of DNA and RNA. Mutations in the DNA and RNA sequence via nucleobase excision or mismatch are influenced by the N-glycosidic bond stabilities of the relevant sequence.[174] N-glycosidic bond stability/cleavage is investigated here because of its role in biochemical processes that occur in vivo, such as nucleobase salvage and DNA repair.[174-176] Modifications on the nucleobase and sugar moiety have been found to affect the stabilities of N-glycosidic bonds.[177-179] Additionally, both theoretical and experimental studies demonstrate that the local environment of a nucleic acid also impacts N-glycosidic bond stabilities.[180-182]

1.7 NUCLEOBASE ORIENTATION AND SUGAR PUCKERING

The nucleobase orientation relative to the N-glycosidic bond is defined by the ∠C4N9C1'O4' dihedral angle for purine nucleosides, and the ∠C2N1C1'O4' dihedral angle for pyrimidine nucleosides. When the dihedral angle falls into the range of 90° to 270°, it is designated as the *anti* orientation. When the dihedral angle falls into the range of -90° to 90°, it is designated as the *syn* orientation. In **Figure 1.3**, dAdo is used to illustrate *anti* and *syn* orientations of purine nucleosides, whereas as dCyd is used to illustrate *anti* and *syn* orientations of pyrimidine nucleosides.

Two related designations for the sugar puckering are used. The first designation assumes that the ring is more envelope like such that endo (puckering toward the 5'-substituent) and exo (puckering away the 5'-substituent) are used to designate which atom is puckered out of the sugar ring plane. The second designation of sugar puckering is defined on the basis of the pseudorotation angle, *P*, of the sugar moiety.[183] Envelope (E) and twist (T) designations are more general and detailed as many stable conformations take on partially twisted structures. E configurations have only one atom puckered out of the plane defined by the other four atoms of the sugar ring, whereas T configurations have two atoms puckered out of the plane defined by the other three atoms of the sugar ring. **Figure 1.4** shows examples of E and T configurations as well as the pseudorotation angle diagram. *P* is calculated using **Equation 1.1**,

$$\tan P = \frac{(v_4 + v_1) - (v_3 + v_0)}{2v_2(\sin 36^\circ + \sin 72^\circ)} \tag{1.1}$$

where the angles, v_0, v_1, v_2, v_3 and v_4, represent the ∠C4'O4′C1′C2′, ∠O4′C1′C2′C3′, ∠C1′C2′C3′C4′, ∠C2′C3′C4′O4′ and ∠C3′C4′O4′C1′ dihedral angles of the sugar moiety,

respectively. In the pseudorotation angle diagram (**Figure 1.4**), v_2 is positive in the upper section of the diagram, and negative in the lower section of the diagram. The E and T designations of sugar puckering can be identified by comparing P and v_2 of each nucleoside. In this nomenclature, superscripts designate endo, whereas subscripts designate exo puckered atoms. The numbers that precede or follow the letters E and T denote the major or minor puckering of the atoms, respectively. For example, ^{2}E designates C2'-endo sugar puckering, and $^2T_3$ indicates that the major sugar puckering as being C2'-endo, and the minor sugar puckering as being C3'-exo, as shown in **Figure 1.4**.

1.8 MOTIVATION AND SYSTEMS INVESTIGATED

A major focus of our research group involves the elucidation of the structures and thermochemical properties of nucleic acid building blocks via tandem mass spectrometry and computational approaches. A previous Ph.D. student in the group, Ranran Wu, investigated the gas-phase conformations and stabilities of the protonated forms of the same 10 DNA and RNA nucleosides examined in this thesis using infrared multiple photon dissociation (IRMPD) action spectroscopy techniques combined with theoretical calculations.[119,125,184-186] She has also elucidated the gas-phase conformations of the protonated forms of the eight canonical DNA and RNA mononucleotides.[187-190] Another former Ph.D. student, Yuan-wei Nei, studied the gas-phase conformations of the deprotonated forms of the canonical DNA and RNA mononucleotides and initiated investigations of their sodium cationized forms using similar techniques.[191,192]

The dissociation mechanisms and energetics associated with N-glycosidic bond cleavage of these same 10 protonated DNA and RNA nucleosides were examined by threshold collision-induced dissociation (TCID) techniques using guided ion beam mass spectrometry (GIBMS) approaches.[193-197] Thermochemical analysis of the resultant TCID data requires detailed mapping of the mechanisms and potential energy surfaces (PESs) for the N-glycosidic bond cleavage reactions observed upon CID of the protonated nucleosides. In these computational works, the most stable low-energy conformers experimentally populated determined from the IRMPD action spectroscopy experiments and theoretical calculations were used as reactant structures. The unimolecular dissociation of the protonated nucleosides was found to involve a sequential two-step mechanism involving elongation of the N-glycosidic bond followed by proton transfer from the sugar moiety to the nucleobase. These latter studies definitively showed that the 2'-hydroxyl substituent of the RNA nucleosides for all five nucleobase, Ade, Cyt, Gua, Thy and Ura, stabilizes the N-glycosidic bond compared with the analogous DNA nucleosides.

In the present work, IRMPD action spectroscopy and theoretical studies of the sodium cationized forms of the same 10 DNA and RNA nucleosides are performed to elucidate the conformations and stabilities of these complexes. Furthermore, sodium cationized adenine mononucleotides and disodium cationized deprotonated adenine mononucleotides are also examined to elucidate the effect of the phosphate moiety on the conformations and stabilities of the adenine nucleosides. These results are compared with previous studies to provide a better understanding of the effects of sodium cationization vs. protonation vs. deprotonation on the gas-phase conformations

of these nucleic acid building blocks. Additionally, these results provide information regarding the reactant structures of these systems to facilitate further studies of the dissociation mechanisms and energetics associated with N-glycosidic bond cleavage of the sodium cationized DNA and RNA nucleosides and N-glycosidic bond and phosphate ester cleavage of the sodium cationized DNA and RNA mononucleotides using a guided ion beam tandem mass spectrometer (GIBMS) techniques.

Energy-resolved collision-induced dissociation (ER-CID) experiments performed in a quadrupole ion trap mass spectrometer (QITMS) under multiple-collision conditions complemented by survival yield analyses are also performed here for the 10 protonated and metal cationized DNA and RNA nucleosides to determine the relative stabilities of these complexes, which in favorable cases directly correlate with their relative N-glycosidic bond stabilities. The effects of modifications and the local environment on the relative N-glycosidic bond stabilities of the nucleosides are obtained from comparative analyses. Compared to GIBMS studies, survival yield analyses cannot provide accurate absolute thermochemical information because internal energy and lifetime effects are not incorporated into the fitting model. However, survival yield analyses do not require such extensive computational works to obtain relative thermochemical data and trends among the precursor ions. Thus, this high-throughput technique is used as a guide for future studies of the absolute energetics associated with N-glycosidic bond cleavage of the sodium cationized DNA and RNA nucleosides and nucleotides using GIBMS approaches.

1.8.1 STRUCTURES OF THE SODIUM CATIONIZED DNA AND RNA NUCLEOSIDES

The effects of sodium cationization on the conformations and stabilities of 10 DNA and RNA nucleosides including eight canonical and two modified nucleosides are elucidated using the combination of IRMPD action spectroscopy and theoretical calculations. Theoretical results for these sodium cationized nucleoside complexes are presented in **Chapter 3**. Geometry optimization and harmonic vibrational frequency calculations are performed at the B3LYP/6-311+G(d,p) level of theory, whereas single point energies are calculated at B3LYP/6-311+G(2d,2p) level of theory. In addition to examining the canonical forms of the nucleosides, tautomerization of the nucleobase residues of the nucleosides is also considered. Water adduction to the low-energy conformers of the sodium cation-pyrimidine nucleoside complexes is also examined to investigate the effects of solvation on the relative stabilities (and to explain unanticipated experimental findings). Results of our IRMPD action spectroscopy studies for these 10 sodium cation-nucleoside complexes are presented in **Chapter 4**. By comparing the measured IRMPD spectra to IR spectra predicted for the stable low-energy conformations computed for each sodium cationized nucleoside complex, the conformations populated in the experiments are determined.

1.8.2 STABILITIES OF PROTONATED AND METAL CATIONIZED DNA AND RNA NUCLEOSIDES

Energy-resolved collision-induced dissociation (ER-CID) experiments of 10 DNA and RNA nucleosides are performed to determine the relative stabilities of these complexes. The survival yield of the precursor ion is calculated at each rf excitation amplitude (rf_{EA}), and then plotted as a function of rf_{EA} to generate the survival yield

curve. By comparing the rf_{EA} required to produce 50% dissociation of the precursor ion ($CID_{50\%}$), the relative stabilities of the DNA and RNA nucleosides are thus determined. In particular, in favorable cases where the fragmentation pathways involve only N-glycosidic bond cleavage, the $CID_{50\%}$ values directly correlate with the relative N-glycosidic bond stabilities. In **Chapter 5**, the relative stabilities of the protonated and sodium cationized forms of 10 DNA and RNA nucleosides including eight canonical and two modified nucleosdies are determined using survival yield analyses. Additionally, the effects of several sugar modifications, including 2'-fluoro substitution, 2'-O-methylation, and inversion of the 2'-stereochemistry, on the relative N-glycosidic bond stabilities are also examined and discussed. These studies are extended to include other metal cations, Li^+, K^+, Rb^+, Cs^+ and Ag^+ for dGuo and Guo to further elucidate the relative propensities of these metal cations for activating the glycosidic bond.

1.8.3 STRUCTURES OF SODIUM CATIONIZED ADENINE MONONUCLEOTIDES

The effects of sodium cationization on the conformations and stabilities of the neutral and deprotonated forms of the adenine mononucleotides are elucidated using the combination of IRMPD action spectroscopy and theoretical calculations. Theoretical results for these sodium cationized adenine mononucleotides complexes are presented in **Chapter 6**. Geometry optimizations and harmonic vibrational frequency calculations are again performed at the B3LYP/6-311+G(d,p) level of theory, whereas single-point energy calculations were calculated with an extended basis set, 6-311+G(2d,2p). Results of our IRMPD action spectroscopy studies of these complexes are presented in **Chapter 7**. By comparing the measured IRMPD spectra to IR spectra predicted for the

stable low-energy conformations computed for each sodium cationized mononucleotide complex, the conformers populated in the experiments are determined.

1.9 REFERENCES

1. O. T. Avery, C. M. MacLeod and M. McCarty, *J. Exp. Med.* 1944, **79**, 137.

2. P. F. Agris, *Nucleic Acids Res.* 2004, **32**, 223.

3. P. F. Agris, *RNA* 2015, **21**, 552.

4. B. X. S. Zhao, I. A. Roundtree and C. He, *Nature Rev. Mol. Cell Biol.* 2017, **18**, 31.

5. M. Duechler, G. Leszczynska, E. Sochacka and B. Nawrot, *Cell. Mol. Life Sci.* 2016, **73**, 3075.

6. L. van Dam, N. Ouwerkerk, A. Brinkmann, J. Raap and M. H. Levitt, *Biophys. J.* 2002, **83**, 2835.

7. A. Rich, A. Nordheim and A. H. J. Wang, *Annu. Rev. Biochem.* 1984, **53**, 791.

8. H. Htun and J. E. Dahlberg, *Science* 1988, **241**, 1791.

9. A. Siddiqui-Jain, C. L. Grand, D. J. Bearss and L. H. Hurley, *Proc. Natl. Acad. Sci. USA* 2002, **99**, 11593.

10. J. Ogawa, S. Takeda, S. X. Xie, H. Hatanaka, T. Ashikari, T. Amachi and S. Shimizu, *Appl. Environ. Microb.* 2001, **67**, 1783.

11. H. Mitsuya, K. J. Weinhold, P. A. Furman, M. H. Stclair, S. N. Lehrman, R. C. Gallo, D. Bolognesi, D. W. Barry and S. Broder, *Proc. Natl. Acad. Sci. USA* 1985, **82**, 7096.

12. C. M. Galmarini, J. R. Mackey and C. Dumontet, *Lancet Oncol.* 2002, **3**, 415.

13. S. K. Mahto and C. S. Chow, *Bioorgan. Med. Chem.* 2008, **16**, 8795.

14. M. Yoshikaw, T. Kato and T. Takenish, *Tetrahedron Lett.* 1967, **50**, 5065.

15. C. C. Richards, *Proc. Natl. Acad. Sci. USA* 1965, **54**, 158.

16. J. A. Fyfe, P. M. Keller, P. A. Furman, R. L. Miller and G. B. Elion, *J. Biol. Chem.* 1978, **253**, 8721.

17. M. L. Lacombe, L. Milon, A. Munier, J. G. Mehus and D. O. Lambeth, *J. Bioenerg. Biomembr.* 2000, **32**, 247.

18. F. Eckstein, *Annu. Rev. Biochem.* 1985, **54**, 367.

19. E. R. Giblett, J. E. Anderson, F. Cohen, B. Pollara and H. J. Meuwissen, *J. Immunol.* 2012, **188**, 936.

20. D. W. Martin and E. W. Gelfand, *Annu. Rev. Biochem.* 1981, **50**, 845.

21. S. Seto, C. J. Carrera, M. Kubota, D. B. Wasson and D. A. Carson, *J. Clin. Invest.* 1985, **75**, 377.

22. B. S. Mitchell, E. Mejias, P. E. Daddona and W. N. Kelley, *Proc. Natl. Acad. Sci. USA* 1978, **75**, 5011.

23. S. Murgia, S. Lampis, P. Zucca, E. Sanjust and M. Monduzzi, *J. Am. Chem. Soc.* 2010, **132**, 16176.

24. O. Adelfinskaya, M. Terrazas, M. Froeyen, P. Marliere, K. Nauwelaerts and P. Herdewijn, *Nucleic Acids Res.* 2007, **35**, 5060.

25. M. Ohmori, K. Ohmori and K. Hasunuma, *Arch. Microbiol.* 1988, **150**, 203.

26. A. Moutinho, P. J. Hussey, A. J. Trewavas and R. Malho, *Proc. Natl. Acad. Sci. USA* 2001, **98**, 10481.

27. H. K. Eltzschig and P. Carmeliet, *N. Engl. J. Med.* 2011, **364**, 656.

28. H. K. Eltzschig, *J. Mol. Med.* 2013, **91**, 141.

29. E. K. Jackson and D. K. Raghvendra, *Annu. Rev. Physiol.* 2004, **66**, 571.

30. E. K. Jackson, *Am. J. Physiol.-Renal Ph.* 2011, **301**, F1160.

31. E. K. Jackson, D. M. Cheng, T. C. Jackson, J. D. Verrier and D. G. Gillespie, *Am. J. Physiol.-Cell Ph.* 2013, **304**, C406.

32. K. S. Lovejoy, R. C. Todd, S. Z. Zhang, M. S. McCormick, J. A. D'Aquino, J. T. Reardon, A. Sancar, K. M. Giacomini and S. J. Lippard, *Proc. Natl. Acad. Sci. USA* 2008, **105**, 8902.

33. T. W. Hambley, *Coordin. Chem. Rev.* 1997, **166**, 181.

34. D. Z. Yang, S. S. G. E. Vanboom, J. Reedijk, J. H. Vanboom and A. H. J. Wang, *Biochemistry-US* 1995, **34**, 12912.

35. A. M. J. Fichtingerschepman, J. L. Vanderveer, J. H. J. Denhartog, P. H. M. Lohman and J. Reedijk, *Biochemistry-US* 1985, **24**, 707.

36. M. Sip, A. Schwartz, F. Vovelle, M. Ptak and M. Leng, *Biochemistry-US* 1992, **31**, 2508.

37. B. Chiavarino, M. E. Crestoni, S. Fornarini, D. Scuderi and J. Y. Salpin, *Inorganic Chemistry* 2015, **54**, 3513.

38. B. Chiavarino, M. E. Crestoni, S. Fornarini, D. Scuderi and J. Y. Salpin, *J. Am. Chem. Soc.* 2013, **135**, 1445.

39. J. Dehand and J. Jordanov, *J. Chem. Soc. Chem. Comm.* 1976, **0**, 598.

40. U. Warnke, C. Rappel, H. Meier, C. Kloft, M. Galanski, C. G. Hartinger, B. K. Keppler and U. Jaehde, *ChemBioChem* 2004, **5**, 1543.

41. N. Farrell, *Platinum-Based Drugs in Cancer Therapy*, Humana Press Inc., New York, **2000**; pp 321-338.

42. E. G. Chapman and V. J. DeRose, *J. Am. Chem. Soc.* 2012, **134**, 256.

43. P. K. Wu, M. Kharatishvili, Y. Qu and N. Farrell, *J. Inorg. Biochem.* 1996, **63**, 9.

44. P. A. Limbach, P. F. Crain and J. A. Mccloskey, *Nucleic Acids Res.* 1994, **22**, 2183.

45. S. Bjelland and E. Seeberg, *Mutat. Res. Fund. Mol. Mech. Mut.* 2003, **531**, 37.

46. C. J. Burrows and J. G. Muller, *Chem. Rev.* 1998, **98**, 1109.

47. H. Wiseman and B. Halliwell, *Biochem. J.* 1996, **313**, 17.

48. M. Masuda, T. Suzuki, M. D. Friesen, J. L. Ravanat, J. Cadet, B. Pignatelli, H. Nishino and H. Ohshima, *J. Biol. Chem.* 2001, **276**, 40486.

49. J. A. Liu, C. J. Petzold, L. E. Ramirez-Arizmendi, J. Perez and H. Kenttamaa, *J. Am. Chem. Soc.* 2005, **127**, 12758.

50. S. Neidle and M. A. Read, *Biopolymers* 2001, **56**, 195.

51. T. Shalaby, G. Fiaschetti, K. Nagasawa, K. Shin-ya, M. Baumgartner and M. Grotzer, *Molecules* 2013, **18**, 12500.

52. S. Lyonnais, C. Hounsou, M. P. Teulade-Fichou, J. Jeusset, E. Le Cam and G. Mirambeau, *Nucleic Acids Res.* 2002, **30**, 5276.

53. C. Perigaud, G. Gosselin and J. L. Imbach, *Bioorg. Med. Chem. Lett.* 1992, **2**, 677.

54. C. Perigaud, G. Gosselin and J. L. Imbach, *Nucleosides Nucleotides Nucleic Acids* 1992, **11**, 903.

55. W. Saenger, *Principles of Nucleic-Acid Structure*, Springer-Verlag, New York, **1984**; pp 20-22.

56. K. Gehring, J. L. Leroy and M. Gueron, *Nature* 1993, **363**, 561.

57. B. Yang and M. T. Rodgers, *J. Am. Chem. Soc.* 2014, **136**, 282.

58. C. Wang, H. Gao, B. L. Gaffney and R. A. Jones, *J. Am. Chem. Soc.* 1991, **113**, 5486.

59. J. L. Leroy, K. Gehring, A. Kettani and M. Gueron, *Biochemistry-US* 1993, **32**, 6019.

60. H. E. Moser and P. B. Dervan, *Science* 1987, **238**, 645.

61. C. Delossantos, M. Rosen and D. Patel, *Biochemistry-US* 1989, **28**, 7282.

62. L. E. Xodo, G. Manzini, F. Quadrifoglio, G. A. Vandermarel and J. H. Vanboom, *Nucleic Acids Res.* 1991, **19**, 5625.

63. S. F. Singleton and P. B. Dervan, *Biochemistry-US* 1992, **31**, 10995.

64. H. A. Day, P. Pavlou and Z. A. E. Waller, *Bioorgan. Med. Chem.* 2014, **22**, 4407.

65. B. Yang and M. T. Rodgers, *J. Am. Soc. Mass Spectrom.* 2015, **26**, 1394.

66. L. S. Ni, M. C. Sung, H. Yu, H. Chokhawala, X. Chen and A. J. Fisher, *Biochemistry-US* 2006, **45**, 2139.

67. J. M. de Muys, H. Gourdeau, N. Nguyen-Ba, D. L. Taylor, P. S. Ahmed, T. Mansour, C. Locas, N. Richard, M. A. Wainberg and R. F. Rando, *Antimicrob. Agents Chemother.* 1999, **43**, 1835.

68. K. Klumpp, G. Kalayanov, H. Ma, S. Le Pogam, V. Leveque, W. R. Jiang, N. Inocencio, A. De Witte, S. Rajyaguru, E. Tai, S. Chanda, M. R. Irwin, C. Sund, A. Winqist, T. Maltseva, S. Eriksson, E. Usova, M. Smith, A. Alker, I. Najera, N. Cammack, J. A. Martin, N. G. Johansson and D. B. Smith, *J. Biol. Chem.* 2008, **283**, 2167.

69. S. B. Kaye, *Br. J. Cancer* 1998, **78**, 1.

70. K. Possinger, *Anti-Cancer Drugs* 1995, **6**, 55.

71. H. E. Krokan, F. Drablos and G. Slupphaug, *Oncogene* 2002, **21**, 8935.

72. R. Shapiro, *Chromosome Damage and Repair*, Plenum Press, New York, **1980**; pp 3-18.

73. H. E. Krokan, R. Standal and G. Slupphaug, *Biochem. J.* 1997, **325**, 1.

74. T. Lindahl, *Nature* 1993, **362**, 709.

75. G. W. Camiener and C. G. Smith, *Biochem. Pharmacol.* 1965, **14**, 1405.

76. T. P. Wang, H. Z. Sable and J. O. Lampen, *J. Biol. Chem.* 1950, **184**, 17.

77. S. S. Brar, M. Watson and M. Diaz, *J. Biol. Chem.* 2004, **279**, 26395.

78. H. M. Shen, S. Ratnam and U. Storb, *Mol. Cell. Biol.* 2005, **25**, 10815.

79. B. K. Tye, P. O. Nyman, I. R. Lehman, S. Hochhauser and B. Weiss, *Proc. Natl. Acad. Sci. USA* 1977, **74**, 154.

80. E. Wist, O. Unhjem and H. Krokan, *Biochim. Biophys. Acta* 1978, **520**, 253.

81. R. K. Singhal, R. Prasad and S. H. Wilson, *J. Biol. Chem.* 1995, **270**, 949.

82. G. Dianov and T. Lindahl, *Curr. Biol.* 1994, **4**, 1069.

83. G. Dianov, A. Price and T. Lindahl, *Mol. Cell. Biol.* 1992, **12**, 1605.

84. H. Kang, K. T. Lee, B. Jung, Y. J. Ko and S. K. Kim, *J. Am. Chem. Soc.* 2002, **124**, 12958.

85. J. Cadet, E. Sage and T. Douki, *Mutat. Res. Fund. Mol. Mech. Mut.* 2005, **571**, 3.

86. S. T. Kim and A. Sancar, *Biochemistry-US* 1991, **30**, 8623.

87. Y. Nosenko, M. Kunitski and B. Brutschy, *J. Phys. Chem. A* 2011, **115**, 9429.

88. S. Nonin and J. L. Leroy, *J. Mol. Biol.* 1996, **261**, 399.

89. T. Ramreddy, M. Kombrabail, G. Krishnamoorthy and B. J. Rao, *J. Phys. Chem. B* 2009, **113**, 6840.

90. A. Zamir, R. W. Holley and M. Marquise, *J. Biol. Chem.* 1965, **240**, 1267.

91. G. R. Bjork and F. C. Neidhardt, *J. Bacteriol.* 1975, **124**, 99.

92. B. C. Chen, S. L. Quinlan and J. G. Reid, *Tetrahedron Lett.* 1995, **36**, 7961.

93. B. C. Chen, S. L. Quinlan, D. R. Stark, J. G. Reid, V. H. Audia, J. G. George, E. Eisenreich, S. P. Brundidge, S. Racha and R. H. Spector, *Tetrahedron Lett.* 1995, **36**, 7957.

94. V. Singh, B. I. Fedeles and J. M. Essigmann, *RNA* 2015, **21**, 1.

95. V. H. Harris, C. L. Smith, W. J. Cummins, A. L. Hamilton, H. Adams, M. Dickman, D. P. Hornby and D. M. Williams, *J. Mol. Biol.* 2003, **326**, 1389.

96. J. D. Watson and F. H. C. Crick, *Nature* 1953, **171**, 964.

97. J. C. Cochrane and S. A. Strobel, *Acc. Chem. Res.* 2008, **41**, 1027.

98. J. C. Cochrane and S. A. Strobel, *RNA* 2008, **14**, 993.

99. J. C. Cochrane, S. V. Lipchock and S. A. Strobel, *Chemistry & Biology* 2007, **14**, 97.

100. C. F. Guerra, F. M. Bickelhaupt, S. Saha and F. Wang, *J. Phys. Chem. A* 2006, **110**, 4012.

101. M. Mons, I. Dimicoli, F. Piuzzi, B. Tardivel and M. Elhanine, *J. Phys. Chem. A* 2002, **106**, 5088.

102. J. L. Alonso, I. Pena, J. C. Lopez and V. Vaquero, *Angew. Chem. Int. Ed.* 2009, **48**, 6141.

103. A. Zhachkina, M. Liu, X. J. Sun, F. S. Amegayibor and J. K. Lee, *J. Org. Chem.* 2009, **74**, 7429.

104. D. L. Barker and R. E. Marsh, *Acta Crystallographica* 1964, **17**, 1581.

105. R. J. Mcclure and B. M. Craven, *Acta Crystallographica Section B-Structural Science* 1973, **B 29**, 1234.

106. E. Nir, M. Muller, L. I. Grace and M. S. de Vries, *Chem. Phys. Lett.* 2002, **355**, 59.

107. M. Szczesniak, K. Szczepaniak, J. S. Kwiatkowski, K. Kubulat and W. B. Person, *J. Am. Chem. Soc.* 1988, **110**, 8319.

108. R. D. Brown, P. D. Godfrey, D. Mcnaughton and A. P. Pierlot, *J. Am. Chem. Soc.* 1989, **111**, 2308.

109. Z. Yang and M. T. Rodgers, *Phys. Chem. Chem. Phys.* 2012, **14**, 4517.

110. B. Yang and M. T. Rodgers, *Phys. Chem. Chem. Phys.* 2014, **16**, 16110.

111. J. S. Kwiatkowski, T. J. Zielinski and R. Rein, *Adv. Quantum Chem.* 1986, **18**, 85.

112. R. Czerminski, B. Lesyng and A. Pohorille, *Int. J. Quantum Chem.* 1979, **16**, 605.

113. I. R. Gould, N. A. Burton, R. J. Hall and I. H. Hillier, *J. MOL. STRUC.-THEOCHEM.* 1995, **331**, 147.

114. H. T. Miles, *Biochim. Biophys. Acta* 1956, **22**, 247.

115. J. P. Kokko, L. Mandell and J. H. Goldstein, *J. Am. Chem. Soc.* 1961, **83**, 2909.

116. J. Y. Salpin, S. Guillaumont, J. Tortajada, L. MacAleese, J. Lemaire and P. Maitre, *ChemPhysChem* 2007, **8**, 2235.

117. Y.-w. Nei, T. E. Akinyemi, J. D. Steill, J. Oomens and M. T. Rodgers, *Int. J. Mass Spectrom.* 2010, **297**, 139.

118. Y.-w. Nei, T. E. Akinyemi, C. M. Kaczan, J. D. Steill, G. Berden, J. Oomens and M. T. Rodgers, *Int. J. Mass Spectrom.* 2011, **308**, 191.

119. R. R. Wu, B. Yang, C. E. Frieler, G. Berden, J. Oomens and M. T. Rodgers, *Phys. Chem. Chem. Phys.* 2015, **17**, 25978.

120. A. O. Alyoubi and R. H. Hilal, *Biophysical Chemistry* 1995, **55**, 231.

121. P. Colarusso, K. Q. Zhang, B. J. Guo and P. F. Bernath, *Chem. Phys. Lett.* 1997, **269**, 39.

122. S. L. Zhang, K. H. Michaelian and G. R. Loppnow, *J. Phys. Chem. A* 1998, **102**, 461.

123. M. T. Rodgers and P. B. Armentrout, *J. Am. Chem. Soc.* 2000, **122**, 8548.

124. M. Kabelac and P. Hobza, *J. Phys. Chem. B* 2006, **110**, 14515.

125. R. R. Wu, B. Yang, C. E. Frieler, G. Berden, J. Oomens and M. T. Rodgers, *J. Am. Soc. Mass Spectrom.* 2016, **27**, 410.

126. W. A. Decatur and M. J. Fournier, *Trends Biochem. Sci.* 2002, **27**, 344.

127. W. A. Cantara, P. F. Crain, J. Rozenski, J. A. McCloskey, K. A. Harris, X. N. Zhang, F. A. P. Vendeix, D. Fabris and P. F. Agris, *Nucleic Acids Res.* 2011, **39**, D195.

128. W. A. Decatur and M. J. Fournier, *J. Biol. Chem.* 2003, **278**, 695.

129. M. A. Machnicka, A. Olchowik, H. Grosjean and J. M. Bujnicki, *RNA Biol.* 2014, **11**, 1619.

130. P. F. Agris, F. A. P. Vendeix and W. D. Graham, *J. Mol. Biol.* 2007, **366**, 1.

131. Y. Motorin and M. Helm, *Biochemistry-US* 2010, **49**, 4934.

132. M. Pastor-Anglada, A. Felipe and F. J. Casado, *Trends Pharmacol. Sci.* 1998, **19**, 424.

133. C. J. McGinn, D. S. Shewach and T. S. Lawrence, *J. Natl. Cancer Inst.* 1996, **88**, 1193.

134. S. Grant, *Adv. Cancer Res.* 1998, **72**, 197.

135. D. L. Nelson and M. M. Cox, *Lehninger Priciples of Biochemistry*, Macmillan Education, Belmont, CA, 6th ed., **2013**; pp 160-161.

136. H. Lodish, A. Berk, S. L. Zipursky, P. Matsudaira, D. Baltimore and J. Darnell, *Molecular Cell Biology*, W. H. Freeman, New York, NY, 4th ed., **2000**; pp 31-63.

137. R. B. Silverman, *The Organic Chemistry of Drug Design and Drug Action*, Elsevier, Amsterdam, The Netherlands, 2nd ed., **2004**; pp 197-198.

138. M. Eisler, *Encyclopedia of Nanoscience and Society*, SAGE Publications, Thousand Oaks, CA, **2010**; pp 839-841.

139. E. Anslyn and D. A. Dougherty, *Modern Physical Organic Chemistry*, University Science, Sausalito, CA, **2004**; pp 207-220.

140. E. C. Constable, *The Metal-Ligand Interaction, in Metals and Ligand Reactivity: An Introduction to the Organic Chemistry of Metal Complexes*, VCH Verlagsgesellschaft mbH: Weinheim, Germany, New, revised and expanded ed., **2005**; pp 46-47.

141. G. Yassaghi, L. Jasikova and J. Roithova, *Int. J. Mass Spectrom.* 2016, **407**, 92.

142. Y. J. Alahmadi, A. Gholami and T. D. Fridgen, *Phys. Chem. Chem. Phys.* 2014, **16**, 26855.

143. M. T. Rodgers and P. B. Armentrout, *Mass Spectrom. Rev.* 2000, **19**, 215.

144. P. B. Armentrout and M. T. Rodgers, *J. Phys. Chem. A* 2000, **104**, 2238.

145. B. S. Fales, N. O. Fujamade, J. Oomens and M. T. Rodgers, *J. Am. Soc. Mass Spectrom.* 2011, **22**, 1862.

146. B. S. Fales, N. O. Fujamade, Y. W. Nei, J. Oomens and M. T. Rodgers, *J. Am. Soc. Mass Spectrom.* 2011, **22**, 81.

147. Y. Zhu, L. A. Hamlow, C. C. He, S. F. Strobehn, J. K. Lee, J. Gao, G. Berden, J. Oomens and M. T. Rodgers, *J. Phys. Chem. B* 2016, **120**, 8892.

148. Y. Zhu, L. A. Hamlow, C. C. He, J. K. Lee, J. Gao, G. Berden, J. Oomens and M. T. Rodgers, *J. Phys. Chem. B* 2017, **121**, 4048.

149. Y. Zhu, L. A. Hamlow, C. C. He, H. A. Roy, N. A. Cunningham, M. U. Munshi, G. Berden, J. Oomens and M. T. Rodgers, *Int. J. Mass Spectrom.* 2017, DOI: https://doi.org/10.1016/j.ijms.2017.04.005.

150. Y. Zhu, H. A. Roy, N. A. Cunningham, S. F. Strobehn, J. Gao, M. U. Munshi, G. Berden, J. Oomens and M. T. Rodgers, *Phys. Chem. Chem. Phys.* 2017, **19**, 17637.

151. Y. Zhu, H. A. Roy, N. A. Cunningham, S. F. Strobehn, J. Gao, M. U. Munshi, G. Berden, J. Oomens and M. T. Rodgers, *J. Am. Soc. Mass Spectrom* 2017, **28**, 2437.

152. N. C. Polfer, J. Oomens and R. C. Dunbar, *ChemPhysChem* 2008, **9**, 579.

153. C. Ruan and M. T. Rodgers, *J. Am. Chem. Soc.* 2004, **126**, 14600.

154. R. Amunugama and M. T. Rodgers, *J. Phys. Chem. A* 2002, **106**, 5529.

155. R. Amunugama and M. T. Rodgers, *J. Phys. Chem. A* 2002, **106**, 9092.

156. R. Amunugama and M. T. Rodgers, *Int. J. Mass Spectrom.* 2003, **227**, 339.

157. R. Amunugama and M. T. Rodgers, *J. Phys. Chem. A* 2002, **106**, 9718.

158. R. Amunugama and M. T. Rodgers, *Int. J. Mass Spectrom.* 2003, **222**, 431.

159. M. T. Rodgers and P. B. Armentrout, *Int. J. Mass Spectrom.* 1999, **185**, 359.

160. R. Amunugama and M. T. Rodgers, *Int. J. Mass Spectrom.* 2000, **195**, 439.

161. Z. Yang and M. T. Rodgers, *J. Am. Chem. Soc.* 2004, **126**, 16217.

162. A. M. Pyle, *J. Biol. Inorg. Chem.* 2002, **7**, 679.

163. G. L. Eichhorn, J. J. Butzow and Y. A. Shin, *J. Biosci.* 1985, **8**, 527.

164. S. Arnott, *Nature* 1984, **312**, 174.

165. R. H. Crabtree, *Science* 1994, **266**, 1591.

166. G. L. Eichhorn, *Coordin. Chem. Rev.* 1993, **128**, 167.

167. D. Sen and W. Gilbert, *Nature* 1988, **334**, 364.

168. W. I. Sundquist and A. Klug, *Nature* 1989, **342**, 825.

169. G. N. Parkinson, M. P. H. Lee and S. Neidle, *Nature* 2002, **417**, 876.

170. S. Burge, G. N. Parkinson, P. Hazel, A. K. Todd and S. Neidle, *Nucleic Acids Res.* 2006, **34**, 5402.

171. S. J. Lippard; and J. M. Berg., *Principles of Bioinorganic Chemistry*, University Science Books, Mill Valley, CA, **1994**; pp 57-69.

172. A. Rich and S. G. Zhang, *Nature Rev. Genet.* 2003, **4**, 566.

173. G. L. Eichhorn and Y. A. Shin, *J. Am. Chem. Soc.* 1968, **90**, 7323.

174. J. T. Stivers and Y. L. Jiang, *Chem. Rev.* 2003, **103**, 2729.

175. P. J. O'Brien, *Chem. Rev.* 2006, **106**, 720.

176. E. M. Moody, J. T. J. Lecomte and P. C. Bevilacqua, *RNA* 2005, **11**, 157.

177. Y. Zheng, Y. Xue and S. G. Yan, *J. Mol. Struc. Theochem* 2008, **860**, 52.

178. G. P. Margison and P. J. Oconnor, *Biochim. Biophys. Acta* 1973, **331**, 349.

179. R. S. Das, M. Samaraweera, M. Morton, J. A. Gascon and A. K. Basu, *Chem. Res. Toxicol* 2012, **25**, 2451.

180. Z. A. Tehrani, A. Fattahi and A. Pourjavadi, *Carbohydr. Res.* 2009, **344**, 771.

181. Z. A. Tehrani, A. Fattahi and A. Pourjavadi, *Journal of Molecular Structure-Theochem* 2009, **913**, 117.

182. R. Rios-Font, J. Bertran, L. Rodriguez-Santiago and M. Sodupe, *J. Phys. Chem. B* 2006, **110**, 5767.

183. C. Altona and M. Sundaralingam, *J. Am. Chem. Soc.* 1972, **94**, 8205.

184. R. R. Wu, B. Yang, G. Berden, J. Oomens and M. T. Rodgers, *J. Phys. Chem. B* 2015, **119**, 2795.

185. R. R. Wu, B. Yang, G. Berden, J. Oomens and M. T. Rodgers, *J. Phys. Chem. B* 2014, **118**, 14774.

186. R. R. Wu, B. Yang, C. E. Frieler, G. Berden, J. Oomens and M. T. Rodgers, *J. Phys. Chem. B* 2015, **119**, 5773.

187. R. R. Wu, C. C. He, L. A. Hamlow, Y.-w. Nei, G. Berden, J. Oomens and M. T. Rodgers, *J. Phys. Chem. B* 2016, **120**, 4616.

188. R. R. Wu, C. C. He, L. A. Hamlow, Y. W. Nei, G. Berden, J. Oomens and M. T. Rodgers, *Phys. Chem. Chem. Phys.* 2016, **18**, 15081.

189. R. R. Wu, L. A. Hamlow, C. C. He, Y. W. Nei, G. Berden, J. Oomens and M. T. Rodgers, *J. Am. Soc. Mass Spectrom.* 2017, **28**, 1638.

190. R. R. Wu, L. A. Hamlow, C. C. He, Y.-w. Nei, G. Berden, J. Oomens and M. T. Rodgers, *Phys. Chem. Chem. Phys.* 2017, DOI: 10.1039/C7CP05521H.

191. Y.-w. Nei, N. Hallowita, J. D. Steill, J. Oomens and M. T. Rodgers, *J. Phys. Chem. A* 2013, **117**, 1319.

192. Y.-w. Nei, K. T. Crampton, G. Berden, J. Oomens and M. T. Rodgers, *J. Phys. Chem. A* 2013, **117**, 10634.

193. R. R. Wu, Y. Chen and M. T. Rodgers, *Phys. Chem. Chem. Phys.* 2016, **18**, 2968.

194. R. R. Wu and M. T. Rodgers, *Phys. Chem. Chem. Phys.* 2016, **18**, 24451.

195. R. R. Wu and M. T. Rodgers, *J. Phys. Chem. B* 2016, **120**, 4803.

196. R. R. Wu and M. T. Rodgers, *Phys. Chem. Chem. Phys.* 2016, **18**, 16021.

197. R. R. Wu and M. T. Rodgers, *J. Am. Soc. Mass Spectrom.* 2017, manuscript in preparation.

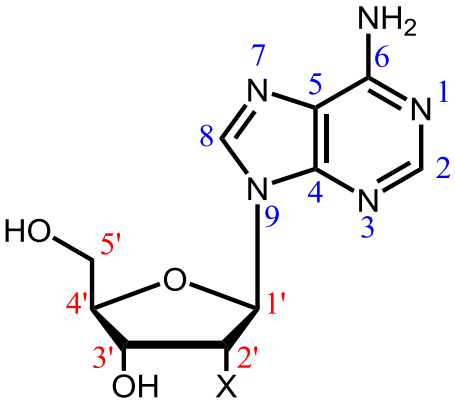

2'-Deoxyadenosine (dAdo)
X=H
Adenosine (Ado)
X=OH

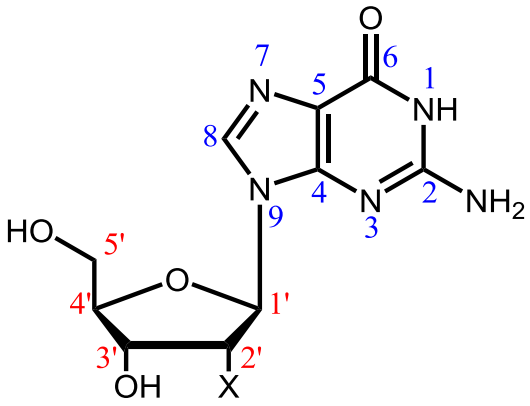

2'-Deoxyguanosine (dGuo)
X=H
Guanosine (Guo)
X=OH

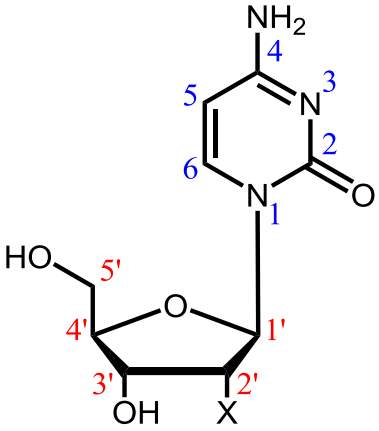

2'-Deoxycytidine (dCyd)
X=H
Cytidine (Cyd)
X=OH

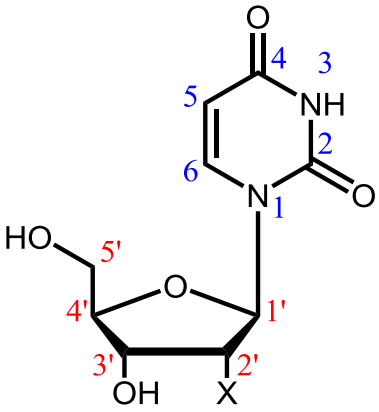

2'-Deoxyuridine (dUrd)
X=H
Uridine (Urd)
X=OH

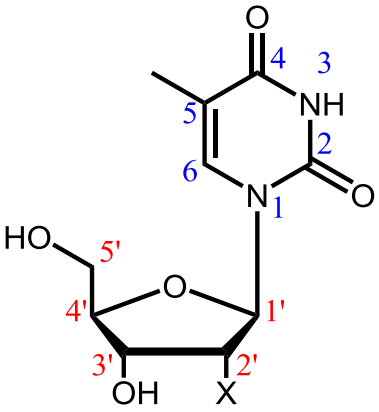

Thymidine (dThd)
X=H
5-Methyluridine (Thd)
X=OH

Figure 1.1 Chemical structures of the adenine, guanine, cytosine, uracil and thymine nucleosides along with their names and three-letter abbreviations. The numbering of each atom of the nucleobase and sugar moiety is also given.

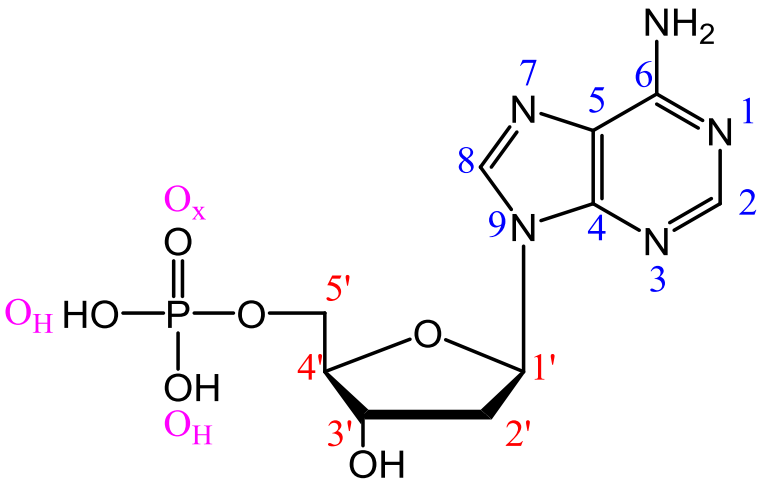

2'-Deoxyadenosine-5'-monophosphate
pdAdo

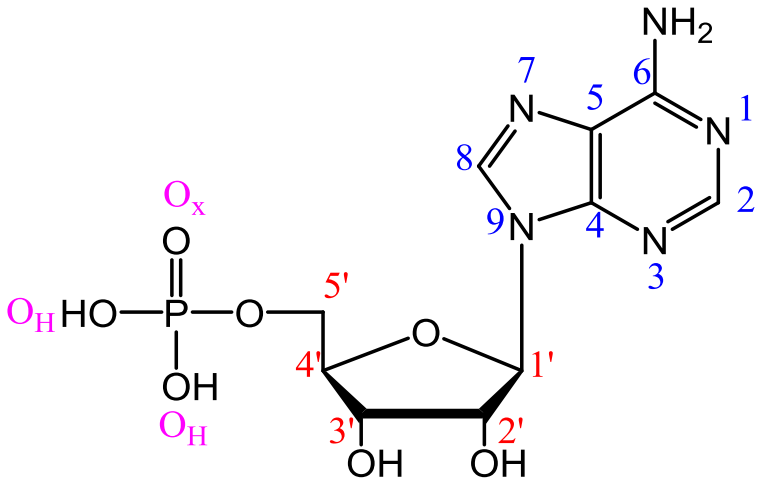

Adenosine-5'-monophosphate
pAdo

Figure 1.2 Chemical structures of 2'-deoxyadenosine-5'-monophosphate (pdAdo) and adenosine-5'-monophosphate (pAdo). The numbering of each atom of the nucleobase, sugar moiety and phosphate group is also given.

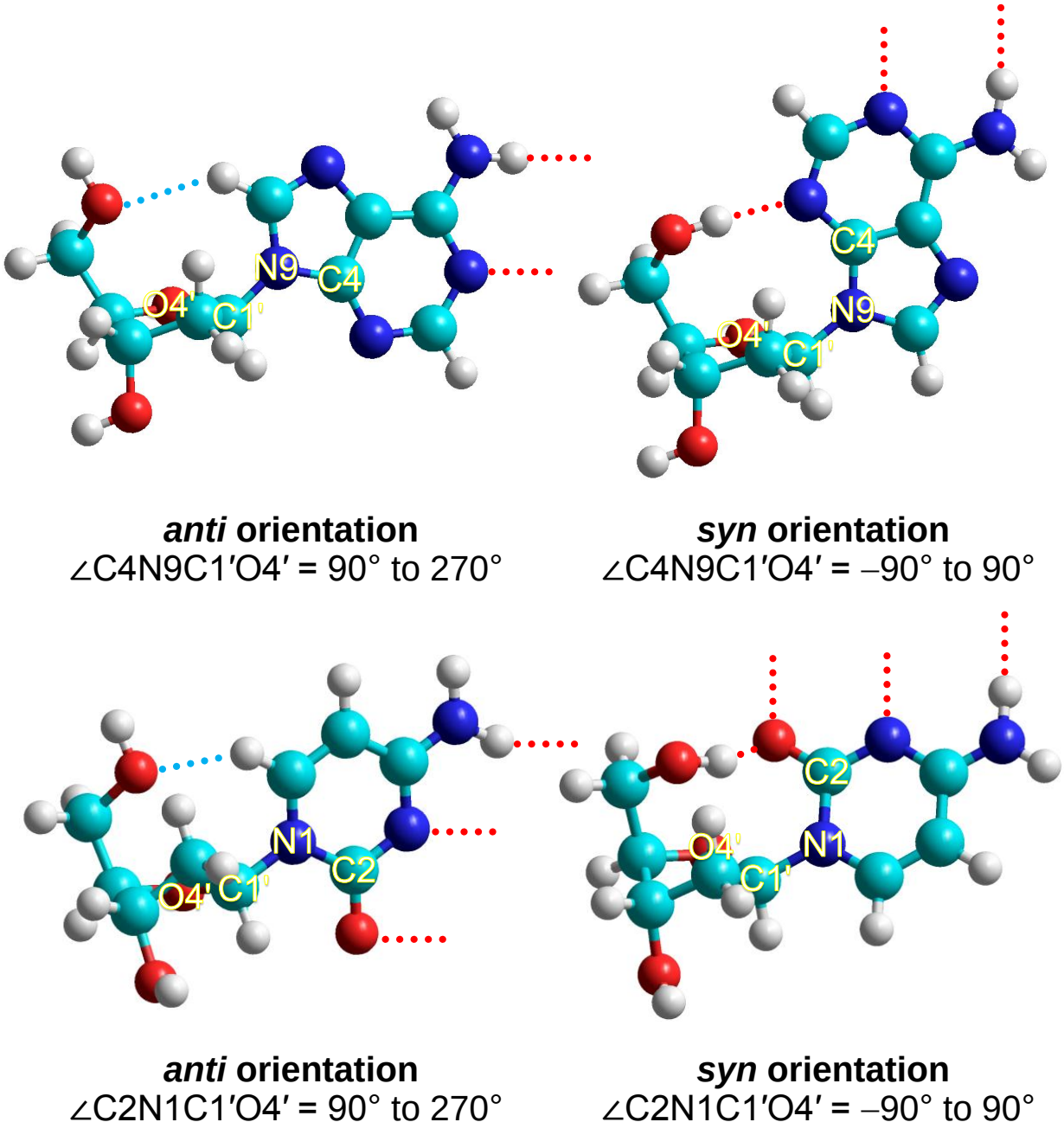

Figure 1.3 Designations of nucleobase orientation (*anti* and *syn*) based on the ∠C4N9C1′O4′ and ∠C2N1C1′O4′ dihedral angles of the purine and pyrimidine nucleosides, respectively.

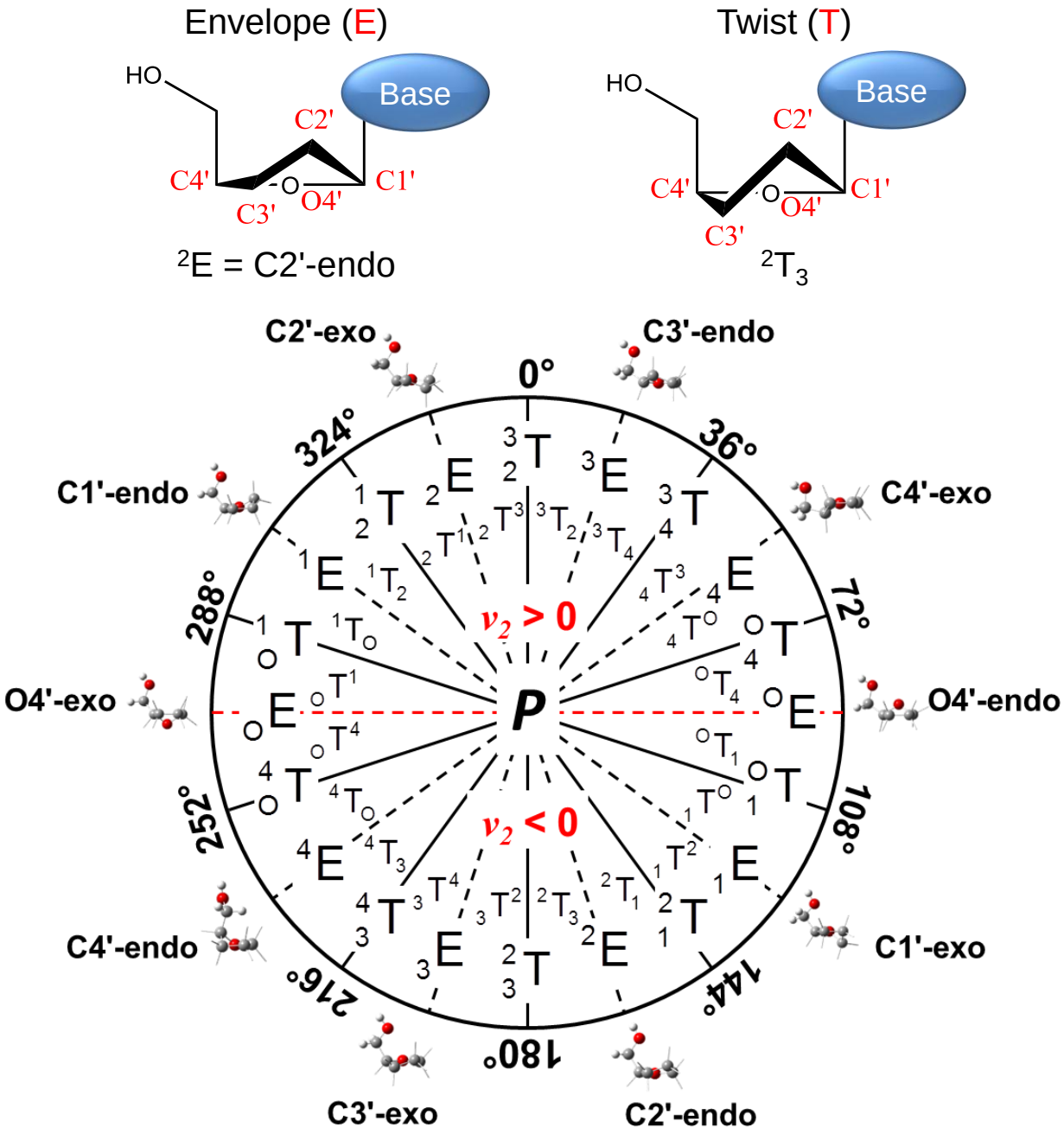

Figure 1.4 Two examples of envelope (E) and twist (T) sugar configurations. E configurations have only one atom puckered out of sugar plane, whereas T configurations have two atoms puckered out of the sugar plane. The pseudorotation phase angle (*P*) diagram is also shown. The sugar puckering is determined by locating *P* in the diagram.

CHAPTER 2 EXPERIMENTAL AND THEORETICAL APPROACHES

2.1 INFRARED MULTIPLE PHOTON DISSOCIATION ACTION SPECTROSCOPY

Infrared multiple photon dissociation (IRMPD) action spectroscopy is a powerful technique that combines mass spectrometry and high-powered wavelength-tunable lasers. In the present work, a free electron laser (FEL) and a table-top optical parametric oscillator/amplifier (OPO) laser were used to examine the unique IR features of mass-isolated precursor ions via their IRMPD fragmentation behavior. The mass spectrometer used to perform the IRMPD action spectroscopy experiments is a custom-built 4.7 T Fourier transform ion cyclotron resonance mass spectrometer (FT-ICR MS). A schematic diagram of the IRMPD experimental setup is shown in **Figure 2.1** and is described in **Section 2.1.1**.The experimental workflow for the IRMPD action spectroscopy studies is illustrated in **Figure 2.2**. The experimental IRMPD tandem mass spectra (MS/MS) of each ion of interest are measured as a function of the laser wavelength (vibrational frequency), converted to IRMPD spectra and compared with the linear IR spectrum calculated for each conformer computed. Good agreement between the experimental IRMPD and calculated IR spectra is interpreted as indicating that that the conformer is populated in the experiments. Significant misalignments between the experimental IRMPD and calculated IR spectra indicate that the corresponding conformer does not have measurable population in the experiments.

2.1.1 EXPERIMENTAL SETUP FOR IRMPD ACTION SPECTROSCOPY EXPERIMENTS

IRMPD action spectroscopy experiments were performed using a custom-built 4.7 T FT-ICR MS coupled to a FEL or an OPO/OPA laser system to examine both the

IR fingerprint (~550 to 1850 cm^{-1}) and hydrogen-stretching (~3300 to 3800 cm^{-1}) regions. The custom-built FT-ICR MS has been described in detail elsewhere.[198-200] The DNA or RNA nucleoside, i.e. 2'-deoxyadenosine (dAdo), adenosine (Ado), 2'-deoxyguanosine (dGuo), guanosine (Guo), 2'-deoxycytidine (dCyd), cytidine (Cyd), 2'-deoxyuridine (dUrd), uridine (Urd), thymidine (dThd) and 5-methyluridine (Thd), along with NaCl was dissolved in a 1:1 (v/v) methanol:water mixture and diluted to a concentration of ~1 mM of the nucleoside and salt to facilitate formation of the sodium cationized nucleosides. The DNA or RNA forms of adenine mononucleotide, i.e. 2'-deoxyadenosine-5'-monophosphate (pdAdo) and adenosine-5'-monophosphate (pAdo), along with NaCl was dissolved in a 1:1 (v/v) methanol:water mixture and diluted to a concentration of ~2 mM of the mononucleotide and 1-2 mM salt. A schematic diagram of the IRMPD action spectroscopy instrumental setup is shown in **Figure 2.1**. Ions were generated using a Micromass “Z-spray” electrospray ionization (ESI) source operated at a flow rate ~10 μL/min. Ions enter the first vacuum region of the mass spectrometer through a limiting orifice cone inlet due to the pressure differential and direct current (dc) potential gradient between the ESI needle and the cone inlet. The cone inlet, which is mounted perpendicularly to the ion path from the ESI needle, and the quadrupole bender (Q bender) is used to prevent direct transfer of neutral solvent droplets from the ESI source. The ions emanating from the ESI source were accumulated in a radio frequency (rf) hexapole ion trap for several seconds to enhance the signal-to noise ratio and affect efficient thermalization of the ions via multiple collisions with the background gases. Ions were pulse extracted from the hexapole through a quadrupole bender, and transferred into the ICR cell via a 1 m long rf octopole ion guide. Ion capturing was

facilitated by electrostatic switching of the dc bias of the octopole, which also avoids collisional heating of the ions.[199] The ICR cell is surrounded by a 4.7 Tesla superconducting magnet. The laser beam in the ICR cell is reflected by the polished gold surface of the ICR cell in a multi-pass fashion, as shown in **Figure 2.1**. This design enables the ion cloud trapped in the ICR cell to overlap multiple times with the FEL and OPO laser beams, such that the IRMPD efficiency is improved. The ions were trapped in the ICR cell for ~300 ms to achieve a room temperature distribution by radiative emission. The precursor ions were isolated using stored waveform inverse Fourier transform (SWIFT) techniques and subsequently irradiated by the FEL or OPO laser to induce IR photodissociation. The FEL typically produces high-energy macropulses, such that efficient IRMPD was achieved in 3-4 s, whereas the reduced output of the OPO laser required 8-9 s of irradiation to achieve similar dissociation efficiency for the experiments performed in this work.

2.1.2 IRMPD YIELD CALCULATION

The IRMPD yield at each frequency was calculated as the ratio of the intensity of the total fragment ion intensity to the total ion intensity, as summarized in **Equation 2.1**,

$$\text{IRMPD yield} = (\sum_i I_{f_i})/(I_P + \sum_i I_{f_i}) \quad (2.1)$$

where I_P is the precursor ion intensity, $\sum_i I_{f_i}$ is the total fragment ion intensity, and $(I_P + \sum_i I_{f_i})$ is the total ion intensity. The IRMPD yields were plotted as a function of vibrational frequency (cm^{-1}) over the IR fingerprint and hydrogen-stretching regions.

Linear normalization with the FEL or OPO laser power was used to correct for variations in the laser power as a function of vibrational frequency.

2.2 ENERGY-RESOLVED COLLISION-INDUCED DISSOCIATION EXPERIMENTS

The energy-resolved collision-induced dissociation (ER-CID) behavior of the protonated and sodium cationized forms of 10 DNA and RNA nucleosides, i.e. dAdo, Ado, dGuo, Guo, dCyd, Cyd, dUrd, Urd, dThd and Thd, were examined using a Bruker amaZon ETD quadrupole ion trap mass spectrometer (QIT MS). The protonated and sodium cationized modified nucleosides were also elucidated using the same technique, including 2'-O-methyladenosine (Adom), 2'-O-methylguanosine (Guom), 2'-O-methylcytidine (Cydm), 2'-O-methyluridine (Urdm), 5,2'-O-dimethyluridine (Thdm), 2'-deoxy-2'-fluoroadenosine (Adofl), 2'-deoxy-2'-fluoroguanosine (Guofl), 2'-deoxy-2'-fluorocytidine (Cydfl), 2'-deoxy-2'-fluorouridine (Urdfl), adenine 9-β-D-arabinofuranoside (araAdo), guanine 9-β-D-arabinofuranoside (areGuo), cytosine 1-β-D-arabinofuranoside (araCyd), uracil 1-β-D-arabinofuranoside (araUrd), 1-methylguanosine (m^1Guo), 7-methylguanosine (m^7Guo), N^2,N^2-dimethylguanosine ($m^2{}_2$Guo) and N2,N2,2'-trimethylguanosine ($m^2{}_2$Guom). The structures of 2'-O-methylnucleosides, 2'-fluoro-nucleosides and ara-nucleosides are shown in **Figure 2.3**, and the methylated guanine nucleosides are shown in **Figure 2.4**. Additionally, several metal cationized dGuo and Guo are examined and compared to protonated and sodium cationized guanine nucleosides to elucidate the effects of local environment on the relative N-glycosidic bond stabilities of these nucleosides, including Li^+, K^+, Rb^+, Cs^+ and Ag^+. A schematic diagram of the QIT MS is shown in **Figure 2.5**. The detailed experimental setup is introduced in **Section 2.2.1**. The experimental workflow for the ER-CID experiments is

illustrated in **Figure 2.6**. The survival yield of a precursor ion is calculated from the CID mass spectra measuredas a function of rf excitation amplitude (rf_{EA}). Four parameter logistic dynamic fitting is applied to fit the survival yield curve and extract the $CID_{50\%}$ value. By comparing the $CID_{50\%}$ values of a family of related ions, the relative stabilities of these precursor ions are determined.

2.2.1 EXPERIMENTAL SETUP FOR ER-CID EXPERIMENTS

All ER-CID experiments were performed using a Bruker amaZon ETD QIT MS. The nucleoside of interest was dissolved in a 1:1 (v/v) methanol:water mixture resulting in a final concentration of 10 to 50 µM. 1% (v/v) acetic acid was added to facilitate formation of the protonated nucleosides, $[Nuo+H]^+$. 10 µM alkali metal chloride was added to promote formation of the alkali metal cationized nucleosides, $[Nuo+M]^+$, whereas 10 µM copper acetate (CuAc) and silver nitrate ($AgNO_3$) were used to produce $[Nuo+Cu]^+$ and $[Nuo+Ag]^+$, respectively. The analyte solution was introduced into the Apollo ESI source at a flow rate of 3 to 5 µL/min to generate the protonated or metal cationized nucleoside ions. These liquid samples were introduced through the nebulizer assembly into the spray chamber at a temperature of ~200℃ and a pressure of 0.69 bar. N_2 used as heated drying gas, and flowing countercurrent to the stream of droplets at a flow rate of 3.0 l/min, was used to aid volatilization, ionization and to carry away any uncharged material. The protonated or metal cationized DNA and RNA nucleosides were focused directly into the entrance of the glass capillary. The capillary voltage was held at 4000 V to transfer ions into a dual ion funnel. The dual ion funnel accepts ions from the ESI source and transfers these ions into a hexapole ion guide. After exiting the second ion funnel through a small aperture, ions enter the subsequent differential

pumping stage. Here, ions are guided using a high precision hexapole into an ion trap module where CID experiments are performed. The ion trap consists of a central ring electrode and a set of two end-cap electrodes. Helium is present into the ion trap to effect efficient trapping and thermalization of the ions. Helium is also used as the collision gas for the ER-CID experiments. A primary rf amplitude is applied to the ring electrode to trap ions. An auxiliary dipolar amplitude is applied to the second end-cap electrode to excite ions. The q_z value for the ER-CID experiments was set to 0.25 to balance the trapping efficiency and low mass cut-off. The fragmentation time was set to 40 ms for all CID experiments. The rf excitation amplitude (rf_{EA}) was increased at a step size of 0.01 V from 0.00 V to the rf_{EA} required to effect complete dissociation of the precursor ion. Each ER-CID experiment was performed three times to assess reproducibility. The CID mass spectra of the protonated and metal cationized nucleosides were acquired using Compass Data Analysis 4.0 software (Bruker Daltonics, Bremen, Germany).

2.2.2 SURVIVAL YIELD ANALYSIS

Survival yield analysis is a robust method to determine the relative stabilities of precursor ions.[147-151,201-204] The survival yield was calculated as each rf_{EA} using **Equation 2.2**,[205]

$$\text{Survival yield} = I_P/(I_P+\sum_i I_{f_i}) \tag{2.2}$$

where I_P and $(I_P+\sum_i I_{f_i})$ are defined as in **Equation 2.1**. A survival yield curve was generated for each system by plotting the survival yield as a function of the rf_{EA}. The $CID_{50\%}$ value, i.e., the rf_{EA} required to effect 50% dissociation of the precursor ion, was

determined using four parameter logistic dynamic fitting based on **Equation 2.3**,

$$\text{Survival yield} = \text{min} + \frac{\text{max-min}}{1+(rf_{EA}/CID_{50\%})^{CID_{slope}}} \quad (2.3)$$

where max and min are the maximum (1) and minimum (0) values of the survival yield, rf_{EA} is the rf excitation amplitude applied, and CID_{slope} is the slope of the declining region of the survival yield curve. The relative stabilities of the protonated and metal cationized nucleosides are elucidated by comparing the $CID_{50\%}$ values determined for these complexes. In particular, in favorable cases where the fragmentation pathways of these complexes involve solely N-glycosidic bond cleavage, the $CID_{50\%}$ values directly correlate with the relative N-glycosidic bond stabilities. Data analyses were performed using SigmaPlot 10.0 software (Systat Software, Inc., San Jose, CA, USA). The survival yields were calculated using custom software developed in our laboratory.

2.3 THEORETICAL CALCULATIONS

The theoretical workflow employed to characterize the structures and predict the IR spectra of the ions of interest is illustrated in **Figure 2.7**. Simulated annealing and complementary electronic structure calculations were performed for the same 10 sodium cationized DNA and RNA nucleosides as well as the sodium cationized complexes of the neutral and deprotonated forms of the adenine mononucleotides. Candidate structures of these complexes were generated from simulated annealing. 10% of the candidate structures were chosen based on the relative stabilities from simulated annealing to perform high level calculations. Geometry optimizations provided the stable low-energy conformers. Vibrational frequencies and their intensities were obtained via frequency analyses. Single point energy calculations using an extended

basis set are performed to improve energetic prediction of the relative stabilities of the stable conformers computed. Thermal corrections and zero point energy based on the computed vibrational frequencies are included to determine the relative stabilities of these conformers at room temperature (298 K), corresponding to the condition under which the experiments are performed. The line spectrum of each conformer was convoluted with a Gaussian distribution and scaled to better reproduce experimental broadening.

2.3.1 SIMULATED ANNEALING

Candidate structures for the sodium cationized nucleosides and mononucleotides were generated using HyperChem software[206] via simulated annealing processes. Conformers with Na^+ binding to each heteroatom of the nucleosides and adenine mononucleotides in a monodentate fashion were used as initial structures for simulated annealing. The chemical structures of the canonical forms of adenine, guanine, cytosine, uracil and thymine nucleosides with the possible binding sites of Na^+ shaded in red are shown in **Figure 2.8**. Additionally, the hydrogen atoms on N1 atom and NH_2 group of guanine can be transferred to N3, O6 or N7 atoms. The hydrogen atom on N3 atom of uracil and thymine can be transferred to O2 or O4 atoms. Therefore, the tautomeric conformers of guanine, uracil and thymine nucleosides with Na^+ binding to each heteroatom were also considered. The chemical structures of the tautomeric forms of guanine, uracil and thymine nucleosides with the possible binding sites of Na^+ shaded in red are shown in **Figure 2.9**. The designation of the tautomeric forms of nucleosides is represented as a lowercase letter “t” followed by one or two numbers. For guanine nucleosides, “t” followed by a single number represents that

tautomerization involves transfer of the N1 proton to the atom indicated, and two numbers represents that tautomerization involves transfer of the N1 and one of the amino protons to the atoms indicated. For uracil and thymine nucleosides, “t” followed by a single number represents that tautomerization involves transfer of the N3 proton to the atom indicated. In the cases of sodium cationized adenine nucleosides, the binding sites of Na^+ examined include the N1, N3, N7, O2', O3', O4', and O5' atoms. In the cases of sodium cationized canonical guanine nucleosides, the binding sites of Na^+ examined include the N3, N7, O6, O2', O3', O4', and O5' atoms. In all cases of sodium cationized tautomeric guanine nucleosides, only nucleobase binding conformers are examined. In the cases of sodium cationized t3 guanine nucleosides, the binding sites of Na^+ examined include the N1, N7, and O6 atoms. In the cases of sodium cationized t6 guanine nucleosides, the binding sites of Na^+ examined include the N1, N3, N7, and O6 atoms. In the cases of sodium cationized t7 guanine nucleosides, the binding sites of Na^+ examined include the N1, N3, and O6 atoms. In the cases of sodium cationized t13 guanine nucleosides, the binding sites of Na^+ examined include the NH, O6, and N7 atoms. In the cases of sodium cationized t16 guanine nucleosides, the binding sites of Na^+ examined include the NH, N3, O6, and N7 atoms. In the cases of sodium cationized t17 guanine nucleosides, the binding sites of Na^+ examined include the NH, N3, and O6 atoms. In the cases of sodium cationized t36 guanine nucleosides, the binding sites of Na^+ examined include the NH, N1, O6, and N7 atoms. In the cases of sodium cationized t37 guanine nucleosides, the binding sites of Na^+ examined include the NH, N1, and O6 atoms. In the cases of sodium cationized t67 guanine nucleosides, the binding sites of Na^+ examined include the NH, N1, N3, and O6 atoms. In the cases of sodium cationized

cytosine nucleosides, the binding sites of Na^+ examined include the O2, N3, O2', O3', O4', and O5' atoms. In the cases of sodium cationized canonical uracil and thymine nucleosides, the binding sites of Na^+ examined include the O2, O4, O2', O3', O4', and O5' atoms. In all cases of sodium cationized tautomeric uracil and thymine nucleosides, only nucleobase binding conformers are examined. In the cases of sodium cationized t2 and t4 uracil and thymine nucleosides, the binding sites of Na^+ examined include the O2, N3, and O4 atoms. The chemical structures of the adenine mononucleotides with the possible binding sites of Na^+ shaded in red are shown in **Figure 2.10**. In the cases of sodium cationized adenine mononucleotides, the binding sites of Na^+ examined include the N1, N3, N7, O2', O3', O4', O5', O_X (oxo atom of phosphate group) and O_H (hydroxyl substituent of phosphate group) atoms. In the cases of sodium cationized deprotonated adenine nucleosides, the binding sites of Na^+ examined include the N1, N3, N7, O2', O3', O4', O5', O_X, and O_H atoms. The theoretical results suggest that Na^+ preferentially binds to N3, O4', O5' O_X, and O_H atoms of deprotonated adenine mononucleotides, thus, the ground conformers of sodium cationized deprotonated adenine mononucleotides are used as initial structures for the simulated annealing of disodium cationized deprotonated adenine mononucleotides. In the cases of disodium cationized deprotonated adenine nucleosides, the first Na^+ binds to the deprotonated adenine mononucleotides in the same fashion as the ground conformers of sodium cationized deprotonated adenine mononucleotides. The binding sites of the second Na^+ examined include the N1, N7, O2', O3', O_X, and O_H atoms. The neutral adenine mononucleotides are also calculated for comparison. Each initial structure of the sodium cationized nucleoside or nucleotide of interest was subjected to 300 cycles of simulated

annealing, where each cycle involved 0.3 ps of thermal heating from 0 to 1000 K, sampling of conformational space for 0.2 ps at 1000 K, the simulation temperature, and 0.3 ps of thermal cooling from 1000 to 0 K. The resulting structure was optimized to a local minimum using the Amber 3 force field. A molecular mechanics (MM) calculation was performed every 1 fs in each cycle, and a snapshot of the lowest energy structure found at the end of each cycle was saved and used as the initial conformation for the subsequent cycle. 30 out of 300 most stable conformers found from each simulated annealing process were chosen and subjected to further analysis via quantum chemical methods. For $[dAdo+Na]^+$ and $[Ado+Na]^+$, 1800 and 2100 candidate conformers were generated from simulated annealing, and 180 and 210 most stable conformers are subjected to further analysis via quantum chemical methods, respectively. For $[dGuo+Na]^+$ and $[Guo+Na]^+$, 11100 and 11400 candidate conformers were generated from simulated annealing, and 1110 and 1140 most stable conformers are subjected to further analysis via quantum chemical methods, respectively. For $[dCyd+Na]^+$ and $[Cyd+Na]^+$, 1500 and 1800 candidate conformers were generated from simulated annealing, and 150 and 180 most stable conformers are subjected to further analysis via quantum chemical methods, respectively. For $[dUrd+Na]^+$ and $[Urd+Na]^+$, 3300 and 3600 candidate conformers were generated from simulated annealing, and 330 and 360 most stable conformers are subjected to further analysis via quantum chemical methods, respectively. For $[dThd+Na]^+$ and $[Thd+Na]^+$, 3300 and 3600 candidate conformers were generated from simulated annealing, and 330 and 360 most stable conformers are subjected to further analysis via quantum chemical methods, respectively. For $[pdAdo+Na]^+$ and $[pAdo+Na]^+$, 2400 and 2700 candidate conformers

were generated from simulated annealing, and 240 and 270 most stable conformers are subjected to further analysis via quantum chemical methods, respectively. For [pdAdo-H+Na] and [pAdo-H+Na], 2400 and 2700 candidate conformers were generated from simulated annealing, and 240 and 270 most stable conformers are subjected to further analysis via quantum chemical methods, respectively. For $[pdAdo-H+2Na]^+$ and $[pAdo-H+2Na]^+$, 1500 and 1800 candidate conformers were generated from simulated annealing, and 150 and 180 most stable conformers are subjected to further analysis via quantum chemical methods, respectively. For pdAdo and pAdo, 300 candidate conformers were generated from simulated annealing, and 30 most stable conformers are subjected to further analysis via quantum chemical methods for both cases.

2.3.2 GEOMETRY OPTIMIZATIONS, FREQUENCY ANALYSES AND SINGLE-POINT ENERGY CALCULATIONS

Geometry optimizations, frequency analyses and single point energy calculations were performed using the Gaussian 09 suite of programs for the candidate conformers of 10 sodium cationized DNA and RNA nucleosdies as well as the sodium cationized complexes of the neutral and deprotonated forms of the adenine mononucleotides and neutral adenine mononucleotides.[207] The candidate conformers subjected to quantum chemical calculations are introduced in **Section 2.3.1**. Geometry optimizations and harmonic vibrational frequency calculations were performed at the B3LYP/6-311+G(d,p) level of theory, whereas single point energies were calculated at the B3LYP/6-311+G(2d,2p) level of theory. This level of theory was chosen because it has been shown to effectively describe the conformations, IR spectra, and relative stabilities of protonated DNA and RNA nucleosides and mononucleotides.[119,125,184-189] The presence of the 2'-hydroxyl substituent of the RNA pyrimidine nucleosides offers the possibility of

unique low-energy binding modes of Na^+ that are not possible for the DNA pyrimidine nucleosides. In particular conformers in which Na^+ binds to the O2 and O2' atoms of the nucleobase and sugar moieties are within 7 kJ/mol of the compuated ground conformers. In order to further assess the importance of the 2'-hydroxyl substituent on the binding of Na^+ to the RNA pyrimidine nucleosides in both the gas phase and solution, the mono and dihydrated forms of the ground and the most stable *anti* oriented bidentate conformers of the sodium cationized RNA pyrimidine nucleosides were also calculated using the same theoretical approaches to elucidate the effect of solvent on the relative stabilities of these complexes. For the sodium cationized uracil nucleosides, single point energies of the ground and most stable *anti* oriented bidentate conformers of $[Urd+Na]^+$ as well as the mono and dihydrated complexes of these conformers were also calculated at the B3LYP/def2-TZVPPD, MP2(full)/6-311+G(2d,2p), and MP2(full)/def2-TZVPPD levels of theory. To further assess the relative stabilities of the ground and three most stable excited tridentate conformers of $[dUrd+Na]^+$, single point energies of these conformers were also calculated at these same levels of theory. Thermal corrections were taken directly from the Gaussian output without scaling of the computed frequencies.

The vibrational frequencies computed for the 10 sodium cationized DNA and RNA nucleosides were scaled by a factor of 0.98-0.99 in the IR fingerprint region, and by a factor of 0.95-0.96 in the hydrogen-stretching region to better reproduce the experimental IRMPD spectra. In previous theoretical and IRMPD action spectroscopy studies of the deprotonated and protonated forms of the common DNA and RNA mononucleotides,[187-192] it was found that the theoretical linear IR spectra calculated at

the B3LYP/6-311+G(d,p) level of theory exhibited the best agreement with the measured IRMPD action spectra when different scaling factors were applied to the bands above and below ~1300 cm^{-1}. Additionally, the previous theoretical and IRMPD studies of phosphorylated species indicated that several spectral features attributed to the modes of the phosphate moiety are red-shifted as compared to the measured frequencies for these vibrational modes.[145,146,208,209] Similar behavior is also observed for the theoretical and experimental spectra presented here, hence, a scaling factor of 0.978 was applied to the calculated harmonic frequencies above 1300 cm^{-1} and 0.990 for frequencies below 1300 cm^{-1} in the IR fingerprint region of the spectra computed for the sodium cationized forms of deprotonated and neutral adenine mononucleotides. In the hydrogen-stretching region, the scaling factor is ~0.955. The vibrational frequencies were convoluted with a 20 cm^{-1} fwhm Gaussian line shape over the IR fingerprint region, and a 15 cm^{-1} fwhm Gaussian line shape over the hydrogen-stretching region to better reproduce the broadening of the IR features observed in the experiments.

2.4 REFERENCES

119. R. R. Wu, B. Yang, C. E. Frieler, G. Berden, J. Oomens and M. T. Rodgers, *Phys. Chem. Chem. Phys.* 2015, **17**, 25978.

125. R. R. Wu, B. Yang, C. E. Frieler, G. Berden, J. Oomens and M. T. Rodgers, *J. Am. Soc. Mass Spectrom.* 2016, **27**, 410.

145. B. S. Fales, N. O. Fujamade, J. Oomens and M. T. Rodgers, *J. Am. Soc. Mass Spectrom.* 2011, **22**, 1862.

146. B. S. Fales, N. O. Fujamade, Y. W. Nei, J. Oomens and M. T. Rodgers, *J. Am. Soc. Mass Spectrom.* 2011, **22**, 81.

147. Y. Zhu, L. A. Hamlow, C. C. He, S. F. Strobehn, J. K. Lee, J. Gao, G. Berden, J. Oomens and M. T. Rodgers, *J. Phys. Chem. B* 2016, **120**, 8892.

148. Y. Zhu, L. A. Hamlow, C. C. He, J. K. Lee, J. Gao, G. Berden, J. Oomens and M. T. Rodgers, *J. Phys. Chem. B* 2017, **121**, 4048.

149. Y. Zhu, L. A. Hamlow, C. C. He, H. A. Roy, N. A. Cunningham, M. U. Munshi, G. Berden, J. Oomens and M. T. Rodgers, *Int. J. Mass Spectrom.* 2017, DOI: https://doi.org/10.1016/j.ijms.2017.04.005.

150. Y. Zhu, H. A. Roy, N. A. Cunningham, S. F. Strobehn, J. Gao, M. U. Munshi, G. Berden, J. Oomens and M. T. Rodgers, *Phys. Chem. Chem. Phys.* 2017, **19**, 17637.

151. Y. Zhu, H. A. Roy, N. A. Cunningham, S. F. Strobehn, J. Gao, M. U. Munshi, G. Berden, J. Oomens and M. T. Rodgers, *J. Am. Soc. Mass Spectrom* 2017, **28**, 2437.

184. R. R. Wu, B. Yang, G. Berden, J. Oomens and M. T. Rodgers, *J. Phys. Chem. B* 2015, **119**, 2795.

185. R. R. Wu, B. Yang, G. Berden, J. Oomens and M. T. Rodgers, *J. Phys. Chem. B* 2014, **118**, 14774.

186. R. R. Wu, B. Yang, C. E. Frieler, G. Berden, J. Oomens and M. T. Rodgers, *J. Phys. Chem. B* 2015, **119**, 5773.

187. R. R. Wu, C. C. He, L. A. Hamlow, Y.-w. Nei, G. Berden, J. Oomens and M. T. Rodgers, *J. Phys. Chem. B* 2016, **120**, 4616.

188. R. R. Wu, C. C. He, L. A. Hamlow, Y. W. Nei, G. Berden, J. Oomens and M. T. Rodgers, *Phys. Chem. Chem. Phys.* 2016, **18**, 15081.

189. R. R. Wu, L. A. Hamlow, C. C. He, Y. W. Nei, G. Berden, J. Oomens and M. T. Rodgers, *J. Am. Soc. Mass Spectrom.* 2017, **28**, 1638.

190. R. R. Wu, L. A. Hamlow, C. C. He, Y.-w. Nei, G. Berden, J. Oomens and M. T. Rodgers, *Phys. Chem. Chem. Phys.* 2017, DOI: 10.1039/C7CP05521H.

191. Y.-w. Nei, N. Hallowita, J. D. Steill, J. Oomens and M. T. Rodgers, *J. Phys. Chem. A* 2013, **117**, 1319.

192. Y.-w. Nei, K. T. Crampton, G. Berden, J. Oomens and M. T. Rodgers, *J. Phys. Chem. A* 2013, **117**, 10634.

198. J. J. Valle, J. R. Eyler, J. Oomens, D. T. Moore, A. F. G. van der Meer, G. von Helden, G. Meijer, C. L. Hendrickson, A. G. Marshall and G. T. Blakney, *Rev. Sci. Instrum.* 2005, **76**, 023103.

199. N. C. Polfer, J. Oomens, D. T. Moore, G. von Helden, G. Meijer and R. C. Dunbar, *J. Am. Chem. Soc.* 2006, **128**, 517.

200. N. C. Polfer and J. Oomens, *Phys. Chem. Chem. Phys.* 2007, **9**, 3804.

201. A. Memboeuf, A. Nasioudis, S. Indelicato, F. Pollreisz, A. Kuki, S. Keki, O. F. van den Brink, K. Vekey and L. Drahos, *Anal. Chem.* 2010, **82**, 2294.

202. F. Derwa, E. Depauw and P. Natalis, *Org. Mass Spectrom.* 1991, **26**, 117.

203. X. H. Guo, M. C. Duursma, P. G. Kistemaker, N. M. M. Nibbering, K. Vekey, L. Drahos and R. M. A. Heeren, *J. Mass Spectrom.* 2003, **38**, 597.

204. A. Memboeuf, L. Jullien, R. Lartia, B. Brasme and Y. Gimbert, *J. Am. Soc. Mass Spectrom.* 2011, **22**, 1744.

205. T. M. Kertesz, L. H. Hall, D. W. Hill and D. F. Grant, *J. Am. Soc. Mass Spectrom.* 2009, **20**, 1759.

206. K. Wolinski, J. F. Hinton, D. S. Wishart, B. D. Sykes, F. M. Richards, A. Pastone, V. Saudek, P. D. Ellis, G. E. Maciel, J. W. McIver Jr., A. C. Blizzard, D. P. Santry, J. A.

Pople, N. S. Ostlund, L. Ducasse, J. Hoarau, M. Pesquer, M. Kondo, I. Ando, R. Chujo, A. Nishioka, E. C. Vauthier, S. Odiot, F. Tonnard, J. D. Baker, M. C. Zerner, D. V. Beveridge, W. P. Anderson, T. R. Cundari, R. C. Bingham, M. J. S. Dewar, D. H. Lo, J. Li, P. C. Mello, K. Jug, W. Tihiel, E. G. Zoebisch, E. F. Healy, J. J. P. Stewart, M. Fraser and D. M. Hayes, HyperChem Computational Chemistry Software Package, hypercube, Inc., Gainsville, FL, version 7.0, 2001.

207. M. J. Frisch, G. W. Trucks, H. B. Schlegel, G. E. Scuseria, M. A. Robb, J. R. Cheeseman, G. Scalmani, V. Barone, B. Mennucci, G. A. Petersson, H. Nakatsuji, M. Caricato, X. Li, H. P. Hratchian, A. F. Izmaylov, J. Bloino, G. Zheng, J. L. Sonnenberg, M. Hada, M. Ehara, K. Toyota, R. Fukuda, J. Hasegawa, M. Ishida, T. Nakajima, Y. Honda, O. Kitao, H. Nakai, T. Vreven, J. A. Montgomery Jr., J. E. Peralta, F. Ogliaro, M. J. Bearpark, J. Heyd, E. N. Brothers, K. N. Kudin, V. N. Staroverov, R. Kobayashi, J. Normand, K. Raghavachari, A. P. Rendell, J. C. Burant, S. S. Iyengar, J. Tomasi, M. Cossi, N. Rega, N. J. Millam, M. Klene, J. E. Knox, J. B. Cross, V. Bakken, C. Adamo, J. Jaramillo, R. Gomperts, R. E. Stratmann, O. Yazyev, A. J. Austin, R. Cammi, C. Pomelli, J. W. Ochterski, R. L. Martin, K. Morokuma, V. G. Zakrzewski, G. A. Voth, P. Salvador, J. J. Dannenberg, S. Dapprich, A. D. Daniels, Ö. Farkas, J. B. Foresman, J. V. Ortiz, J. Cioslowski and D. J. Fox, Gaussian 09, Gaussian, Inc., Wallingford, CT, revision C.01, 2009.

208. M. T. Rodgers, P. B. Armentrout, J. Oomens and J. D. Steill, *J. Phys. Chem. A* 2008, **112**, 2258.

209. C. F. Correia, P. O. Balaj, D. Scuderi, P. Maitre and G. Ohanessian, *J. Am. Chem. Soc.* 2008, **130**, 3359.

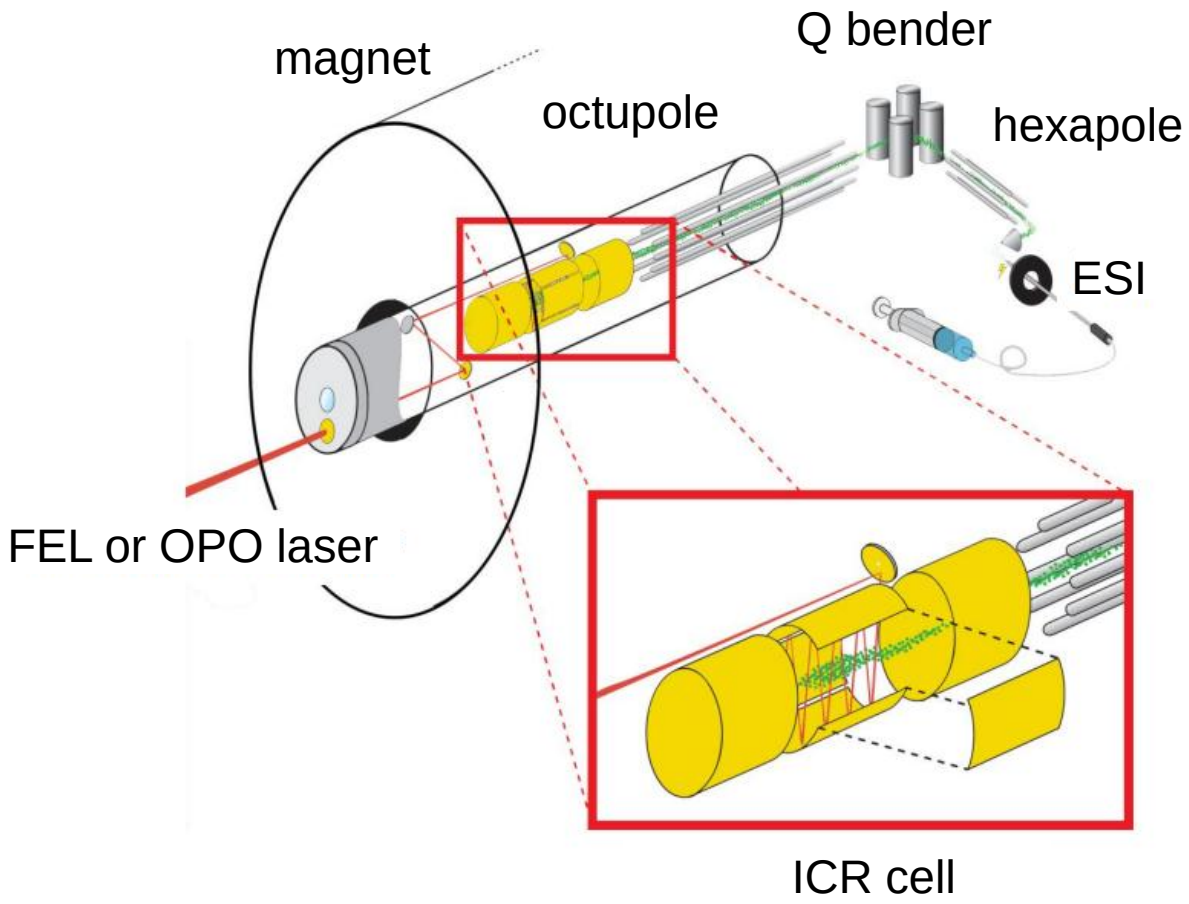

Figure 2.1 Schematic diagram of the FT-ICR MS coupled to an FEL or OPO/OPA laser. Precursor ions were generated using an ESI source, and accumulated in an rf hexapole ion trap for several seconds. Ions were pulse extracted through a quadrupole bender, and transferred into the ICR cell. Precursor ions were mass isolated and interacted with the laser beam to induce IR photodissociation.

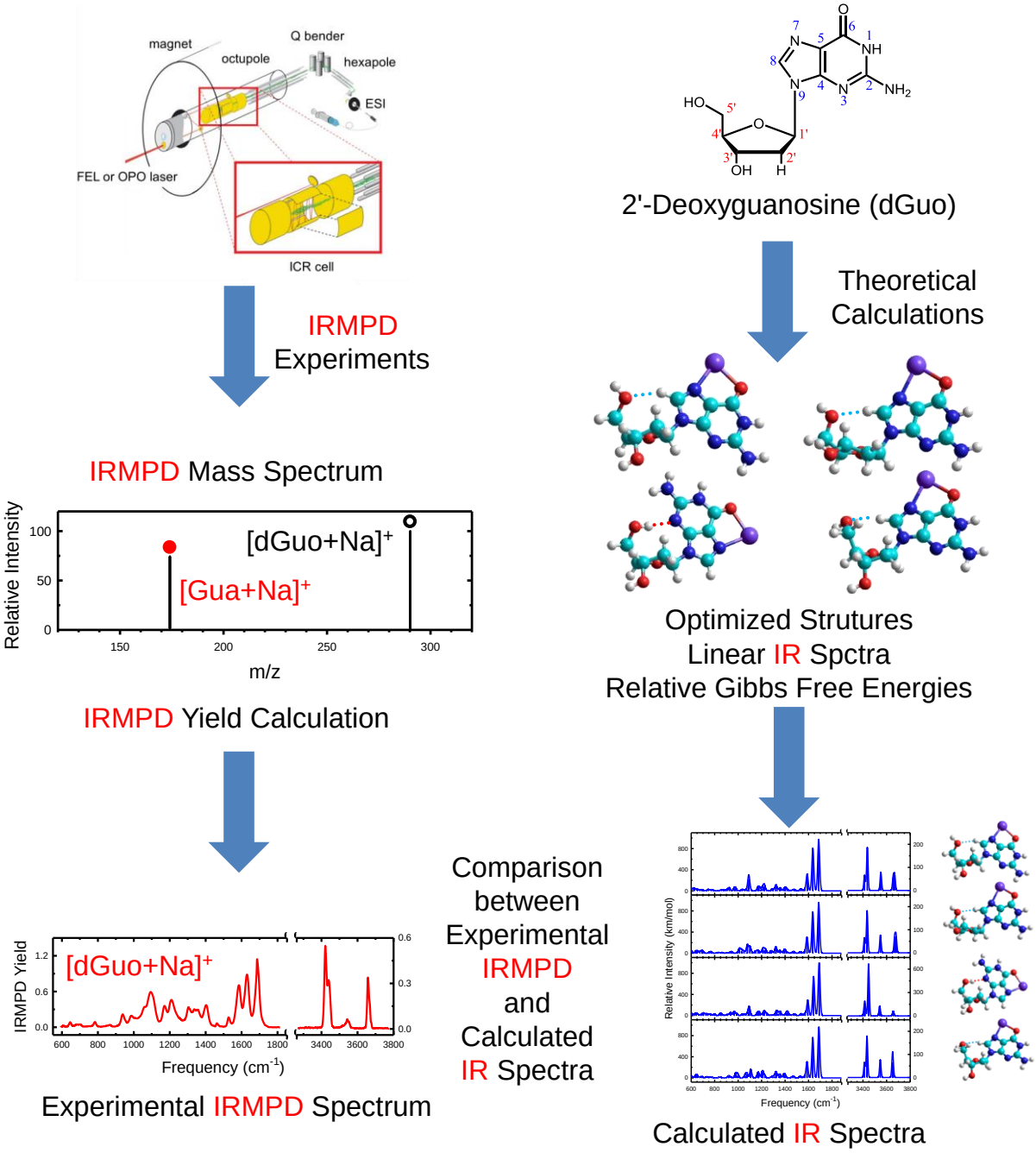

Figure 2.2 Experimental workflow for IRMPD action spectroscopy experiments. MS/MS experiments are performed as a function of laser output (wavelength/vibrational frequency). Experimental IRMPD spectra were computed from the wavelength-dependent IRMPD MS/MS spectra. The linear IR spectra were obtained from theoretical calculation. Comparison between the experimental IRMPD and calculated IR spectra enable determination of stable low-energy conformers populated in the experiments.

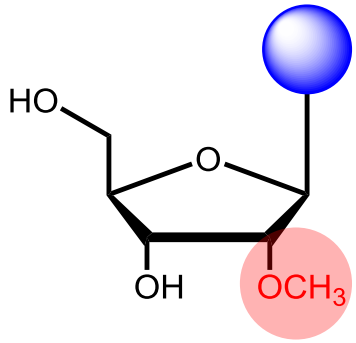

Nuom

Adom, Cydm, Guom, Urdm, Thdm

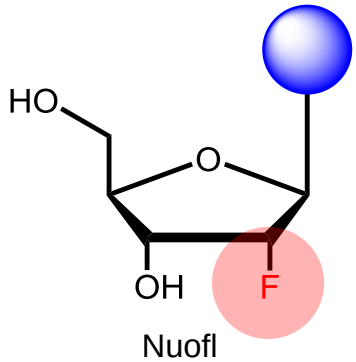

Nuofl

Adofl, Cydfl, Guofl, Urdfl

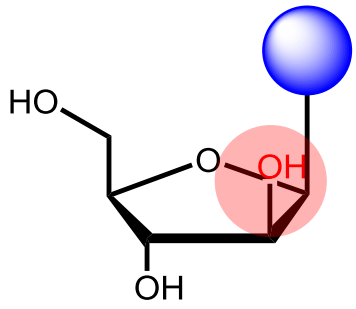

araNuo

araAdo, araCyd, araGuo, araUrd

Figure 2.3 Chemical structures of 2'-O-methylated, 2'-fluoro-substituted and the arabinose nucleoside analogs along with their three-letter and modification abbreviations. The sugar modifications are shaded in red.

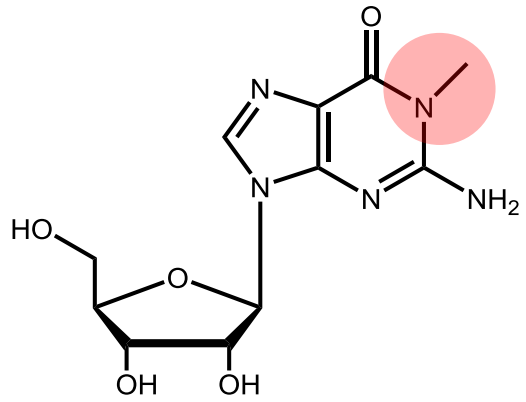

1-Methylguanosine
m^1Guo

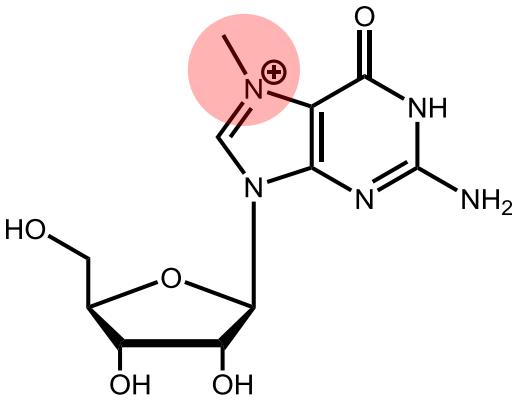

7-Methylguanosine
m^7Guo

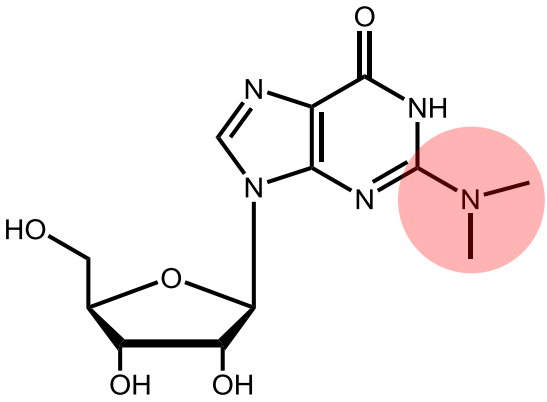

N^2,N^2-Dimethylguanosine
m^2_2Guo

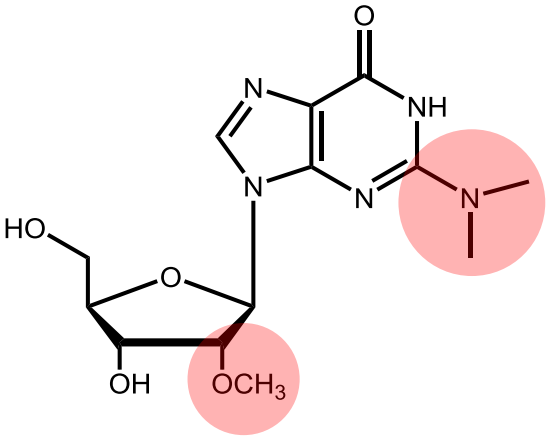

$N^2,N^2,2'$-Trimethylguanosine
m^2_2Guom

Figure 2.4 Chemical structures of methylated guanosines along with three-letter and substitution abbreviations. The modifications are shaded in red.

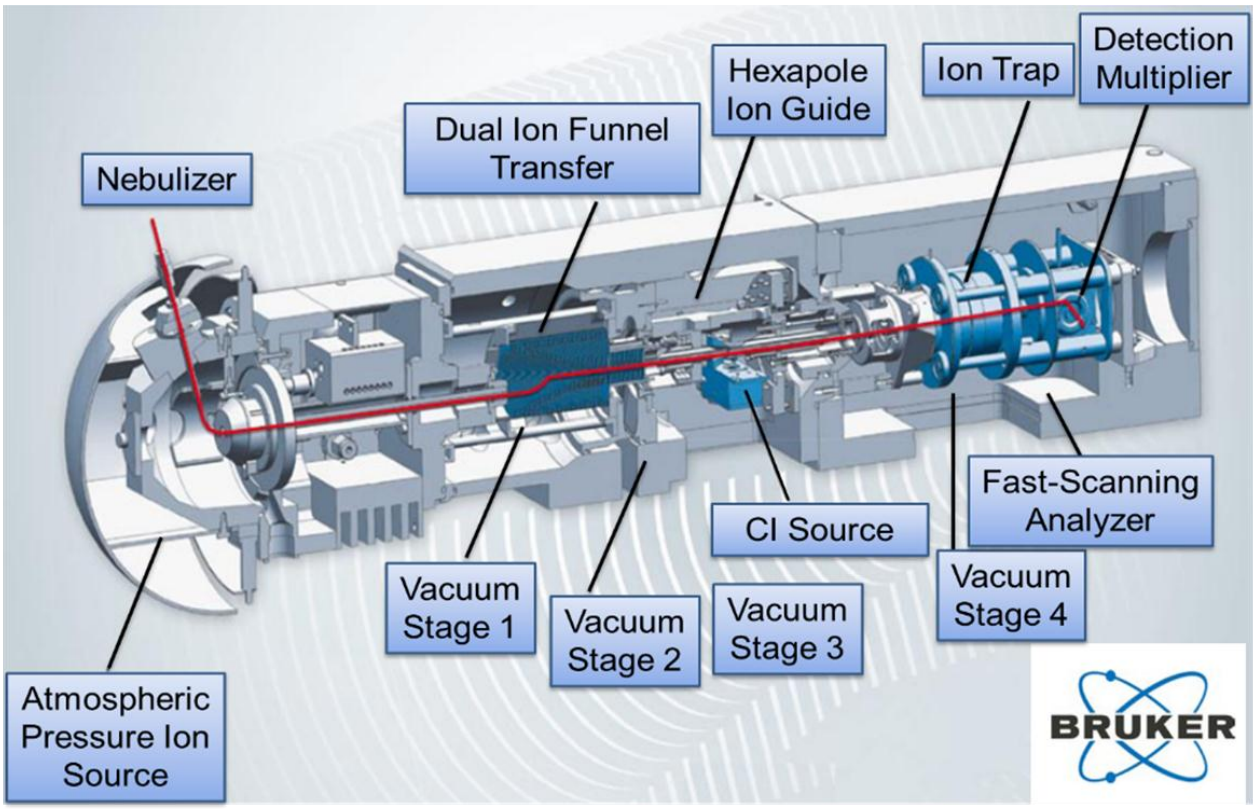

Figure 2.5 Schematic diagram of the QIT MS. Ions are generated using an ESI source, and transferred into a dual ion funnel through a heated capillary. An rf hexapole ion guide is used to transfer the ions into the ion trap. Precursor ions were mass isolated, subjected to rf excitation to increase their kinetic energy, and collided with the He buffer gas to effect collision-induced dissociation.

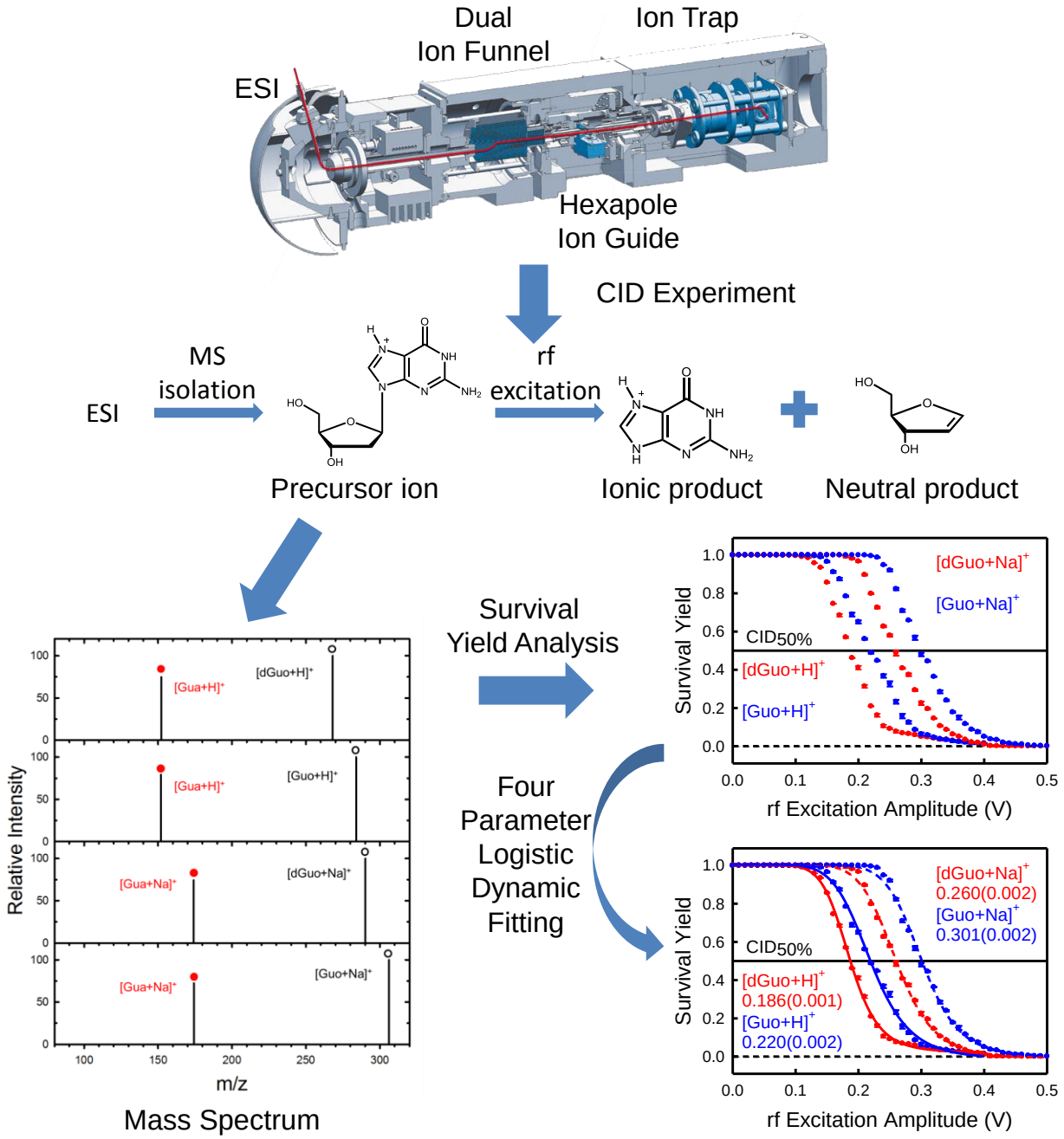

Figure 2.6 Experimental workflow for ER-CID experiments using QIT MS. Mass spectra of the precursor ion were obtained as a function of the rf_{EA}. Survival yield was calculated and plotted as a function of rf_{EA} to generate the survival yield curve. The $CID_{50\%}$ value of each precursor ion was determined using four parameter logistic dynamic fitting of the survival yield curve. Comparisons among related systems elucidate trends in the stability of the precursor ions.

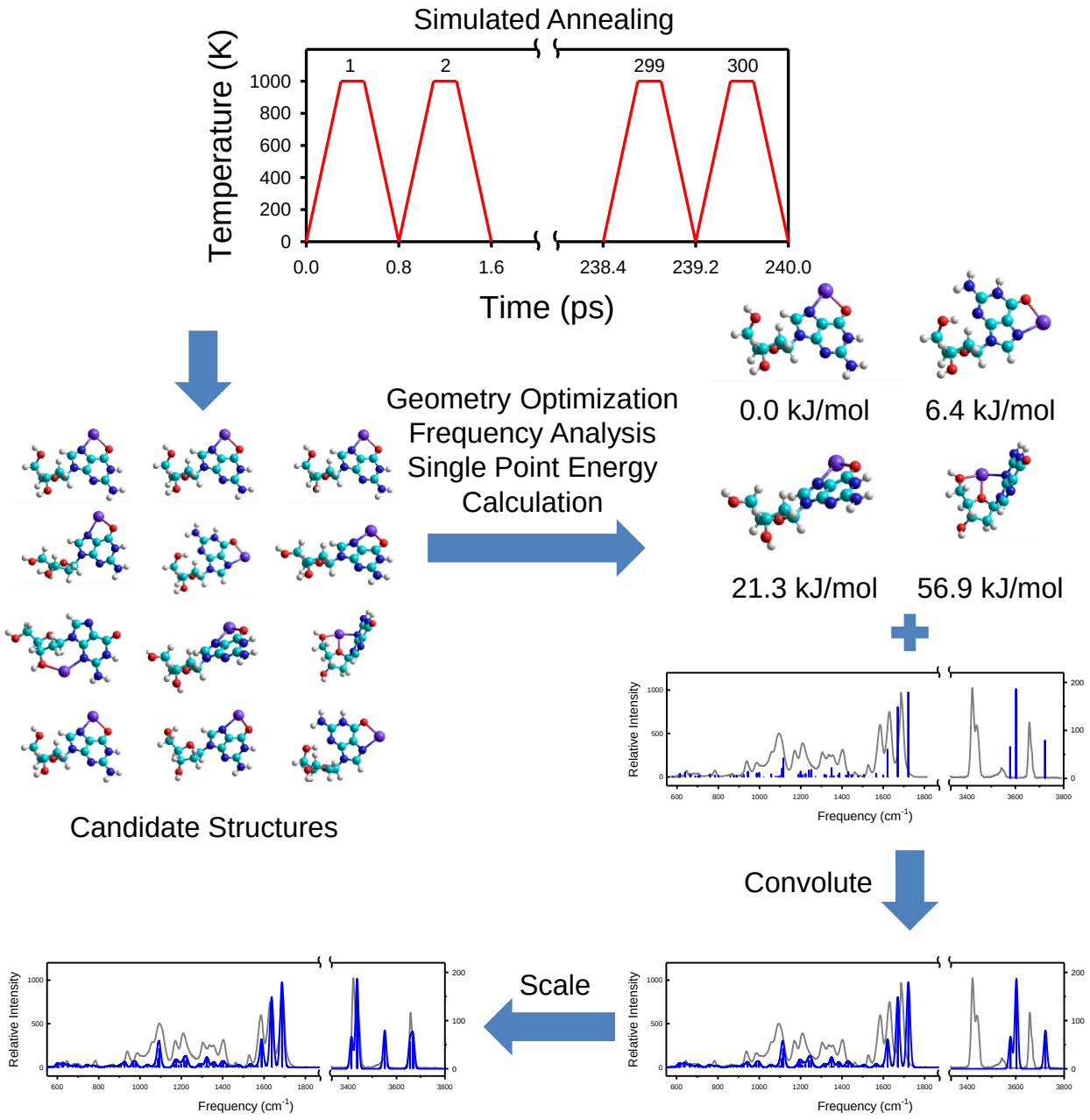

Figure 2.7 Theoretical workflow for computational work. Candidate structures are generated by simulated annealing procedures. 30 out of 300 most stable candidate structures from each simulated annealing are chosen to perform electronic structure calculations. Geometry optimizations, frequency analyses and single point energy calculations provided the structures, linear IR spectra and energetics of low-energy conformers. The line spectrum is convoluted and scaled to better reproduce the experimental IRMPD spectrum.

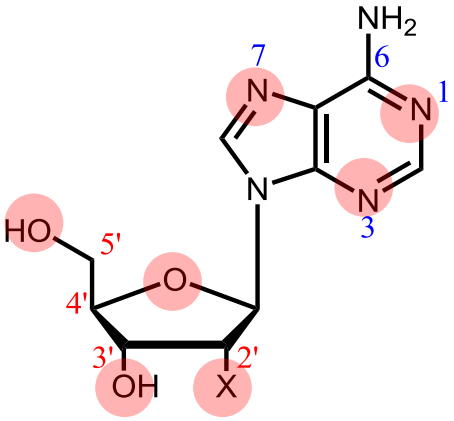

2'-Deoxyadenosine (dAdo)
X=H
Adenosine (Ado)
X=OH

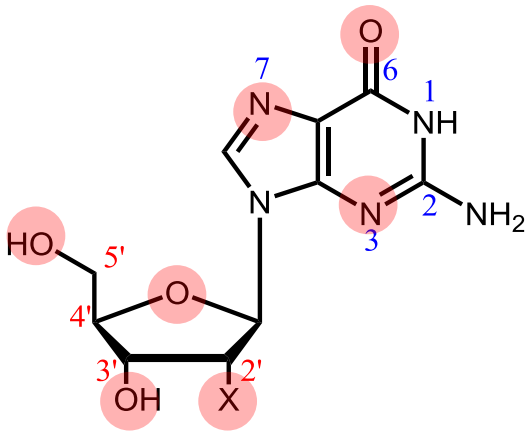

2'-Deoxyguanosine (dGuo)
X=H
Guanosine (Guo)
X=OH

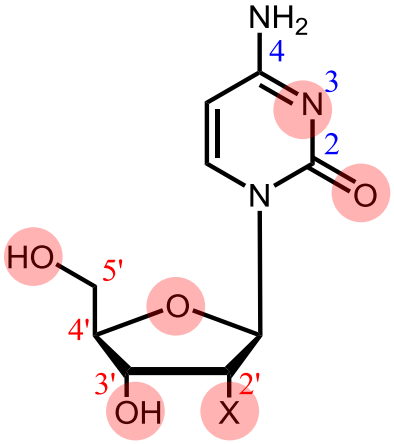

2'-Deoxycytidine (dCyd)
X=H
Cytidine (Cyd)
X=OH

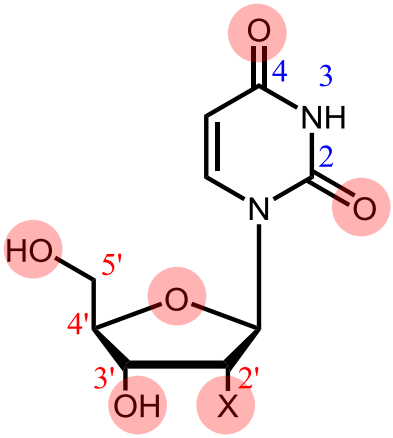

2'-Deoxyuridine (dUrd)
X=H
Uridine (Urd)
X=OH

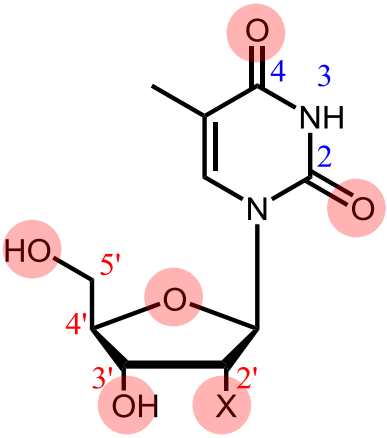

Thymidine (dThd)
X=H
5-Methyluridine (Thd)
X=OH

Figure 2.8 Chemical structures of the canonical forms of adenine, guanine, cytosine, uracil and thymine nucleosides along with their names and three-letter abbreviations. Heteroatoms that are the possible binding sites of the sodium cation are shaded in red.

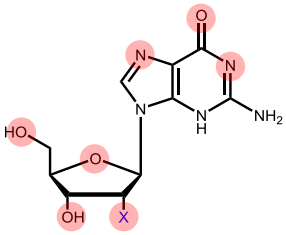

dGuot3 or Guot3

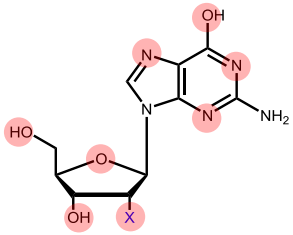

dGuot6 or Guot6

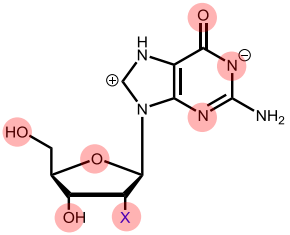

dGuot7 or Guot7

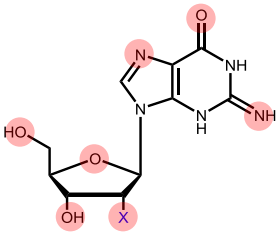

dGuot13 or Guot13

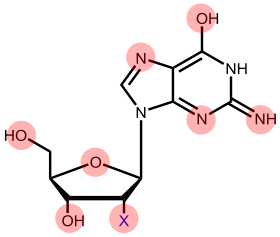

dGuot16 or Guot16

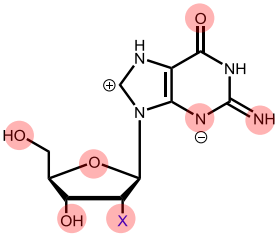

dGuot17 or Guot17

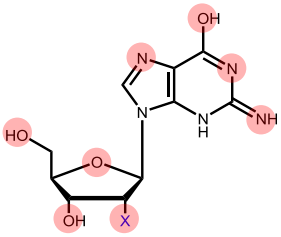

dGuot36 or Guot36

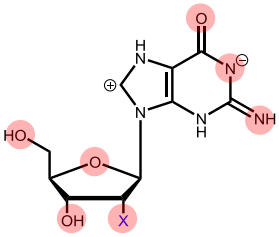

dGuot37 or Guo37

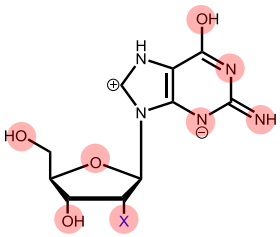

dGuot67 or Guot67

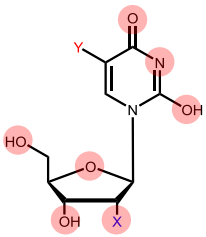

dUrdt2 or Urdt2
dThdt2 or Thdt2

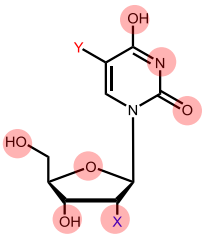

dUrdt4 or Urdt4
dThdt4 or Thdt4

X = H, DNA nucleosides
X = OH, RNA nucleosides
Y = H, uracil nucleosides
Y = CH_3, thymine nucleosides

Figure 2.9 Chemical structures of the tautomeric forms of guanine, uracil, and thymine nucleosides along with their abbreviations. Heteroatoms that are the possible binding sites of the sodium cation are shaded in red.

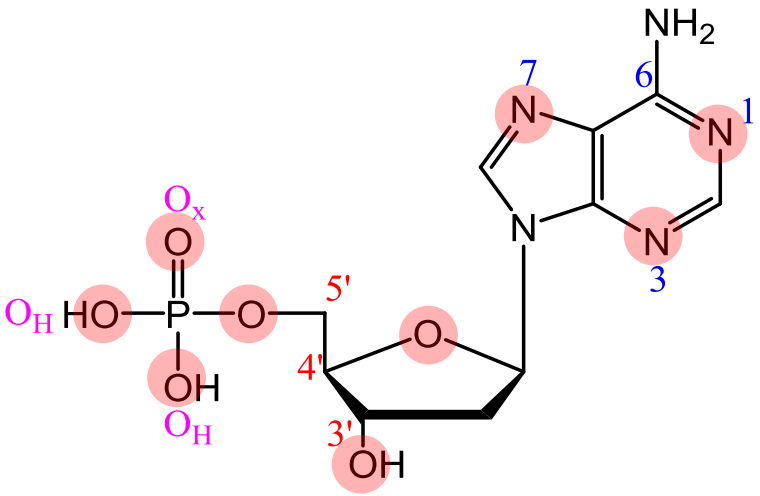

2'-Deoxyadenosine-5'-monophosphate
pdAdo

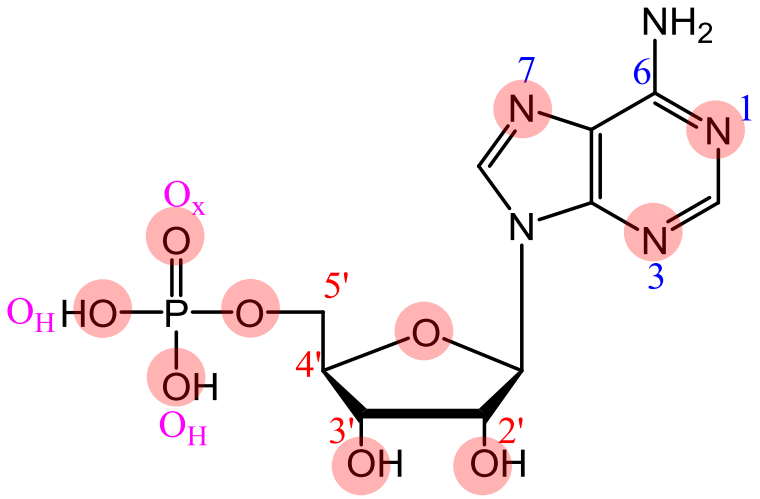

Adenosine-5'-monophosphate
pAdo

Figure 2.10 Chemical structures of 2'-deoxyadenosine-5'-monophosphate (pdAdo) and adenosine-5'-monophosphate (pAdo) along with potential binding sites of Na^+ shaded in red.

CHAPTER 3 THEORETICAL RESULTS AND DISCUSSION

Portions of this chapter were reprinted with permission from the followed research publications. Y. Zhu, L. A. Hamlow, C. C. He, S. F. Strobehn, J. K. Lee, J. Gao, G. Berden, J. Oomens and M. T. Rodgers, *J. Phys. Chem. B* 2016, **120**, 8892. Copyright 2016 American Chemistry Society. Y. Zhu, L. A. Hamlow, C. C. He, J. K. Lee, J. Gao, G. Berden, J. Oomens and M. T. Rodgers, *J. Phys. Chem. B* 2017, **121**, 4048. Copyright 2017 American Chemistry Society. Y. Zhu, L. A. Hamlow, C. C. He, H. A. Roy, N. A. Cunningham, M. U. Munshi, G. Berden, J. Oomens and M. T. Rodgers, *Int. J. Mass Spectrom.* 2017, https://doi.org/10.1016/j.ijms.2017.04.005. Copyright 2017 Elsevier B.V. Y. Zhu, H. A. Roy, N. A. Cunningham, S. F. Strobehn, J. Gao, M. U. Munshi, G. Berden, J. Oomens and M. T. Rodgers, *Phys. Chem. Chem. Phys.* 2017, **19**, 17637. Copyright 2017 Royal Society of Chemistry. Y. Zhu, H. A. Roy, N. A. Cunningham, S. F. Strobehn, J. Gao, M. U. Munshi, G. Berden, J. Oomens and M. T. Rodgers, *J. Am. Soc. Mass Spectrom*. 2017, **28**, 2437. Copyright 2017 American Society for Mass Spectrometry.

3.1 INTRODUCTION

The computational methods employed to characterize the stable conformations of the sodium cationized DNA and RNA nucleosides are described in detail in **Chapter 2**. In this chapter, the stable low-energy conformations calculated for 10 sodium cationized DNA and RNA nucleosides at B3LYP/6-311+G(2d,2p)//B3LYP/6-311+G(d,p) level of theory are presented.[147-151] The stable low-energy conformers of each sodium cationized nucleoside shown in this chapter include all populated conformers (determined in **Chapter 4**) and the most stable conformer of each type of Na^+ binding.

As discussed in **Chapter 2.3**, the presence of the 2'-hydroxyl substituent of RNA pyrimidine nucleosides offers the possibility of a unique low-energy binding mode of Na^+ that is not possible for DNA pyrimidine nucleosides, thus, the mono and dihydrated ground and the most stable *anti* oriented bidentate conformers of the sodium cationized RNA formed pyrimidine nucleosides were also calculated to elucidate the effect of water molecules on the relative stabilities of these complexes.

3.2 NOMENCLATURE OF SODIUM CATIONIZED NUCLEOSIDES

The nomenclature employed to describe the stable low-energy conformers of the sodium cationized DNA and RNA nucleosides and specifically, the binding geometry, relative stability, and tautomeric conformation of the nucleobase, employs an uppercase letter to indicate the number of chelation interactions between the sodium cation and nucleoside (T for tridentate, B for bidentate, and M for monodentate), followed by a number that indicates the order of relative Gibbs free energies at 298 K of the conformers found for that mode of Na^+ binding (1, 2, 3, etc.), followed by the atoms to which Na^+ is bound in parentheses, which is appended by t, when the nucleobase is in a minor tautomeric form.

3.3 THEORETICAL RESULTS

3.3.1 STABLE LOW-ENERGY CONFORMERS OF SODIUM CATIONIZED ADENINE NUCLEOSIDES

Figures 3.1 and **3.2** show representative stable low-every conformers of the sodium cationized adenine nucleosides along with their relative Gibbs free energies, nucleobase orientations and sugar puckerings. For $[dAdo+Na]^+$, 48 stable low-energy conformers were found within 100 kJ/mol of the ground conformer. Among these conformers, 10 unique modes of Na^+ binding were found, including T(N3O4'O5'),

B(N3O4'), B(O4'O5'), B(N7NH_2), B(N3O3'), B(N7O5'), B(N1NH_2), B(N3O5'), T(N7NH_2O5'), and M1(N3). For $[Ado+Na]^+$, 58 stable low-energy conformers were found within 100 kJ/mol of the ground conformer. Among these conformers, 9 unique modes of Na^+ binding were found, including T(N3O4'O5'), B(N3O2'), T(N3O2'O3'), B(N3O4'), B(O4'O5'), B(N7NH_2), B(N1NH_2), B(N7O5'), T(N7NH_2O5'), and M1(N1). In the ground conformers of the $[dAdo+Na]^+$ and $[Ado+Na]^+$, the sodium cation binds in a tridentate fashion to the N3, O4′ and O5′ atoms forming 5- and 6-membered chelation rings, with adenine in a *syn* orientation and puckering of the sugar moieties that is C2'-endo ($^2T_1$) and C1'-exo ($_1T^O$), respectively. Conformers that bind via bidentate interaction with the N3 and O4′ atoms are >33 kJ/mol less stable, indicating that the chelation interaction with the O5′ atom is an important contributor to the binding. *Anti*-oriented N3 binding conformers of $[dAdo+Na]^+$ and $[Ado+Na]^+$ are much less stable, by > 65 kJ/mol for dAdo and almost 20 kJ/mol for Ado. Conformers that bind via monodentate interaction with the N3 atom are only found for $[dAdo+Na]^+$, however, the most stable of these conformers, M1(N3), is > 95 kJ/mol less stable than the ground conformer. All stable conformers that bind to the N1 or N7 atoms also chelate with the amino substituent or the 5′-hydroxyl substituent. Both *anti*- and *syn* orientations are found with the *anti*-conformers favored over *syn*. The interaction between the sodium cation and the NH_2 substituent disrupts the conjugated structure of adenine, and changes the hybridization of the amino nitrogen from sp^2 to sp^3. Sodium cation chelation with N7 and O5′ is observed in both $[dAdo+Na]^+$ and $[Ado+Na]^+$, but is much less favorable with the most stable conformers of this type > 70 kJ/mol less stable than the corresponding ground conformers. A monodentate conformer binding to the N1 atom is only found for

$[Ado+Na]^+$, M1(N1), and this conformer is 96.1 kJ/mol less stable. Bidentate binding of the sodium cation to the sugar via the O4′ and O5′ atoms is found in the B1(O4′O5′) conformer of $[dAdo+Na]^+$, and the B1(O4′O5′) and B2(O4′O5′) conformers of $[Ado+Na]^+$. These conformers are computed to be > 40 kJ/mol less stable than their corresponding tridentate ground conformers. The 2′-hydroxyl substituent of $[Ado+Na]^+$ forms a hydrogen bond with the N3 atom of adenine in the B1(O4'O5') conformer and limits rotation about the N-glycosidic bond. Therefore, the missing interaction between the sodium cation and adenine leads to significant destabilization of the B1(O4'O5') conformer. A more detailed discussion of the theoretical results and descriptions of the sodium cationized adenine nucleosides can be found in **Reference 146**.

3.3.2 COMPARISONS OF THE STABLE LOW-ENERGY CONFORMERS OF THE PROTONATED AND SODIUM CATIONIZED ADENINE NUCLEOSIDES

Ranran Wu reported the IRMPD action spectroscopic and theoretical studies of the gas-phase conformations and energetics of protonated adenine nucleosides.[184] She found that N3 atom is the most favorable protonation site for both $[dAdo+H]^+$ and $[Ado+H]^+$. N3 protonation enables a strong intramolecular hydrogen-bonding interaction between $N3H^+$ and O5′ to be formed leading to rotation of adenine to a *syn* orientation and an approximately C2′-endo ($^2T_1$) configuration of the sugar. In contrast, protonation at N1 and N7 are found to be much less favorable such that N1 protonated conformers are observed in minor abundance and N7 conformers are not present in measurable abundance, consistent with the computed stabilities which follow the order: N3 > N1 > N7. For $[dAdo+H]^+$, the N1 binding conformers are at least 25.3 kJ/mol less stable, and the N7 binding conformers are at least 33.6 kJ/mol less stable than the ground conformer. For $[Ado+H]^+$, the relative Gibbs free energies of N1 binding conformers

reduce to at least 21.8 kJ/mol, whereas the relative Gibbs free energies of N7 binding conformers increase to at least 37.2 kJ/mol. Similarly, the sodium cation prefers to bind to the N3, O4′ and O5′ atoms and also requires that adenine rotate to a *syn* orientation. However, because the sodium cation is much larger and can form multiple chelating interactions, the O4′ atom is also involved in the binding of Na^+, and thus forms 5- and 6-membered rings in the ground conformers of $[dAdo+Na]^+$ and $[Ado+Na]^+$. Interaction of the sodium cation with the O4′ atom influences the sugar puckering, which shifts from C2′-endo (^2E) in the protonated systems toward O4′-endo (^OE) in the sodium cationized systems, with multiple low-energy conformers exhibiting puckering of the sugar moiety that lie between these limiting configurations. Sodium cation binding to the N1 or N7 atoms is much less favorable and not observed in the experiments. For $[dAdo+Na]^+$, the N7 binding conformers are at least 65.0 kJ/mol less stable, whereas the N1 binding conformers are at least 73.1 kJ/mol less stable than the ground conformer. For $[Ado+Na]^+$, the relative Gibbs free energies of the N7 and N1 binding conformers are similar to those found for $[dAdo+Na]^+$, but are slightly more favorable such that the most stable N7 binding conformer is 60.3 kJ/mol, whereas the most stable N1 binding conformer is 67.1 kJ/mol less favorable than the ground conformer. The binding affinities follow the order: N3 > N7 > N1. Thus, the sodium cation alters the relative affinities for N1 and N7 binding compared to a proton. Additionally, the N1 and N7 binding conformers of $[dAdo+Na]^+$ and $[Ado+Na]^+$ are much less stable than the corresponding ground conformers. The glycosidic bonds of the sodium cationized adenine nucleosides are shorter than those of the protonated species (1.458 Å in $[dAdo+Na]^+$ and 1.448 Å in $[Ado+Na]^+$ vs. 1.465 Å in $[dAdo+H]^+$ and 1.459 Å in

$[Ado+H]^+$), indicating that sodium cationization is less effective at activating the glycosidic bond than protonation.

3.3.3 STABLE LOW-ENERGY CONFORMERS OF SODIUM CATIONIZED GUANINE NUCLEOSIDES

Figures 3.3 and **3.4** show representative stable low-every conformers of the sodium cationized guanine nucleosides along with their relative Gibbs free energies, nucleobase orientations and sugar puckerings. For $[dGuo+Na]^+$, 43 stable low-energy confomrers were found within 140 kJ/mol of the ground conformer. Among all canonical form of conformers, 4 unique modes of Na^+ binding were found, including B(O6N7), T(N3O4'O5'), B(O4'O5'), and B(N3O3'). Among all tautomeric forms of conformers, 9 unique modes of Na^+ binding were found, including B(O6N7)t3, B(N1O6)t7, T(N3O4'O5')t6, B(O6N7)t13, T(N3O4'O5')t16, B(N1NH)t36, T(N3O4'O5')t17, B(N1NH)t67, and B(N1O6)t37. For $[Guo+Na]^+$, 46 stable low-energy conformers were found within 145 kJ/mol of the ground conformer. Among all canonical form of conformers, 7 modes of Na^+ binding were found, including B(O6N7), T(N3O4'O5'), B(N3O2'), T($N3NH_2O2'$), B(N3O4'), B(O2'O3'), and B(O3'O4'). Among all tautomeric forms of conformers, 9 unique modes of Na^+ binding were found, including B(O6N7)t3, B(N1O6)t7, T(N3O4'O5')t6, B(O6N7)t13, B(N1NH)t36, T(N3O4'O5')t16, B(N1NH)t37, B(N3O2')t17, and B(N1NH)t67. The ground conformers of $[dGuo+Na]^+$ and $[Guo+Na]^+$ are very similar, Na^+ binds to the O6 and N7 atoms of the guanine nucleobase, forming a 5-membered chelation ring. The nucleobase orientation in both ground conformers is *anti*, whereas the sugar puckering is C2′-endo ($^2T_3$). For $[dGuo+Na]^+$, *syn* orientated B(O6N7) binding conformers are at least 6.4 kJ/mol less stable than the ground conformer, whereas for $[Guo+Na]^+$, *syn* orientated conformers are more competitive

such that the most stable B(O6N7) *syn* conformer is only 0.5 kJ/mol less stable than the ground conformer. For both $[dGuo+Na]^+$ and $[Guo+Na]^+$, the N3 atom of guanine is found to be a much less favorable binding site for Na^+ such that the most stable N3 binding conformers are > 56.9 kJ/mol less stable than the B1(O6N7) ground conformers. Conformers that bind solely to the sugar moiety of both $[dGuo+Na]^+$ and $[Guo+Na]^+$ are much less favorable than the corresponding ground conformers. The relative Gibbs free energies of sugar binding conformers exceed those of the corresponding B1(O6N7) ground conformers by at least 106 kJ/mol. Thus, the oxygen atoms of the sugar are not important binding sites for Na^+ in $[dGuo+Na]^+$ and $[Guo+Na]^+$. Conformers involving minor tautomers of the guanine residue are found to be much less stable (by at least 32.2 and 34.2 kJ/mol) than the canonical B1(O6N7) ground conformers, respectively. A more detailed discussion of the theoretical results and descriptions of the sodium cationized guanine nucleosides can be found in **Reference 147**.

3.3.4 COMPARISONS OF THE STABLE LOW-ENERGY CONFORMERS OF THE PROTONATED AND SODIUM CATIONIZED GUANINE NUCLEOSIDES

Ranran Wu reported the IRMPD action spectroscopic and theoretical studies of the gas-phase conformations and energetics of protonated guanine nucleosides.[185] She found that the most favorable protonation site is the N7 atom of guanine. The larger size and the electrostatic nature of the binding to Na^+ allows multiple chelation interactions in $[dGuo+Na]^+$ and $[Guo+Na]^+$, forming a 5-membered chelation ring. In contrast, the proton only binds to the N7 atom of guanine. Additionally, O6 and N3 are found to be much less favorable protonation sites for dGuo and Guo, with the relative Gibbs free energies of O6 and N3 binding conformers at least 35 and 41 kJ/mol less favorable than

the corresponding ground conformers, respectively, such that the proton affinities follow the order: N7 > O6 > N3. For the sodium cationized guanine nucleosides, N3 is also a less favorable binding site for Na^+ than B(O6N7), with the relative Gibbs free energies of N3 binding conformers at least 56 kJ/mol less favorable than the ground conformers, i.e., the binding affinities follow the order: O6N7 > N3. For both protonated guanine nucleosides, guanine exhibits a preference for the *anti* orientation, whereas the sugar prefers C3′-endo ($^3T_2$) puckering. The sodium cationized guanine nucleosides exhibit structural factors similar to protonated guanine nucleosides, except for the sugar puckering, where the C2′-endo ($^2T_3$) configuration for $[dGuo+Na]^+$ and $[Guo+Na]^+$ is preferred. However, the guanine orientation and sugar puckering do not significantly change the calculated IR spectra of the sodium cationized guanine nucleosides. Therefore, B(O6N7) binding conformers of $[dGuo+Na]^+$ and $[Guo+Na]^+$ with both anti and syn orientations and a variety of sugar puckerings coexist in the experiments. The glycosidic bonds of the sodium cationized guanine nucleosides are shorter than those of the protonated species (1.469 Å in $[dGuo+Na]^+$ and 1.463 Å in $[Guo+Na]^+$ vs. 1.508 Å in $[dGuo+H]^+$ and 1.498 Å in $[Guo+H]^+$), indicating that sodium cationization is less effective at activating the glycosidic bond than protonation. A noncanonical hydrogen-bonding interaction between H8 and O5′ is observed in the ground conformers of all of the species.

3.3.5 STABLE LOW-ENERGY CONFORMERS OF SODIUM CATIONIZED CYTOSINE NUCLEOSIDES

Figures 3.5 and **3.6** show representative stable low-every conformers of the sodium cationized cytosine nucleosides along with their relative Gibbs free energies, nucleobase orientations and sugar puckerings. For $[dCyd+Na]^+$, 43 stable low-energy

conformers were found within 90 kJ/mol of the ground conformer. Among these conformers, 7 unique modes of Na^+ binding were found, including T(O2O4'O5'), B(O2N3), B(O2O5'), B(O2O4'), B(O2O3'), T(O2N3O5'), and B(O3'O5'). For [Cyd+Na]+, 56 stable low-energy conformers were found within 120 kJ/mol of the ground conformer. Among these conformers, 8 unique modes of Na^+ binding were found, including T(O2O4'O5'), B(O2O2'), B(O2N3), B(O2O5'), B(O2O3'), T(O2O2'O3'), T(O2N3O5'), and M(O2'). The ground conformers of both $[dCyd+Na]^+$ and $[Cyd+Na]^+$ exhibit a *syn* nucleobase orientation and O4'-endo sugar puckering with Na^+ binding to the O2, O4' and O5' atoms of the cytosine nucleosides to form 5 and 6-membered chelation rings. Although both structures exhibit O4'-endo sugar puckering, the 2'-hydroxy substituent induces small changes to the overall structure such that the sugar puckerings of $[dCyd+Na]^+$ and $[Cyd+Na]^+$ are ${}^{O}T_1$ and ${}^{O}T_4$, respectively. The 2'-hydroxyl substituent of $[Cyd+Na]^+$ stabilizes the *anti* oriented bidentate cytosine and sugar binding conformers, such that B1(O2O2') is only 4.3 kJ/mol less stable than the ground conformer, whereas for $[dCyd+Na]^+$, the most stable *anti* oriented cytosine and sugar binding conformer, B1(O2O3'), is 47.1 kJ/mol less stable than the ground conformer. Both *anti* and *syn* oriented cytosine binding conformers are found for $[dCyd+Na]^+$ and $[Cyd+Na]^+$, with a preference for an *anti* orientation over *syn*. All conformers in which the sodium cation binds solely to the cytosine residue exhibit bidentate chelation to the O2 and N3 atoms, B(O2N3). The B1(O2N3) conformers of both $[dCyd+Na]^+$ and $[Cyd+Na]^+$ prefer C2'-endo (${}^{2}T_3$) sugar puckering, and are 15.4 and 16.5 kJ/mol less stable than the corresponding ground conformers, respectively. Thus, B(O2N3) is a less favorable mode of Na^+ binding for both $[dCyd+Na]^+$ and $[Cyd+Na]^+$. Sodium cation binding solely

to the sugar moiety provides much less favorable binding for both $[dCyd+Na]^+$ and $[Cyd+Na]^+$. The most stable sugar binding conformers, B1(O3'O5') of $[dCyd+Na]^+$ and B1(O2'O3') of $[Cyd+Na]^+$, are 62.4 and 37.9 kJ/mol less stable than the corresponding T1(O2O4'O5') ground conformers.

Figure 3.7 compares the structures and relative Gibbs free energies of the T1(O2O4'O5') and B1(O2O2') conformers of $[Cyd+Na]^+$ and their mono and bis water adducts. For $[Cyd+Na]^+$, B1(O2O2') is only 4.3 kJ/mol less stable than the ground T1(O2O4'O5') conformer. One water molecule stabilizes the B1(O2O2') conformer, resulting in a decrease of the relative Gibbs free energy to 2.0 kJ/mol vs. T1(O2O4'O5'). Binding of a second water molecule to the T1(O2O4'O5') and B1(O2O2') conformers inverses the relative Gibbs free energies such that T1(O2O4'O5')•$2H_2O$ is 12.6 kJ/mol less stable than B1(O2O2')•$2H_2O$. These results suggest that $[Cyd+Na]^+$ prefers an *anti* orientation with Na^+ binding to the O2 and O2' atoms in aqueous solution. A more detailed discussion of the theoretical results and descriptions of the sodium cationized cytosine nucleosides can be found in **Reference 148**.

3.3.6 COMPARISONS OF THE STABLE LOW-ENERGY CONFORMERS OF THE PROTONATED AND SODIUM CATIONIZED CYTOSINE NUCLEOSIDES

Ranran Wu reported the IRMPD action spectroscopic and theoretical studies of the gas-phase conformations and energetics of protonated cytosine nucleosides.[186] B3LYP/6-311+G(2d,2p)//B3LYP/6-311+G(d,p) level of theory suggests that N3 atom is the most favorable protonation site for cytosine nucleosides, whereas MP2(full)/6-311+G(2d,2p)//B3LYP/6-311+G(d,p) level of theory suggests that O2 atom is the most favorable protonation site for cytosine nucleosides. Both the ground N3 and O2 protonated conformers prefer an *anti* orientation of the cytosine residue and C2'-endo

sugar puckering. A noncanonical hydrogen bond between C5H and O5' is found in all N3 and O2 protonated conformers of dCyd and Cyd. However, Na^+ prefers to bind to both the cytosine nucleobase and sugar moiety. The theory suggests that the ground conformers of both sodium cationized cytosine nucleosides involve tridentate binding of Na^+ to the cytosine nucleosides via the atoms O2, O4' and O5' with a *syn* orientation of uracil and O4'-endo sugar puckering. The *anti* oriented O2 binding conformers of $[dCyd+Na]^+$ and $[Cyd+Na]^+$ are at least 47.1 and 4.3 kJ/mol less stable than the corresponding ground conformer, respectively. When the Na^+ binds to N3 atom, it always binds to O2 atom as well. The most stable B1(O2N3) conformers of $[dCyd+Na]^+$ and $[Cyd+Na]^+$ are 15.4 and 16.5 kJ/mol less stable vs. the corresponding ground conformers, respectively. The N-glycosidic bonds of $[dCyd+Na]^+$ and $[Cyd+Na]^+$, 1.457 Å and 1.452 Å, are shorter than those of $[dCyd+H]^+$ and $[Cyd+H]^+$, which are 1.529 Å and 1.488 Å for the N3 protonated conformers, and 1.506 Å and 1.494 Å for the O2 protonated conformers, respectively, indicating that sodium cationization is less effective at activating the glycosidic bond than protonation.

3.3.7 STABLE LOW-ENERGY CONFORMERS OF SODIUM CATIONIZED URACIL NUCLEOSIDES

Figures 3.8 and **3.9** show representative stable low-every conformers of the sodium cationized uracil nucleosides along with their relative Gibbs free energies, nucleobase orientations and sugar puckerings. For $[dUrd+Na]^+$, 106 stable low-energy conformers were found within 100 kJ/mol of the ground conformer. Among all canonical form of conformers, 8 unique modes of Na^+ binding were found, including T(O2O4'O5'), B(O2O4'), M1(O4), B(O2O5'), B(O3'O5'), M(O2), B(O2O3'), and B(O4O5'). Among all tautomeric forms of complexes, 7 unique modes of Na^+ binding were found, including

T(O2O4'O5')t4, B(O2N3)t4, B(O2O4')t4, T(O2N3O5')t4, B(N3O4)t2, M(O4)t2, and B(O2O3')t4. For $[Urd+Na]^+$, 138 stable low-energy conformers were found within 100 kJ/mol of the ground conformer. Among all canonical form of conformers, 8 unique modes of Na^+ binding were found, including T(O2O4'O5'), B(O2O2'), T(O2O2'O3'), B(O2'O3'), M(O4), B(O2O4'), B(O2O5'), and B(O4O5'). Among all tautomeric forms of complexes, 7 unique modes of Na^+ binding were found, including T(O2O4'O5')t4, B(O2N3)t4, B(O2O5')t4, B(N3O4)t2, B(O2O2')t4, M(O4)t2, and T(O2N3O5')t4. The ground conformers of $[dUrd+Na]^+$ and $[Urd+Na]^+$ exhibit very parallel structures, where Na^+ binds via tridentate coordination to the O2, O4' and O5' atoms, with a *syn* orientation of the uracil nucleobase. The sugar puckerings of the ground conformers of $[dUrd+Na]^+$ and $[Urd+Na]^+$ are similar as both exhibit O4'-endo sugar puckering, however minor differences in the pseudorotation phase angle lead to different designations in the envelope (E) vs twist (T) nomenclature, ${}^{O}T_1$ for $[dUrd+Na]^+$ and ${}^{O}T_4$ for $[Urd+Na]^+$. The most stable *anti* oriented O2 binding conformers of $[Urd+Na]^+$ are only 6.1 kJ/mol less stable than the ground conformer, whereas those of $[dUrd+Na]^+$ are 49.0 kJ/mol less stable than the ground conformer, indicating that the 2'-deoxy modification destabilizes the *anti* oriented O2 binding conformers of these complexes. The most stable O4 binding conformers, M1(O4) of $[dUrd+Na]^+$ and $[Urd+Na]^+$, are found to be 29.5 kJ/mol and 27.4 kJ/mol less stable than the corresponding ground conformers, respectively. Additionally, the most stable sugar binding conformers, B1(O3'O5') of $[dUrd+Na]^+$ and B1(O2'O3') of $[Urd+Na]^+$, are 43.5 and 22.9 kJ/mol less stable than the corresponding T1(O2O4'O5') conformers, indicating that the nucleobase contributes most to the stability and binding preferences of $[dUrd+Na]^+$ and $[Urd+Na]^+$,

and that the 2'-hydroxyl substituent of Urd is critical to the structure and stability of $[Urd+Na]^+$. Both the sodium cationized t2 and t4 tautomeric uracil nucleosides are less favorable than the corresponding canonical ground conformers of $[dUrd+Na]^+$ and $[Urd+Na]^+$. The most stable mode of sodium cation binding to the t4 tautomers, T1(O2O4'O5')t4, is 23.0 and 16.6 kJ/mol less stable than the T1(O2O4'O5') conformers of canonical $[dUrd+Na]^+$ and $[Urd+Na]^+$, respectively. The most stable mode of sodium cation binding to the t2 tautomers, B1(N3O4)t2, is even less favorable than binding to t4. The B1(N3O4)t2 conformers of $[dUrd+Na]^+$ and $[Urd+Na]^+$ are 63.8 and 49.4 kJ/mol less favorable than the corresponding ground conformers, respectively. Thus, binding of a sodium cation is not strong enough to stabilize the minor tautomeric forms of the uracil nucleosides vs their canonical counterparts.

The conformations and relative Gibbs free energies of the T1(O2O4'O5') and B1(O2O2') conformers and their mono and bis water adducts of $[Urd+Na]^+$ are compared in **Figure 3.10**. The *anti* oriented B1(O2O2') conformer is only 6.1 kJ/mol less stable than the *syn* oriented T1(O2O4'O5') conformer. Binding of one water molecule to $[Urd+Na]^+$ inverts the relative Gibbs free energies of these complexes, such that the *syn* oriented T1(O2O4'O5')•H_2O conformer is 1.6 kJ/mol less stable than the *anti* oriented B1(O2O2')•H_2O conformer. Binding of a second water molecule further stabilizes *anti* oriented $[Urd+Na]^+$, such that the *syn* oriented T1(O2O4'O5')•$2H_2O$ conformer is 3.9 kJ/mol less stable than the *anti* oriented B1(O2O2')•$2H_2O$ conformer. These results suggest that $[Urd+Na]^+$ prefers an *anti* orientation with the sodium cation binding to the O2 and O2' atoms of Urd in aqueous solution. A more detailed discussion of the

theoretical results and descriptions of the sodium cationized uracil nucleosides can be found in **Reference 149**.

3.3.8 COMPARISONS OF THE STABLE LOW-ENERGY CONFORMERS OF THE PROTONATED AND SODIUM CATIONIZED URACIL NUCLEOSIDES

Ranran Wu reported the IRMPD action spectroscopic and theoretical studies of the gas-phase conformations and energetics of protonated uracil nucleosides.[119] The ground conformer calculated for $[Urd+H]^+$ is the 2,4-dihydroxy tautomer (t24) with an *anti* orientation of uracil and C2'-endo sugar puckering, whereas the ground conformer calculated for $[dUrd+H]^+$ is the O4 protonated conformer with an *anti* orientation of uracil and C3'-endo sugar puckering. The O4 protonated conformer of $[Urd+H]^+$ and the t24 tautomer of $[dUrd+H]^+$ are only 2.9 and 0.7 kJ/mol less favorable than the corresponding ground conformers, respectively. The O2 protonated conformers of $[Urd+H]^+$ and $[dUrd+H]^+$ are at least 8.0 kJ/mol and 8.8 kJ/mol less stable than the corresponding ground conformers, respectively. Overall, the relative stabilities of the low-energy conformers of protonated Urd and dUrd follow the order: t24 ≈ O4 > O2. In contrast, the same level of theory suggest that the ground conformers of both sodium cationized uracil nucleosides involve tridentate binding of Na^+ to the canonical tautomer via the atoms O2, O4' and O5' with a *syn* orientation of uracil and O4'-endo sugar puckering. The O4 binding conformers of $[Urd+Na]^+$ and $[dUrd+Na]^+$ are at least 27.4 and 29.5 kJ/mol less stable than the corresponding ground conformer, respectively. The most favorable mode of sodium cation binding to the t4 tautomers of Urd and dUrd also involve tridentate binding to O2, O4' and O5', but are less stable by 16.6 and 23.0 kJ/mol, respectively. Sodium cation binding to the t2 tautomers of Urd and dUrd is even less favorable, exhibiting much higher relative Gibbs free energies of 49.4 and 63.8

kJ/mol, respectively. Overall, the relative stabilities of the low-energy conformers of $[Urd+Na]^+$ and $[dUrd+Na]^+$ follow the order: O2 > t4 > O4 > t2. Clearly the strength of binding of the proton vs. the sodium cation, and hydrogen-bonding vs. multiple chelation interactions are important in determining the relative stabilities of the stable conformers of these systems.

3.3.9 STABLE LOW-ENERGY CONFORMERS OF SODIUM CATIONIZED THYMINE NUCLEOSIDES

Figures 3.11 and **3.12** show representative stable low-energy conformers of the sodium cationized thymine nucleosides along with their relative Gibbs free energies, nucleobase orientations and sugar puckerings. For $[dThd+Na]^+$, 80 stable low-energy conformers were found within 100 kJ/mol of the ground conformer. Among all canonical form of conformers, 6 unique modes of Na^+ binding were found, including T(O2O4'O5'), B(O2O4'), M(O4), B(O3'O5'), B(O2O3'), and M(O2). Among all tautomeric forms of conformers, 4 unique modes of Na^+ binding were found, including B(O2O5')t4, T(O2O4'O5')t4, B(O2N3)t4, and B(N3O4)t2. For $[Thd+Na]^+$, 86 stable low-energy conformer were found within 100 kJ/mol of the ground conformer. Among all canonical form of conformers, 6 unique modes of Na^+ binding were found, including T(O2O4'O5'), B(O2O2'), T(O2O2'O3'), B(O2'O3'), B(O2O4'), and M(O4). Among all tautomeric forms of conformers, 3 unique modes of Na^+ binding were found, including B(O2O5')t4, B(O2N3)t4, and B(N3O4)t2. The ground conformers calculated for $[dThd+Na]^+$ and $[Thd+Na]^+$ are highly parallel. Both dThd and Thd exhibit a preference for a tridentate mode of Na^+ binding to the O2, O4' and O5' atoms, forming 5- and 6-membered chelation rings, with a *syn* orientation of Thy, and similar O4'-endo sugar puckering. The sugar puckering shifts from ${}^{O}T_1$ for $[dThd+Na]^+$ to ${}^{O}T_4$ for $[Thd+Na]^+$ due to the influence

of the hydrogen-bonding interaction between the 2'- and 3'-hydroxyl substituents. The main difference between the two lowest energy conformers is an additional hydrogen-bonding interaction between the 2'- and 3'-hydroxyl substituents found for $[Thd+Na]^+$. Elimination of one (or both) chelation interactions between Na^+ and the O5' (and O4') atoms of the sugar moiety significantly increases the relative Gibbs free energy, by at least 30.0 kJ/mol for $[dThd+Na]^+$ and 59.2 kJ/mol for $[Thd+Na]^+$. All *anti* oriented bidentate O2 and O3' binding conformers of $[dThd+Na]^+$ are much less favorable, and are at least 51.4 kJ/mol less stable than the lowest energy conformer. The bidentate O2 binding conformers of $[Thd+Na]^+$ that exhibit an *anti* orientation of Thy are at least 6.6 kJ/mol less stable than the ground conformer. Lack of one chelation interaction between Na^+ and the O5' atom of the sugar moiety increases the relative Gibbs free energy by at least 31.9 kJ/mol vs. the ground conformer. No stable monodentate O2 binding conformer is found for $[Thd+Na]^+$. Unique tridentate O2, O2' and O3' binding conformers are obviously only found for $[Thd+Na]^+$, and are at least 19.2 kJ/mol less stable than the ground conformer. The lowest energy O4 binding conformers calculated for both $[dThd+Na]^+$ and $[Thd+Na]^+$ are M1(O4) conformers, which are 39.4 and 35.4 kJ/mol less stable than the corresponding ground conformers, respectively. No stable bidentate or tridentate O4 binding conformers are found for either $[dThd+Na]^+$ or $[Thd+Na]^+$. Clearly, the change in preference for O2 over O4 binding to the thymine nucleobase for the thymine nucleosides is driven by the additional stabilization provided by multiple chelation interactions of Na^+ with the thymine nucleobase and the sugar moiety. The lowest energy sugar binding conformers calculated for $[dThd+Na]^+$ and $[Thd+Na]^+$ are the B1(O3'O5') conformer of $[dThd+Na]^+$ and the B1(O2'O3') conformer of $[Thd+Na]^+$,

which are 46.8 and 25.0 kJ/mol less stable than the corresponding ground conformers, respectively. These results suggest that the stability and binding preferences of these species are dominated by the thymine nucleobase, and secondarily by additional chelation interactions with the sugar moiety. However, the 2'-hydroxyl substituent of Thd is also an important determinant of the conformation and stability of $[Thd+Na]^+$. All tautomeric $[dThd+Na]^+$ and $[Thd+Na]^+$ are found to be less favorable than the canonical forms of these species. The lowest energy sodium cationized t4 conformers of $[dThd+Na]^+$ and $[Thd+Na]^+$ are 42.0 and 37.6 kJ/mol less stable than the corresponding ground conformers, respectively. Therefore, conformers involving Na^+ binding to minor tautomeric forms of the thymine nucleosides are unlikely to be important in the experiments.

The conformations and relative Gibbs free energies of the T1(O2O4'O5') and B1(O2O2') conformers and their mono and bis water adducts of $[Thd+Na]^+$ are compared in **Figure 3.13**. The *anti* oriented B1(O2O2') conformer is only 6.6 kJ/mol less stable than the *syn* oriented T1(O2O4'O5') conformer. Binding of one water molecule to $[Thd+Na]^+$ preferentially stabilizes the B1(O2O2') conformer, such that the *anti* oriented B1(O2O2')•H_2O conformer is now very slightly favored (by 0.1 kJ/mol) over the *syn* oriented T1(O2O4'O5')•H_2O conformer. Binding of a second water molecule further stabilizes the *anti* oriented B1(O2O2') conformer of $[Thd+Na]^+$ relative to the *syn* oriented T1(O2O4'O5') conformer such that T1(O2O4'O5')•$2H_2O$ is 9.8 kJ/mol less stable than the *anti* oriented B1(O2O2')•$2H_2O$ conformer. These results suggest that $[Thd+Na]^+$ prefers an *anti* orientation with the sodium cation binding to the O2 and O2' atoms of Thd in aqueous solution. A more detailed discussion of the theoretical results

and descriptions of the sodium cationized thymine nucleosides can be found in **Reference 150**.

3.3.10 COMPARISONS OF THE STABLE LOW-ENERGY CONFORMERS OF THE PROTONATED AND SODIUM CATIONIZED THYMINE NUCLEOSIDES

Ranran Wu reported the IRMPD action spectroscopic and theoretical studies of the gas-phase conformations and energetics of protonated thymine nucleosides.[125] For both $[dThd+H]^+$ and $[Thd+H]^+$, the ground conformers are 2,4-dihydroxy tautomers with *anti* orientations of the thymine nucleobase, where the 2- and 4-hydroxyl hydrogen atoms point toward the N3 atom, and exhibit C2'-endo sugar puckering. The lowest energy O2 protonated Thy nucleosides are only 4.1 and 5.2 kJ/mol less favorable than the corresponding lowest energy conformers, respectively, whereas the lowest energy O4 protonated thymine nucleosides are 3.3 and 6.2 kJ/mol less stable, respectively, i.e., the protonation preferences of $[dThd+H]^+$ follow the order: t24 > O4 > O2. In contrast, the protonation preferences of $[Thd+H]^+$ follow the order: t24 > O2 > O4. In spite of the similar computed relative stabilities, evidence for O4 protonated species was not found. For the sodium cationized thymine nucleosides, the ground conformer of $[dThd+Na]^+$ involves tridentate binding of Na^+ to the canonical form of dThd via the O2, O4', and O5' atoms, with a *syn* orientation of the thymine nucleobase and O4'-endo ($^{O}T_1$) sugar puckering. The ground conformer of $[Thd+Na]^+$ exhibits a very similar conformation, but the O4'-endo sugar puckering changes to $^{O}T_4$ due to the hydrogen-bonding interaction between the 2'- and 3'-hydroxyl substituents. The relative stabilities of different forms of $[dThd+Na]^+$ follow the order: O2 > O4 > t4 > sugar > t2. In contrast, the relative stabilities of different forms of $[Thd+Na]^+$ follow the order: O2 > sugar > O4 > t4 > t2. The difference in the order of the relative stabilities of $[dThd+Na]^+$ and $[Thd+Na]^+$

indicates that the 2'-hydroxyl substituent of Thd stabilizes the sugar binding conformers relative to dThd. Compared to protonation, sodium cationization is unable to sufficiently stabilize the minor tautomers of the thymine nucleosides, such that the canonical forms of $[dThd+Na]^+$ and $[Thd+Na]^+$ have lower relative Gibbs free energies and are the only forms populated in the experiments.

3.4 CONCLUSIONS

Theory suggests that the ground conformers of the sodium cationized DNA and RNA nucleosides are highly parallel. For all sodium cationized DNA and RNA nucleosides, Na^+ is preferentially bound to both the nucleobase and sugar moieties, except for the sodium cationized guanine nucleosides, where Na^+ binds solely to guanine nucleobase. A variety of stable conformers exhibit different sugar puckerings, but in general, changes in the sugar puckering only have a minor effect on the relative Gibbs energy, compared to the Na^+ binding mode and nucleobase orientation. A hydrogen-bonding interaction is observed in all sodium cationized RNA nucleosides, due to the additional 2'-hydroxyl substituent. For all pyrimidine nucleosides, the B1(O2O2') conformer with an *anti* orientation of the nucleobase is competitive with the tridentate T1(O2O4'O5') ground conformers. Binding of one or two water molecules to the sodium cationized RNA pyrimidine nucleosides inverts the relative stabilities of the T1(O2O4'O5') and B1(O2O2') conformers of these complexes, indicating that $[Cyd+Na]^+$, $[Urd+Na]^+$ and $[Thd+Na]^+$ prefer an *anti* orientation with the sodium cation binding to the O2 and O2' atoms of the nucleoside in aqueous solution.

3.5 REFERENCES

119. R. R. Wu, B. Yang, C. E. Frieler, G. Berden, J. Oomens and M. T. Rodgers, *Phys. Chem. Chem. Phys.* 2015, **17**, 25978.

125. R. R. Wu, B. Yang, C. E. Frieler, G. Berden, J. Oomens and M. T. Rodgers, *J. Am. Soc. Mass Spectrom.* 2016, **27**, 410.

147. Y. Zhu, L. A. Hamlow, C. C. He, S. F. Strobehn, J. K. Lee, J. Gao, G. Berden, J. Oomens and M. T. Rodgers, *J. Phys. Chem. B* 2016, **120**, 8892.

148. Y. Zhu, L. A. Hamlow, C. C. He, J. K. Lee, J. Gao, G. Berden, J. Oomens and M. T. Rodgers, *J. Phys. Chem. B* 2017, **121**, 4048.

149. Y. Zhu, L. A. Hamlow, C. C. He, H. A. Roy, N. A. Cunningham, M. U. Munshi, G. Berden, J. Oomens and M. T. Rodgers, *Int. J. Mass Spectrom.* 2017, DOI: https://doi.org/10.1016/j.ijms.2017.04.005.

150. Y. Zhu, H. A. Roy, N. A. Cunningham, S. F. Strobehn, J. Gao, M. U. Munshi, G. Berden, J. Oomens and M. T. Rodgers, *Phys. Chem. Chem. Phys.* 2017, **19**, 17637.

151. Y. Zhu, H. A. Roy, N. A. Cunningham, S. F. Strobehn, J. Gao, M. U. Munshi, G. Berden, J. Oomens and M. T. Rodgers, *J. Am. Soc. Mass Spectrom* 2017, **28**, 2437.

184. R. R. Wu, B. Yang, G. Berden, J. Oomens and M. T. Rodgers, *J. Phys. Chem. B* 2015, **119**, 2795.

185. R. R. Wu, B. Yang, G. Berden, J. Oomens and M. T. Rodgers, *J. Phys. Chem. B* 2014, **118**, 14774.

186. R. R. Wu, B. Yang, C. E. Frieler, G. Berden, J. Oomens and M. T. Rodgers, *J. Phys. Chem. B* 2015, **119**, 5773.

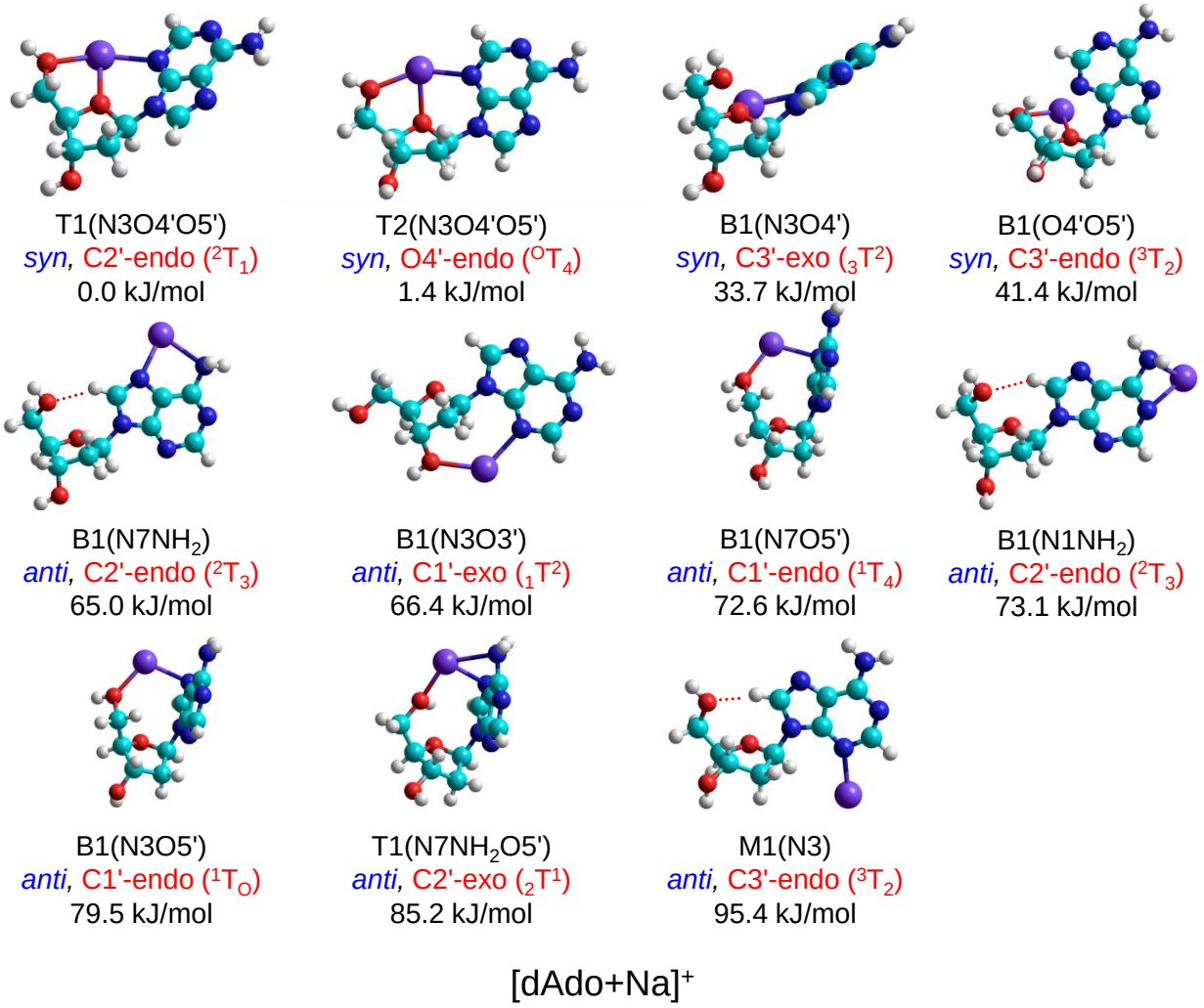

Figure 3.1 Select stable B3LYP/6-311+G(d,p) conformers of $[dAdo+Na]^+$. The Na^+ binding modes, orientations of the adenine nucleobase, sugar puckering, and the relative 298 K Gibbs free energies at the B3LYP/6-311+G(2d,2p) level of theory are also listed for each structure.

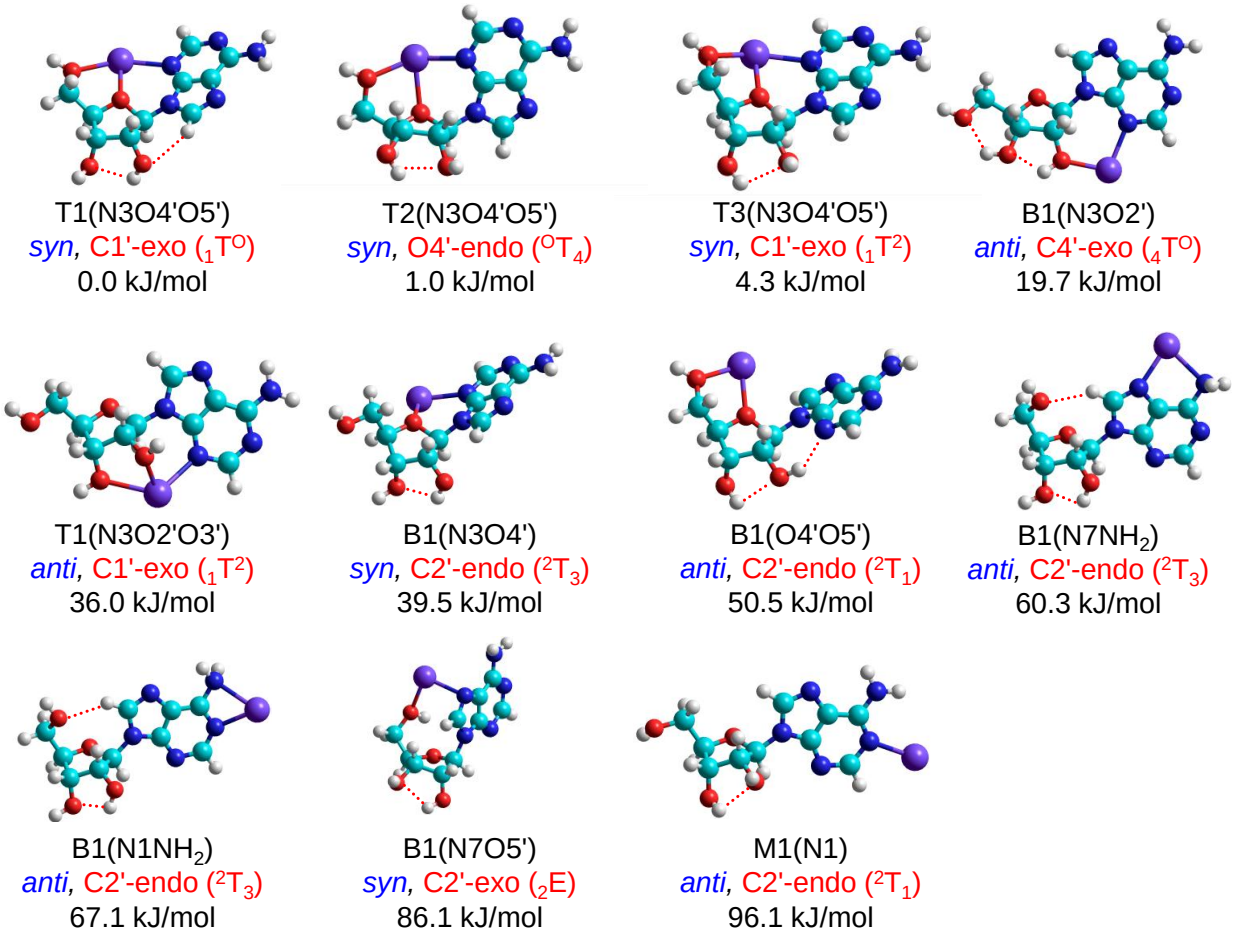

[Ado+Na]$^+$

Figure 3.2 Select stable B3LYP/6-311+G(d,p) conformers of [Ado+Na]$^+$. The Na$^+$ binding modes, orientations of the adenine nucleobase, sugar puckering, and the relative 298 K Gibbs free energies at the B3LYP/6-311+G(2d,2p) level of theory are also listed for each structure.

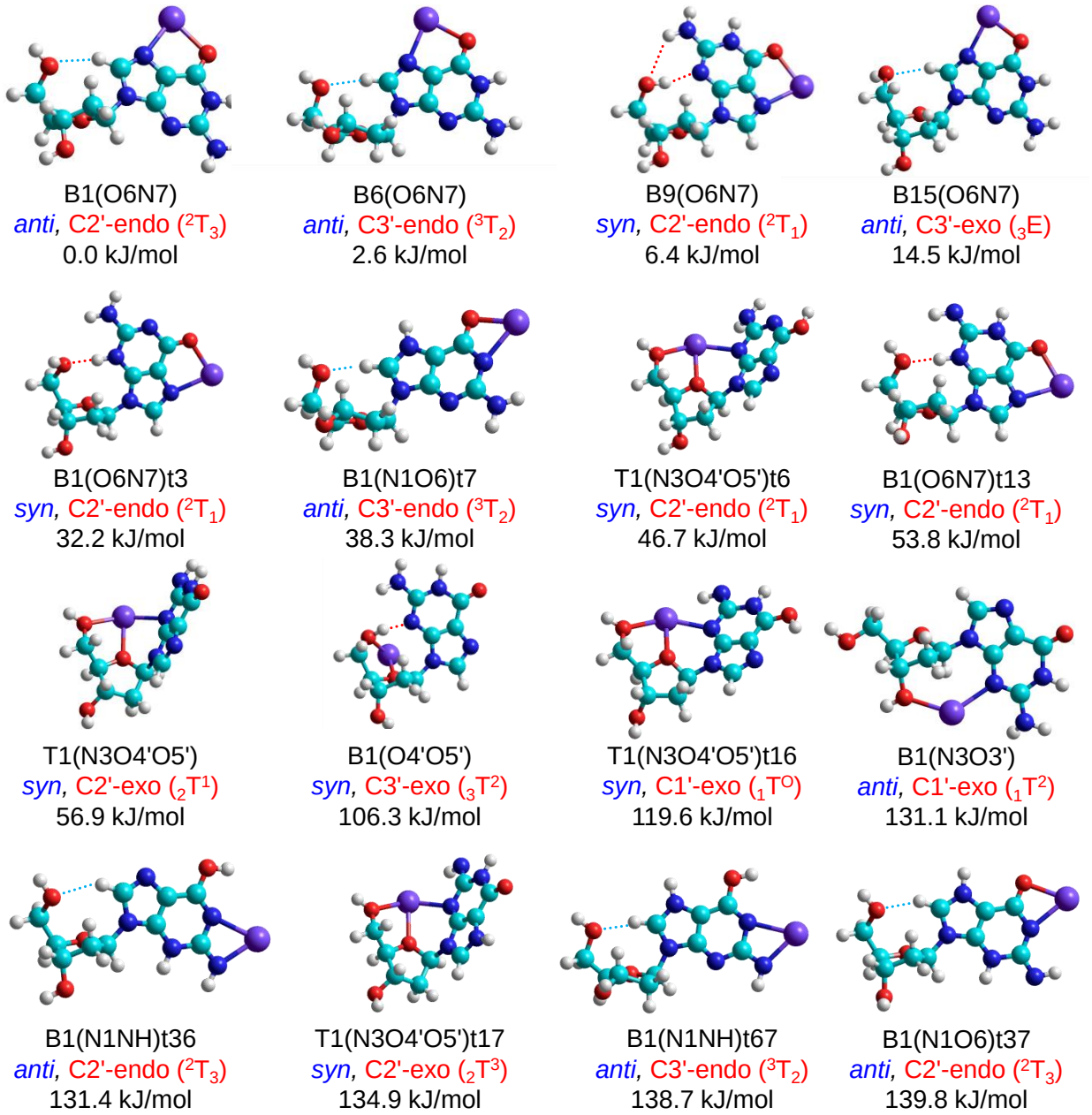

[dGuo+Na]$^+$

Figure 3.3 Select stable B3LYP/6-311+G(d,p) conformers of [dGuo+Na]$^+$. The Na$^+$ binding modes, orientations of the guanine nucleobase, sugar puckering, and the relative 298 K Gibbs free energies at the B3LYP/6-311+G(2d,2p) level of theory are also listed for each structure.

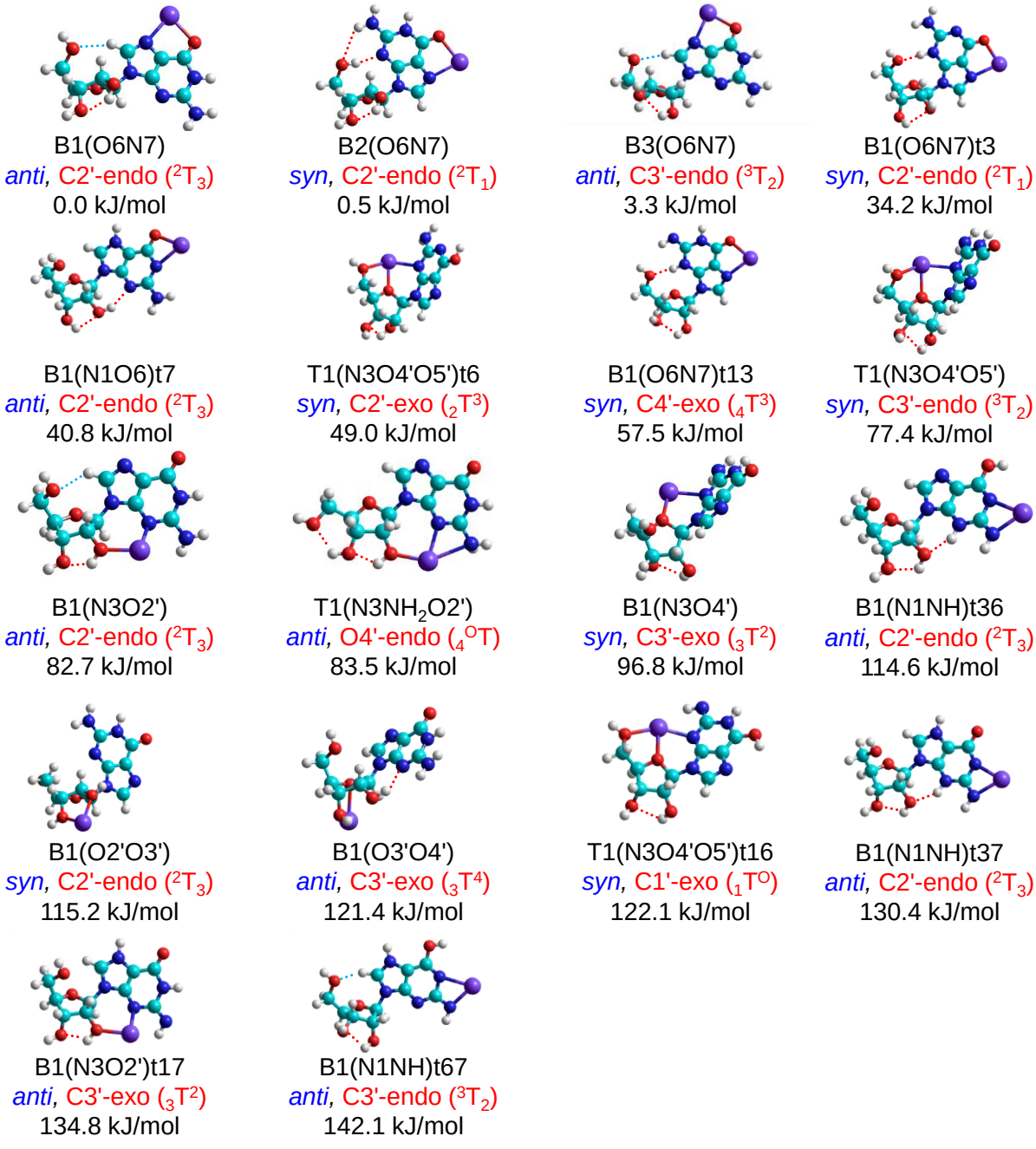

[Guo+Na]$^+$

Figure 3.4 Select stable B3LYP/6-311+G(d,p) conformers of [Guo+Na]$^+$. The Na$^+$ binding modes, orientations of the guanine nucleobase, sugar puckering, and the relative 298 K Gibbs free energies at the B3LYP/6-311+G(2d,2p) level of theory are also listed for each structure.

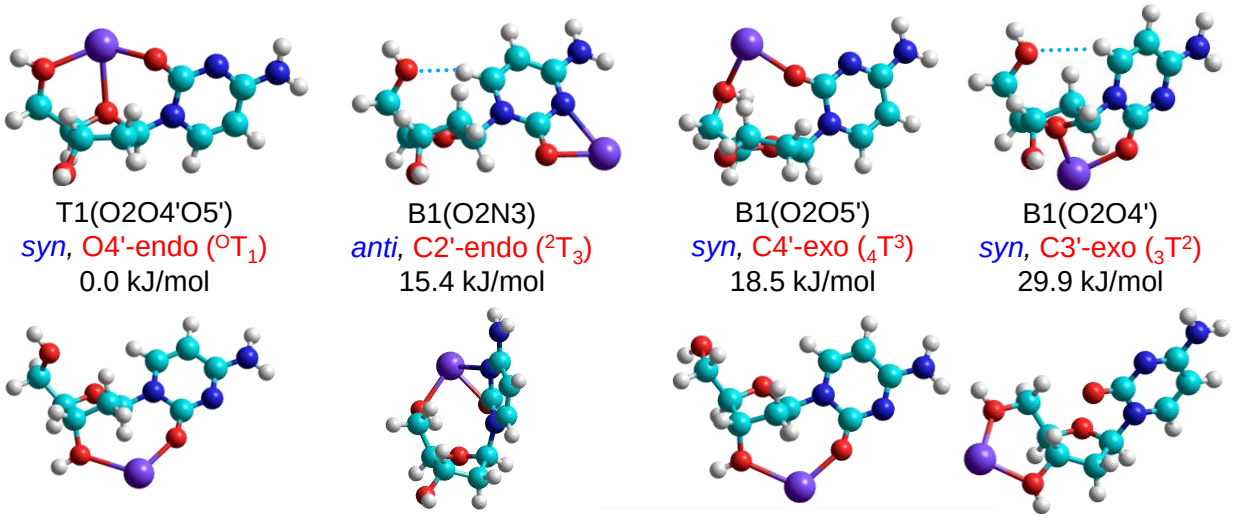

[dCyd+Na]$^{+}$

Figure 3.5 Selected stable B3LYP/6-311+G(d,p) conformers of [dCyd+Na]$^{+}$. The Na^{+} binding modes, orientations of the cytosine nucleobase, sugar puckering, and the relative 298 K Gibbs free energies at the B3LYP/6-311+G(2d,2p) level of theory are also listed for each structure.

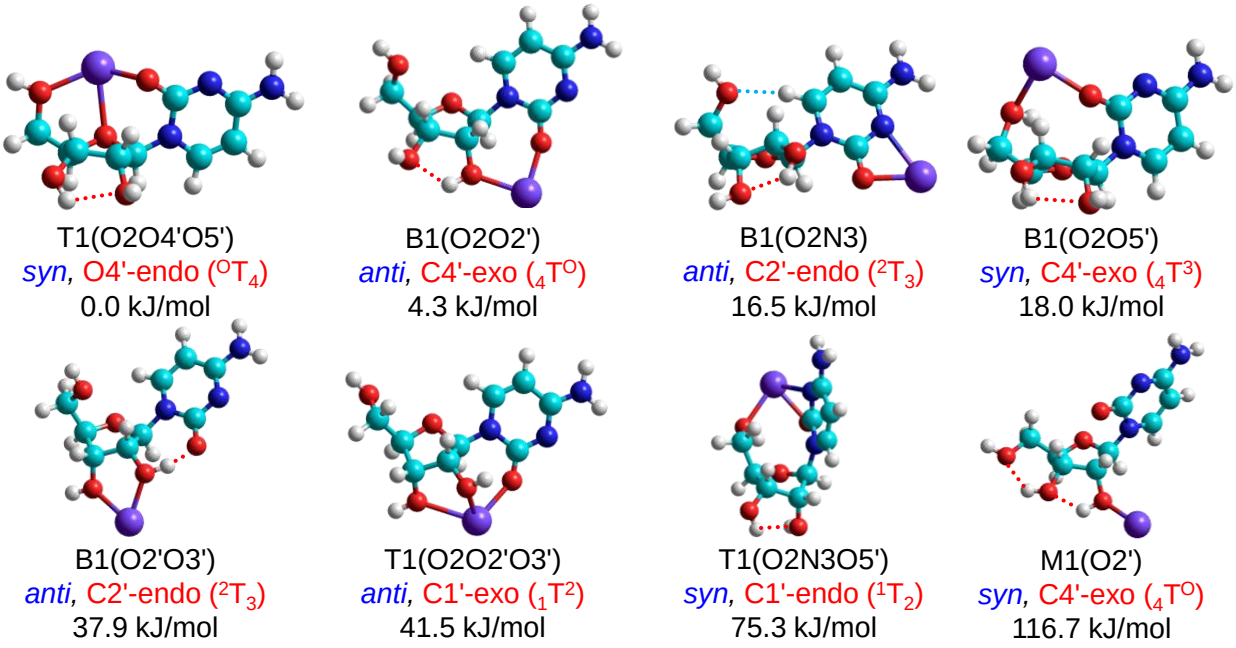

[Cyd+Na]$^{+}$

Figure 3.6 Select stable B3LYP/6-311+G(d,p) conformers of [Cyd+Na]$^{+}$. The Na^{+} binding modes, orientations of the cytosine nucleobase, sugar puckering, and the relative 298 K Gibbs free energies at the B3LYP/6-311+G(2d,2p) level of theory are also listed for each structure.

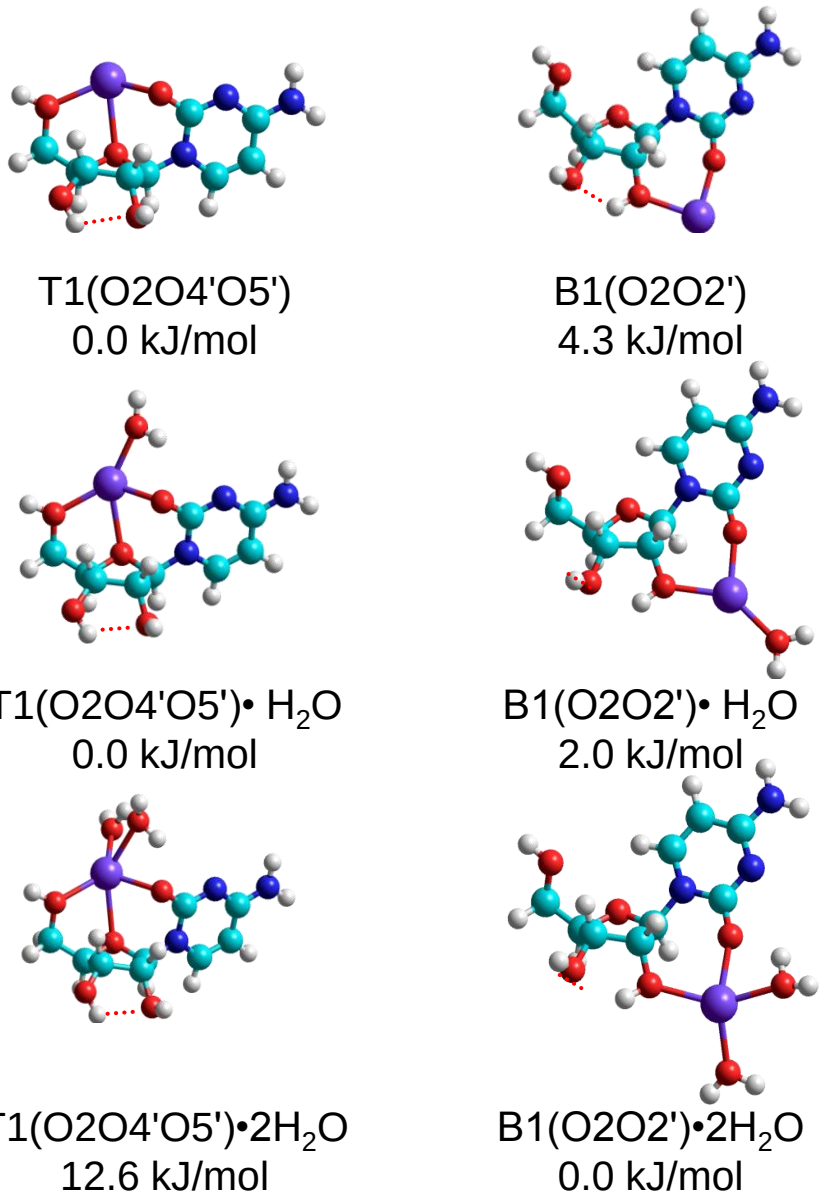

$[Cyd+Na]^+ \bullet nH_2O \quad (n = 0–2)$

Figure 3.7 Structures of the T1(O2O4'O5') and B1(O2O2') conformers of $[Cyd+Na]^+$ and their mono and bis water adducts ($[Cyd+Na]^+ \bullet nH2O$, n=1, 2). The relative Gibbs free energies calculated at B3LYP/6-311+G(2d,2p)//B3LYP/6-311+G(d,p) level of theory are also shown.

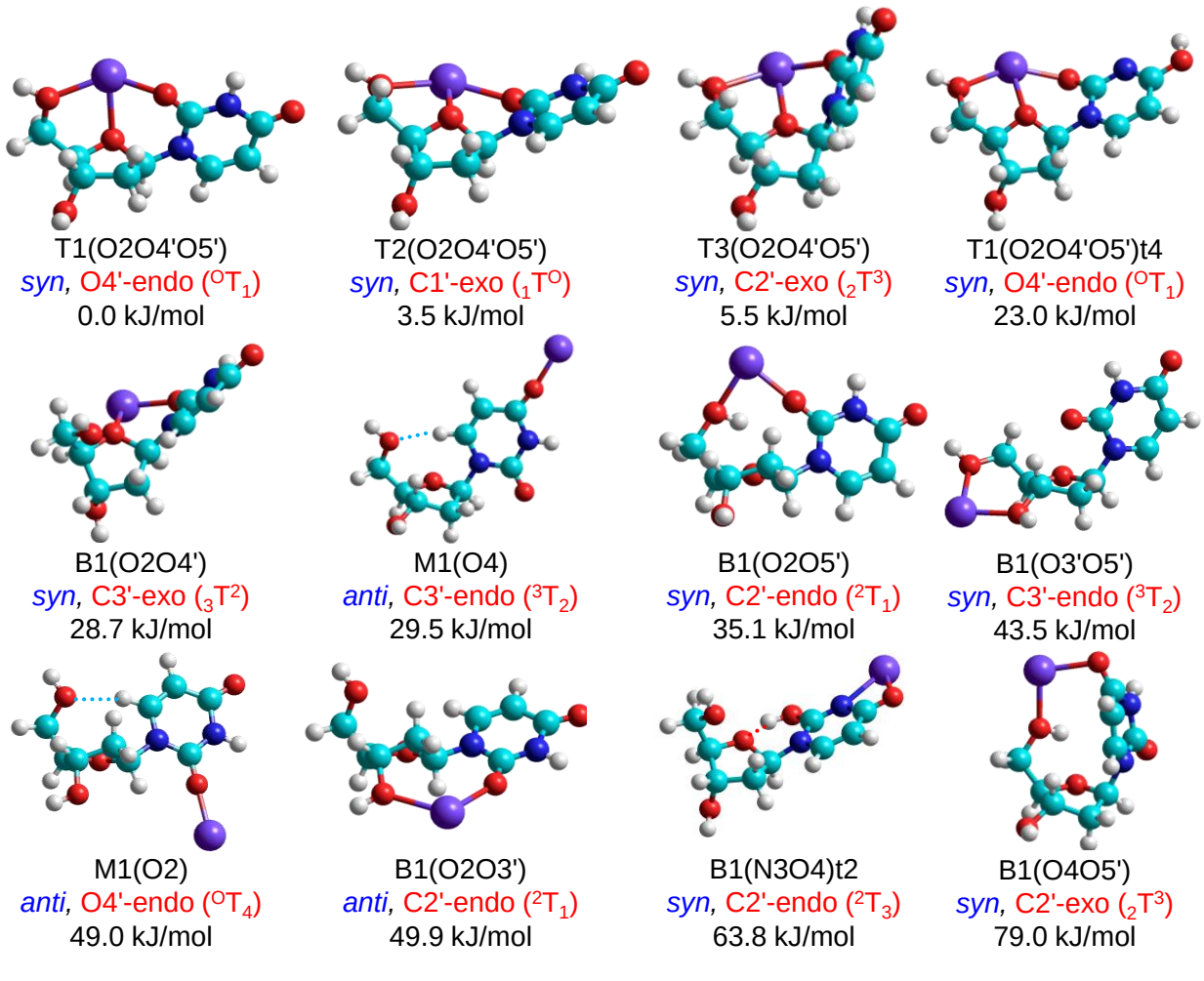

[dUrd+Na]+

Figure 3.8 Select stable B3LYP/6-311+G(d,p) conformers of [dUrd+Na]+. The Na+ binding modes, orientations of the uracil nucleobase, sugar puckering, and the relative 298 K Gibbs free energies at the B3LYP/6-311+G(2d,2p) level of theory are also listed for each structure.

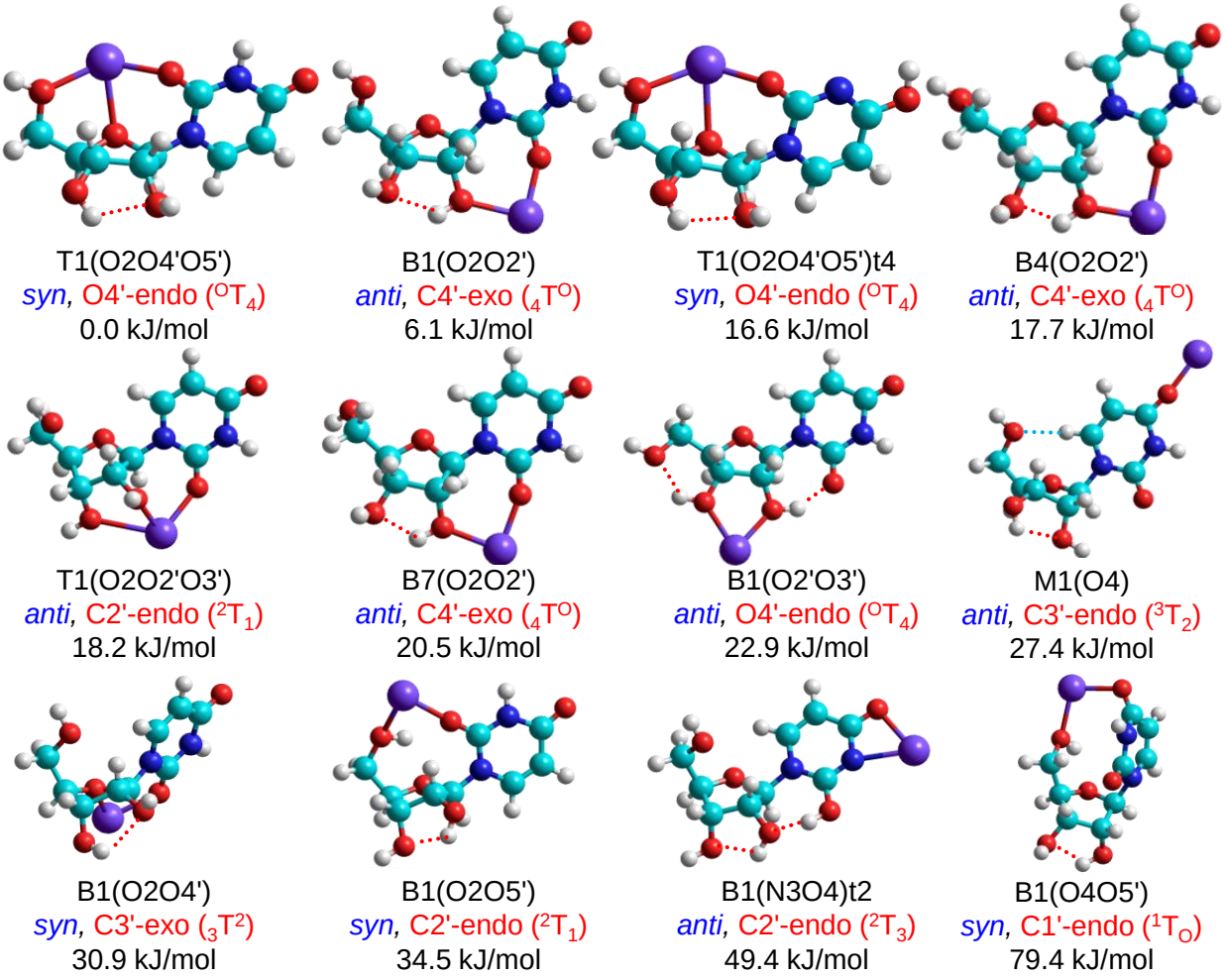

[Urd+Na]$^+$

Figure 3.9 Select stable B3LYP/6-311+G(d,p) conformers of [Urd+Na]$^+$. The Na$^+$ binding modes, orientations of the uracil nucleobase, sugar puckering, and the relative 298 K Gibbs free energies at the B3LYP/6-311+G(2d,2p) level of theory are also listed for each structure.

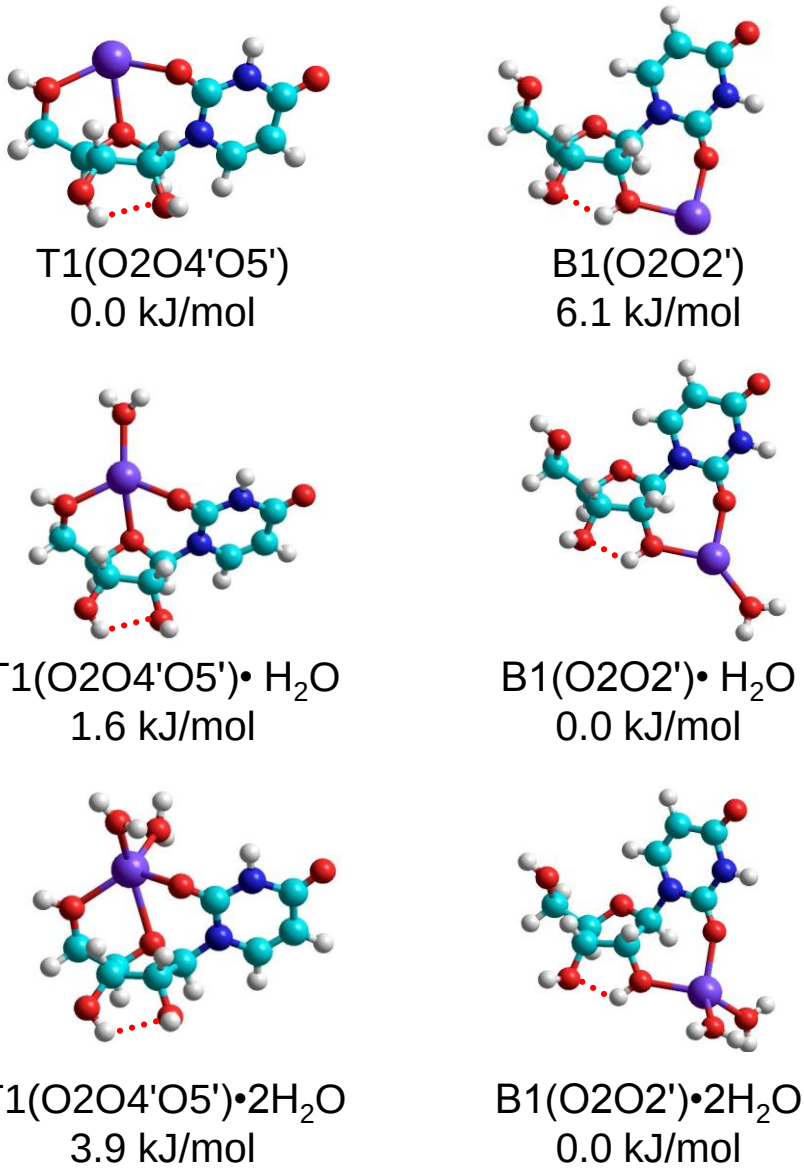

$[Urd+Na]^+ \bullet nH_2O \quad (n = 0–2)$

Figure 3.10 Structures of the T1(O2O4'O5') and B1(O2O2') conformers of $[Urd+Na]^+$ and their mono and bis water adducts ([Urd+Na]+•nH2O, n=1, 2). The relative Gibbs free energies calculated at B3LYP/6-311+G(2d,2p)//B3LYP/6-311+G(d,p) level of theory are also shown.

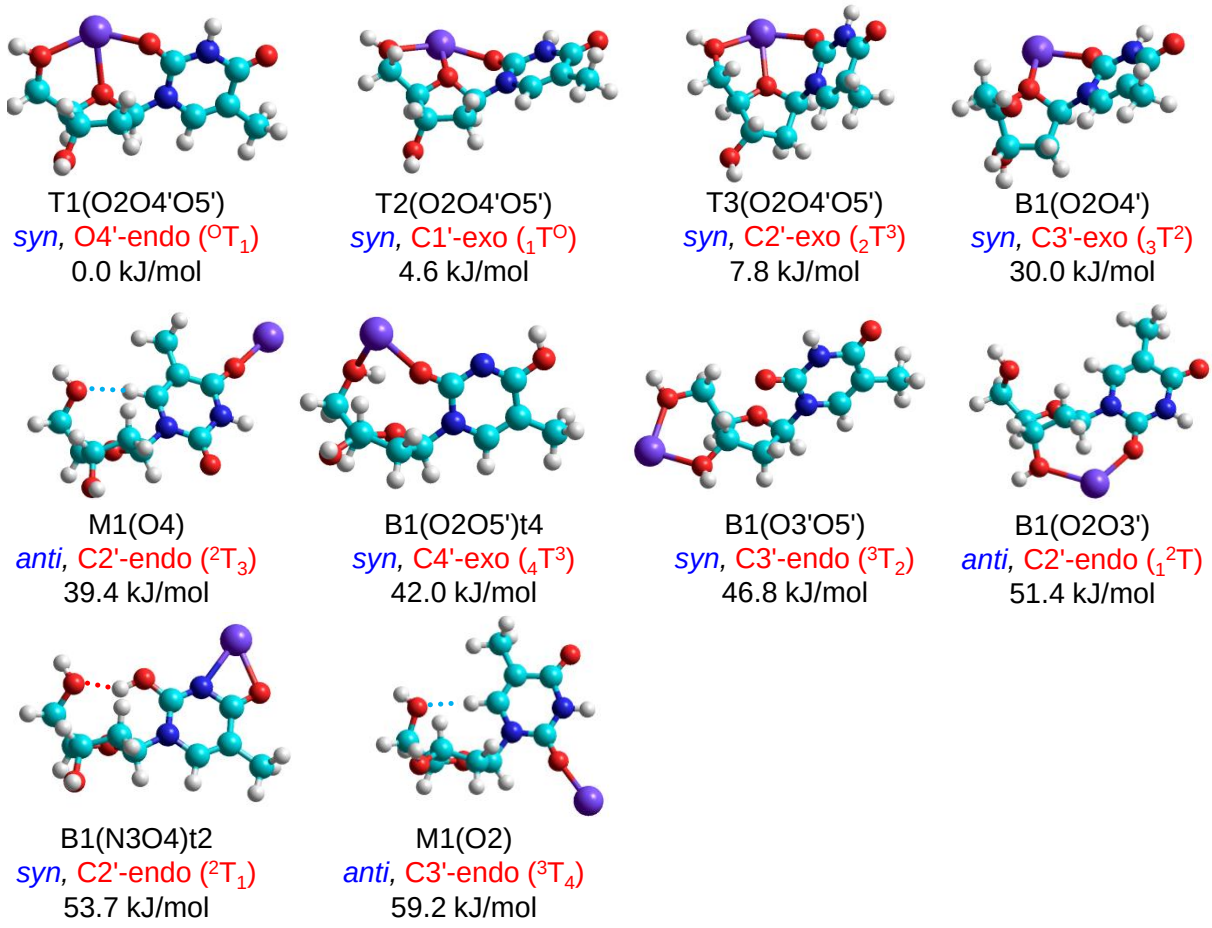

[dThd+Na]$^+$

Figure 3.11 Select stable B3LYP/6-311+G(d,p) conformers of [dThd+Na]$^+$. The Na$^+$ binding modes, orientations of the thymine nucleobase, sugar puckering, and the relative 298 K Gibbs free energies at the B3LYP/6-311+G(2d,2p) level of theory are also listed for each structure.

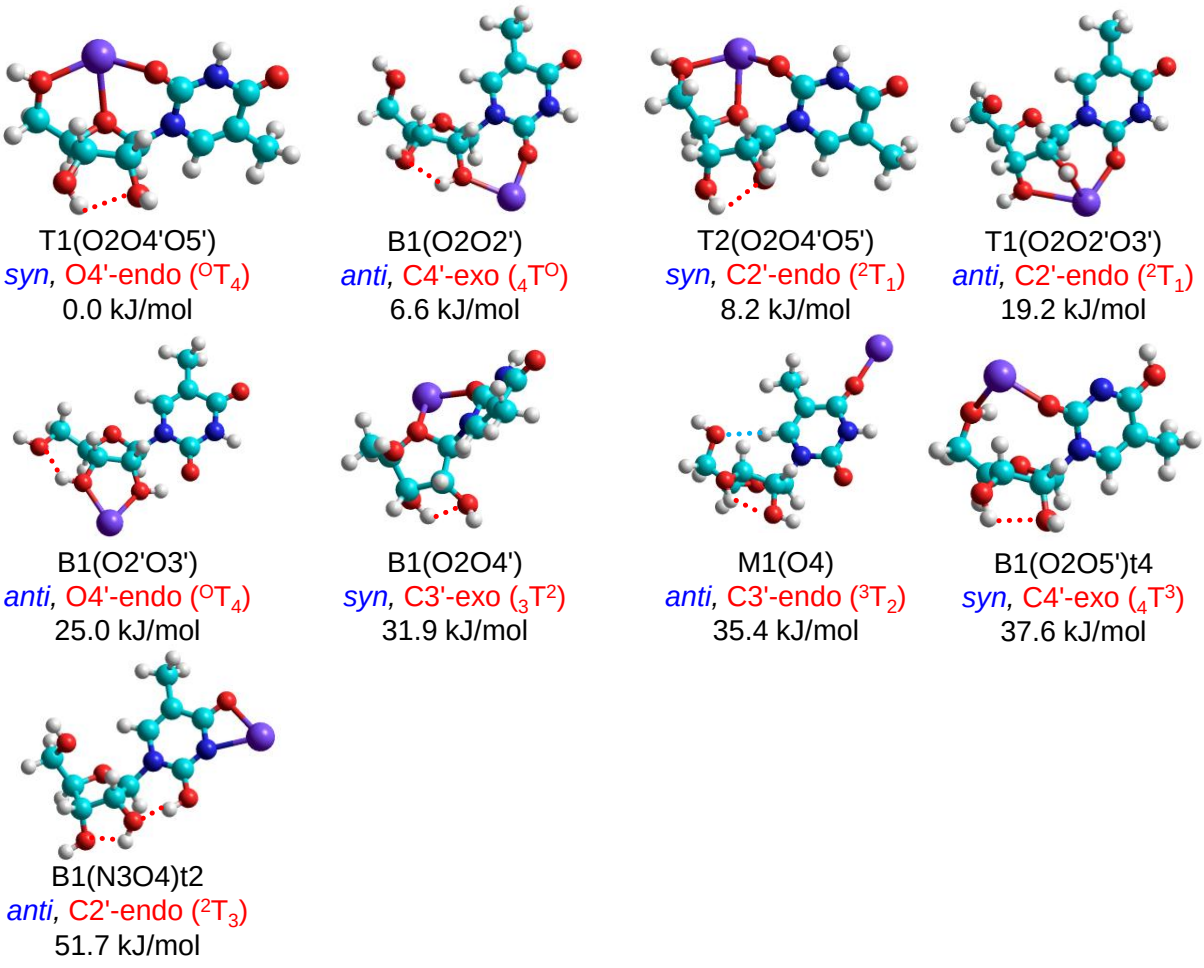

[Thd+Na]$^+$

Figure 3.12 Select stable B3LYP/6-311+G(d,p) conformers of [Thd+Na]$^+$. The Na$^+$ binding modes, orientations of the thymine nucleobase, sugar puckering, and the relative 298 K Gibbs free energies at the B3LYP/6-311+G(2d,2p) level of theory are also listed for each structure.

T1(O2O4'O5')
0.0 kJ/mol

B1(O2O2')
6.6 kJ/mol

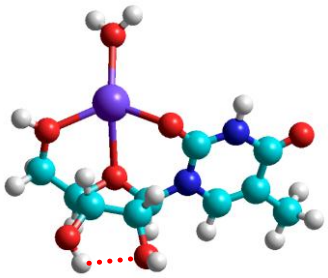

T1(O2O4'O5')• H_2O
0.1 kJ/mol

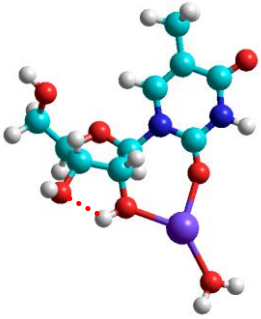

B1(O2O2')• H_2O
0.0 kJ/mol

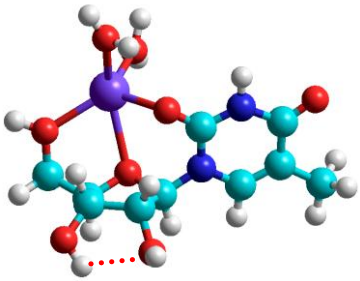

T1(O2O4'O5')•2H_2O
9.8 kJ/mol

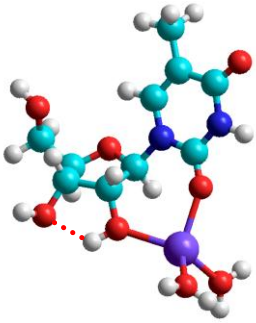

B1(O2O2')•2H_2O
0.0 kJ/mol

$[Thd+Na]^+•nH_2O$ (n = 0–2)

Figure 3.13 Structures of the T1(O2O4'O5') and B1(O2O2') conformers of $[Thd+Na]^+$ and their mono and bis water adducts ($[Thd+Na]^+$•nH2O, n=1, 2). The relative Gibbs free energies calculated at B3LYP/6-311+G(2d,2p)//B3LYP/6-311+G(d,p) level of theory are also shown.

CHAPTER 4 CHARACTERIZATION OF THE STABLE CONFORMATIONS OF SODIUM CATIONIZED DNA AND RNA NUCLEOSIDES VIA IRMPD ACTION SPECTROSCOPY

Portions of this chapter were reprinted with permission from the followed research publications. Y. Zhu, L. A. Hamlow, C. C. He, S. F. Strobehn, J. K. Lee, J. Gao, G. Berden, J. Oomens and M. T. Rodgers, *J. Phys. Chem. B* 2016, **120**, 8892. Copyright 2016 American Chemistry Society. Y. Zhu, L. A. Hamlow, C. C. He, J. K. Lee, J. Gao, G. Berden, J. Oomens and M. T. Rodgers, *J. Phys. Chem. B* 2017, **121**, 4048. Copyright 2017 American Chemistry Society. Y. Zhu, L. A. Hamlow, C. C. He, H. A. Roy, N. A. Cunningham, M. U. Munshi, G. Berden, J. Oomens and M. T. Rodgers, *Int. J. Mass Spectrom.* 2017, https://doi.org/10.1016/j.ijms.2017.04.005. Copyright 2017 Elsevier B.V. Y. Zhu, H. A. Roy, N. A. Cunningham, S. F. Strobehn, J. Gao, M. U. Munshi, G. Berden, J. Oomens and M. T. Rodgers, *Phys. Chem. Chem. Phys.* 2017, **19**, 17637. Copyright 2017 Royal Society of Chemistry. Y. Zhu, H. A. Roy, N. A. Cunningham, S. F. Strobehn, J. Gao, M. U. Munshi, G. Berden, J. Oomens and M. T. Rodgers, *J. Am. Soc. Mass Spectrom*. 2017, **28**, 2437. Copyright 2017 American Society for Mass Spectrometry.

4.1 INTRODUCTION

Our motivation for elucidating the gas-phase conformations of the sodium cationized DNA and RNA nucleosides is discussed in detail in **Chapter 1**. The experimental IRMPD spectra of 10 sodium cationized DNA and RNA nucleosides were acquired via IRMPD action spectroscopy experiments in both the IR fingerprint and hydrogen-stretching regions, including $[dAdo+Na]^+$, $[Ado+Na]^+$, $[dGuo+Na]^+$, $[Guo+Na]^+$, $[dCyd+Na]^+$, $[Cyd+Na]^+$, $[dUrd+Na]^+$, $[Urd+Na]^+$, $[dThd+Na]^+$ and $[Thd+Na]^+$. The

experimental procedures were described in **Section 2.1**. The linear IR spectra of each conformer were calculated at B3LYP/6-311+G(2d,2p)//B3LYP/6-311+G(d,p) level of theory, as introduced in **Section 2.3**. The conformations of these sodium cationized DNA and RNA nucleosides populated by electrospray ionization (ESI) are determine here by comparing the calculated IR spectra predicted for each stable conformer computed and discussed in **Chapter 3** with the experimental IRMPD spectrum.[147-151] Ranran Wu, a previous Ph.D. student in our group, studied the gas-phase conformations of the protonated forms of these same 10 DNA and RNA nucleosides via IRMPD action spectroscopy experiments and theoretical approaches.[119,125,184-186] Results for the sodium cationized DNA and RNA nucleosides are compared to those for the protonated DNA and RNA nucleosides to elucidate the effects of sodium cationization vs. protonation on the gas-phase conformations of DNA and RNA nucleosides. In this chapter, the sodium cationized adenine nucleosides are examined in detail and used as examples to introduce the methodology employed for spectral comparisons and determination of important conformers in the experiments. The same methodology is applied to all systems investigated including the sodium cationized guanine, cytosine, uracil, and thymine nucleosides, however, for these latter systems, the discussion presented focuses only on the conformers of these sodium cationized nucleosides that are populated in the experiments.

4.2 EXPERIMENTAL IRMPD SPECTRA OF SODIUM CATIONIZED DNA AND RNA NUCLEOSIDES

The experimental IRMPD spectra of 10 sodium cationized DNA and RNA nucleosides are compared in **Figure 4.1**. Three thypes of photodissociation pathways were observed in the experiments as summarized in **Reactions 4.1**–**4.3**,

$$[\text{Nuo+Na}]^+ + n\,h\nu \rightarrow \text{Na}^+ + \text{Nuo} \quad (4.1)$$

$$[\text{Nuo+Na}]^+ + n\,h\nu \rightarrow [\text{Nue+Na}]^+ + (\text{Nuo}-\text{Nue}) \quad (4.2)$$

$$[\text{Nuo+Na}]^+ + n\,h\nu \rightarrow [\text{Nuo}-\text{Nue+Na}]^+ + \text{Nue} \quad (4.3)$$

where Nuo is the precursor nucleoside and Nue is the associated nucleobase. **Reaction 4.1** corresponds to simple noncovalent bond cleavage resulting in loss of the intact nucleoside. **Reactions 4.2** and **4.3** involve glycosidic bond cleavage with the sodium cation retained either by the nucleobase or sugar moiety, respectively. All three photodissociation pathways, **Reactions 4.1-4.3** were observed for $[\text{dAdo+Na}]^+$ in the IR fingerprint region, whereas only **Reaction 4.2** was seen in the hydrogen-stretching region. In contrast, the only photodissociation pathway observed for $[\text{Ado+Na}]^+$ was the loss of the intact nucleoside, **Reaction 4.1** in both the IR fingerprint and hydrogen-stretching regions. The only photodissociation pathway observed for the guanine and cytosine nucleosides in both the IR fingerprint and hydrogen-stretching regions involved N-glycosidic bond cleavage with the sodium cation retained by guanine as summarized in **Reaction 4.2**. **Reactions 4.2** and **4.3** were observed for $[\text{dUrd+Na}]^+$ in both spectral regions. In contrast, only **Reaction 4.1** was observed for $[\text{Urd+Na}]^+$ in the IR fingerprint region, whereas all three photodissociation pathways, **Reactions 4.1**-**4.3** were seen in the hydrogen-stretching region. IR photodissociation of $[\text{dThd+Na}]^+$ induced by either the FELIX or the OPO laser produced both simple cleavage of the noncovalent interaction between Na^+ and the nucleoside, **Reaction 4.1**, and cleavage of the N-glycosidic bond with Na^+ retained by the thymine nucleobase, **Reaction 4.2**. In contrast, IR photodissociation of $[\text{Thd+Na}]^+$ induced by the FEL led solely to simple loss of the neutral nucleoside, **Reaction 4.1**, whereas in the hydrogen-stretching region, both

Reactions 4.1 and **4.2** were observed. The observation of **Reaction 4.3** in the dAdo, dUrd, and Urd systems indicates that the sugar is a competitive binder of Na^+ in these systems. Likewise, these results suggest that Gua and Cyt bind to Na^+ more strongly than Ade, Ura, and Thy, because **Reaction 4.2** but not **Reaction 4.3** was observed in the IRMPD action spectroscopy experiments for the sodium cationized guanine and cytosine nucleosides. Because no N-glycosidic bond cleavage was observed upon IRMPD of $[Ado+Na]^+$, it can be concluded that Ado has the strongest N-glycosidic bond among these 10 nucleosides, consistent with the ER-CID results discussed in **Chapter 5** and previous TCID studies of the protonated DNA and RNA nucleosides.[193-197]

Overall, the IR features observed in the experiments for the sodium cationized DNA vs. RNA nucleosides are highly parallel, except for the adenine and guanine nucleosides. Compared to the DNA forms of the sodium cationized adenine and guanine nucleosides, an additional IR absorption at ~3590 cm^{-1} is only observed for the RNA forms of these complexes; this feature is associated with the additional 2'-hydroxyl substituent. The IRMPD yields of the RNA forms of the sodium cationized DNA and RNA nucleosides are generally lower than those of the analogous DNA forms of these complexes, suggesting that the additional 2'-hydroxyl substituent of the RNA nucleosides stabilizes the N-glycosidic bond. However, other factors may also contribute to the disparity in the IRMPD yields for these systems.

4.3 SODIUM CATIONIZED ADENINE NUCLEOSIDES

4.3.1 CONFORMERS OF SODIUM CATIONIZED 2'-DEOXYADENOSINE POPULATED BY ESI

The measured IRMPD spectrum and calculated IR spectra of the two low-energy conformers of $[dAdo+Na]^+$ that provide the best matches to the measured IRMPD

spectrum are compared in **Figure 4.2**. The measured IRMPD spectrum and calculated IR spectra of the most stable conformer determined for each mode of Na^+ binding are compared in **Figure 4.3**. Overall, the IR spectrum predicted for the ground T1(N3O4′O5′) conformer exhibits the best agreement with the measured IRMPD spectrum in both the IR fingerprint and hydrogen-stretching regions. The interaction between the sodium cation and the N3, O4′ and O5′ atoms forming stable 5- and 6-membered chelation rings to the nucleobase and sugar moieties provides maximum stability to the complex. T2(N3O4′O5′), which differs from the ground conformer by rotation of the 3′-hydroxyl substituent and the nucleobase about the N-glycosidic bond as well as the sugar puckering, which destabilize this structure by 1.4 kJ/mol, also exhibits good agreement with the measured IRMPD spectrum. The primary difference between the calculated IR spectra of T1(N3O4′O5′) and T2(N3O4′O5′) is the width of the peak at 3659 cm^{-1}, which is quite narrow for T1(N3O4′O5′), and much broader peak for T2(N3O4′O5′). The sharpness of the corresponding feature in the measured IRMPD spectrum suggests that T1(N3O4′O5′) is the major contributor, and that T2(N3O4′O5′) is probably only present in low abundance in the experiments.

Other stable structures involving binding to N3 are found, but are much less stable. Sodium cation binding to the N3 and O3′ atoms rotates the adenine residue to an *anti* orientation in B1(N3O3′), and increases the relative Gibbs free energy significantly. The absence of the IR band at 930 cm^{-1}, and the split of the IR feature at 3659 cm^{-1} indicate that B1(N3O3′) is not present in measurable abundance in the experiments. As a result of the absence of additional chelation interactions with the sugar moiety, the monodentate conformer, M1(N3), exhibits a different sugar puckering

and nucleobase orientation and is significantly less stable (> 95 kJ/mol). Therefore, the IR spectrum predicted for M1(N3) exhibits distinct shifts in the low frequency region, and a split of the IR band at 3659 cm^{-1}. The IR features predicted in the hydrogen-stretching region for the B1(N7NH_2) and B1(N1NH_2) conformers exhibit obvious disagreement with the experimental IRMPD spectrum due to the binding interaction between the sodium cation and the amino substituent of adenine. The Na^+-NH_2 interaction leads to significant variation in the IR features at 1636 cm^{-1} and 1583 cm^{-1}, respectively. In addition, the N1 and N7 binding conformers are significantly less stable, which also suggests that they are unlikely to be accessed in the experiments. For B1(O4′O5′), sodium cation binding solely to the sugar moiety increases the relative Gibbs free energy by 41.4 kJ/mol. The additional peak at 960 cm^{-1} and the blue shifted IR feature at 3690 cm^{-1} in the calculated IR spectrum indicate that B1(O4′O5′) is not present in measurable abundance in the experiments.

In summary, the IR spectrum of the ground T1(N3O4′O5′) conformer exhibits very good agreement with the measured IRMPD spectrum. Therefore, it can be concluded that the sodium cation prefers N3 binding to adenine and chelates with the O4′ and O5′ atoms of the sugar moiety as indicated by the computed relative stabilities of the stable conformers. Furthermore, other tridentate N3 binding conformers with a *syn*-orientation of adenine exhibit only minor shifts in the FELIX region. Broadening at the base of the feature at 3659 cm^{-1}, indicates that these conformers may be present, but if so are present in low abundance in the experiments. Because no evidence for peak splitting at 3659 cm^{-1} is observed in the measured spectrum, B1(N3O3′) and M1(N3) do not have measurable populations in the experiments. Due to the huge shifts

at 1636 cm^{-1} and the absence of the IR feature at 3433 cm^{-1}, all N1 and N7 binding conformers are unlikely accessed in the experiments. B1(O4′O5′), in which the sodium cation binds to the sugar moiety, exhibits significant shifts and broadening in the calculated IR spectrum, indicating that this conformer also does not have a measurable abundance in the experiments. A more detailed discussion of the comparisons between the experimental IRMPD and calculated IR spectra of $[dAdo+Na]^+$ can be found in **Reference 146**.

4.3.2 CONFORMERS OF SODIUM CATIONIZED ADENOSINE POPULATED BY ESI

The measured IRMPD and calculated IR spectra of the two low-energy conformers of $[Ado+Na]^+$ that provide the best matches to the measured IRMPD spectrum are compared in **Figure 4.4**. The measured IRMPD spectrum and calculated IR spectra of the most stable conformers of $[Ado+Na]^+$ with each binding modes of Na^+ are compared in **Figure 4.5**. The T1(N3O4′O5′), T2(N3O4′O5′), and T3(N3O4′O5′) conformers show very good agreement with the measured IRMPD spectrum in the FELIX and OPO regions. However, because the calculated IR spectrum of T2(N3O4′O5′) is virtually identical to that of T1(N3O4′O5′), it is not included in **Figure 4.4**. The shape/broadening at the base of the IRMPD features observed at 3599 and 3659 cm^{-1}, suggests that both conformers are present in the experiments. However, theory does not do a good job of predicting the frequency of the IR feature associated with the O5′H stretch as there is a blue shift of this feature in all of the computed IR spectra. Therefore, T1(N3O4′O5′) again appears to be the dominant conformer populated in the experiments based on the peak width of the feature near 3659 cm^{-1}. N3 binding conformers exhibiting an *anti* orientation of adenine, B1(N3O2′) and

T1(N3O2′O3′), do not have measurable population in the experiments, due to the significant mismatches observed in the OPO region and high relative Gibbs free energies. The absence of a chelation interaction with O5′ makes B1(N3O4′) 39.5 kJ/mol less stable than the ground conformer, and the IR band predicted at 960 cm^{-1} is not observed in the measured IRMPD spectrum. The N7 or N1 binding modes are less favorable due to the relatively high Gibbs free energy compared with the ground conformer. As found for $[dAdo+Na]^+$, the IR features predicted in the OPO region for B1(N7NH_2) and B1(N1NH_2) exhibit obvious disagreement with the measured IRMPD action spectrum, which is due to the chelation between the sodium cation and the NH_2 substituent. Both the relative Gibbs free energies and the shifts in the IR features of the N1 or N7 binding conformers suggest that the sodium cation prefers to bind to N3 rather than N1 or N7 of adenine. For the bidentate conformer, B1(O4′O5′), the lack of a chelation interaction between Na^+ and adenine make this conformer 50.5 kJ/mol less stable than the ground conformer. Additionally, poor agreement of the calculated IR spectrum of B1(O4′O5′) also indicates that this bidentate conformer cannot be present in significant abundance in the experiments.

In summary, based on comparisons between the measured IRMPD and calculated IR spectra of $[Ado+Na]^+$ in the FELIX and OPO regions, it can be concluded that N1 or N7 binding conformers are not measurably populated in the experiments. Good agreement is achieved for tridentate complexes that bind via N3, O4′ and O5′, and in particular, for the T1(N3O4′O5′), T2(N3O4′O5′), and T3(N3O4′O5′) conformers with puckering of the sugar moiety that is approximately C1′-exo, but lies between C2′-endo and O4′-endo, and a *syn* orientation of adenine indicating that these conformers

may be present in the experiments. T1(N3O4′O5′) and T2(N3O4′O5′) are likely present at higher populations than T3(N3O4′O5′) as a result of the greater similarity in their predicted IR spectra regarding the feature observed at 3659 cm^{-1}. It can be concluded that the *anti* orientated N3 binding conformers, B1(N3O2′) and T1(N3O2′O3′), do not have measurable populations in the experiments due to the significant differences between the computed and measured spectra in the OPO region. Both high Gibbs free energy and mismatch of the calculated IR spectrum suggest that B1(N3O4′) has very low abundance in the experiments. A more detailed discussion of the comparisons between the experimental IRMPD and calculated IR spectra of $[Ado+Na]^+$ can be found in **Reference 146**.

4.3.3 VIBRATIONAL ASSIGNMENTS FOR SODIUM CATIONIZED ADENINE NUCLEOSIDES

Vibrational assignments for $[dAdo+Na]^+$ and $[Ado+Na]^+$ based on comparison of the IRMPD spectrum and the IR spectra predicted for the ground T1(N3O4′O5′) conformers are listed in **Table 4.1**. The measured IRMPD spectra of $[dAdo+Na]^+$ and $[Ado+Na]^+$ are highly parallel, and only small shifts (< 10 cm^{-1}) are observed for each vibrational mode. Two notable differences in the IRMPD spectra of $[dAdo+Na]^+$ and $[Ado+Na]^+$ are however observed. In the IR fingerprint region, the IRMPD feature associated with C2′-C3′ stretching at 930 cm^{-1} is only observed for $[dAdo+Na]^+$. In the hydrogen-stretching region, the weak IR feature at ~3600 cm^{-1} reflects the 2′-hydroxyl stretch, which is obviously only observed for $[Ado+Na]^+$. As summarized in the table, the features below 1550 cm^{-1} and above 3550 cm^{-1} are associated with the sugar moiety, whereas those between these limits arise from the nucleobase. Both spectral regions are important to the assignment of the structures populated in the experiments. In

general, the gross structural features of these complexes (i.e., the mode of cation binding and nucleobase orientation) are readily deduced from the IR signatures observed in either the IR fingerprint or hydrogen-stretching region. However, both spectral regions are important for elucidating minor structural differences and for definitively establishing the dominant conformers populated in the experiments.

4.3.4 COMPARISONS OF THE CONFORMERS OF PROTONATED VS. SODIUM CATIONIZED ADENINE NUCLEOSIDES POPULATED BY ESI

Our previous IRMPD action spectroscopy and theoretical study of the gas-phase conformations and energetics of $[dAdo+H]^+$ and $[Ado+H]^+$, found N3 to be the most favorable protonation site for both $[dAdo+H]^+$ and $[Ado+H]^+$.[184] The ground structures of protonated and sodium cationized adenine nucleosides are shown in **Figure 4.6** for comparison. N3 protonation enables a strong intramolecular hydrogen-bonding interaction between $N3H^+$ and O5′ to be formed leading to rotation of adenine to a *syn* orientation and an approximately C2′-endo ($^2T_1$) configuration of the sugar. Similarly, the sodium cation prefers to bind to the N3, O4′ and O5′ atoms and also requires that adenine rotate to a *syn* orientation. However, because the sodium cation is much larger and can form multiple chelating interactions, the O4′ atom is also involved in the binding of Na^+, and thus forms 5- and 6-membered chelation rings in the ground conformers of $[dAdo+Na]^+$ and $[Ado+Na]^+$. The glycosidic bonds of the sodium cationized adenine nucleosides are shorter than those of the protonated species (1.458 Å in $[dAdo+Na]^+$ and 1.448 Å in $[Ado+Na]^+$ vs. 1.465 Å in $[dAdo+H]^+$ and 1.459 Å in $[Ado+H]^+$), indicating that sodium cationization is less effective at activating the glycosidic bond than protonation.

4.4 SODIUM CATIONIZED GUANINE NUCLEOSIDES

4.4.1 CONFORMERS OF SODIUM CATIONIZED 2'-DEOXYGUANOSINE POPULATED BY ESI

The measured IRMPD spectrum and calculated IR spectra of the most stable B(O6N7) binding conformers of $[dGuo+Na]^+$ that exhibit good agreement with the measured IRMPD spectrum are compared in **Figure 4.7**. The calculated IR spectrum of the ground conformer, B1(O6N7) exhibits very good agreement with the measured IRMPD spectrum. However, the intensities of the IR features predicted at 3413 and 3436 cm^{-1} are inverted compared with the corresponding features in the measured IRMPD spectrum. The calculated IR spectra of other similar low-energy B(O6N7) conformers, which also exhibit C2'-endo ($^2T_3$) sugar puckering and an *anti* orientation, are highly parallel, and therefore, these conformers, may also be populated in the experiments. The IR feature at 3670 cm^{-1} predicted for *anti* oriented B(O6N7) conformers with C3'-endo sugar puckering exhibits a slight blue shift compared with the measured IRMPD spectrum, which indicates that these conformers may be populated in the experiments, but if so, with lower abundance than the more stable B(O6N7) conformers with C2'-endo sugar puckering. The IR feature associated with O5'H stretching predicted for B9(O6N7) blue shifts by 9 cm^{-1} to 3444 cm^{-1} vs B1(O6N7), but is still reasonably well aligned with the measured IRMPD spectrum. Slight blue shifts of the IR features at 1536, 1591, 1642 and 3655 cm^{-1} for B9(O6N7) vs. those of B1(O6N7) and the observed features in the measure IRMPD spectrum suggest that B9(O6N7) may also be present, but if present, is present in very low abundance. The calculated IR spectrum of B15(O6N7) shows good agreement with the experimental IRMPD spectrum, which indicates B(O6N7) conformers with C3'-exo sugar puckering may be

accessed in the experiments with low populations. Changes in the sugar puckering do not significantly impact the calculated IR spectra, only a minor blue shift of the IR feature at 3673 cm^{-1} by ~10 cm^{-1} is found. However, the relative Gibbs free energies of these conformers suggest that the conformers with sugar puckerings that differ from C2'-endo do not have large populations in the experiments.

In summary, the sodium cation prefers bidentate binding to the O6 and N7 atoms of guanine via a 5-membered chelation ring with *anti* and *syn* orientations of the nucleobase being populated in the experiments. The *syn* orientation is slightly less favorable than *anti*, based on the computed relative Gibbs free energies and minor shifts in the calculated IR spectrum. C2'-endo puckering is preferred over other sugar puckerings. The O6N7 bidentate binding conformers with C2'-endo puckering of $[dGuo+Na]^+$ are the dominant species present in the experiments. A more detailed discussion of the comparisons between the experimental IRMPD and calculated IR spectra of $[dGuo+Na]^+$ can be found in **Reference 147**.

4.4.2 CONFORMERS OF SODIUM CATIONIZED GUANOSINE POPULATED BY ESI

The measured IRMPD spectrum and calculated IR spectra of the most stable B(O6N7) conformers of $[Guo+Na]^+$ that exhibit good spectral alignment with the measured IRMPD spectrum are compared in **Figure 4.8**. Similar to $[dGuo+Na]^+$, the calculated IR spectrum of both *anti* and *syn* orientated B(O6N7) binding conformers exhibit good agreement with the measured IRMPD spectrum. Both C2'-endo and C3'-endo puckerings are represented among these conformers, with a preference for C2'-endo puckering, that is, *anti* oriented B(O6N7) conformers with C3'-endo sugar puckering are likely present in lower populations. The predicted IR spectra for the

B(O6N7) conformers with other sugar puckerings show significant spectral misalignments with the measured IRMPD spectrum, which suggests that these conformers with high relative Gibbs free energies do not have measurable populations in the experiments.

In summary, *anti* and *syn* orientated B(O6N7) binding conformers with a preference for C2'-endo puckering are the dominant conformers populated in the experiments. The *syn* orientated B(O6N7) binding conformers if present likely have lower populations, due to the relative Gibbs free energy and minor shifts in the calculated IR spectrum. A detailed discussion of the comparisons between the experimental IRMPD and calculated IR spectra of $[Guo+Na]^+$ can be found in **Reference 147**.

4.4.3 VIBRATIONAL ASSIGNMENTS FOR SODIUM CATIONIZED GUANINE NUCLEOSIDES

Vibrational assignments for the $[dGuo+Na]^+$ and $[Guo+Na]^+$ conformers based on the IR spectra predicted for the ground B1(O6N7) conformers of these complexes are listed in **Table 4.2**. The measured IRMPD spectra of $[dGuo+Na]^+$ and $[Guo+Na]^+$ exhibit high similarity with shifts of <10 cm^{-1} observed for each vibrational mode. Three minor differences enable differentiation of $[dGuo+Na]^+$ from $[Guo+Na]^+$. The relatively strong IR feature at 650 cm^{-1} in the measured IRMPD spectrum of $[dGuo+Na]^+$, which is related to sugar ring bending, is very weak for $[Guo+Na]^+$. The IR feature at 938 cm^{-1} associated with C2′-C3′ stretching is only observed for $[dGuo+Na]^+$. Its absence in the IRMPD spectrum of $[Guo+Na]^+$ is likely caused by a tightening of this vibration associated with the hydrogen-bonding interaction between the 2'- and 3'-hydroxyls. The

IR feature at 3577 cm^{-1}, which is associated with 2′-hydroxyl stretching is obviously only observed for $[Guo+Na]^+$.

4.4.4 COMPARISONS OF THE CONFORMERS OF PROTONATED VS. SODIUM CATIONIZED GUANINE NUCLEOSIDES POPULATED BY ESI

Previous IRMPD action spectroscopy and theoretical study of the gas-phase conformations and energetics of $[dGuo+H]^+$ and $[Guo+H]^+$, indicated that the most favorable protonation site is the N7 atom of guanine.[185] The ground conformers of protonated and sodium cationized guanine nucleosides are compared in **Figure 4.9**. The larger size and the electrostatic nature of the binding to Na^+ allows multiple chelation interactions in $[dGuo+Na]^+$ and $[Guo+Na]^+$, forming a 5-membered chelation ring. In contrast, the proton only binds to the N7 atom of guanine. For both protonated guanine nucleosides, guanine exhibits a preference for the *anti* orientation, whereas the sugar prefers C3′-endo ($^3T_2$) puckering. The sodium cationized guanine nucleosides exhibit structural factors similar to protonated guanine nucleosides, except for the sugar puckering, where the C2′-endo ($^2T_3$) configuration for $[dGuo+Na]^+$ and $[Guo+Na]^+$ is preferred. However, the guanine orientation and sugar puckering do not significantly change the calculated IR spectra of the sodium cationized guanine nucleosides. Therefore, B(O6N7) binding conformers of $[dGuo+Na]^+$ and $[Guo+Na]^+$ with both *anti* and *syn* orientations and a variety of sugar puckerings may coexist in the experiments. The glycosidic bonds of the sodium cationized guanine nucleosides are shorter than those of the protonated species (1.469 Å in $[dGuo+Na]^+$ and 1.463 Å in $[Guo+Na]^+$ vs. 1.508 Å in $[dGuo+H]^+$ and 1.498 Å in $[Guo+H]^+$), indicating that sodium cationization is less effective at activating the glycosidic bond than protonation. A noncanonical

hydrogen-bonding interaction between H8 and O5′ is observed in the ground conformers of all of the species.

4.5 SODIUM CATIONIZED CYTOSINE NUCLEOSIDES

4.5.1 CONFORMERS OF SODIUM CATIONIZED 2'-DEOXYCYTIDINE POPULATED BY ESI

The measured IRMPD spectrum of $[dCyd+Na]^+$ is compared to the IR spectra predicted for stable conformers that exhibit good agreement in **Figure 4.10**. The calculated IR spectrum for the ground conformer, T1(O2O4'O5'), which binds to dCyd via tridentate interaction with the cytosine and sugar moieties, exhibits very good agreement with the measured IRMPD spectrum of $[dCyd+Na]^+$ although the predicted spectral features exhibit small shifts relative to the measured IRMPD spectrum in the hydrogen-stretching region. Changes in the sugar puckering of tridentate T(O2O4'O5') conformers induces splitting of the IR feature at 3664 cm^{-1}, which is not seen in the measured IRMPD spectrum, indicating that if present, these conformers do not have significant populations in the experiments. The IR spectra predicted for conformers that bind via bidentate interaction with the cytosine and sugar moieties, B1(O2O4') and B6(O2O3') show reasonably good agreement with the experimental IRMPD spectrum even though the relative Gibbs free energies calculated for these species, 29.9 kJ/mol and 62.2 kJ/mol, suggest that they should not be present in significant populations. However, minor shifts in the calculated IR spectra of B1(O2O4') and B6(O2O3') indicate that if these conformers are indeed present, they must have low populations in the experiments.

In summary, Na^+ interacting with both the cytosine and sugar moieties provides the most favorable mode of binding for $[dCyd+Na]^+$, with a preference for binding to the

O2, O4' and O5' atoms to form 5- and 6-membered chelation rings. Several sugar puckerings are found among the conformers populated in the experiments, including: O4'-endo ($^{O}T_1$) in T1(O2O4O5), C3'-exo ($_3T^2$) in B1(O2O4'), and C1'-exo ($_1T^2$) in B6(O2O3'). In all other cases, changes in the sugar puckering lead to spectral mismatches between theory and experiment, even when the conformers exhibit similar Na^+ binding modes and cytosine orientations. A more detailed discussion of the comparisons between the experimental IRMPD and calculated IR spectra of $[dCyd+Na]^+$ can be found in **Reference 148**.

4.5.2 CONFORMERS OF SODIUM CATIONIZED CYTIDINE POPULATED BY ESI

The calculated IR spectra of $[Cyd+Na]^+$ conformers that exhibit good agreement with the measured IRMPD spectrum are compared in **Figure 4.11**. In contrast to $[dCyd+Na]^+$, an additional IR feature associated with free O2'-H stretching in the hydrogen-stretching region is observed in the calculated IR spectrum predicted for the T1(O2O4'O5') ground conformer that is not experimentally observed, indicating T1(O2O4'O5') is not an dominant contributor in the experiments in spite of its computed stability. Similar T(O2O4'O5') conformers are eliminated from the experiments for the same reason. However, the calculated IR spectrum of the B1(O2O2') conformer, which is computed to be 4.3 kJ/mol less stable than the ground conformer, exhibits very good agreement with the measured IRMPD spectrum of $[Cyd+Na]^+$. The splitting of the feature between 3400 and 3475 cm^{-1} in the calculated IR spectrum of B1(O2O2') is observed as an unresolved feature at 3440 cm^{-1} with a shoulder on the red side, indicating that B1(O2O2') is likely the dominant conformer populated in the experiments. Only minor shifts are predicted in the calculated IR spectra of conformers that exhibit

similar binding, cytosine orientation, and sugar puckering, suggesting that these conformers may be also populated in the experiments. The presence of B(O2O2') conformers in the experiments is understood based on the computed relative stabilities of the T1(O2O4'O5') and B(O2O2') conformers when solvated by one and two water molecules (see **Figure 3.8**). The inversion of the relative stabilities of these conformers in the presence of as little as two molecules suggests that B(O2O2') conformers are dominant in solution and kinetically trapped in the ESI desolvation process, and thus are dominantly populated in the experiments.

In a previous study, Tehrani and co-workers performed DFT calculations for $[dCyd+Na]^+$ and $[Cyd+Na]^+$ at the B3LYP/6-311++G(d,p) level of theory.[180] Their results suggested that the preferred binding sites of Na^+ for $[dCyd+Na]^+$ are O2, O4' and O5' atoms, with a *syn* nucleobase orientation and C2'-endo sugar puckering, parallel to that found here. In contrast, for $[Cyd+Na]^+$, they found that Na^+ prefers to bind to the O2 and O2' atoms, with an *anti* orientation of the nucleobase and C3'-exo sugar puckering, similar to the excited low-energy conformers computed here. In order to allow direct comparison with our results, the low-energy conformers determined in their work were recalculated using the computational approach employed in this work. However, the most stable O2 and O2' binding conformer they found is calculated to be 7.6 kJ/mol less stable than the T1(O2O4'O5') conformer and 3.3 kJ/mol less stable than the B1(O2O2') conformer, indicating that the low-energy conformers they found are not ground conformers even though our IRMPD experiments suggest that these binding modes are indeed populated in the experiments, a result of kinetic trapping. Interestingly, the calculated IR spectrum of the T1(O2O2'O3') conformer shows very good agreement

with the experimental IRMPD spectrum in spite of the relatively high Gibbs free energy calculated for this conformer, 41.5 kJ/mol.

In summary, B(O2O2') conformers with an *anti* orientation of cytosine and C4'-exo ($_4T^O$) sugar puckering are the domiant conformers populated in the experiments. The T1(O2O2'O3') conformer with an *anti* orientation and C2'-endo ($^2T_3$) sugar puckering may also be populated, but given its relatively high Gibbs free energy, it is likely only present in low abundance. Minor shifts predicted in the calculated IR spectra of B(O2O2') conformers that exhibit different sugar puckerings, or that are stabilized by an additional intramolecular hydrogen-bonding interaction, indicate that these conformers are not likely populated in large abundance. A more detailed discussion of the comparisons between the experimental IRMPD and calculated IR spectra of $[Cyd+Na]^+$ can be found in **Reference 148**.

4.5.3 VIBRATIONAL ASSIGNMENTS FOR SODIUM CATIONIZED CYTOSINE NUCLEOSIDES

Table 4.3 lists vibrational assignments for $[dCyd+Na]^+$ based on the T1(O2O4'O5') conformer and for $[Cyd+Na]^+$ based on the B1(O2O2') conformer. Overall, the experimental IRMPD spectra of $[dCyd+Na]^+$ and $[Cyd+Na]^+$ are highly parallel, except that the IRMPD yield of $[dCyd+Na]^+$ is at least four times greater than that of $[Cyd+Na]^+$ in the IR fingerprint region, whereas the IRMPD yield of $[dCyd+Na]^+$ is only slightly greater than that of $[Cyd+Na]^+$ in the hydrogen-stretching region. A strong IR feature associated with sugar ring bending at 855 cm^{-1} is observed in the calculated IR spectrum of $[dCyd+Na]^+$ in the FELIX region, whereas this IR feature is very weak in the calculated IR spectrum of $[Cyd+Na]^+$. Additionally, the IR features predicted for

$[dCyd+Na]^+$ between 914 and 1028 cm^{-1} representing sugar ring stretching are much stronger than those predicted for $[Cyd+Na]^+$.

4.5.4 COMPARISONS OF THE CONFORMERS OF PROTONATED VS. SODIUM CATIONIZED CYTOSINE NUCLEOSIDES POPULATED BY ESI

Our previous studies of $[dCyd+H]^+$ and $[Cyd+H]^+$ indicated that N3 and O2 protonated tautomeric conformations of dCyd and Cyd coexist in the gas phase.[186] The dominant populated conformers of protonated and sodium cationized cytosine nucleosides are compared in **Figure 4.12**. Both N3 and O2 protonated cytosine nucleosides prefer an *anti* orientation of the cytosine residue and C2'-endo sugar puckering. A noncanonical hydrogen bond between C5H and O5' is found in all N3 and O2 protonated conformers of dCyd and Cyd. In contrast, Na^+ is found to bind to both the cytosine nucleobase and sugar moiety via the O2, O4' and O5' atoms. For $[dCyd+Na]^+$, both *syn* and *anti* oriented conformers are populated in the experiments, with a preference for the *syn* orientation of cytosine. A variety of sugar puckerings are represented among the conformers populated, including: O4'-endo ($^{O}T_1$), C3'-exo ($_3T^2$) and C1-exo ($_1T^2$), for $[dCyd+Na]^+$. For $[Cyd+Na]^+$, B(O2O2') conformers with an *anti* orientation and C4'-exo ($_4T^{O}$) sugar puckering and the T1(O2O2'O3') conformer with an *anti* orientation and C2'-endo ($^2T_3$) sugar puckering are the dominant conformers populated in the experiments. The N-glycosidic bonds of $[dCyd+Na]^+$ and $[Cyd+Na]^+$, 1.457 Å and 1.452 Å, are shorter than those of $[dCyd+H]^+$ and $[Cyd+H]^+$, which are 1.529 Å and 1.488 Å for the N3 protonated conformers, and 1.506 Å and 1.494 Å for the O2 protonated conformers, respectively, indicating that sodium cationization is less effective at activating the glycosidic bond than protonation.

4.6 SODIUM CATIONIZED URACIL NUCLEOSIDES

4.6.1 CONFORMERS OF SODIUM CATIONIZED 2'-DEOXYURIDINE POPULATED BY ESI

Figure 4.13 compares the experimental IRMPD spectrum of $[dUrd+Na]^+$ and the calculated IR spectra predicted for low-energy conformers that exhibit good spectral alignment. Overall, the calculated IR spectrum of the ground conformer of $[dUrd+Na]^+$ exhibits the best agreement with the measured IRMPD spectrum. Na^+ preferentially binds to the O2, O4' and O5' atoms of dUrd to form 5- and 6-membered chelation rings. The sugar exhibits O4'-endo ($^{O}T_1$) sugar puckering and uracil exhibits a *syn* orientation. Additionally, the calculated IR spectra of T2(O2O4'O5'), and T3(O2O4'O5') with C1'-exo ($_1T^{O}$), and C2'-exo ($_2T^{3}$) sugar puckerings exhibit very good agreement with the experimental IRMPD spectrum. However, the theoretical IR spectra of the other T(O2O4'O5') conformers with other sugar puckerings exhibit significant spectral mismatches with the experimental IRMPD spectrum, such that the T(O2O4'O5') conformers with other sugar puckerings do not have significant populations in the experiments. Both high Gibbs free energies and significant misalignments between the measured IRMPD and calculated IR spectra suggest that the O4 binding and sugar binding conformers as well as minor tautomers are not populated in the experiments.

In summary, T1-T3(O2O4'O5') conformers of $[dUrd+Na]^+$ with O4'-endo ($^{O}T_1$), C1'-exo ($_1T^{O}$) and C2'-exo ($_2T^{3}$) sugar puckerings are dominantly populated in the experiments. The T(O2O4'O5') conformers with other sugar puckerings may be present but do not have large populations in the experiments. A more detailed discussion of the comparisons between the experimental IRMPD and calculated IR spectra of $[dUrd+Na]^+$ can be found in **Reference 149**.

4.6.2 CONFORMERS OF SODIUM CATIONIZED URIDINE POPULATED BY ESI

Figure 4.14 compares the experimental IRMPD spectrum of $[Urd+Na]^+$ and the calculated IR spectra predicted for the ground conformer and low-energy conformers that exhibit good spectral alignment. The IR spectrum predicted for the ground conformer, T1(O2O4'O5') of $[Urd+Na]^+$, exhibits additional IR bands at 984 and 3577 cm^{-1} and a slight blue shift of the feature at ~1688 cm^{-1} that are not observed experimentally, indicating that the ground conformer is not measurably populated by ESI, even though theory suggests that the T1(O2O4'O5') conformer exhibits the lowest relative Gibbs free energy. The relatively strong IR band predicted between 3550 and 3600 cm^{-1} is associated with the free O2'H stretch. Therefore, all conformers that do not involve binding of Na^+ to the O2' atom are not populated in the experiments. Overall, the calculated IR spectra of B1, B4, and B7(O2O2') with C4'-exo ($_4T^O$) sugar puckering show good agreement with the measured IRMPD spectrum of $[Urd+Na]^+$, such that these three conformers may be populated in the experiments. Thees complexes differ only in the rotation of 5'-hydroxyl substituent, such that the IR spectra calculated for theses complexes are highly parallel. The distances between the C6H and O5' atoms of the B1, B4, and B7(O2O2') conformers are 3.2, 4.2 and 4.1 Å, respectively. A shoulder to the red of the IR band at ~3438 cm^{-1} in the IR spectrum predicted for B1(O2O2') better reproduces the asymmetry of the IR feature at ~3420 cm^{-1} observed in the measured IRMPD spectrum, suggesting that the B1(O2O2') conformer may be present in higher population than B4 and B7(O2O2').

In summary, B1, B4 and B7(O2O2') conformers with C4'-exo ($_4T^O$) sugar puckering and an *anti* orientation of uracil are dominantly populated in the experiments.

An additional IR feature is predicted in the hydrogen-stretching region for all conformers that do not involve Na^+ binding to the O2' atom, which is not experimentally observed such that we can conclude that these conformers are not present even though theory suggests that the T1(O2O4'O5') conformer is the ground conformer. The inversion of the order of the relative Gibbs free energies calculated for the solvated T1(O2O4'O5') and B1(O2O2') conformers suggests that B(O2O2') conformers are dominantly present in solution, and are kinetically trapped in the ESI desolvation process. Thus, bidentate *anti* oriented B(O2O2') conformers are dominant in the experiments. In contrast, conformers involving O4 binding, sugar binding, and tautomeric $[Urd+Na]^+$ are not populated by ESI as obvious differences between the calculated IR spectra of these conformers and the experimental IRMPD spectrum of $[Urd+Na]^+$ are found. A more detailed discussion of the comparisons between the experimental IRMPD and calculated IR spectra of $[Urd+Na]^+$ can be found in **Reference 149**.

4.6.3 VIBRATIONAL ASSIGNMENTS FOR SODIUM CATIONIZED URACIL NUCLEOSIDES

The vibrational assignments listed in **Table 4.4** of the measured IRMPD spectra of $[dUrd+Na]^+$ and $[Urd+Na]^+$ are based on the ground T1(O2O4'O5') conformer of $[dUrd+Na]^+$ and the low-energy B1(O2O2') conformer of $[Urd+Na]^+$, which exhibit good agreement with the experimental IRMPD spectra. In the IR fingerprint region, the weak IRMPD features associated with N3–H wagging, uracil twisting, and C5–H and C6–H wagging are not observed for $[Urd+Na]^+$ as result of the very low IRMPD yields. The relatively strong IRMPD feature at ~948 cm^{-1} associated with C2'–C3' stretch is only observed for $[dUrd+Na]^+$, whereas this IRMPD feature is not observed for $[Urd+Na]^+$ because the additional hydrogen-bonding interaction between the 2'- and 3'-hydroxyl

substituents reduces the flexibility of the sugar ring of $[Urd+Na]^+$, such that the IRMPD yield associated with the vibrations of the sugar ring of $[Urd+Na]^+$ are significantly lower. Three strong IRMPD absorptions arising from C5–C6, C2=O, and C4=O stretches of $[Urd+Na]^+$ are slightly red shifted, by 10-16 cm^{-1} vs. those of $[dUrd+Na]^+$. The measured spectra of sodium cationized uracil nucleosides in the hydrogen-stretching region are highly parallel. Two strong IRMPD bands at 3420 cm^{-1} and 3664 cm^{-1} are observed. However, the IRMPD feature at 3420 cm^{-1} observed for $[dUrd+Na]^+$ is contributed by the N3–H stretch, whereas this IRMPD feature observed for $[Urd+Na]^+$ is contributed by both the N3–H and O2'–H stretches. The strong IRMPD absorption at 3664 cm^{-1} arises from O3'–H and O5'–H stretches, and is observed for both $[dUrd+Na]^+$ and $[Urd+Na]^+$.

4.6.4 COMPARISONS OF THE CONFORMERS OF PROTONATED VS. SODIUM CATIONIZED URACIL NUCLEOSIDES POPULATED BY ESI

Our previous studies of $[dUrd+H]^+$ and $[Urd+H]^+$ indicated that 2,4-dihydroxy tautomers and O4 protonated conformations of dUrd and Urd coexist in the gas phase.[119] The most populated conformers of protonated and sodium cationized uracil nucleosides are shown in **Figure 4.15** for comparison. The ground conformer calculated for $[dUrd+H]^+$ is the O4 protonated conformer with an *anti* orientation of uracil and C3'-endo sugar puckering, whereas the ground conformer calculated for $[Urd+H]^+$ is the 2,4-dihydroxy tautomer (t24) with an *anti* orientation of uracil and C2'-endo sugar puckering. The t24 tautomer of $[dUrd+H]^+$ and the O4 protonated conformer of $[Urd+H]^+$ are only 0.7 and 2.9 kJ/mol less favorable than the corresponding ground conformers, respectively. The spectral comparisons between the measured IRMPD and calculated IR spectra indicate that the O4 protonated and t24 tautomer of $[dUrd+H]^+$ and $[Urd+H]^+$ coexist in the gas phase. In contrast, the same level of theory suggest that the ground

conformers of both sodium cationized uracil nucleosides involve tridentate binding of Na^+ to the canonical tautomer via the atoms O2, O4' and O5' with a *syn* orientation of uracil and O4'-endo sugar puckering. The spectral comparisons between the measured IRMPD and calculated IR spectra indicate *anti* oriented bidentate B(O2O2') conformers of $[Urd+Na]^+$ are dominantly populated in the experiments. Clearly the strength of binding of the proton vs. the sodium cation, and hydrogen-bonding vs. multiple chelation interactions are important in determining the relative stabilities of the stable conformers of these systems. Compared to protonation, sodium cationization is unable to sufficiently stabilize the minor tautomers of the uracil nucleosides, such that the canonical forms of $[dUrd+Na]^+$ and $[Urd+Na]^+$ have lower relative Gibbs free energies and are the only forms populated in the experiments.

4.7 SODIUM CATIONIZED THYMINE NUCLEOSIDES

4.7.1 CONFORMERS OF SODIUM CATIONIZED THYMIDINE POPULATED BY ESI

Figure 4.16 compares the experimental IRMPD and calculated IR spectra of $[dThd+Na]^+$ for several conformers that exhibit good agreement. Overall, the calculated IR spectra of the T1, T2, and T3(O2O4'O5') conformers exhibit the best agreement with the experimental IRMPD spectrum. These conformers all exhibit tridentate binding of Na^+, with a *syn* orientation of Thy, but with different sugar puckerings, O4'-endo ($^{O}T_1$), C1'-exo ($_1T^{O}$) and C2'-exo ($_2T^3$), respectively. Changes of the sugar puckering and rotation of the N-glycosidic bond lead to the splitting of the IR feature predicted at ~3664 cm^{-1}, indicating that the T(O2O4'O5') conformers with other sugar puckerings do not have measurable populations in the experiments. Both high Gibbs free energies and significant misalignments between the measured IRMPD and calculated IR spectra

suggest that O4 binding and sugar binding conformers as well as minor tautomers of $[dThd+Na]^+$ are clearly not populated in the experiments.

In summary, the T1, T2, and T3(O2O4'O5') conformers are dominantly populated in the experiments. Na^+ preferentially binds to O2, O4' and O5' atoms of thymidine in a tridentate fashion. Thy exhibits a *syn* orientation and several different sugar puckerings, O4'-endo ($^{O}T_1$), C1'-exo ($_1T^{O}$) and C2'-exo ($_2T^3$). All O4 binding and sugar binding conformers are not present in the experiments. Likewise, it is very clear that all sodium cationized tautomeric dThd are also not populated in the experiments. These findings are also consistent with the computed relative Gibbs free energies for these conformers of $[dThd+Na]^+$. A more detailed discussion of the comparisons between the experimental IRMPD and calculated IR spectra of $[dThd+Na]^+$ can be found in **Reference 150**.

4.7.2 CONFORMERS OF SODIUM CATIONIZED 5-METHYLURIDINE POPULATED BY ESI

Figure 4.17 compares the experimental IRMPD and calculated IR spectra of $[Thd+Na]^+$ for conformers that exhibit good agreement. The IR spectrum calculated for the B1(O2O2') conformer of $[Thd+Na]^+$, which exhibits an *anti* orientation of the Thy nucleobase and C4'-exo ($_4T^{O}$) sugar puckering, exhibits good agreement with the experimental IRMPD spectrum; the slight broadening of the IR feature calculated at ~3420 cm^{-1} well reproduces the weak shoulder to the blue of IR feature observed. The other stable structures that exhibit a very similar conformation, i.e. B4 and B5(O2O2') exhibit virtually identical IR spectra (not shown) and thus may also be populated in the experiments. For all T(O2O4'O5') conformers, a moderate IR feature is predicted between ~3540 and 3630 cm^{-1} in the calculated IR spectra, which contributes to the

very weak IR absorption at ~3605 cm^{-1} in the experimental IRMPD spectrum of $[Thd+Na]^+$. Among all T(O2O4'O5') conformers, the IR spectrum calculated for the T2(O2O4'O5') conformer shows the best agreement with the experimental IRMPD spectrum, but slight red and blue shifts are observed for the two intense peaks predicted at ~3420 and 3682 cm^{-1}, respectively, suggesting that the T2(O2O4'O5') conformer of $[Thd+Na]^+$ is a less important contributor than B1(O2O2') in the experiments. For the lowest energy T1(O2O4'O5') conformer, this IR feature shifts to the red compared to the measured IRMPD spectrum, suggesting that the lowest energy T1(O2O4'O5') conformer may have low population in the experiments. Overall, the T(O2O4'O5') conformers have low abundances in the experiments. The calculated IR spectrum of the *anti* oriented tridentate O2 binding conformer, T1(O2O2'O3'), exhibits reasonably good agreement with the experimental IRMPD spectrum, where slight misalignments of the calculated IR spectrum from ~971 to 1166 cm^{-1} are observed, indicating that the T(O2O2'O3') conformers may also be populated in the experiments, but are probably present in lower abundance than the B1(O2O2') conformer. Similar to $[dThd+Na]^+$, the IR spectra calculated for all O4 binding and sugar binding conformers exhibit obvious spectral mismatches, such that these conformers are not present in the experiments. The two intense IR features in the high end of the IR fingerprint region are associated with the C2=O and C4=O stretches, and the IR feature at ~3420 cm^{-1} is associated with the N3–H stretch. Thus, all t2 and t4 conformers where the N3 proton has shifted to the O2 or O4 atoms are not populated, due to the significant shifts of the IR bands associated with the C2=O, C4=O and N3–H stretches.

In summary, *anti* oriented bidentate O2 binding conformers of $[Thd+Na]^+$ are dominantly populated, and *anti* oriented tridentate O2 binding conformers may also be populated, but have lower abundance than the B(O2O2') conformers. *Syn* oriented tridentate and bidentate O2 binding conformers may also be minor contributors in the experiments. Kinetic trapping of B(O2O2') conformers occurs in the ESI desolvation process, consistent with the inversion of the relative stabilities of the solvated T1(O2O4'O5') and B1(O2O2') conformers. In contrast, all conformers involving O4 binding, sugar binding, and tautomeric $[Thd+Na]^+$ are not important in the experiments. These findings are again consistent with the computed relative Gibbs free energies for the conformers of $[Thd+Na]^+$. A more detailed discussion of the comparisons between the experimental IRMPD and calculated IR spectra of $[Thd+Na]^+$ can be found in **Reference 150**.

4.7.3 VIBRATIONAL ASSIGNMENTS FOR SODIUM CATIONIZED THYMINE NUCLEOSIDES

Table 4.5 lists vibrational mode assignments for $[dThd+Na]^+$ and $[Thd+Na]^+$ based on the lowest energy conformer of $[dThd+Na]^+$ and the dominantly populated B1(O2O2') conformer of $[Thd+Na]^+$. In general, the IR features observed for $[dThd+Na]^+$ and $[Thd+Na]^+$ in the experiments are highly similar. The relatively strong IR features at ~772, 862 and 944 cm^{-1} associated with Thy twisting, C6-H wagging and sugar breathing, respectively, are only observed in the measured IRMPD spectrum of $[dThd+Na]^+$. This may be associated with inefficient dissociation of $[Thd+Na]^+$ at these low frequencies. The intense IR feature with a shoulder to the red at ~1680 cm^{-1} is contributed by C5=C6 and C2=O stretches. The intense IR feature at ~1750 cm^{-1} is associated with the C4=O stretch. Additionally, the strong IR band at 3420 cm^{-1}

represents N3–H stretching, which only occurs in the canonical forms of dThd and Thd. These spectral signatures provide strong evidence that all tautomeric $[dThd+Na]^+$ and $[Thd+Na]^+$ are not populated. In the measured IRMPD spectrum of $[Thd+Na]^+$, the IR band at 3420 cm^{-1} along with the small shoulder to the blue is contributed by the N3–H and 2'-hydroxyl stretches.

4.7.4 COMPARISONS OF THE CONFORMERS OF PROTONATED VS. SODIUM CATIONIZED THYMINE NUCLEOSIDES POPULATED BY ESI

Our previous studies of $[dThd+H]^+$ and $[Thd+H]^+$ indicated that 2,4-dihydroxy tautomer and O2 protonated conformations of dThd and Thd coexist in the gas phase.[125] The most populated conformers of protonated and sodium cationized thymine nucleosides are compared in **Figure 4.18**. For both $[dThd+H]^+$ and $[Thd+H]^+$, the lowest energy conformers are 2,4-dihydroxy tautomers (t24) with *anti* orientations of the Thy nucleobase, where the 2- and 4-hydroxyl hydrogen atoms point toward the N3 atom, and exhibit C2'-endo sugar puckering. The lowest energy O2 protonated Thy nucleosides are only 4.1 and 5.2 kJ/mol less favorable than the corresponding lowest energy conformers, respectively. The spectral comparisons between the measured IRMDP and calculated IR spectra indicate that both t24 tautomer and O2 protonated conformer coexist in the gas phase. For the sodium cationized Thy nucleosides, the lowest energy conformer of $[dThd+Na]^+$ involves tridentate binding of Na^+ to the canonical form of dThd via the O2, O4', and O5' atoms, with a *syn* orientation of the Thy nucleobase and O4'-endo ($^{O}T_1$) sugar puckering. The lowest energy conformer of $[Thd+Na]^+$ exhibits a very similar conformation, but the O4'-endo sugar puckering changes to $^{O}T_4$ due to the hydrogen-bonding interaction between the 2'- and 3'-hydroxyl substituents. However, spectral comparisons between the measured IRMPD and

calculated IR spectra indicate *anti* oriented bidentate B(O2O2') conformers of $[Thd+Na]^+$ are dominantly populated in the experiments. Compared to protonation, sodium cationization is unable to sufficiently stabilize the minor tautomers of the thymine nucleosides, such that the canonical forms of $[dThd+Na]^+$ and $[Thd+Na]^+$ have lower relative Gibbs free energies and are the only forms populated in the experiments.

4.8 CONCLUSIONS

The gas-phase conformations of 10 sodium cationized DNA and RNA nucleosides are determined via IRMPD action spectroscopy experiments and electronic structure calculations. In all cases, the sodium cation preferentially binds to both the nucleobase and sugar moieties, except for the guanine nucleosides where the sodium cation binds solely to guanine nucleobase. Theory suggests that the DNA and RNA forms of sodium cationized nucleosides exhibit highly parallel conformations. A hydrogen-bonding interaction between 2'- and 3'-hydroxyl substituents is observed in all sodium cationized RNA nucleosides due to the additional 2'-hydroxyl substituent. However, the comparisons between the experimental IRMPD and calculated IR spectra demonstrate that for pyrimidine nucleosides, the stable low-energy B1(O2O2') conformers with *anti* orientation of the nucleobase are dominantly populated in the experiments. In contrast, the ground T1(O2O4'O5') conformers with *syn* orientation of the nucleobase do not have large population. Additional binding of one or two water molecules to the sodium cationized RNA nucleosides inverts the relative Gibbs free energies of the T1(O2O4'O5') and B1(O2O2') conformers such that $[Cyd+Na]^+$, $[Urd+Na]^+$ and $[Thd+Na]^+$ exhibit an *anti* orientation with the sodium cation binding to

the O2 and O2' atoms of the pyrimidine nucleosides in aqueous solution, and the stable low-energy B1(O2O2') conformers are kinetically trapped during ESI process.

4.9 REFERENCES

119. R. R. Wu, B. Yang, C. E. Frieler, G. Berden, J. Oomens and M. T. Rodgers, *Phys. Chem. Chem. Phys.* 2015, **17**, 25978.

125. R. R. Wu, B. Yang, C. E. Frieler, G. Berden, J. Oomens and M. T. Rodgers, *J. Am. Soc. Mass Spectrom.* 2016, **27**, 410.

147. Y. Zhu, L. A. Hamlow, C. C. He, S. F. Strobehn, J. K. Lee, J. Gao, G. Berden, J. Oomens and M. T. Rodgers, *J. Phys. Chem. B* 2016, **120**, 8892.

148. Y. Zhu, L. A. Hamlow, C. C. He, J. K. Lee, J. Gao, G. Berden, J. Oomens and M. T. Rodgers, *J. Phys. Chem. B* 2017, **121**, 4048.

149. Y. Zhu, L. A. Hamlow, C. C. He, H. A. Roy, N. A. Cunningham, M. U. Munshi, G. Berden, J. Oomens and M. T. Rodgers, *Int. J. Mass Spectrom.* 2017, DOI: https://doi.org/10.1016/j.ijms.2017.04.005.

150. Y. Zhu, H. A. Roy, N. A. Cunningham, S. F. Strobehn, J. Gao, M. U. Munshi, G. Berden, J. Oomens and M. T. Rodgers, *Phys. Chem. Chem. Phys.* 2017, **19**, 17637.

151. Y. Zhu, H. A. Roy, N. A. Cunningham, S. F. Strobehn, J. Gao, M. U. Munshi, G. Berden, J. Oomens and M. T. Rodgers, *J. Am. Soc. Mass Spectrom* 2017, **28**, 2437.

180. Z. A. Tehrani, A. Fattahi and A. Pourjavadi, *Carbohydr. Res.* 2009, **344**, 771.

184. R. R. Wu, B. Yang, G. Berden, J. Oomens and M. T. Rodgers, *J. Phys. Chem. B* 2015, **119**, 2795.

185. R. R. Wu, B. Yang, G. Berden, J. Oomens and M. T. Rodgers, *J. Phys. Chem. B* 2014, **118**, 14774.

186. R. R. Wu, B. Yang, C. E. Frieler, G. Berden, J. Oomens and M. T. Rodgers, *J. Phys. Chem. B* 2015, **119**, 5773.

193. R. R. Wu, Y. Chen and M. T. Rodgers, *Phys. Chem. Chem. Phys.* 2016, **18**, 2968.

194. R. R. Wu and M. T. Rodgers, *Phys. Chem. Chem. Phys.* 2016, **18**, 24451.

195. R. R. Wu and M. T. Rodgers, *J. Phys. Chem. B* 2016, **120**, 4803.

196. R. R. Wu and M. T. Rodgers, *Phys. Chem. Chem. Phys.* 2016, **18**, 16021.

197. R. R. Wu and M. T. Rodgers, *J. Am. Soc. Mass Spectrom.* 2017, manuscript in preparation.

Table 4.1 Vibrational Assignments for $[dAdo+Na]^+$ and $[Ado+Na]^+$ [α]

Vibrational Mode	$[dAdo+Na]^+$	$[Ado+Na]^+$
C2′–C3′ stretching	930	–
Sugar ring stretching	960 to 1150	976 to ~1146
Sugar hydrogen bending	1269	1269
Nucleobase ring stretching	1583	1590
NH_2 scissoring and C–NH_2 stretching	1636	1640
NH_2 symmetric stretching	3433	3433
NH_2 asymmetric stretching	3551	3549
2′-hydroxyl stretching	–	3599
3′- and 5′-hydroxyl stretching	3659	3659

[α]All values are given in cm^{-1}. Assignments are based on the IR spectra predicted for the T1(N3O4'O5') conformers of $[dAdo+Na]^+$ and $[Ado+Na]^+$.

Table 4.2 Vibrational Assignments for $[dGuo+Na]^+$ and $[Guo+Na]^+$ [α]

Vibrational Mode	$[dGuo+Na]^+$	$[Guo+Na]^+$
Sugar ring bending	650	–
C2′–C3′ stretching	938	–
Sugar ring stretching	970 to 1145	976 to 1153
Sugar hydrogen bending	1145 to 1280	1153 to 1267
Nucleobase ring stretching	1280 to 1480	1287 to 1443
Nucleobase ring stretching	1526	1526
NH_2 scissoring	1588	1586
C–NH_2 stretching	1628	1629
C=O stretching	1685	1687
N1–H stretching	3420	3417
NH_2 symmetric stretching	3440	3435
NH_2 asymmetric stretching	3542	3543
2′-hydroxyl stretching	–	3577
3′- and 5′-hydroxyl stretching	3658	3662

[α]All values are given in cm^{-1}. Assignments are based on the IR spectra predicted for the B1(O6N7) conformers of $[dGuo+Na]^+$ and $[Guo+Na]^+$.

Table 4.3 Vibrational Assignments for $[dCyd+Na]^+$ and $[Cyd+Na]^+$ [α]

Vibrational Mode	$[dCyd+Na]^+$	$[Cyd+Na]^+$
Cytosine twisting	793	–
Sugar ring bending	855	–
Sugar ring stretching	914 to 1168	950 to 1168
Sugar hydrogen bending	1168 to 1329	1168 to 1325
Cytosine hydrogen rocking	1369	1369
NH_2 scissoring and cytosine hydrogen rocking	1482	1477
Cytosine stretching	1525	1523
NH_2 stretching	1601	1601
C=O and C–NH_2 stretching	1662	1659
NH_2 symmetric stretching and 2'-hydroxyl stretching	–	3445
NH_2 symmetric stretching	3444	–
NH_2 asymmetric stretching	3563	3564
3′- and 5′-hydroxyl stretching	3664	3666

[α]All values are given in cm^{-1}. Assignments are based on the IR spectra predicted for the T1(O2O4'O5') conformer of $[dCyd+Na]^+$ and the B1(O2O2') conformer of $[Cyd+Na]^+$.

Table 4.4 Vibrational Assignments for $[dUrd+Na]^+$ and $[Urd+Na]^+$ [α]

Vibrational Mode	$[dUrd+Na]^+$	$[Urd+Na]^+$
N3 H wagging	674	–
Uracil twisting	777	–
C5–H and C6–H wagging	802	–
C2'–C3' stretching	948	–
Sugar ring stretching	970 to 1164	970 to 1170
Sugar hydrogen bending	1164 to 1328	1170 to 1324
Uracil hydrogen rocking	1328 to 1512	1324 to 1470
C5–C6 stretching	1644	1634
C2=O stretching	1690	1674
C4=O stretching	1783	1769
N3–H stretching	3420	3420
2′-hydroxyl stretching	–	3420
3′- and 5′-hydroxyl stretching	3664	3664

[α]All values are given in cm^{-1}. The experimental bands are assigned based on the IR spectra predicted for the T1(O2O4'O5') conformer of $[dUrd+Na]^+$ and the B1(O2O2') conformer of $[Urd+Na]^+$.

Table 4.5 Vibrational Assignments for $[dThd+Na]^+$ and $[Thd+Na]^+$ [α]

Vibrational Mode	$[dThd+Na]^+$	$[Thd+Na]^+$
Thy ring twisting	772	–
C6–H wagging	862	–
Sugar ring breathing	944	–
Sugar ring stretching	964 to 1150	971 to 1166
Sugar H bending	1150 to 1320	1166 to 1310
Thy ring H rocking	1320 to 1490	1310 to 1512
C5–C6 stretching	1640	1641
C2=O stretching	1680	1671
C4=O stretching	1750	1746
N3–H stretching	3420	3420
2′O–H stretching	–	3435
3′O–H and 5′O–H stretching	3664	3664

[α]All values are given in cm^{-1}. Assignments are based on the IR spectra predicted for the T1(O2O4'O5') conformer of $[dThd+Na]^+$ and the dominantly populated B1(O2O2') conformer of $[Thd+Na]^+$.

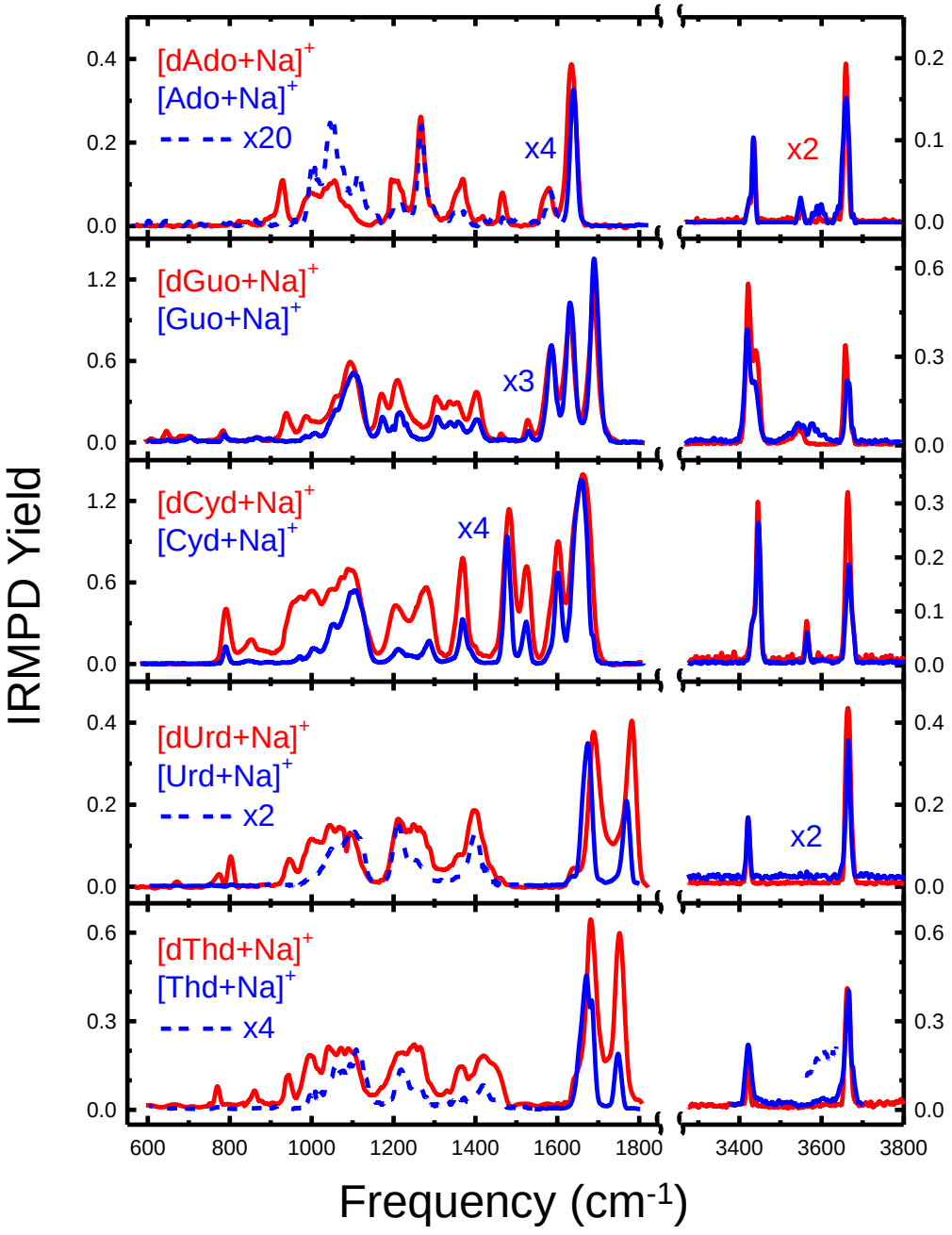

Figure 4.1 Experimental IRMPD action spectra of the sodium cationized forms of 10 DNA and RNA nucleosides in the IR fingerprint and hydrogen-stretching regions. To facilitate comparisons, several of the IR spectra have been scaled so that the IRMPD yields of the DNA and analogous RNA nucleosides are of similar intensity.

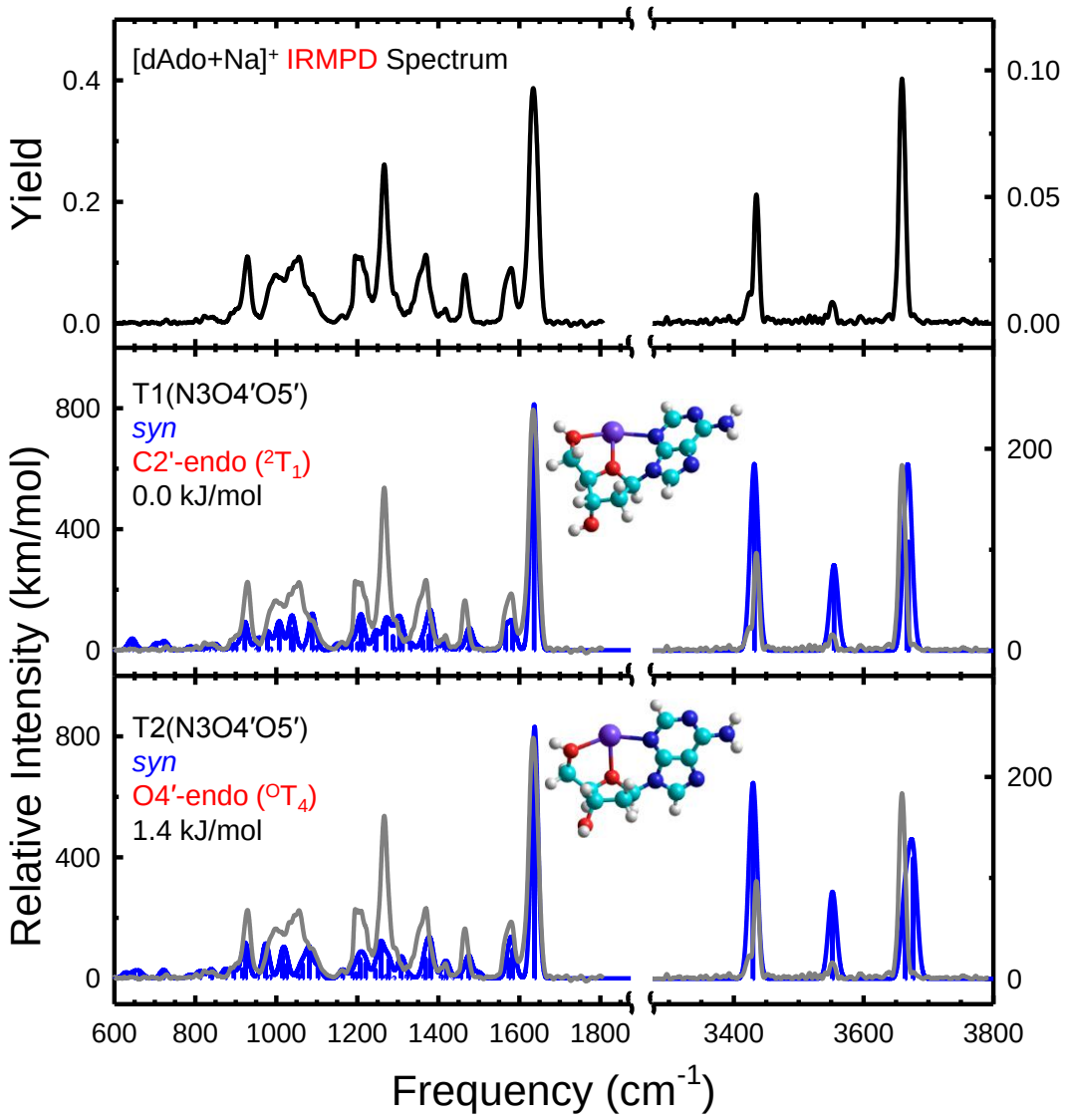

Figure 4.2 Comparison of the experimental IRMPD action spectrum of $[dAdo+Na]^+$ with the B3LYP/6-311+G(d,p) optimized structures and calculated linear IR spectra for representative low-energy conformers that best match the measured IRMPD spectrum. The nucleobase orientation, sugar puckering, and B3LYP/6-311+G(2d,2p) relative Gibbs free energies at 298 K are also shown.

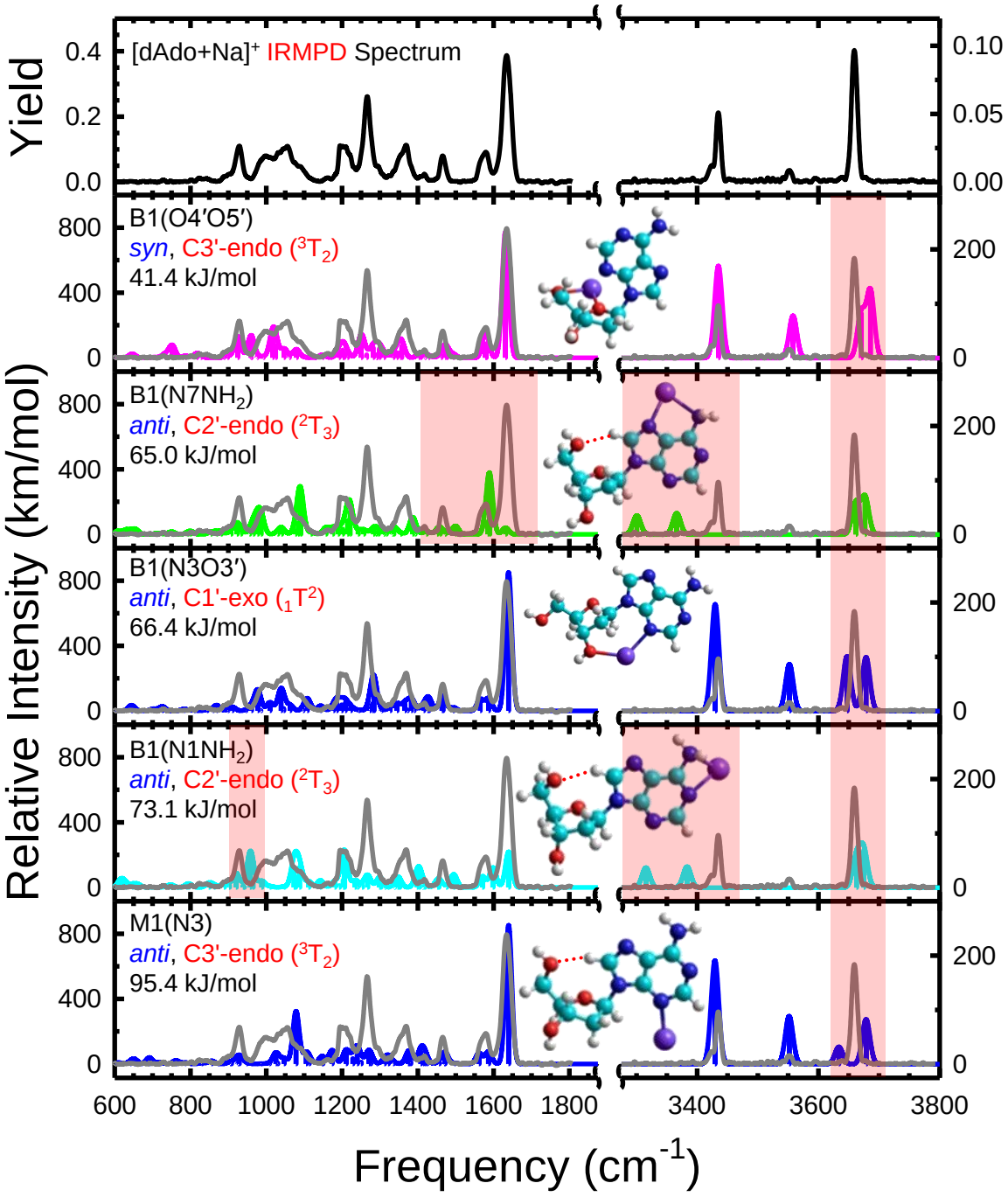

Figure 4.3 Comparison of the experimental IRMPD action spectrum of $[dAdo+Na]^+$ with the B3LYP/6-311+G(d,p) optimized structures and calculated linear IR spectra for the most stable conformers of each mode of Na^+ binding. The nucleobase orientation, sugar puckering, and B3LYP/6-311+G(2d,2p) relative Gibbs free energies at 298 K are also shown. Mismatches are shaded in red.

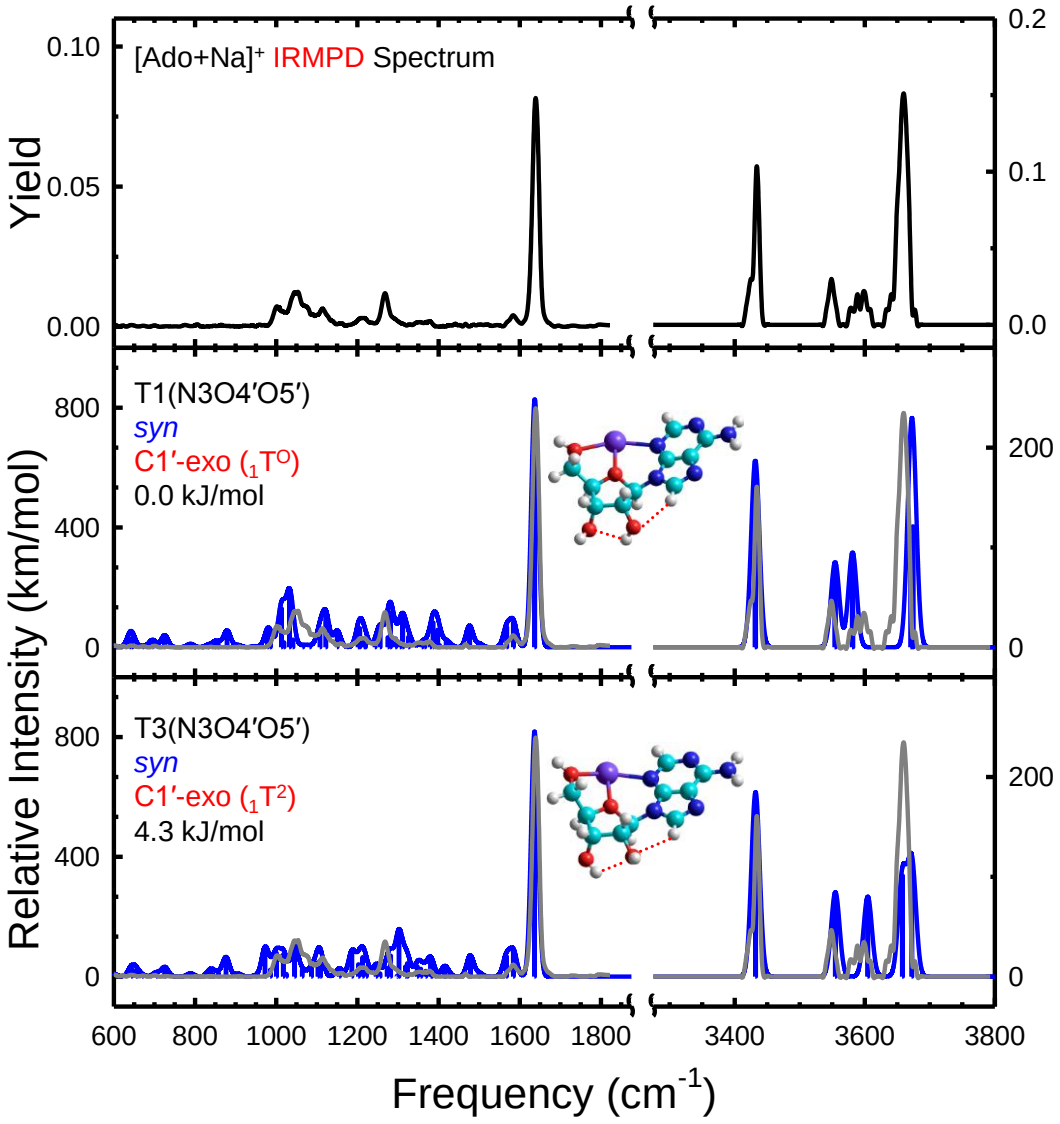

Figure 4.4 Comparison of the experimental IRMPD action spectrum of $[Ado+Na]^+$ with the B3LYP/6-311+G(d,p) optimized structures and calculated linear IR spectra for representative low-energy conformers that best match the measured IRMPD spectrum. The nucleobase orientation, sugar puckering, and B3LYP/6-311+G(2d,2p) relative Gibbs free energies at 298 K are also shown.

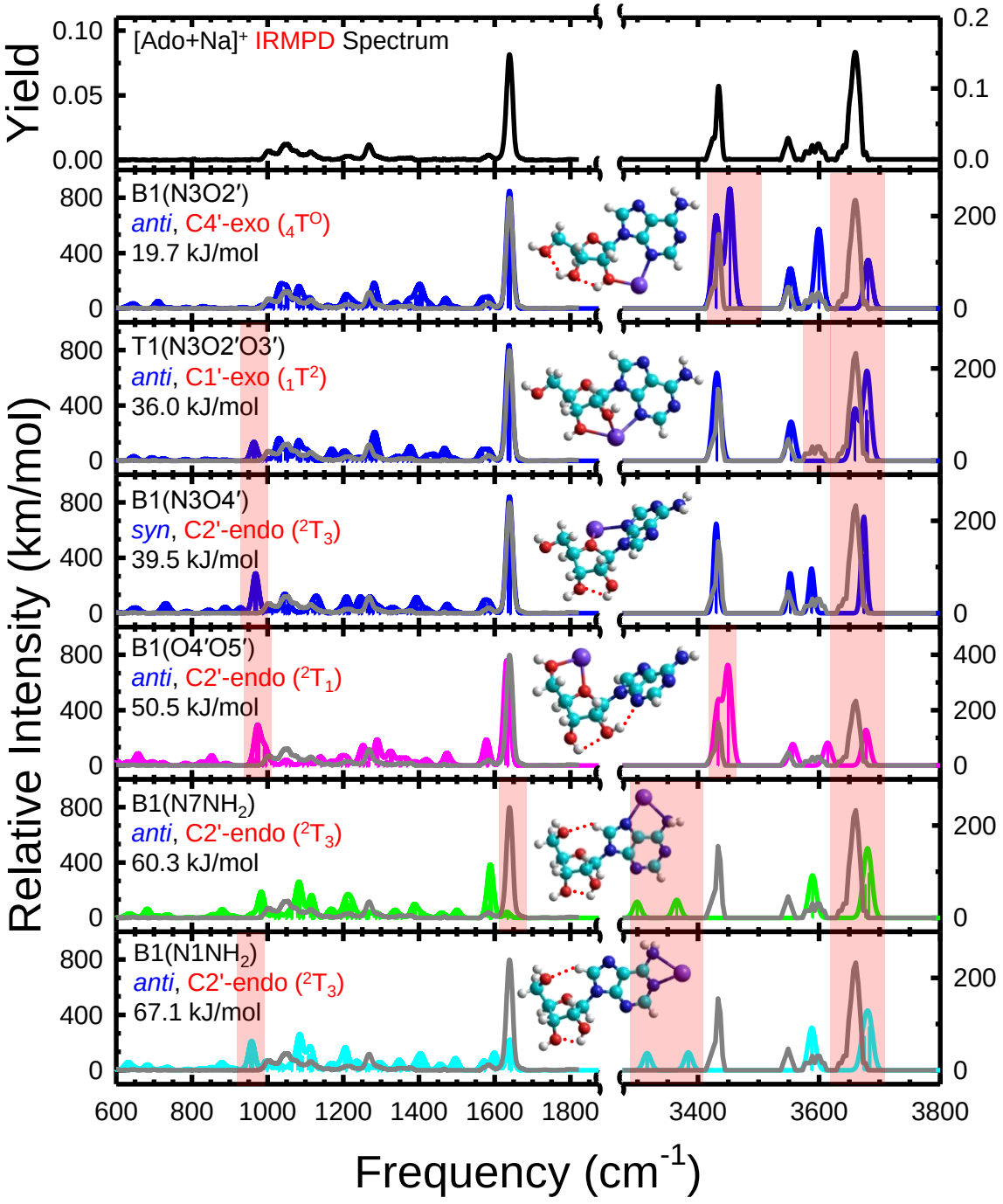

Figure 4.5 Comparison of the experimental IRMPD action spectrum of $[Ado+Na]^+$ with the B3LYP/6-311+G(d,p) optimized structures and calculated linear IR spectra for the most stable conformers of each mode of Na^+ binding. The nucleobase orientation, sugar puckering, and B3LYP/6-311+G(2d,2p) relative Gibbs free energies at 298 K are also shown. Mismatches are shaded in red.

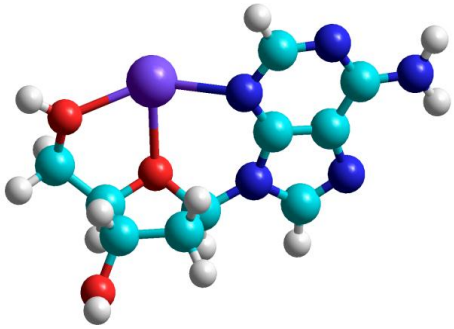

[dAdo+Na]$^+$
T1(N3O5'O4')
syn, C2'-endo ($^2T_1$)

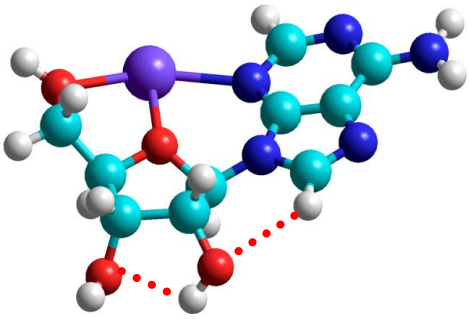

[Ado+Na]$^+$
T1(N3O4'O5')
syn, C1'-exo ($_1T^2$)

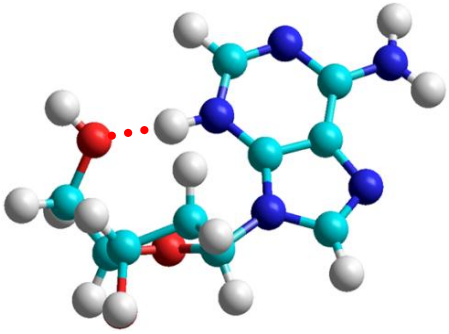

[dAdo+H]$^+$
(N3)1
syn, C2'-endo ($^2T_1$)

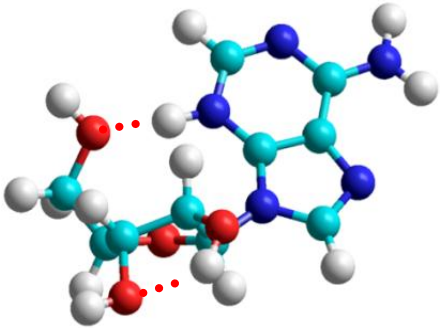

[Ado+H]$^+$
(N3)1
syn, C2'-endo ($^2T_1$)

Figure 4.6 The ground T1(N3O4'O5') conformers of [dAdo+Na]$^+$ and [Ado+Na]$^+$ which are dominantly populated are shown along with the nucleobase orientation and sugar puckering. The most populated N3 protonated conformers of [dAdo+H]$^+$ and [Ado+H]$^+$ are also shown along with the nucleobase orientation and sugar puckering and are taken from **Reference 183**.

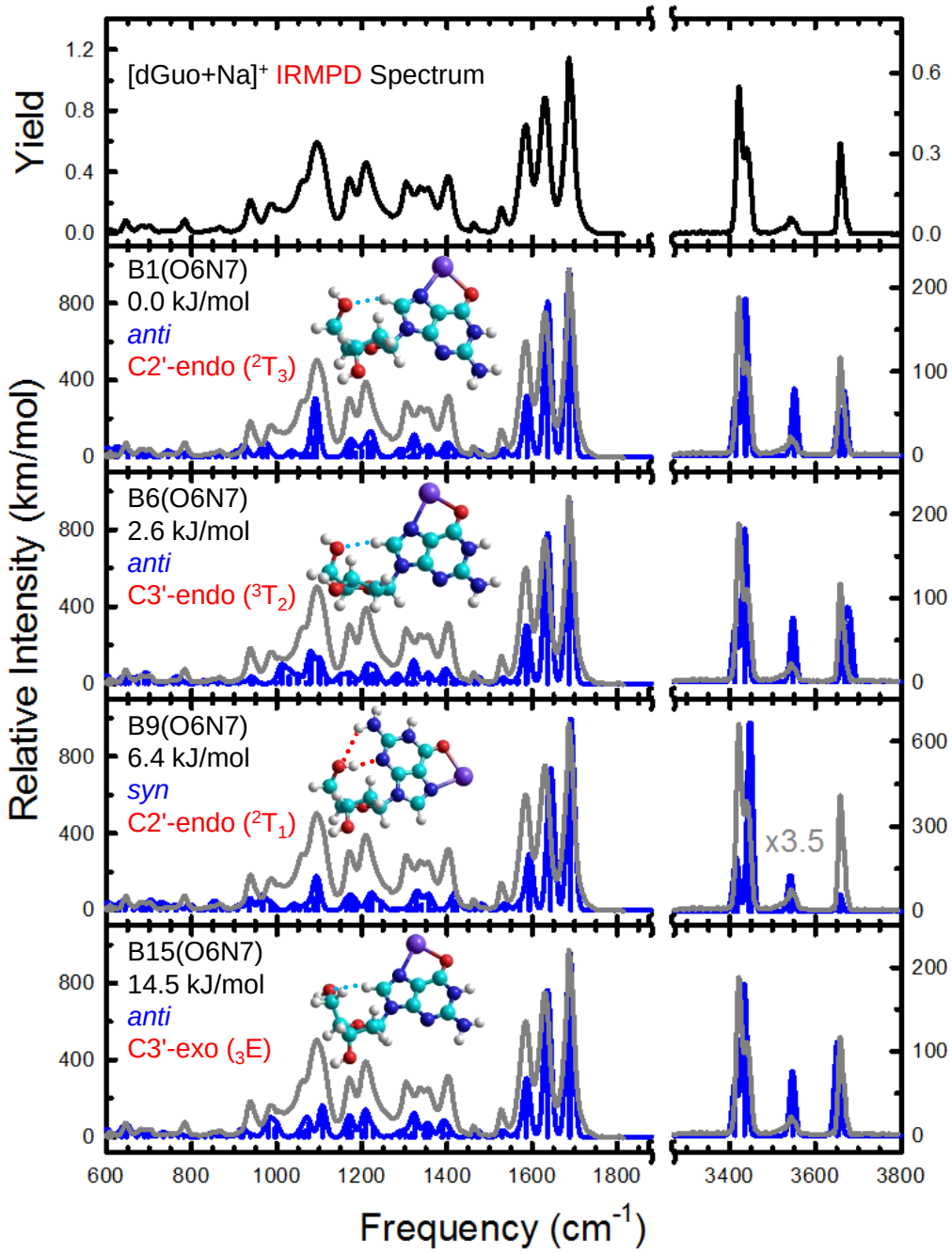

Figure 4.7 Comparison of the experimental IRMPD action spectrum of $[dGuo+Na]^+$ with the B3LYP/6-311+G(d,p) optimized structures and calculated linear IR spectra for representative low-energy conformers that best match the measured IRMPD spectrum. The nucleobase orientation, sugar puckering, and B3LYP/6-311+G(2d,2p) relative Gibbs free energies at 298 K are also shown.

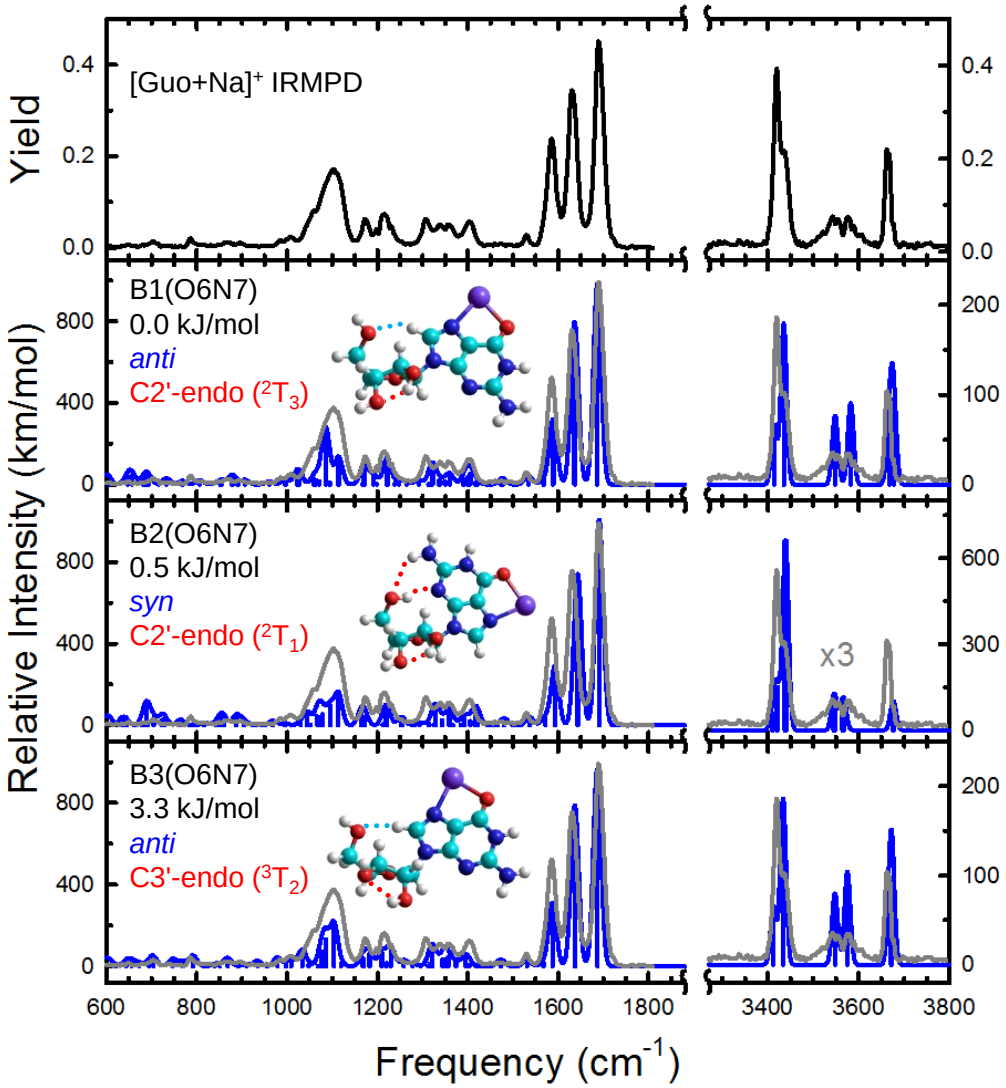

Figure 4.8 Comparison of the experimental IRMPD action spectrum of $[Guo+Na]^+$ with the B3LYP/6-311+G(d,p) optimized structures and calculated linear IR spectra for representative low-energy conformers that best match the measured IRMPD spectrum. The nucleobase orientation, sugar puckering, and B3LYP/6-311+G(2d,2p) relative Gibbs free energies at 298 K are also shown.

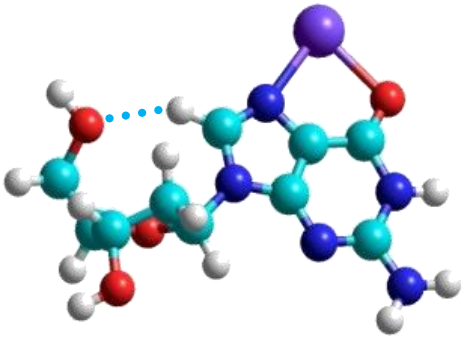

[dGuo+Na]$^+$
B1(O6N7)
anti, C2'-endo ($^2T_3$)

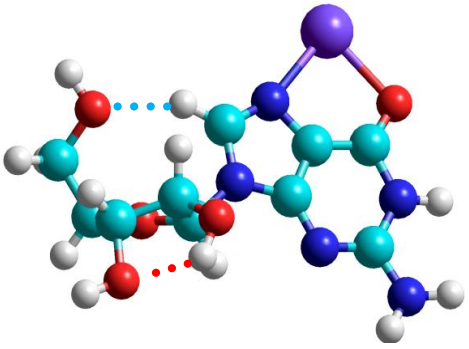

[Guo+Na]$^+$
B1(O6N7)
anti, C2'-endo ($^2T_3$)

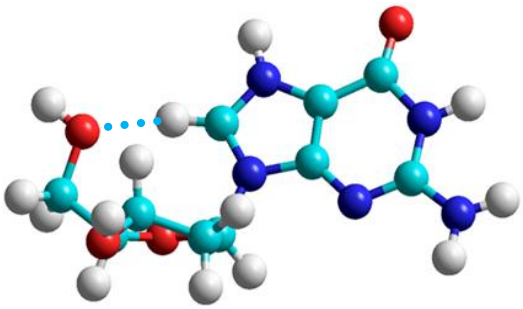

[dGuo+H]$^+$
(N7)1
anti, C3'-endo ($^3T_2$)

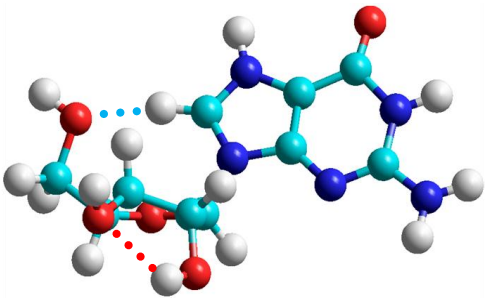

[Guo+H]$^+$
(N7)1
anti, C3'-endo ($^3T_2$)

Figure 4.9 The ground B1(O6N7) conformers of [dGuo+Na]$^+$ and [Guo+Na]$^+$ which are dominantly populated are shown along with the nucleobase orientation and sugar puckering. The most populated N7 protonated conformers of [dGuo+H]$^+$ and [Guo+H]$^+$ are also shown along with the nucleobase orientation and sugar puckering and are taken from **Reference 184**.

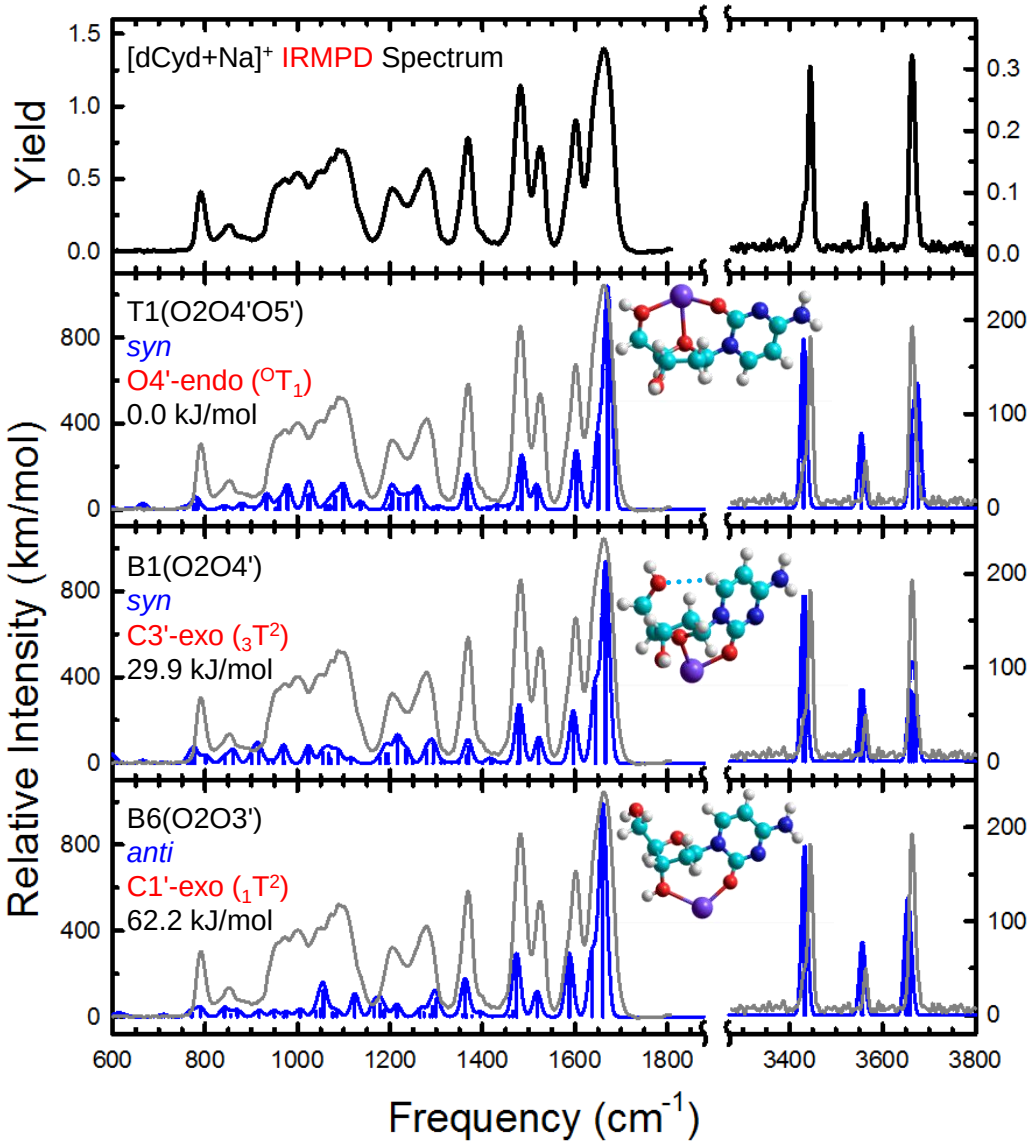

Figure 4.10 Comparison of the experimental IRMPD action spectrum of $[dCyd+Na]^+$ with the B3LYP/6-311+G(d,p) optimized structures and calculated linear IR spectra for representative low-energy conformers that best match the measured IRMPD spectrum. The nucleobase orientation, sugar puckering, and B3LYP/6-311+G(2d,2p) relative Gibbs free energies at 298 K are also shown.

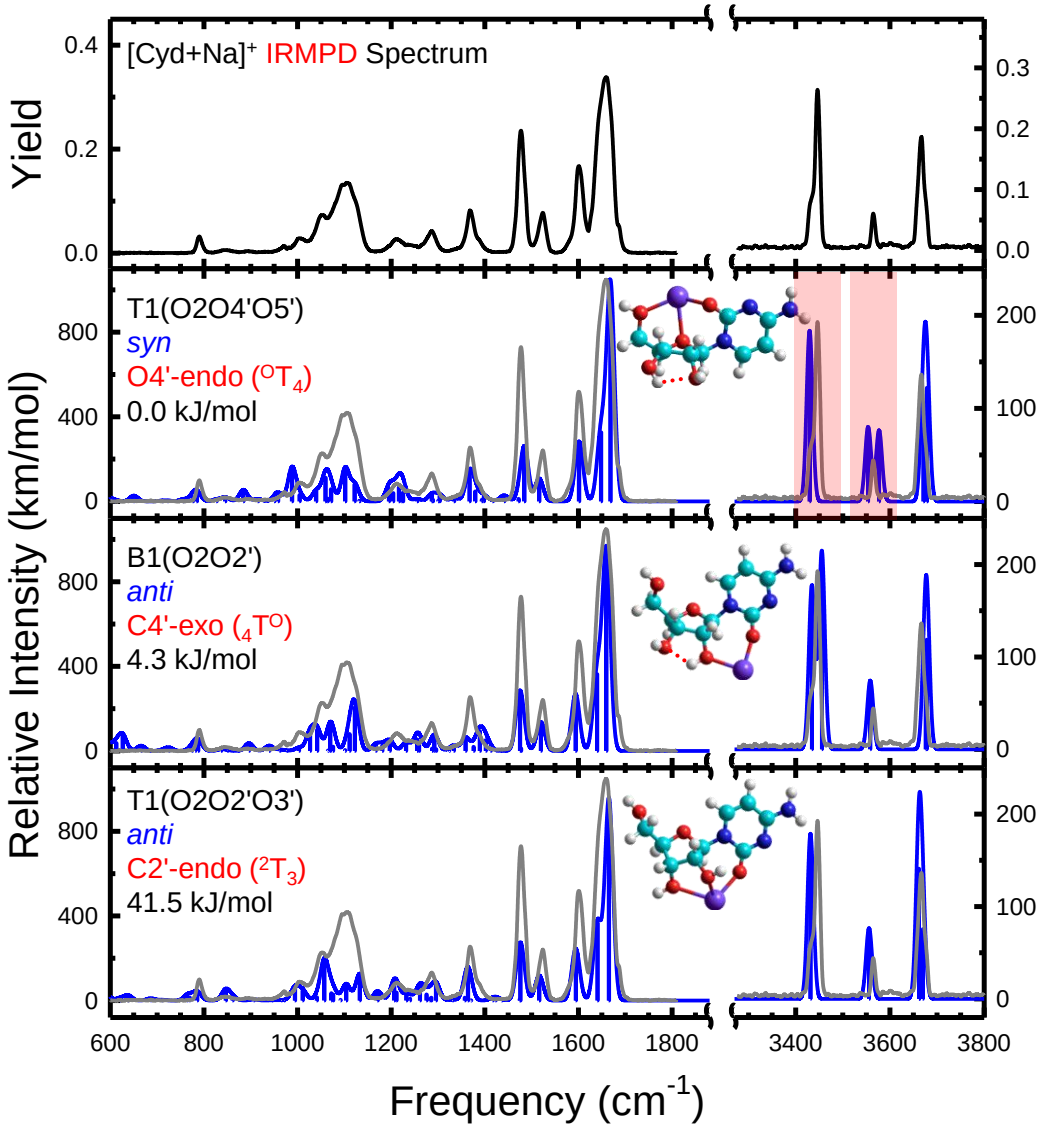

Figure 4.11 Comparison of the experimental IRMPD action spectrum of $[Cyd+Na]^+$ with the B3LYP/6-311+G(d,p) optimized structures and calculated linear IR spectra for the ground conformer and representative low-energy conformers that best match the measured IRMPD spectrum. The nucleobase orientation, sugar puckering, and B3LYP/6-311+G(2d,2p) relative Gibbs free energies at 298 K are also shown.

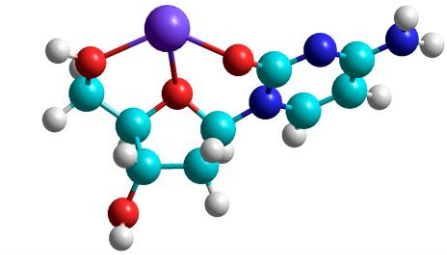

[dCyd+Na]$^+$
T1(O2O4′O5′)
syn, O4′-endo ($^{O}T_1$)

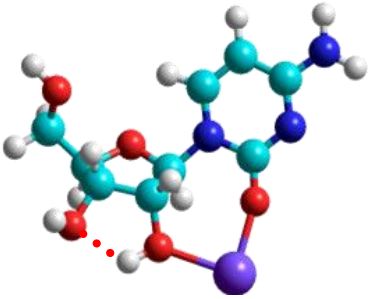

[Cyd+Na]$^+$
B1(O2O2′)
anti, O4′-exo ($_4T^{O}$)

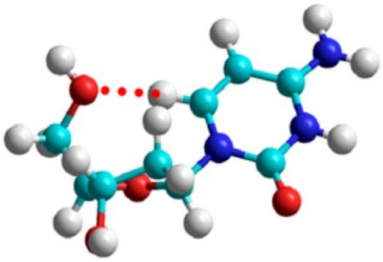

[dCyd+H]$^+$
(N3)1
anti, C2′-endo ($^2T_3$)

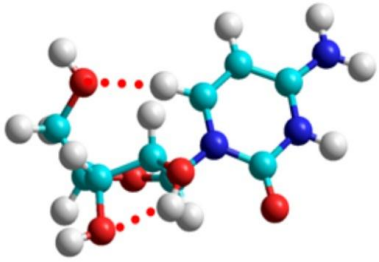

[Cyd+H]$^+$
(N3)1
anti, C2′-endo ($^2T_3$)

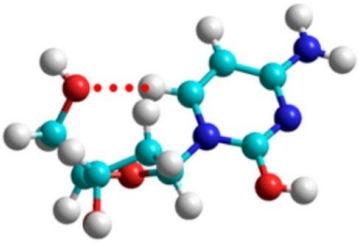

[dCyd+H]$^+$
(O2)1
anti, C2′-endo ($^2T_3$)

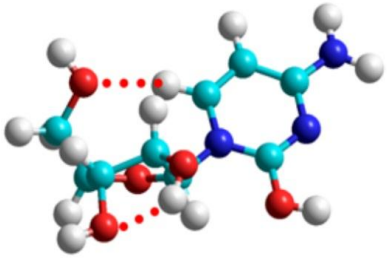

[Cyd+H]$^+$
(O2)1
anti, C2′-endo ($^2T_3$)

Figure 4.12 The T1(O2O4′O5′) conformer of [dCyd+Na]$^+$ and the B1(O2O2′) conformer of [Cyd+Na]$^+$ that are dominantly populated are shown along with the nucleobase orientation and sugar puckering. The most populated N3 and O2 protonated conformers of [dCyd+H]$^+$ and [Cyd+H]$^+$ are also shown along with the nucleobase orientation and sugar puckering and are taken from **Reference 185**.

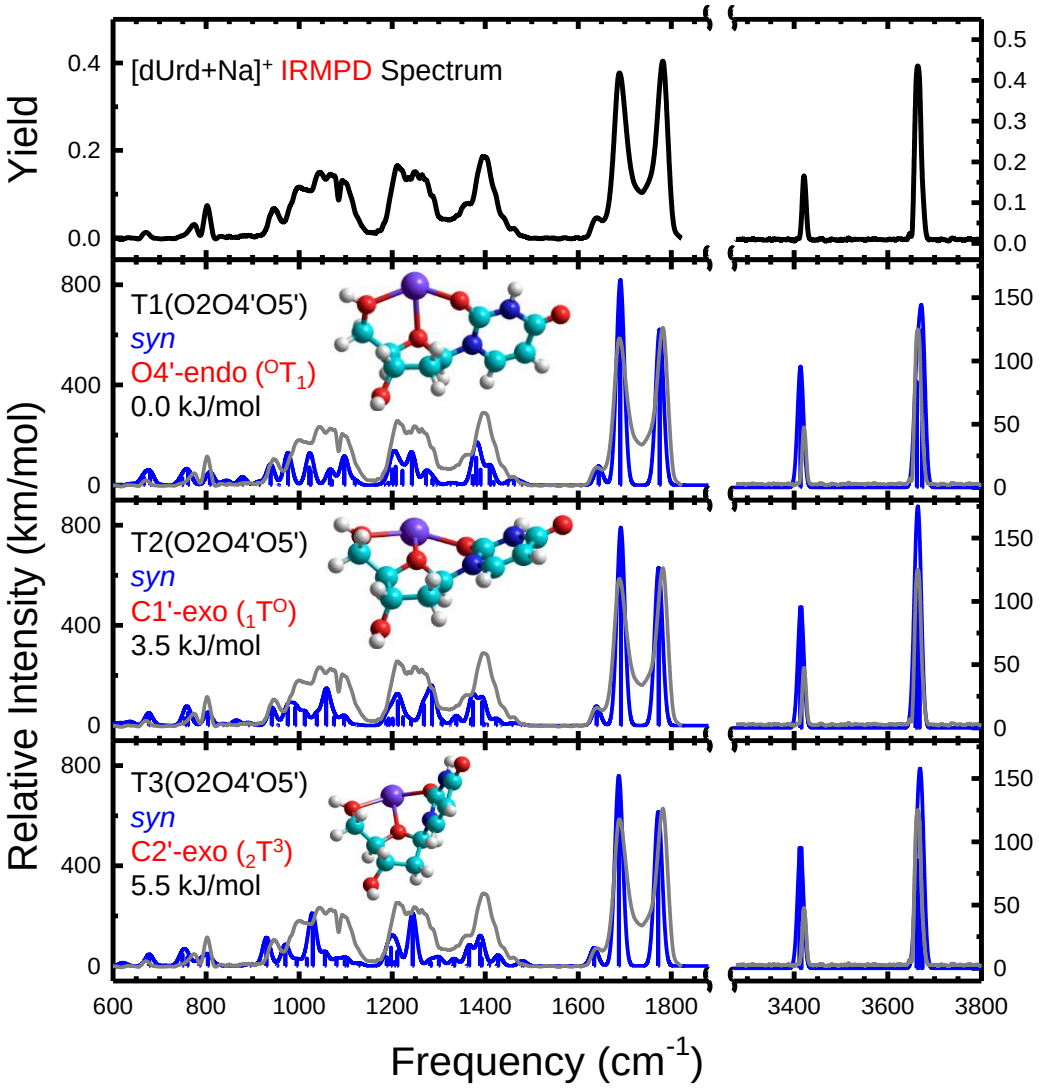

Figure 4.13 Comparison of the experimental IRMPD action spectrum of $[dUrd+Na]^+$ with the B3LYP/6-311+G(d,p) optimized structures and calculated linear IR spectra for representative low-energy conformers that best match the measured IRMPD spectrum. The nucleobase orientation, sugar puckering, and B3LYP/6-311+G(2d,2p) relative Gibbs free energies at 298 K are also shown.

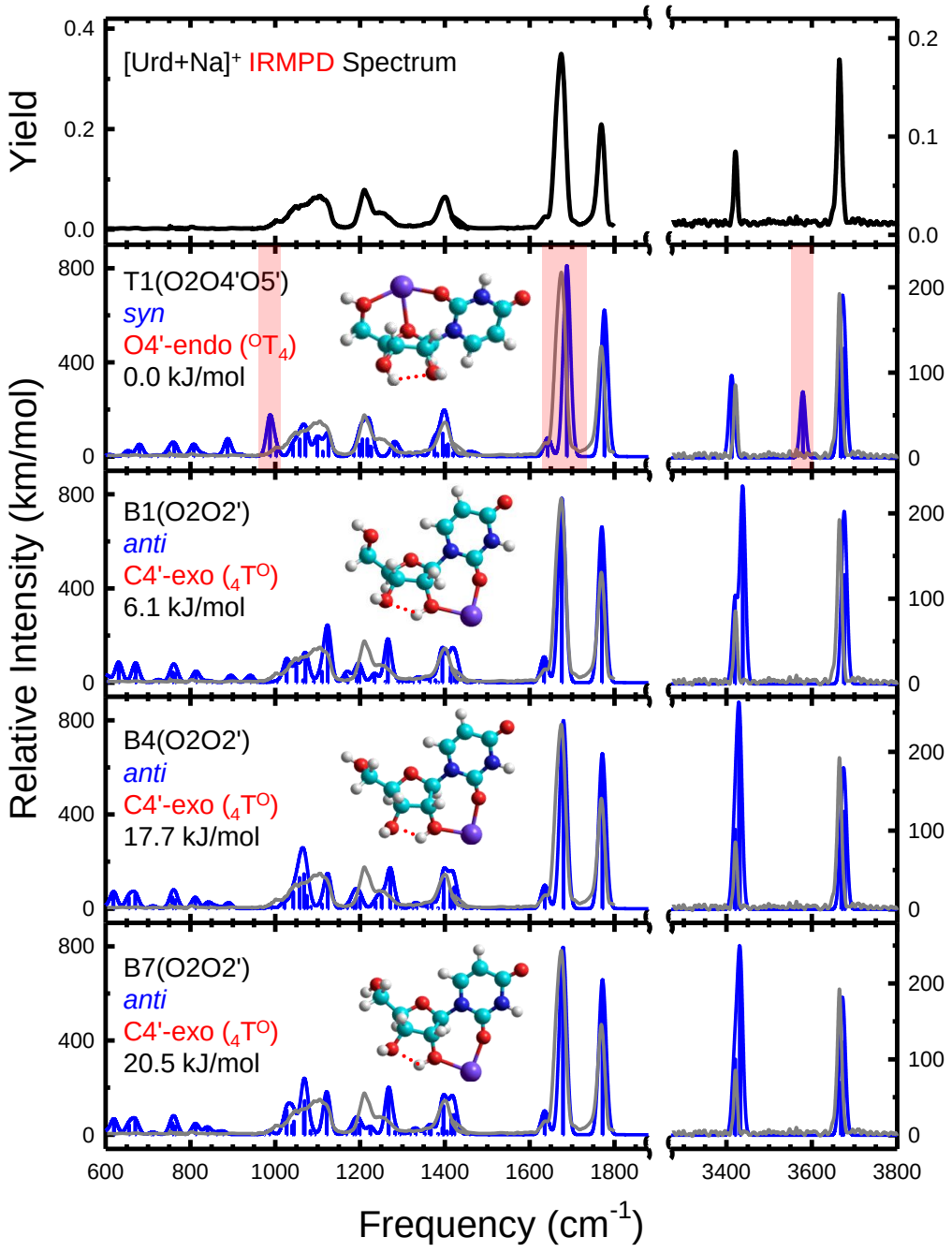

Figure 4.14 Comparison of the experimental IRMPD action spectrum of $[Urd+Na]^+$ with the B3LYP/6-311+G(d,p) optimized structures and calculated linear IR spectra for the ground conformer and representative low-energy conformers that best match the measured IRMPD spectrum. The nucleobase orientation, sugar puckering, and B3LYP/6-311+G(2d,2p) relative Gibbs free energies at 298 K are also shown.

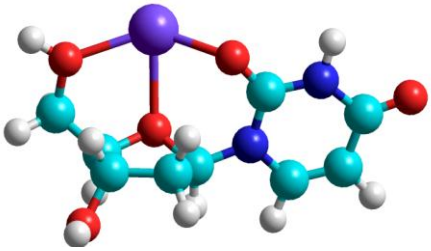

[dUrd+Na]$^+$
T1(O2O4′O5′)
syn, O4′-endo ($^{O}T_1$)

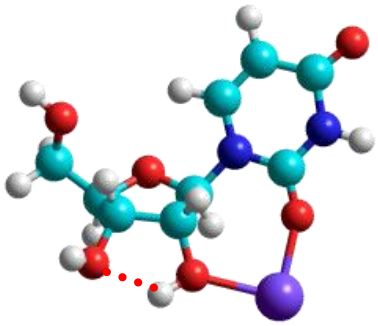

[Urd+Na]$^+$
B1(O2O2′)
anti, C4′-exo ($_4T^{O}$)

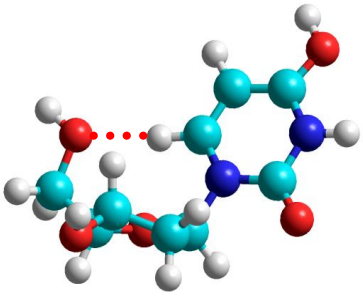

[dUrd+H]$^+$
(O4)1
anti, C3′-endo ($^3T_2$)

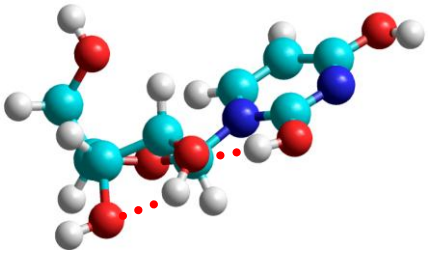

[Urd+H]$^+$
(t24)1
anti, C2′-endo ($^2T_3$)

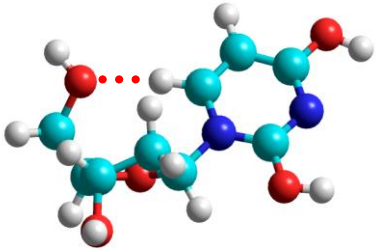

[dUrd+H]$^+$
(t24)1
anti, C2′-endo ($^2T_3$)

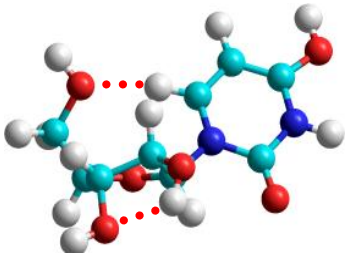

[Urd+H]$^+$
(O4)1
anti, C2′-endo ($^2T_3$)

Figure 4.15 The T1(O2O4′O5′) conformer of [dUrd+Na]$^+$ and the B1(O2O2′) conformer of [Urd+Na]$^+$ that are dominantly populated are shown along with the nucleobase orientation and sugar puckering. The most populated t24 and O4 protonated conformers of [dUrd+H]$^+$ and [Urd+H]$^+$ are also shown along with the nucleobase orientation and sugar puckering and are taken from **Reference 119**.

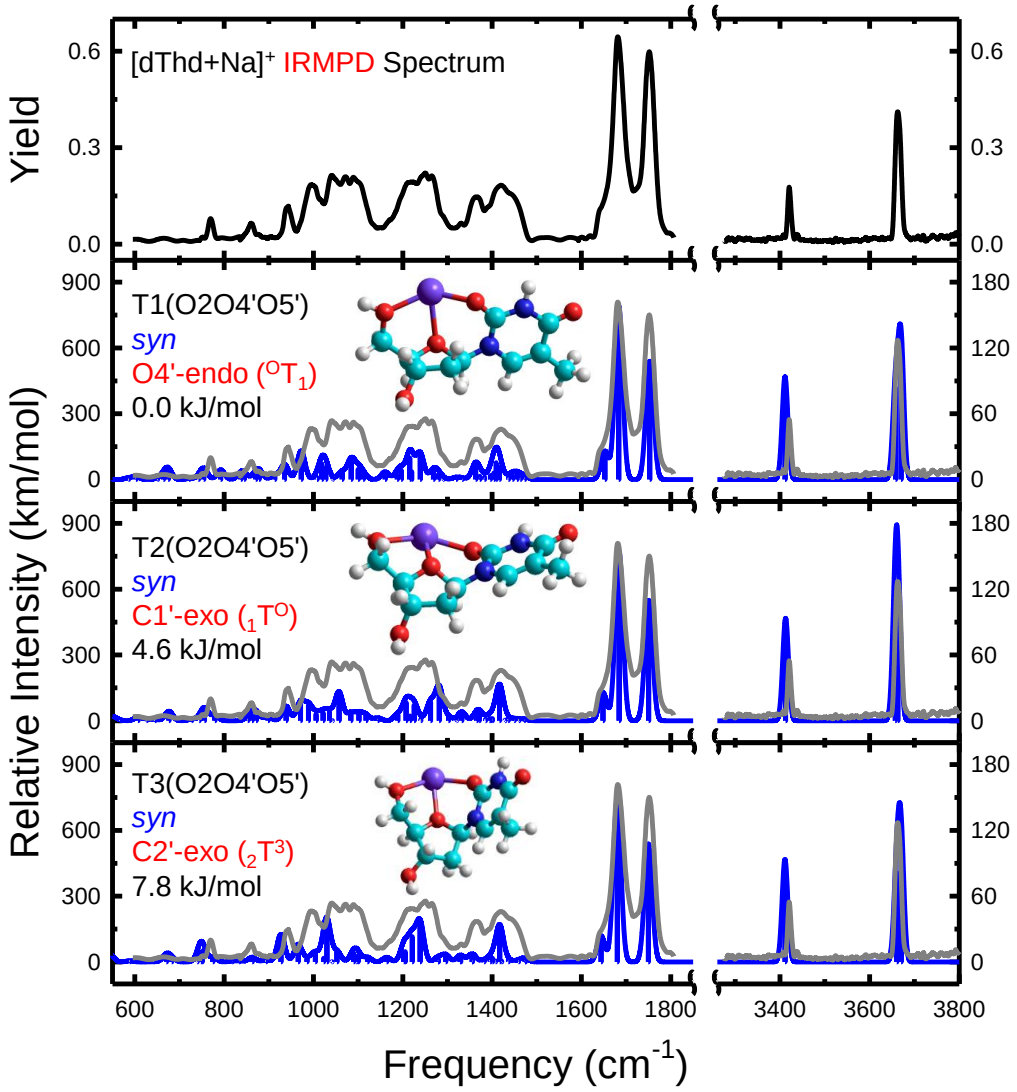

Figure 4.16 Comparison of the experimental IRMPD action spectrum of $[dThd+Na]^+$ with the B3LYP/6-311+G(d,p) optimized structures and calculated linear IR spectra for representative low-energy conformers that best match the measured IRMPD spectrum. The nucleobase orientation, sugar puckering, and B3LYP/6-311+G(2d,2p) relative Gibbs free energies at 298 K are also shown.

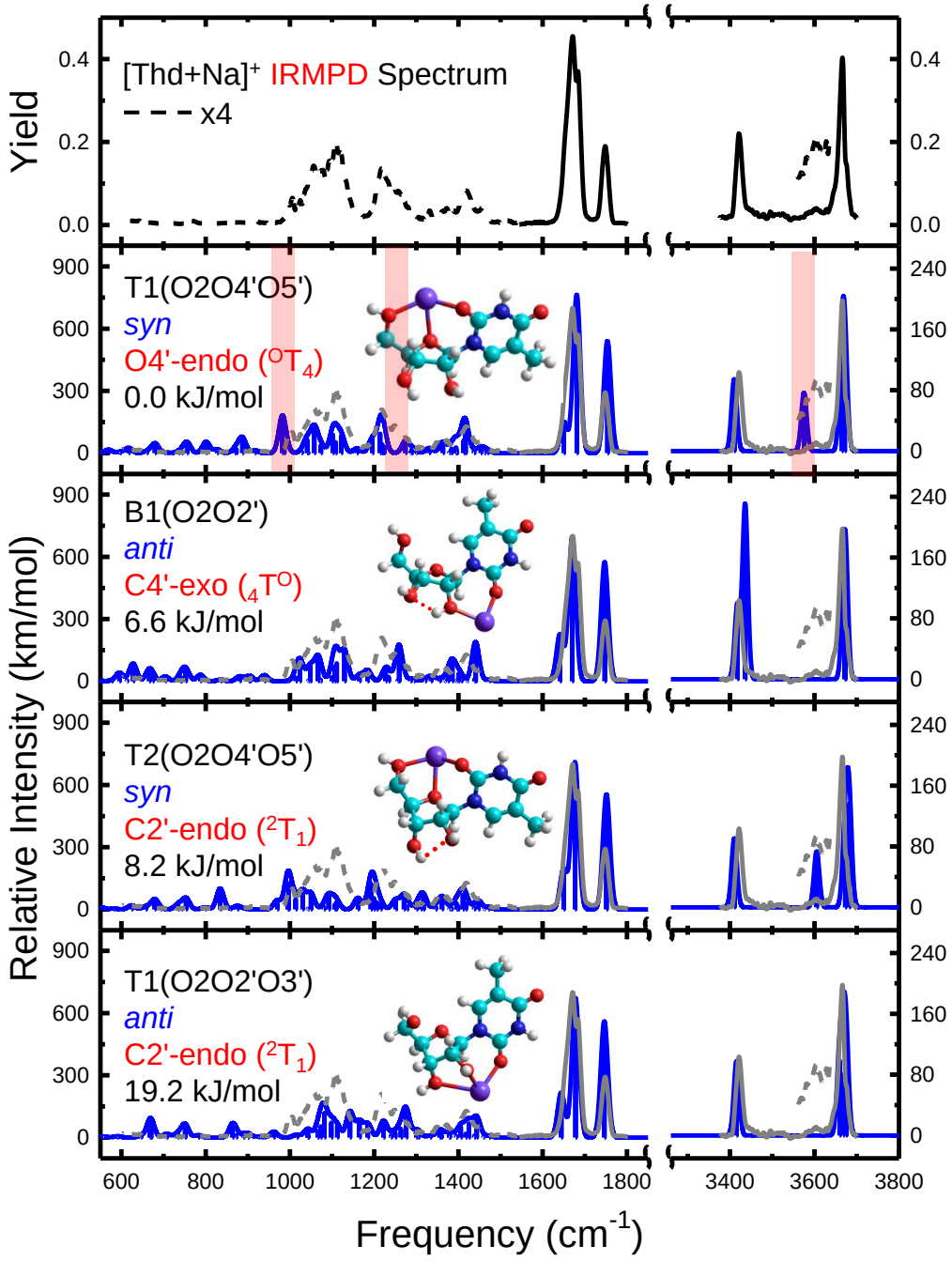

Figure 4.17 Comparison of the experimental IRMPD action spectrum of $[Thd+Na]^+$ with the B3LYP/6-311+G(d,p) optimized structures and calculated linear IR spectra for the ground conformer and representative low-energy conformers that best match the measured IRMPD spectrum. The nucleobase orientation, sugar puckering, and B3LYP/6-311+G(2d,2p) relative Gibbs free energies at 298 K are also shown.

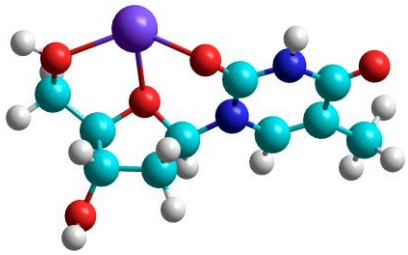

$[dThd+Na]^+$
T1(O2O4′O5′)
syn, O4′-endo ($^{O}T_1$)

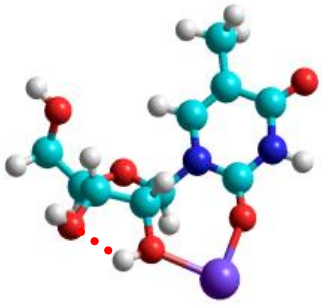

$[Thd+Na]^+$
B1(O2O2′)
anti, C4′-exo ($_4T^{O}$)

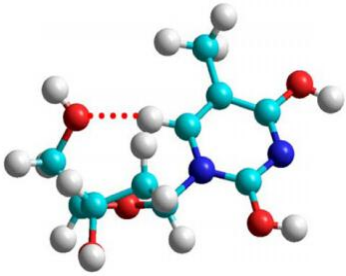

$[dThd+H]^+$
(t24)1
anti, C2′-endo ($^2T_3$)

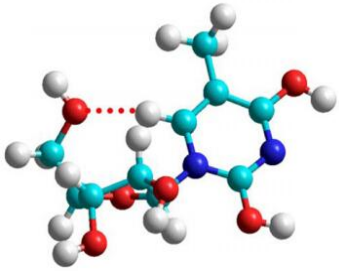

$[Thd+H]^+$
(t24)1
anti, C2′-endo ($^2T_3$)

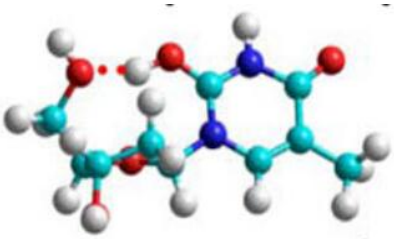

$[dThd+H]^+$
(O2)1
syn, C2′-endo ($^2T_3$)

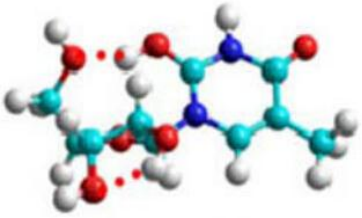

$[Thd+H]^+$
(O2)1
syn, C2′-endo ($^2T_3$)

Figure 4.18 The T1(O2O4′O5′) conformer of $[dThd+Na]^+$ and the B1(O2O2′) conformer of $[Thd+Na]^+$ that are dominantly populated are shown along with the nucleobase orientation and sugar puckering. The most populated t24 and O4 protonated conformers of $[dThd+H]^+$ and $[Thd+H]^+$ are also shown along with the nucleobase orientation and sugar puckering and are taken from **Reference 125**.

CHAPTER 5 ER-CID EXPERIMENTS AND SURVIVAL YIELD ANALYSES

Portions of this chapter were reprinted with permission from the followed research publications. Y. Zhu, L. A. Hamlow, C. C. He, S. F. Strobehn, J. K. Lee, J. Gao, G. Berden, J. Oomens and M. T. Rodgers, *J. Phys. Chem. B* 2016, **120**, 8892. Copyright 2016 American Chemistry Society. Y. Zhu, L. A. Hamlow, C. C. He, J. K. Lee, J. Gao, G. Berden, J. Oomens and M. T. Rodgers, *J. Phys. Chem. B* 2017, **121**, 4048. Copyright 2017 American Chemistry Society. Y. Zhu, L. A. Hamlow, C. C. He, H. A. Roy, N. A. Cunningham, M. U. Munshi, G. Berden, J. Oomens and M. T. Rodgers, *Int. J. Mass Spectrom.* 2017, https://doi.org/10.1016/j.ijms.2017.04.005. Copyright 2017 Elsevier B.V. Y. Zhu, H. A. Roy, N. A. Cunningham, S. F. Strobehn, J. Gao, M. U. Munshi, G. Berden, J. Oomens and M. T. Rodgers, *Phys. Chem. Chem. Phys.* 2017, **19**, 17637. Copyright 2017 Royal Society of Chemistry. Y. Zhu, H. A. Roy, N. A. Cunningham, S. F. Strobehn, J. Gao, M. U. Munshi, G. Berden, J. Oomens and M. T. Rodgers, *J. Am. Soc. Mass Spectrom*. 2017, **28**, 2423. Copyright 2017 American Society for Mass Spectrometry.

5.1 INTRODUCTION

The motivations for elucidation of the relative stabilities of DNA and RNA nucleosides are introduced in **Chapter 1**. In order to determine the relative stabilities of DNA and RNA nucleosides, energy-resolved collision-induced dissociation (ER-CID) experiments were performed using an amaZon ETD quadrupole ion trap mass spectrometer (QIT MS). The experimental procedures were introduced in **Section 2.2.1**. The survival yields of the precursor ions at each rf excitation amplitude (rf_{EA}) were calculated as described in **Section 2.2.2**, and then plotted as a function of rf_{EA} to

generate the survival yield plots. In this chapter, the relative stabilities of the protonated and sodium cationized forms of 10 DNA and RNA nucleosides are elucidated, including 2'-deoxyadenosine (dAdo), adenosine (Ado), 2'-deoxyguanosine (dGuo), guanosine (Guo), 2'-deoxycytidine (dCyd), cytidine (Cyd), 2'-deoxyuridine (dUrd), uridine (Urd), thymidine (dThd), and 5-methyluridine (Thd).[147-151] These results provide insight regarding the effects of protonation vs. sodium cationization on the relative stabilities of DNA and RNA nucleosides, as well as the effects of 2'-hydroxyl substituent of RNA nucleosides on the relative stabilities of these species. Furthermore, in favorable cases where the fragmentation pathways of these complexes involve solely N-glycosidic bond cleavage, the $CID_{50\%}$ values, which are the rf_{EA} required to produce 50% dissociation of the precursor ions, are directly correlated with the relative N-glycosidic bond stabilities. In addition, the effects of modifications of nucleosides and local environment on the relative stabilities of DNA and RNA nucleosides are also introduced. In present work, several sugar modifications, including 2'-fluoro substitution, 2'-O-methylation, and inversion of the 2'-stereochemistry on the relative N-glycosidic bond stabilities are also examined and discussed. The systems examined in present work are the protonated and sodium cationized forms of these modified nucleosides. The 2'-fluoro substituted nucleosides examined include 2'-deoxy-2'-fluoroadenosine (Adofl), 2'- deoxy-2'-fluorocytidine (Cydfl), 2'- deoxy-2'-fluoroguanosine (Guofl), and 2'- deoxy-2'-fluorouridine (Urdfl). The 2'-O-methylated nucleosides examined include 2'-O-methyladenosine (Adom), 2'-O-methylguanosine (Guom), 2'-O-methylcytidine (Cydm), 2'-O-methyluridine (Urdm), 2'-O-methylthymidine (Thdm). The arabinose nucleosides examined include adenine 9-β-D-arabinofuranoside (araAdo), guanine 9-β-D-

arabinofuranoside (areGuo), cytosine 1-β-D-arabinofuranoside (araCyd), and uracil 1-β-D-arabinofuranoside (araUrd), Several methylated guanosines are also elucidated to examine the effects of the positions of methylation on the relative N-glycosidic bond stabilities of guanosines. The methylated guanosines examined include 1-methylguanosine (m_1Guo), 7-methylguanosine (m_7Guo), N_2,N_2-dimethylguanosine (m_{22}Guo), and N2,N2,2'-trimethylguanosine (m_{22}Guom). The chemical structures of these modified nucleosides are shown in **Figures 2.3** and **2.4**. These studies are extended to include other metal cations, Li^+, K^+, Rb^+, Cs^+, and Ag^+ for dGuo and Guo to further elucidate the relative propensities of these metal cations for activating the N-glycosidic bond. In this chapter, the CID mass spectra and survival yield analyses of protonated and sodium cationized DNA and RNA nucleosides are discussed in detail. For the studies of the effects of modifications and the local environment on the relative stabilities of the DNA and RNA nucleosides, I mainly focus on comparisons of the $CID_{50\%}$ values of these complexes, but the mode of cation binding also comes in to play.

5.2 ENERGY-RESOLVED COLLISION-INDUCED DISSOCIATION OF PROTONATED AND SODIUM CATIONIZED DNA AND RNA NUCLEOSIDES

All CID fragmentation pathways observed for the protonated and sodium cationized DNA and RNA nucleosides are summarized in **Reactions 5.1-5.10**,

$$[\text{Nuo+M}]^+ \xrightarrow{n\ \text{He}} [\text{Nue+M}]^+ + (\text{Nuo}-\text{Nue}) \quad (5.1)$$

$$[\text{Nuo+M}]^+ \xrightarrow{n\ \text{He}} [\text{Nuo}-\text{Nue+M}]^+ + \text{Nue} \quad (5.2)$$

$$[\text{Nuo+M}]^+ \xrightarrow{n\ \text{He}} \text{M}^+ + \text{Nuo} \quad (5.3)$$

$$[\text{Nuo+M}]^+ \xrightarrow{n\ \text{He}} [\text{Nuo}-\text{W+M}]^+ + \text{W} \quad (5.4)$$

$$[\text{Nuo+M}]^+ \xrightarrow{n\ \text{He}} [\text{Nuo}-2\text{W+M}]^+ + 2\text{W} \quad (5.5)$$

$$[\text{Nuo+M}]^+ \xrightarrow{n\,\text{He}} [\text{Nuo–Nue–W+M}]^+ + \text{Nue} + \text{W} \quad (5.6)$$

$$[\text{Nuo+M}]^+ \xrightarrow{n\,\text{He}} [\text{Nuo–Nue–2W+M}]^+ + \text{Nue} + 2\text{W} \quad (5.7)$$

$$[\text{Nuo+M}]^+ \xrightarrow{n\,\text{He}} [\text{Nue+W+M}]^+ + (\text{Nuo–Nue–W}) \quad (5.8)$$

$$[\text{Nuo+M}]^+ \xrightarrow{n\,\text{He}} [\text{Nuo–K+M}]^+ + \text{K} \quad (5.9)$$

$$[\text{Nuo+M}]^+ \xrightarrow{n\,\text{He}} [\text{Nuo–K–W+M}]^+ + \text{K} + \text{W} \quad (5.10)$$

where Nuo represents nucleoside, and Nue represents nucleobase. M is a proton or sodium cation. W represents a water molecule, and K represents ketene ($H_2C=C=O$).

5.2.1 CID MASS SPECTRA OF PROTONATED AND SODIUM CATIONIZED ADENINE NUCLEOSIDES

The CID mass spectra of the protonated and sodium cationized adenine nucleosides at an rf excitation amplitude near $CID_{50\%}$ are compared in **Figure 5.1**. For $[dAdo+H]^+$ and $[Ado+H]^+$, the only fragmentation pathway observed is N-glycosidic bond cleavage leading to the production of protonated adenine, **Reaction 5.1**. For $[dAdo+Na]^+$, two fragmentation pathways are observed, both involving N-glycosidic bond cleavage with the sodium cation competitively retained by the adenine nucleobase or the sugar moiety, **Reactions 5.1** and **5.2**. It is likely that **Reaction 5.3** also occurs, but cannot be detected as its ionic product, Na^+, has an m/z below the low-mass cut-off of the QIT MS. In contrast, for $[Ado+Na]^+$, although the intensity of the precursor ion decreases as the rf excitation voltage is increased, no CID products are observed. The lack of detectable CID products suggests that $[Ado+Na]^+$ undergoes CID solely by **Reaction 5.3**, indicating that the glycosidic bond of Ado is stronger than that of dAdo. Clearly, these slow-heating methods, IRMPD and multiple-collision CID, produce similar activation and fragmentation behavior.

5.2.2 CID MASS SPECTRA OF PROTONATED AND SODIUM CATIONIZED GUANINE NUCLEOSIDES

the CID mass spectra of the protonated and sodium cationized guanine nucleosides at an rf excitation amplitude near $CID_{50\%}$ are compared in **Figure 5.2**. In all cases, the CID mass spectra are very simple exhibiting only a single fragmentation pathway corresponding to N-glycosidic bond cleavage with the proton or sodium cation retained by the guanine nucleobase, as summarized in **Reaction 5.1**. Again we observe that activation by multiple low-energy collisions results in the same unimolecular decomposition pathway as activation by absorption of multiple IR photons.

5.2.3 CID MASS SPECTRA OF PROTONATED AND SODIUM CATIONIZED CYTOSINE NUCLEOSIDES

The CID mass spectra of the protonated and sodium cationized cytosine nucleosides at an rf excitation amplitude near $CID_{50\%}$ are compared in **Figure 5.3**. The major fragmentation pathway observed for the protonated and sodium cationized cytosine nucleosides involves N-glycosidic bond cleavage leading to detection of either the protonated or sodium cationized cytosine nucleobase, as shown in **Reaction 5.1**. **Reaction 5.1** is the only CID pathway observed for $[dCyd+H]^+$, $[Cyd+H]^+$, and $[dCyd+Na]^+$. Two very minor fragmentation pathways are observed in the CID mass spectrum of $[Cyd+Na]^+$, N-glycosidic bond cleavage where the sodium cation is retained by the sugar, $[Cyd\text{-}Cyt+Na]^+$ (**Reaction 5.2**), and loss of water, $[Cyd\text{-}H_2O+Na]^+$ (**Reaction 5.4**). Yet again, the fragmentation behavior induced by multiple low-energy collisions is highly parallel to that observed for multiple photon absorption, and the minor fragmentation pathways that are only observed for $[Cyd+Na]^+$ suggest that

$[dCyd+Na]^+$ and $[Cyd+Na]^+$ may exhibit different conformations, consistent with the results of IRMPD action spectroscopy experiments of sodium cytosine nucleosides, as discussed in **Section 4.5**.

5.2.4 CID MASS SPECTRA OF PROTONATED AND SODIUM CATIONIZED URACIL NUCLEOSIDES

The CID mass spectra of the protonated and sodium cationized uracil nucleosides at an rf excitation amplitude near $CID_{50\%}$ are compared in **Figure 5.4**. The major fragmentation pathways of $[Urd+H]^+$, $[dUrd+Na]^+$ and $[Urd+Na]^+$ involve N-glycosidic bond cleavage with the proton retained by uracil, and the sodium cation retained by either uracil or the sugar moiety as summarized in **Reactions 5.1** and **5.2**. **Reactions 5.1** and **5.2** are also observed in the CID mass spectrum of $[dUrd+H]^+$, but are only minor reaction pathways. For $[dUrd+H]^+$, the major fragmentation pathways involve elimination of one or two W molecules, **Reactions 5.4** and **5.5**. Three additional minor fragmentation pathways are also observed for $[dUrd+H]^+$, all of which involve N-glycosidic bond cleavage and water elimination, **Reactions 5.6**, **5.7**, and **5.8**. Three minor CID pathways are also observed for $[Urd+H]^+$ that involve fragmentation of the sugar moiety via elimination of W, **Reaction 5.4**, elimination of K, **Reaction 5.9**, or elimination of both W and K, **Reaction 5.10**. The differences in the CID behavior of $[Urd+H]^+$ vs. $[dUrd+H]^+$ also suggest that the structures accessed in the experiments differ somewhat for $[Urd+H]^+$ and $[dUrd+H]^+$, consistent with the findings in the IRMPD study of these species.[119]

Figure 5.5 shows the mass spectra for MS^3 experiments of $[dUrd-W+H]^+$, $[dUrd-2W+H]^+$, $[dUrd-Ura+H]^+$ and $[Urd-K+H]^+$. $[dUrd-2W+H]^+$ may come from a successive loss of W from $[dUrd-W+H]^+$. Loss of (W+Ura) observed for $[dUrd+H]^+$ may come from

successive losses of Ura from $[dUrd\text{-}W+H]^+$ and of W from $[dUrd\text{-}Ura+H]^+$. Loss of (K+W) observed for $[Urd+H]^+$ may come from a successive loss of W from $[Urd\text{-}K+H]^+$. The MS^3 experiment for $[Urd\text{-}W+H]^+$ could not be performed due to the very low intensity of this peak across the entire rf_{EA} range.

5.2.5 CID MASS SPECTRA OF PROTONATED AND SODIUM CATIONIZED THYMINE NUCLEOSIDES

The CID mass spectra of protonated and sodium cationized thymine nucleosides at an rf excitation amplitude near $CID_{50\%}$ are compared in **Figure 5.6**. N-glycosidic bond cleavage processes are observed as the dominant fragmentation pathways for $[Thd+H]^+$, $[dThd+Na]^+$, and $[Thd+Na]^+$, where the cation, H^+ or Na^+, is retained either by the thymine nucleobase or the sugar as summarized in **Reactions 5.1** and **5.2**. In all cases, **Reaction 5.1** is favored over **Reaction 5.2**. Indeed **Reaction 5.2** is observed as a minor fragmentation pathway for $[Thd+H]^+$ over the entire range of rf_{EA}. In contrast, **Reaction 5.1** and CID pathways that involve elimination of K, or both K and one W molecule as summarized in **Reactions 5.9** and **5.10** become more competitive for $[dThd+H]^+$. Four additional minor fragmentation pathways are also observed for $[dThd+H]^+$ that involve elimination of one or two W molecules, or elimination of the thymine nucleobase and one or two W molecules, as summarized in **Reactions 5.4**, **5.5**, **5.6** and **5.7**. **Reaction 5.4** is also observed as a minor fragmentation pathway for $[Thd+H]^+$.

Figure 5.7 shows MS^3 mass spectra for $[dThd\text{-}W+H]^+$, $[dThd\text{-}2W+H]^+$, $[dThd\text{-}K+H]^+$ and $[dThd+K\text{-}W]^+$. However, MS^3 experiments of $[dThd\text{-}Thy+H]^+$, $[dThd\text{-}Thy\text{-}W+H]^+$ and $[dThd\text{-}Thy\text{-}2W+H]^+$ could not be performed due to their low intensities in the CID experiments of $[dThd+H]^+$. $[dThd\text{-}Thy\text{-}W+H]^+$ and $[dThd\text{-}Thy\text{-}2W+H]^+$ are mainly

contributed by successive loss of Thy from $[dThd\text{-}W+H]^+$ and $[dThd\text{-}2W+H]^+$, respectively. It is clear that when glycosidic bond cleavage occurs after elimination of water that the proton is preferentially retained by the dehydrated sugar moiety. **Reaction 5.10** may occur from successive loss of W from of $[dThd\text{-}K+H]^+$. A unique MS^3 fragment, $[dThd\text{-}K\text{-}W\text{-}CH_2O+H]^+$, is observed upon dissociation of $[dThd\text{-}K+H]^+$. The successive loss of W or K is observed from the MS^3 experiment of $[dThd\text{-}K\text{-}W+H]^+$.

5.3 RELATIVE STABILITIES OF PROTONATED AND SODIUM CATIONIZED DNA AND RNA NUCLEOSIDES

5.3.1 SURVIVAL YIELD ANALYSES OF PROTONATED AND SODIUM CATIONIZED ADENINE NUCLEOSIDES

Survival yield analyses of $[dAdo+H]^+$, $[Ado+H]^+$ and $[dAdo+Na]^+$ are compared in **Figure 5.8**. Because the only fragmentation pathway observed for $[dAdo+H]^+$, $[Ado+H]^+$ and $[dAdo+Na]^+$ involves N-glycosidic bond cleavage, the trends in the $CID_{50\%}$ values provide a direct measure of the relative N-glycosidic bond stabilities. The $CID_{50\%}$ value of $[Ado+H]^+$ exceeds that of $[dAdo+H]^+$, which suggests that the 2′-hydroxyl substituent of Ado stabilizes the N-glycosidic bond. This result is consistent with TCID results recently reported for these adenine nucleosides, where the activation energies at 0 K for N-glycosidic bond cleavage of N3 protonated $[dAdo+H]^+$ and $[Ado+H]^+$ were measured as 147.6±4.8 and 164.0± 4.8 kJ/mol, respectively.[196] These trends are also consistent with the computed C1–N9 glycosidic bond lengths discussed in **Section 3.2.1**. The same conclusion can be drawn by comparing the fragmentation behavior of $[dAdo+Na]^+$ and $[Ado+Na]^+$. The only CID fragmentation pathway of $[Ado+Na]^+$ is the loss of neutral adenosine, which is empirical evidence that suggests that the N-glycosidic bond of $[Ado+Na]^+$ is more stable than that of $[dAdo+Na]^+$. In summary, the N-glycosidic bond of

dAdo is less stable than that of Ado for both the protonated and sodium cationized species. In addition, the N-glycosidic bonds of sodium cationized dAdo and Ado are more stable than those of protonated dAdo and Ado, respectively. Thus, sodium cationization activates the N-glycosidic bond less effectively than protonation.

5.3.2 SURVIVAL YIELD ANALYSES OF PROTONATED AND SODIUM CATIONIZED GUANINE NUCLEOSIDES

Survival yield analyses for the protonated and sodium cationized guanine nucleosides, $[dGuo+H]^+$, $[Guo+H]^+$, $[dGuo+Na]^+$, and $[Guo+Na]^+$, are compared in **Figure 5.9**. The only fragmentation pathway observed for these species involves N-glycosidic bond cleavage, therefore, trends in the $CID_{50\%}$ values directly correlate with the relative stabilities of the N-glycosidic bonds in these systems. The $CID_{50\%}$ of $[Guo+H]^+$ is greater than that of $[dGuo+H]^+$, indicating that the 2′-hydroxyl substituent of Guo stabilizes the N-glycosidic bond. This result is consistent with previous TCID results for $[dGuo+H]^+$ and $[Guo+H]^+$.[193] The same conclusion can be drawn via comparison of the $CID_{50\%}$ values of $[dGuo+Na]^+$ and $[Guo+Na]^+$. These results are also consistent with the bond lengths from DFT calculations discussed in **Section 3.2.2**, where the N-glycosidic bond lengths of the RNA nucleosides are slightly shorter than those of the analogous DNA nucleosides. Overall, the N-glycosidic bonds of sodium cationized guanine nucleosides are more stable than those of the analogous protonated guanine nucleosides, clearly indicating that sodium cationization activates the N-glycosidic bond, but less effectively than protonation.

5.3.3 SURVIVAL YIELD ANALYSES OF PROTONATED AND SODIUM CATIONIZED CYTOSINE NUCLEOSIDES

Survival yield analyses for the protonated and sodium cationized cytosine nucleosides, $[dCyd+H]^+$, $[Cyd+H]^+$, $[dCyd+Na]^+$, and $[Cyd+Na]^+$, are compared in **Figure 5.10**. Because the major fragmentation pathways observed for the protonated and sodium cationized cytosine nucleosides exclusively involve N-glycosidic bond cleavage, the survival yield analyses enable the relative stabilities of the N-glycosidic bonds of these species to be elucidated. The increase in the $CID_{50\%}$ values observed for both the protonated and sodium cationized species from dCyd to Cyd indicates that the 2'-hydroxyl substituent stabilizes the N-glycosidic bond. This conclusion is consistent with previous TCID results for the protonated cytosine nucleosides.[195] The sodium cationized cytosine nucleosides exhibit higher $CID_{50\%}$ value than the analogous protonated cytosine nucleosides, indicating that sodium cationization activates the N-glycosidic bond less effectively than protonation.

5.3.4 SURVIVAL YIELD ANALYSES OF PROTONATED AND SODIUM CATIONIZED URACIL NUCLEOSIDES

Survival yield analyses for the protonated and sodium cationized uracil nucleosides, $[dUrd+H]^+$, $[Urd+H]^+$, $[dUrd+Na]^+$, and $[Urd+Na]^+$, are compared in **Figure 5.11**. The $CID_{50\%}$ values indicate that the overall relative stabilities of these species follow the order: $[dUrd+H]^+ < [Urd+H]^+ < [dUrd+Na]^+ < [Urd+Na]^+$. In particular, the fragmentation pathways of the sodium cationized uridine nucleosides only involve cleavage of the N-glycosidic bond. Therefore, the $CID_{50\%}$ values of $[Urd+Na]^+$ and $[dUrd+Na]^+$ directly correlate with the relative N-glycosidic bond stabilities. The $CID_{50\%}$

value of $[Urd+Na]^+$ exceeds that of $[dUrd+Na]^+$, indicating that the 2'-deoxy modification of dUrd destabilizes the N-glycosidic bond vs. that of Urd.

5.3.5 SURVIVAL YIELD ANALYSES OF PROTONATED AND SODIUM CATIONIZED THYMINE NUCLEOSIDES

Survival yield curves for the protonated and sodium cationized thymine nucleosides, $[dThd+H]^+$, $[Thd+H]^+$, $[dThd+Na]^+$, and $[Thd+Na]^+$, are compared in **Figure 5.12**. Based on the $CID_{50\%}$ values, the overall relative stabilities of these species follow the order: $[dThd+H]^+ < [Thd+H]^+ < [dThd+Na]^+ < [Thd+Na]^+$. In particular, the dominant fragmentation pathways observed for $[Thd+H]^+$, $[dThd+Na]^+$ and $[Thd+Na]^+$ involve only N-glycosidic bond cleavage. Thus, the $CID_{50\%}$ values of these species directly correlate with the relative stabilities of the N-glycosidic bonds in these complexes. However, the **Reactions 5.8** and **5.9** of $[dThd+H]^+$ become more competitive, such that the $CID_{50\%}$ value of $[dThd+H]^+$ may not directly correlate to the N-glycosidic bond stability. The $CID_{50\%}$ value of $[Thd+Na]^+$ is higher than that of $[Thd+H]^+$, indicating that sodium cationization activates the N-glycosidic bond less effectively than protonation. Likewise, the $CID_{50\%}$ value of $[Thd+Na]^+$ exceeds that of $[dThd+Na]^+$, indicating that the 2'-hydroxy modification of Thd stabilizes the N-glycosidic bond compared to dThd.

5.4 THE EFFECTS OF MODIFICATIONS ON THE RELATIVE STABILITIES OF DNA AND RNA NUCLEOSIDES

5.4.1 EFFECTS OF 2'-MODIFICATIONS ON THE RELATIVE STABILITIES OF DNA AND RNA NUCLEOSIDES

The $CID_{50\%}$ values for a series of protonated and sodium cationized modified DNA and RNA nucleosides are compared in **Figure 5.13**. This study focuses on the effect of modifications on the relative stabilities of protonated and sodium cationized nucleosides, including 2'-O-methylation, 2'-fluoro-substitution and the arabinose analogs,

which involve inversion of the 2'-stereochemistry. The chemical structures of these modified nucleosides are shown in **Figure 2.3**. In all cases, the $CID_{50\%}$ values of the sodium cationized nucleosides exceed those of the corresponding protonated nucleosides, indicating that sodium cationization activates the N-glycosidic bond less effectively than protonation. 2'-Fluoro nucleosides exhibit the highest $CID_{50\%}$ values among these nucleosides, indicating that the 2'-fluoro substituent significantly stabilizes the N-glycosidic bond. In contrast, the DNA nucleosides exhibit the lowest $CID_{50\%}$ values among these nucleosides, indicating that the 2'-hydrogen atom is least effective at stabilizing the N-glycosidic bond. The $CID_{50\%}$ values of 2'-O-methyl nucleosides are similar to the corresponding RNA nucleosides, suggesting that 2'-O-methyl substituent has a similar influence on the N-glycosidic bond stabilities as compared to the 2'-hydroxyl substituent. Similarly, the arabinose analogs exhibit $CID_{50\%}$ values that are similar to the corresponding RNA nucleosides, suggesting that changing the orientation of 2'-hydroxyl substituent has only a slight impact on the N-glycosidic bond stabilities.

5.4.2 THE EFFECTS OF METHYL SUBSTITUENTS ON THE RELATIVE STABILITIES OF GUANOSINE

The $CID_{50\%}$ values for a series of protonated and sodium cationized methylated guanosines are compared in **Figure 5.14**. This study focuses on the effects of methylation on the relative stabilities of protonated and sodium guanosine, including 1-methylguanosine (m^1Guo), 2'-O-methylguanosine (Guom), 7-methylguanosine (m^7Guo), N^2,N^2-dimethylguanosine ($m^2{}_2$Guo) and N^2,N^2,2'-O-trimethylguanosine ($m^2{}_2$Guom). The chemical structures of these methylated guanosines are shown in **Figure 2.4**. For the protonated methylated guanosines, $[m^2{}_2Guom+H]^+$ exhibits the highest $CID_{50\%}$ value, whereas $[m^1Guo+H]^+$ exhibits the lowest $CID_{50\%}$ value among these nucleosides. The

$CID_{50\%}$ values of all sodium cationized methylated guanosine exceed those of the corresponding protonated methylated guanosine, consistent with the conclusions from **Section 5.3**. Interestingly, the $CID_{50\%}$ value of $[m^7Guo+Na]^+$ is much lower than that of the other sodium cationized methylated guanosines because methylation at the N7 position alters the Na^+ binding site. This conclusion is consistent with the IRMPD action spectroscopy and theoretical studies of $[dGuo+Na]^+$ and $[Guo+Na]^+$ discussed in **Section 3.2.2** and **4.4**, whereas Na^+ prefers to bind to O6 and N7 positions of guanine nucleosides.

5.5 THE EFFECTS OF LOCAL ENVIRONMENT ON THE RELATIVE STABILITIES OF GUANINE NUCLEOSIDES

5.5.1 CID MASS SPECTRA OF PROTONATED AND METAL CATIONIZED GUANINE NUCLEOSIDES

The CID mass spectra for a series of protonated and metal cationized dGuo complexes at an rf excitation amplitude near $CID_{50\%}$ are compared in **Figure 5.15**. The only fragmentation pathway observed for $[dGuo+M]^+$ involves N-glycosidic bond cleavage with the proton or the metal cation retained by the guanine nucleobase, where M = H^+, Li^+, Na^+, K^+, Rb^+ and Ag^+. For $[dGuo+Cs]^+$, the only fragmentation pathway observed is the simple cleavage of the noncovalent interaction between Cs^+ and dGuo.

The CID mass spectra for a series of protonated and metal cationized Guo complexes at an rf excitation amplitude near $CID_{50\%}$ are compared in **Figure 5.16**. The only fragmentation pathway observed for $[Guo+M]^+$ involves N-glycosidic bond cleavage with the proton or the metal cation retained by the guanine nucleobase, where M = H^+, Li^+, Na^+, K^+, and Ag^+. For $[Guo+Rb]^+$ and $[Guo+Cs]^+$, the only fragmentation pathway observed is simple cleavage of the noncovalent interaction between Rb^+ or Cs^+ and

dGuo, respectively. Due to the low mass cut-off of the CID experiments using the QIT MS, Rb^+ cannot be observed in the CID mass spectrum of $[Guo+Rb]^+$.

In summary, the fragmentation behavior of metal cationized dGuo and Guo are related to the size of the metal cation. The binding between the metal cation and the nucleoside become weaker as the metal cation becomes larger. Thus, the loss of metal cation becomes more competitive as the size of the metal cation bound to the nucleoside becomes larger. As a result, only the metal cation is observed as a CID product in the spectra of $[dGuo+Cs]^+$, $[Guo+Rb]^+$ and $[Guo+Cs]^+$.

5.5.2 SURVIVAL YIELD ANALYSES OF PROTONATED AND METAL CATIONIZED GUANINE NUCLEOSIDES

Survival yield curves for $[dGuo+M]^+$, where M = H^+, Li^+, Na^+, K^+, Rb^+ and Ag^+ are compared in **Figure 5.17**. The relative stabilities of protonated and metal cationized dGuo follow the order: $[dGuo+H]^+ < [dGuo+Ag]^+ < [dGuo+Li]^+ \sim [dGuo+Na]^+ < [dGuo+K]^+ < [dGuo+Rb]^+$. Survival yield curves for $[Guo+M]^+$, where M = H^+, Li^+, Na^+, K^+, and Ag^+ are compared in **Figure 5.18**. The relative stabilities of protonated and metal cationized Guo follow the order: $[Guo+Ag]^+ < [dGuo+H]^+ < [dGuo+Li]^+ < [dGuo+Na]^+ < [dGuo+K]^+$. These results indicate that the local endearment significantly impact the relative N-glycosidic bond stabilities of DNA and RNA nucleosides. The relative stabilities of alkali metal cationized dGuo and Guo follow the order of increasing size of the alkali metal. However, the N-glycosidic bond of $[dGuo+Ag]^+$ is more stable than that of $[dGuo+H]^+$, whereas the N-glycosidic bond of $[Guo+Ag]^+$ is less stable than that of $[dGuo+H]^+$. These contrasting observations may be due to different conformations of silver cationized dGuo and Guo being accessed in the experiments.

5.6 CONCLUSIONS

Survival yield analysis is a robust technique to determine the relative stabilities of DNA and RNA nucleosides. In particular, the $CID_{50\%}$ value can be directly used to determine the relative N-glycosidic bond stability when all fragmentation pathways involve solely N-glycosidic bond cleavage. In general, the 2'-hydroxyl substituents of RNA nucleosides stabilize the N-glycosidic bond compared with the corresponding DNA nucleosides. Sodium cationization activates the N-glycosidic bond less effectively than protonation. 2'-Fluoro nucleosides exhibit the highest $CID_{50\%}$ values, indicating that 2'-floro substituent significantly stabilizes the N-glycosidic bond compared with the canonical DNA and RNA nucleosides. The $CID_{50\%}$ values of 2'-O-methyl nucleosides are similar to the corresponding RNA nucleosides, suggesting that 2'-O-methyl substituent has similar influence on the N-glycosidic bond stabilities as compared to the 2'-hydroxyl substituent. Similarly, the arabinose analogs exhibit similar $CID_{50\%}$ values with the corresponding RNA nucleosides, suggesting that changing the stereochemistry of 2'-hydroxyl and 2'-hydrogen substituents only slightly impacts the N-glycosidic bond stabilities. The survival yield analyses of protonated and sodium cationized methylated guanosine find that the position of the methyl substituent is important to the impact on the relative N-glycosidic bond stabilities of these nucleosides. Interestingly, the $CID_{50\%}$ value of $[m^7Guo+Na]^+$ is significantly lower than those of other sodium cationized methylated guanosines, because methylation at the N7 position alters the Na^+ binding site. The fragmentation behavior of metal cationized dGuo and Guo are related to the size of the metal cation. The binding between the metal cation and the nucleoside become weaker as the metal cation becomes larger. Thus, the loss of metal cation

becomes more competitive as the size of the metal cation bound to the nucleoside increases. The order of relative stabilities of alkali metal cationized dGuo and Guo is consistent with the order of increasing size of the alkali metal. The different relative stabilities of protonated and silver cationized dGuo and Guo may be due to different conformations of silver cationized dGuo and Guo being accessed in the experiments, suggesting that further IRMPD studies of these $[dGuo+Ag]^+$ and $[Guo+Ag]^+$ complexes would be of interest.

5.7 REFERENCES

119. R. R. Wu, B. Yang, C. E. Frieler, G. Berden, J. Oomens and M. T. Rodgers, *Phys. Chem. Chem. Phys.* 2015, **17**, 25978.

147. Y. Zhu, L. A. Hamlow, C. C. He, S. F. Strobehn, J. K. Lee, J. Gao, G. Berden, J. Oomens and M. T. Rodgers, *J. Phys. Chem. B* 2016, **120**, 8892.

148. Y. Zhu, L. A. Hamlow, C. C. He, J. K. Lee, J. Gao, G. Berden, J. Oomens and M. T. Rodgers, *J. Phys. Chem. B* 2017, **121**, 4048.

149. Y. Zhu, L. A. Hamlow, C. C. He, H. A. Roy, N. A. Cunningham, M. U. Munshi, G. Berden, J. Oomens and M. T. Rodgers, *Int. J. Mass Spectrom.* 2017, DOI: https://doi.org/10.1016/j.ijms.2017.04.005.

150. Y. Zhu, H. A. Roy, N. A. Cunningham, S. F. Strobehn, J. Gao, M. U. Munshi, G. Berden, J. Oomens and M. T. Rodgers, *Phys. Chem. Chem. Phys.* 2017, **19**, 17637.

151. Y. Zhu, H. A. Roy, N. A. Cunningham, S. F. Strobehn, J. Gao, M. U. Munshi, G. Berden, J. Oomens and M. T. Rodgers, *J. Am. Soc. Mass Spectrom* 2017, **28**, 2437.

193. R. R. Wu, Y. Chen and M. T. Rodgers, *Phys. Chem. Chem. Phys.* 2016, **18**, 2968.

195. R. R. Wu and M. T. Rodgers, *J. Phys. Chem. B* 2016, **120**, 4803.

196. R. R. Wu and M. T. Rodgers, *Phys. Chem. Chem. Phys.* 2016, **18**, 16021.

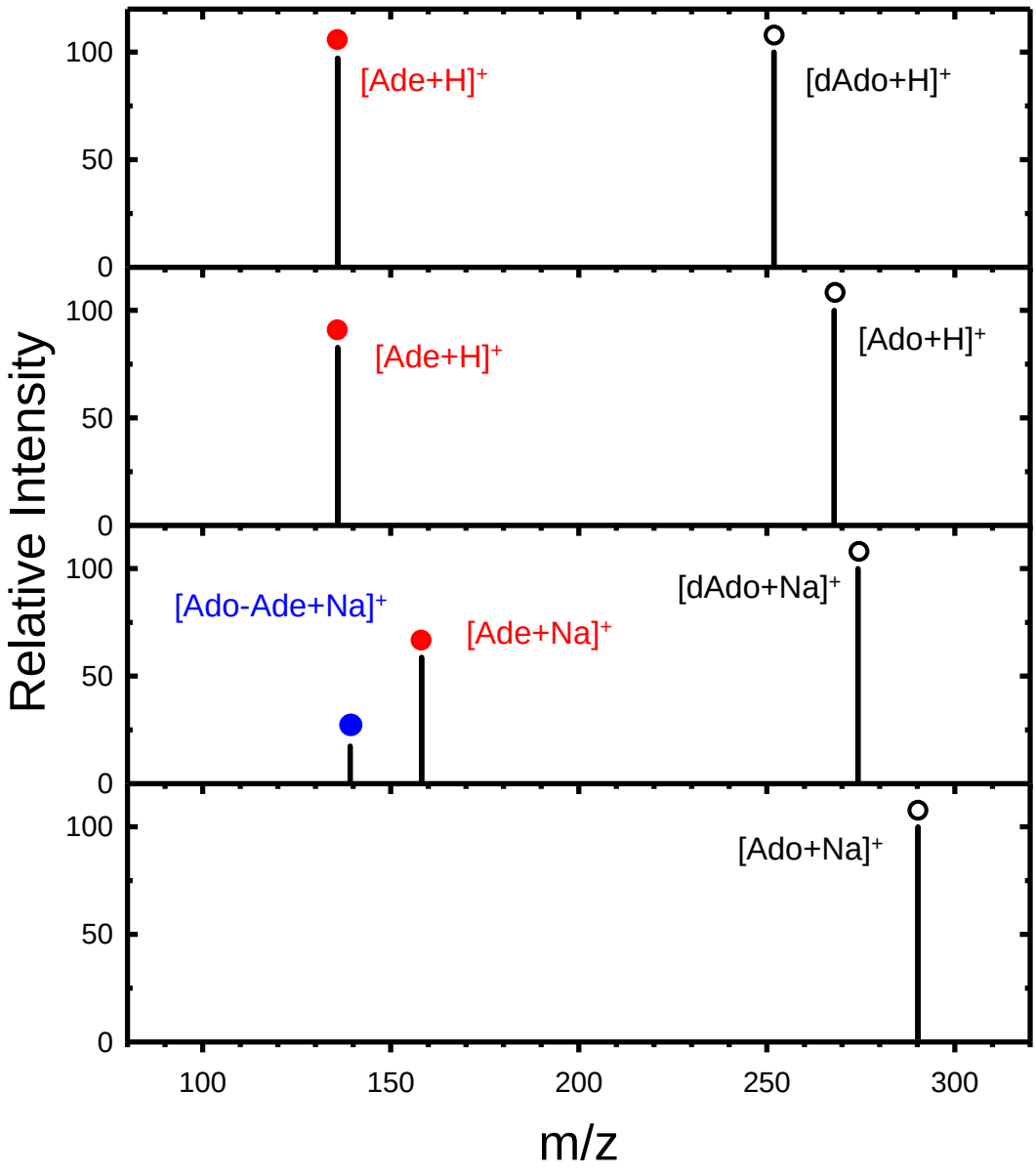

Figure 5.1 CID mass spectra of protonated and sodium cationized adenine nucleosides at an rf excitation amplitude (rf_{EA}) that produces ~50% dissociation. No CID fragments were observed for $[Ado+Na]^+$ due to the low-mass cut-off of the QIT MS. The only CID pathways observed involve N-glycosidic bond cleavage.

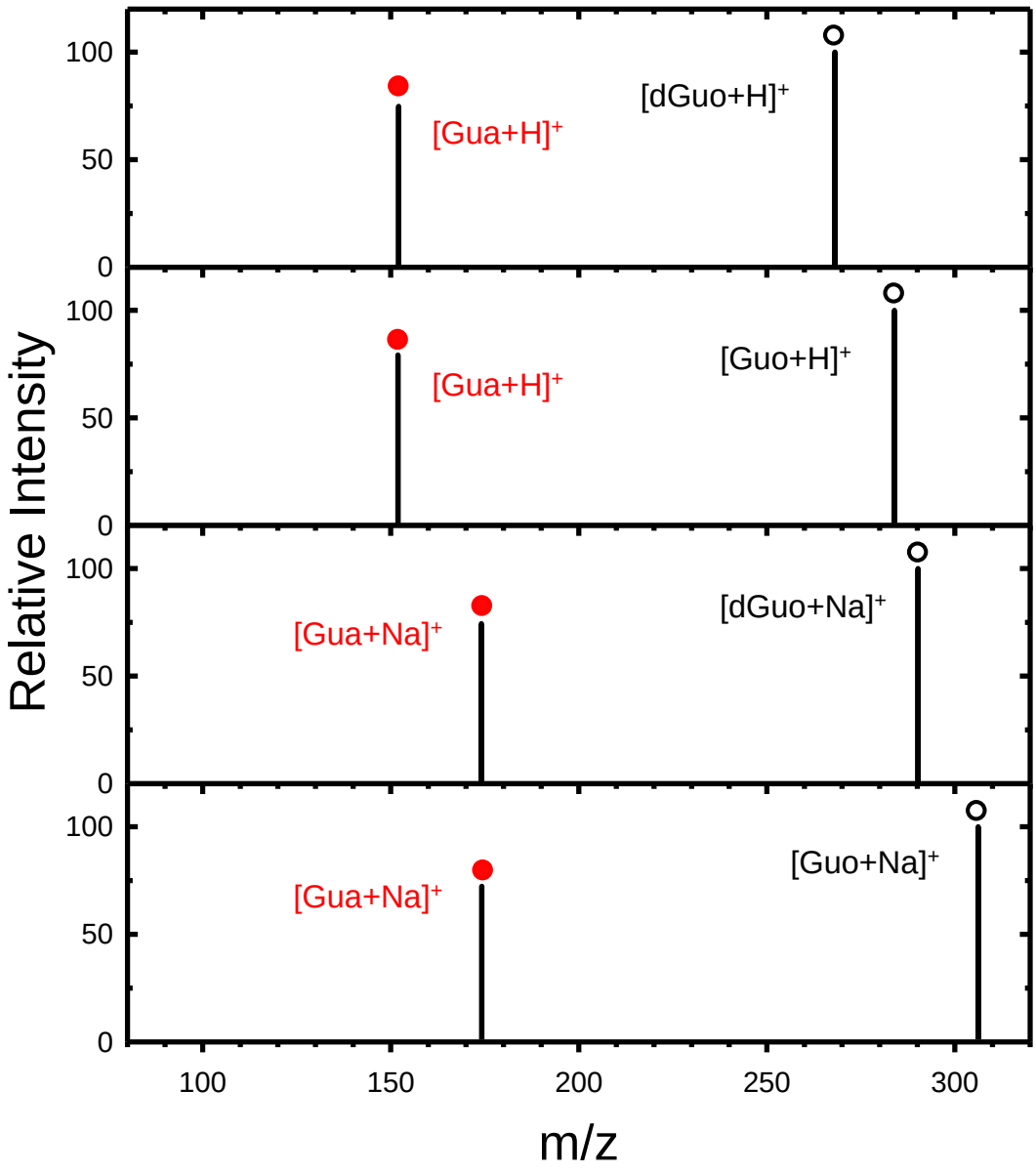

Figure 5.2 CID mass spectra of protonated and sodium cationized guanine nucleosides at an rf excitation amplitude (rf_{EA}) that produces ~50% dissociation. The only CID pathway observed involves N-glycosidic bond cleavage with the cation retained by the nucleobase, Gua.

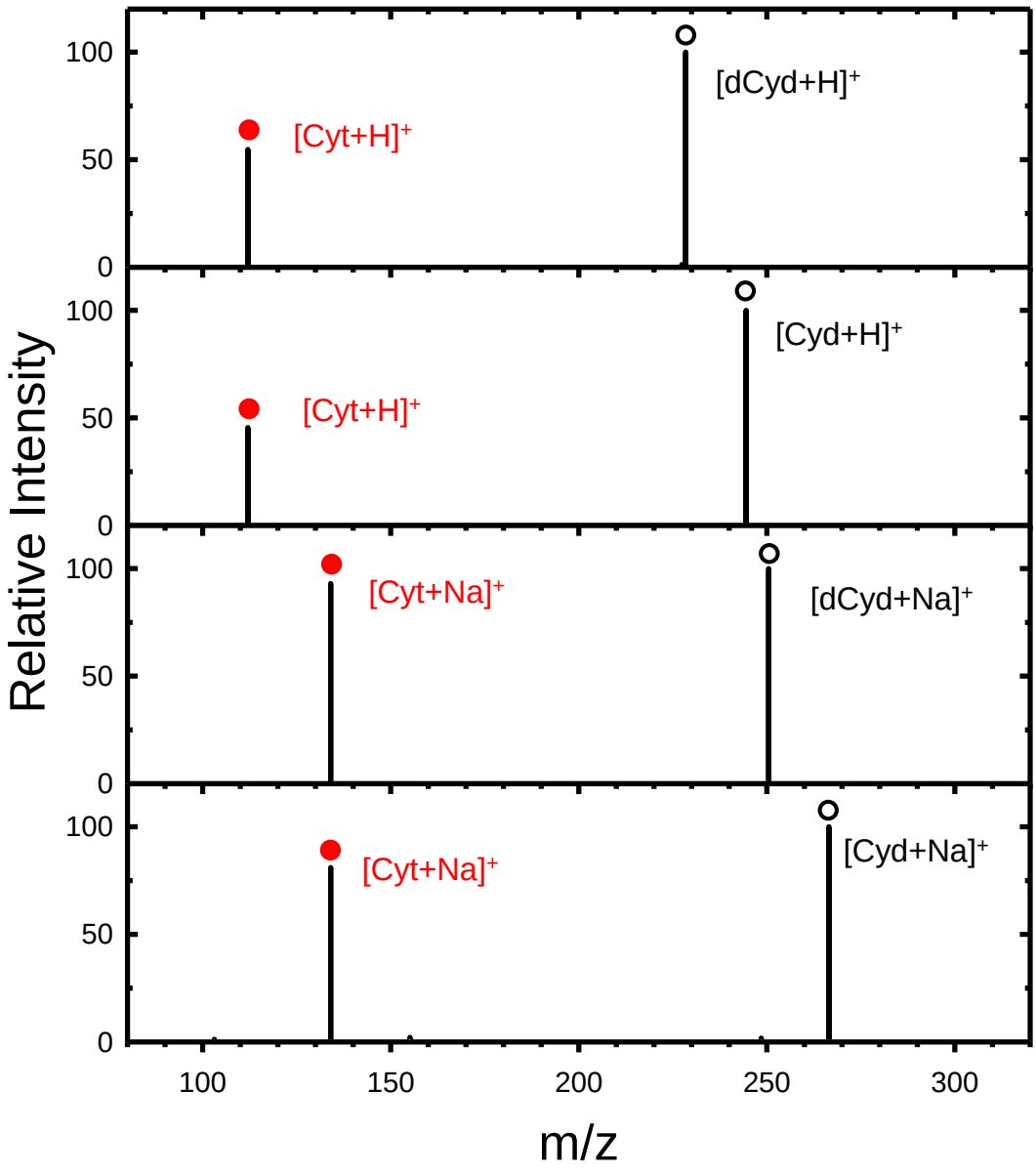

Figure 5.3 CID mass spectra of protonated and sodium cationized cytosine nucleosides at an rf excitation amplitude (rf_{EA}) that produces ~50% dissociation. The only CID pathway observed involves N-glycosidic bond cleavage with the cation retained by the nucleobase, Cyt.

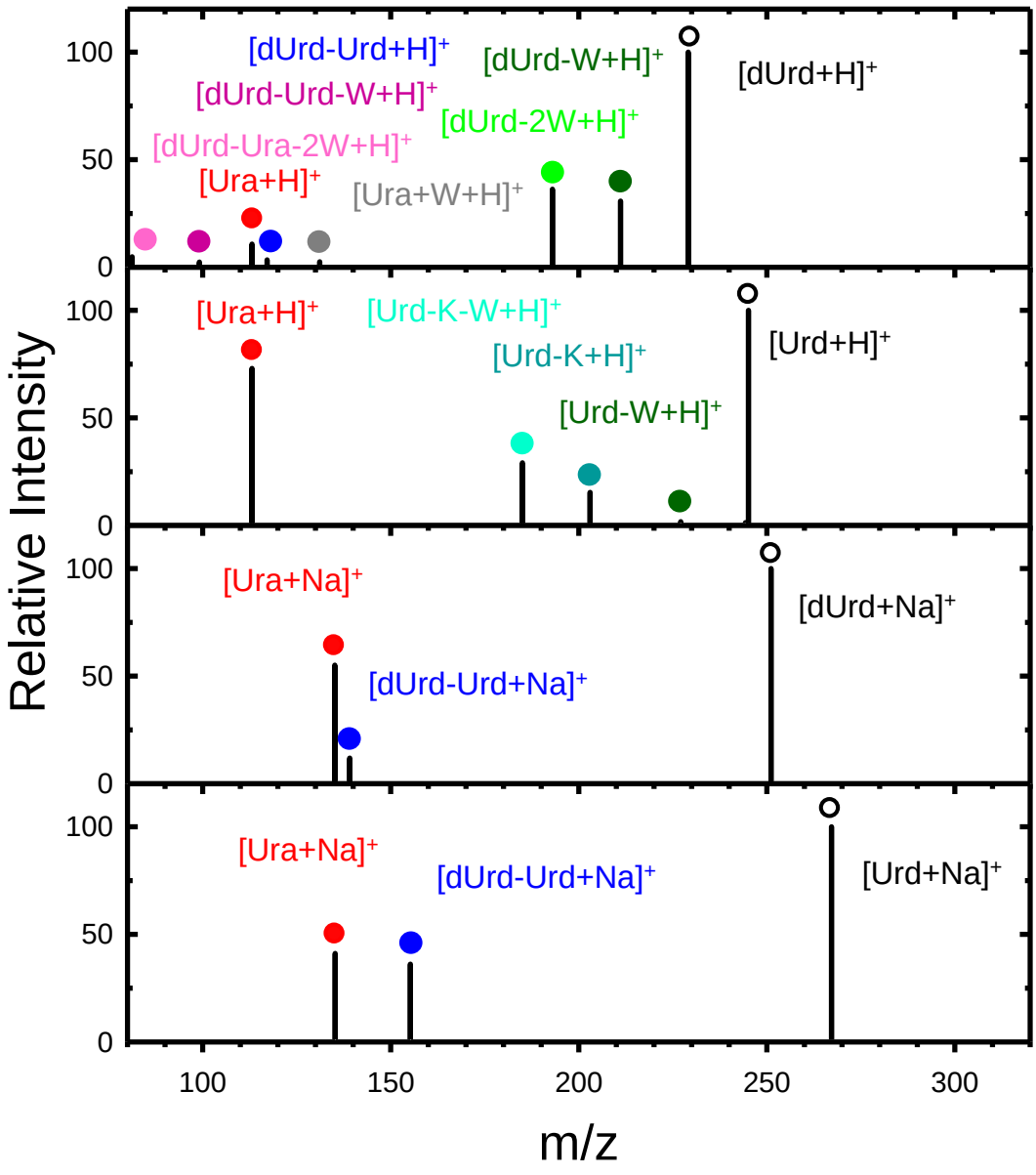

Figure 5.4 CID mass spectra of protonated and sodium cationized uracil nucleosides at an rf excitation amplitude (rf_{EA}) that produces ~50% dissociation. Although N-glycosidic bond cleavage pathways are observed for all complexes, a variety of neutral loss pathways are also observed for the protonated systems.

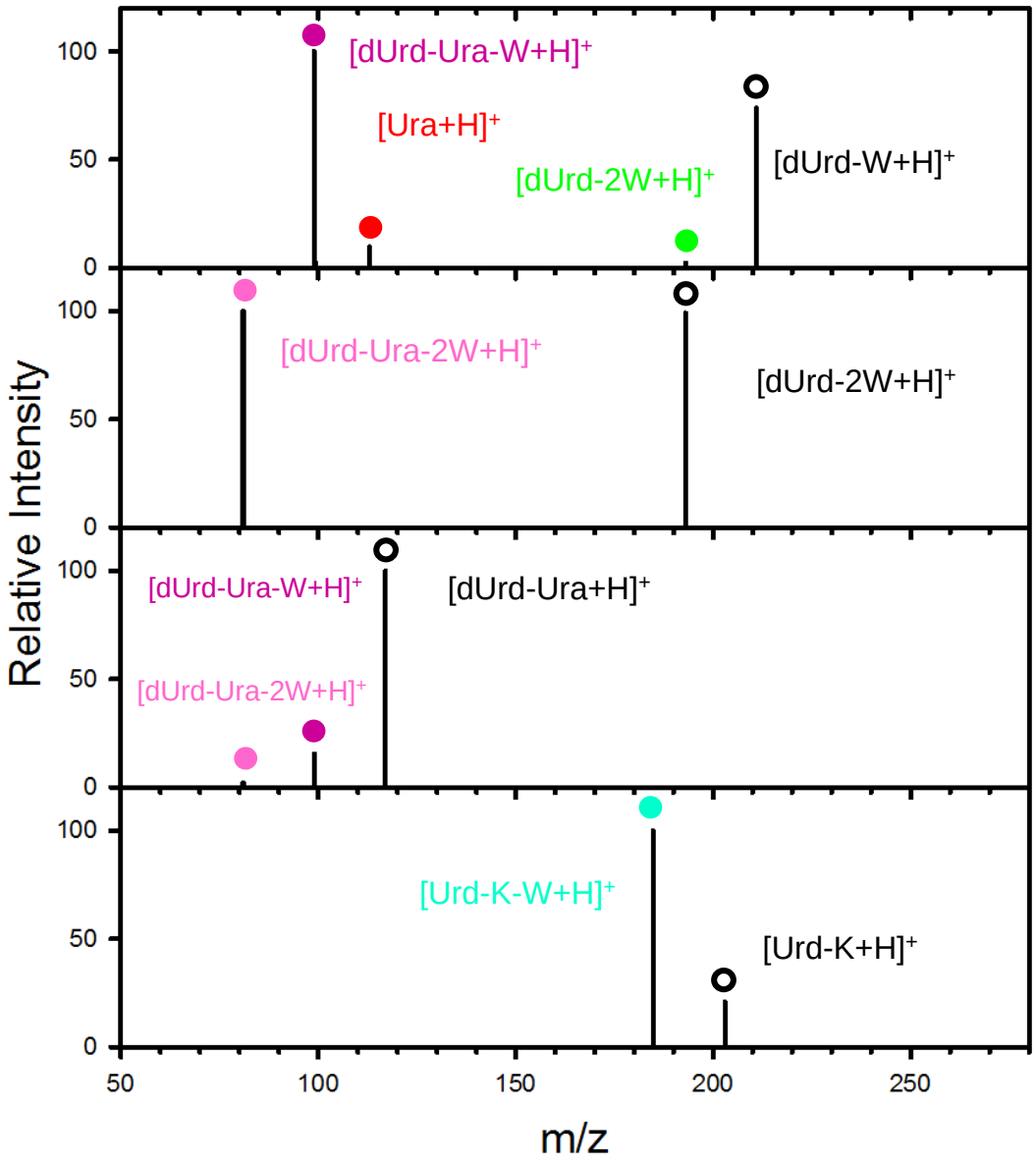

Figure 5.5 MS^3 spectra of $[dUrd\text{-}W+H]^+$, $[dUrd\text{-}Ura+H]^+$, $[dUrd\text{-}2W+H]^+$, and $[Urd\text{-}K+H]^+$.

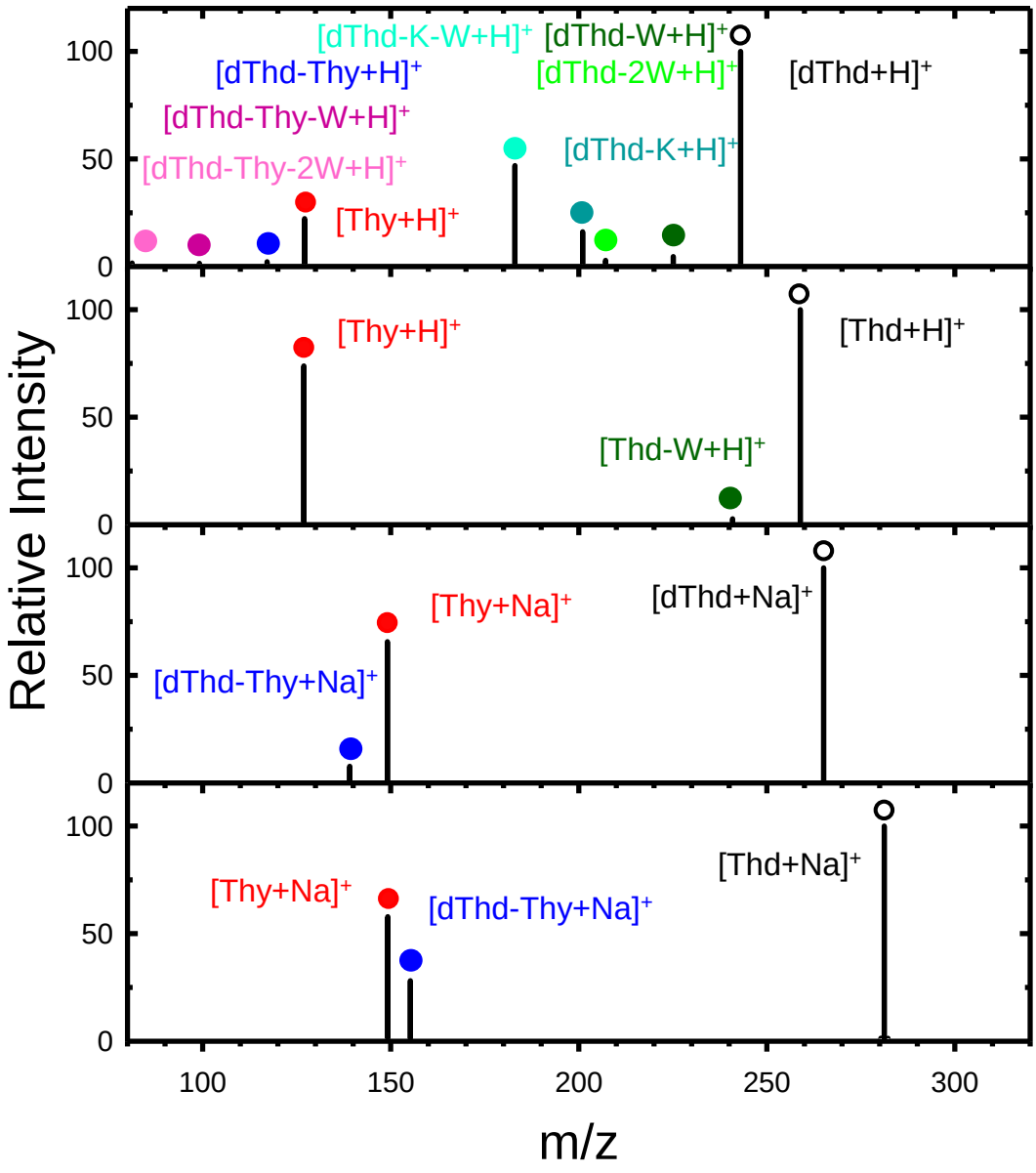

Figure 5.6 CID mass spectra of protonated and sodium cationized thymine nucleosides at an rf excitation amplitude (rf_{EA}) that produces ~50% dissociation. Although N-glycosidic bond cleavage pathways are observed for all complexes, a variety of neutral loss pathways are also observed for the protonated systems.

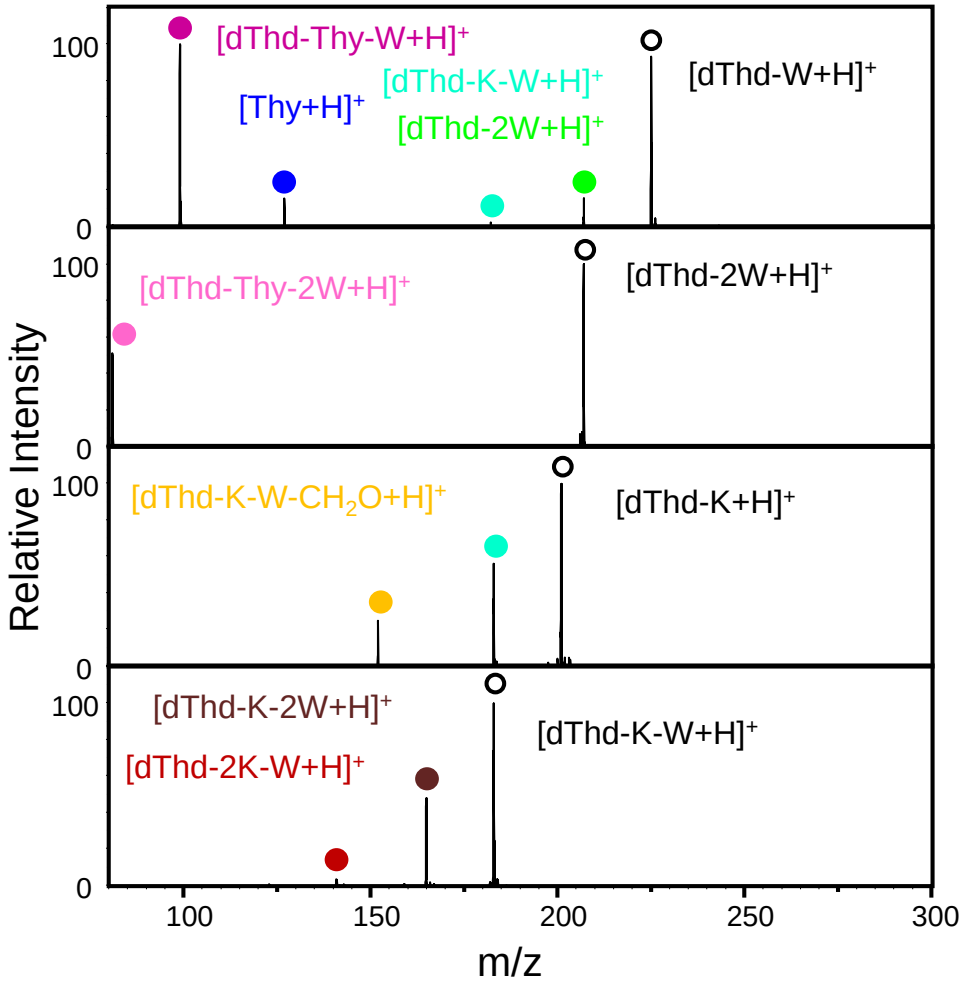

Figure 5.7 MS^3 spectra of $[dThd\text{-}W+H]^+$, $[dThd\text{-}2W+H]^+$, $[dThd\text{-}K+H]^+$ and $[dThd\text{-}K\text{-}W+H]^+$.

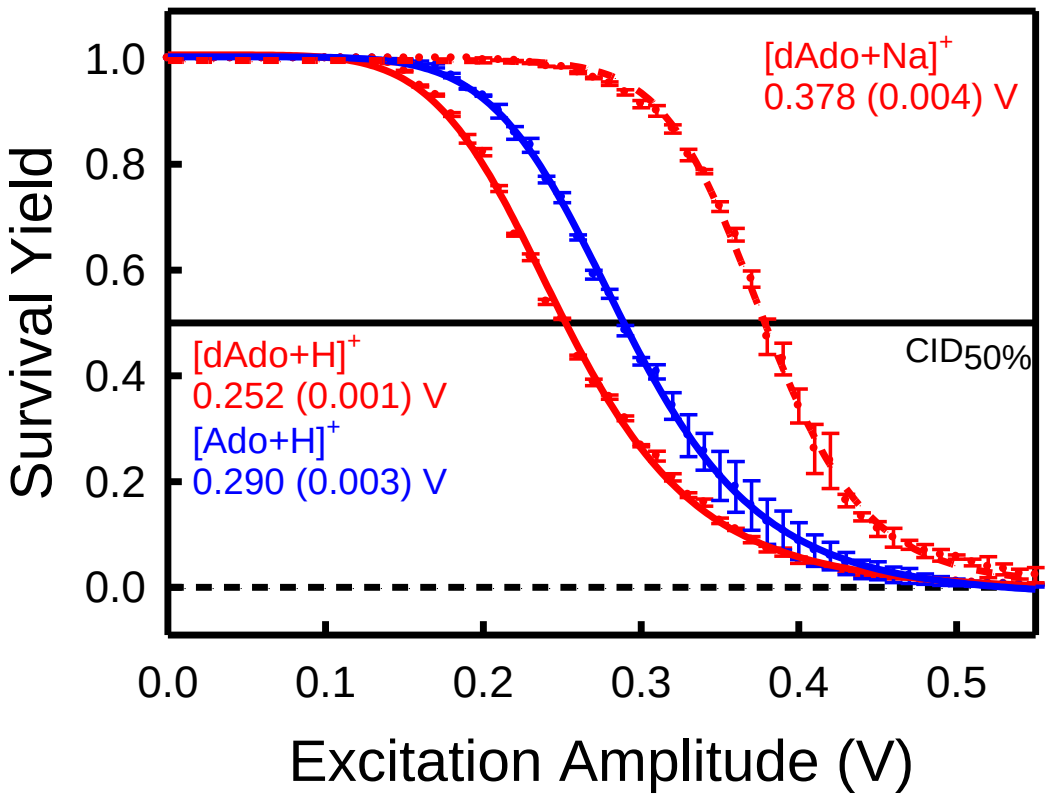

Figure 5.8 Survival yield analyses of protonated and sodium cationized adenosine nucleosides and their corresponding $CID_{50\%}$ values. Values (in parentheses) represent the standard deviation for fits to the average of three measurements.

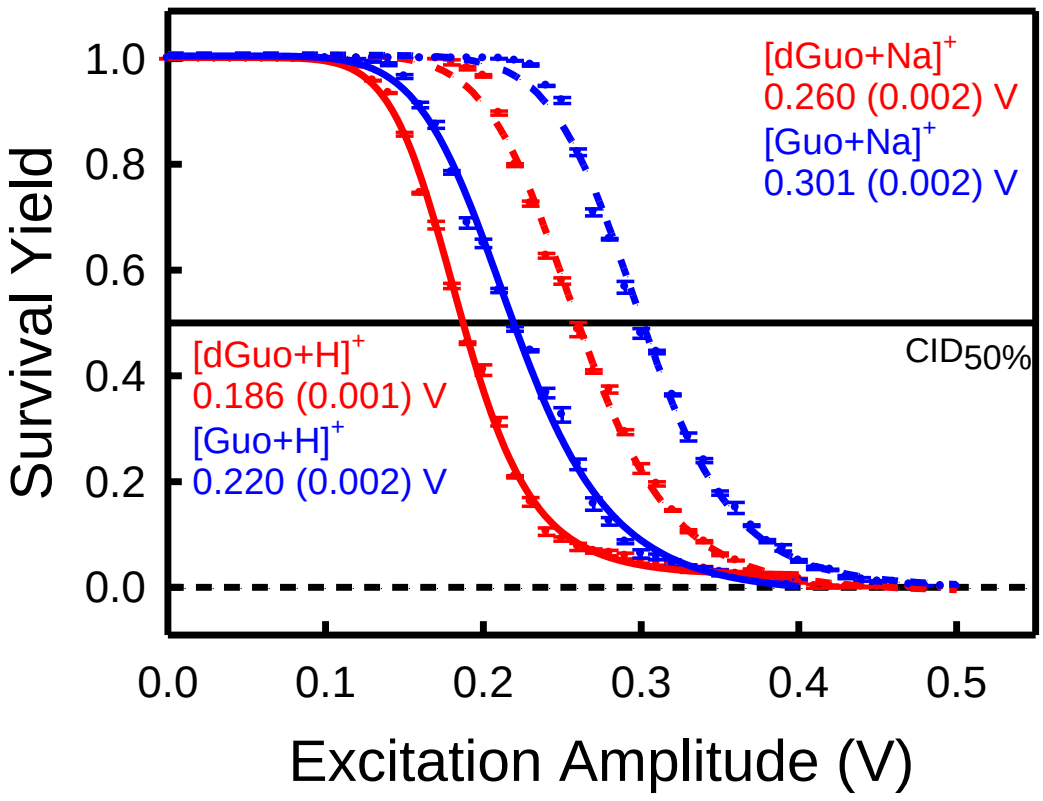

Figure 5.9 Survival yield analyses of protonated and sodium cationized guanine nucleosides and their corresponding $CID_{50\%}$ values. Values (in parentheses) represent the standard deviation for fits to the average of three measurements.

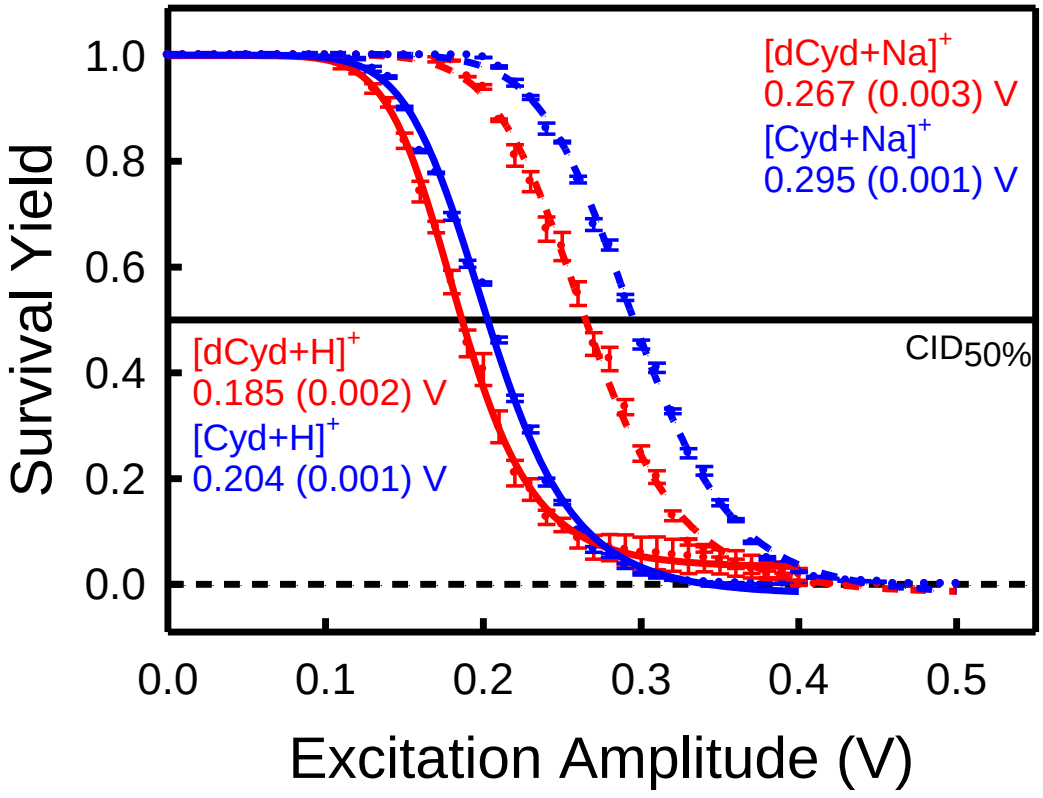

Figure 5.10 Survival yield analyses of protonated and sodium cationized cytosine nucleosides and their corresponding $CID_{50\%}$ values. Values (in parentheses) represent the standard deviation for fits to the average of three measurements.

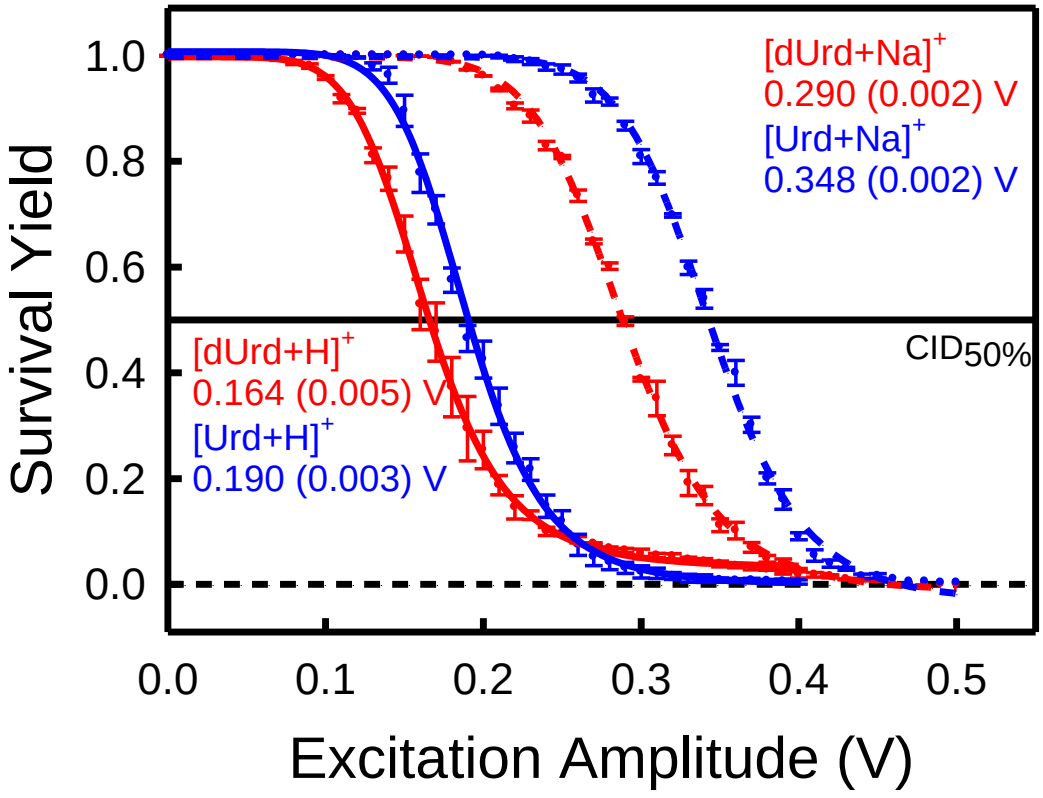

Figure 5.11 Survival yield analyses of protonated and sodium cationized uracil nucleosides and their corresponding $CID_{50\%}$ values. Values (in parentheses) represent the standard deviation for fits to the average of three measurements.

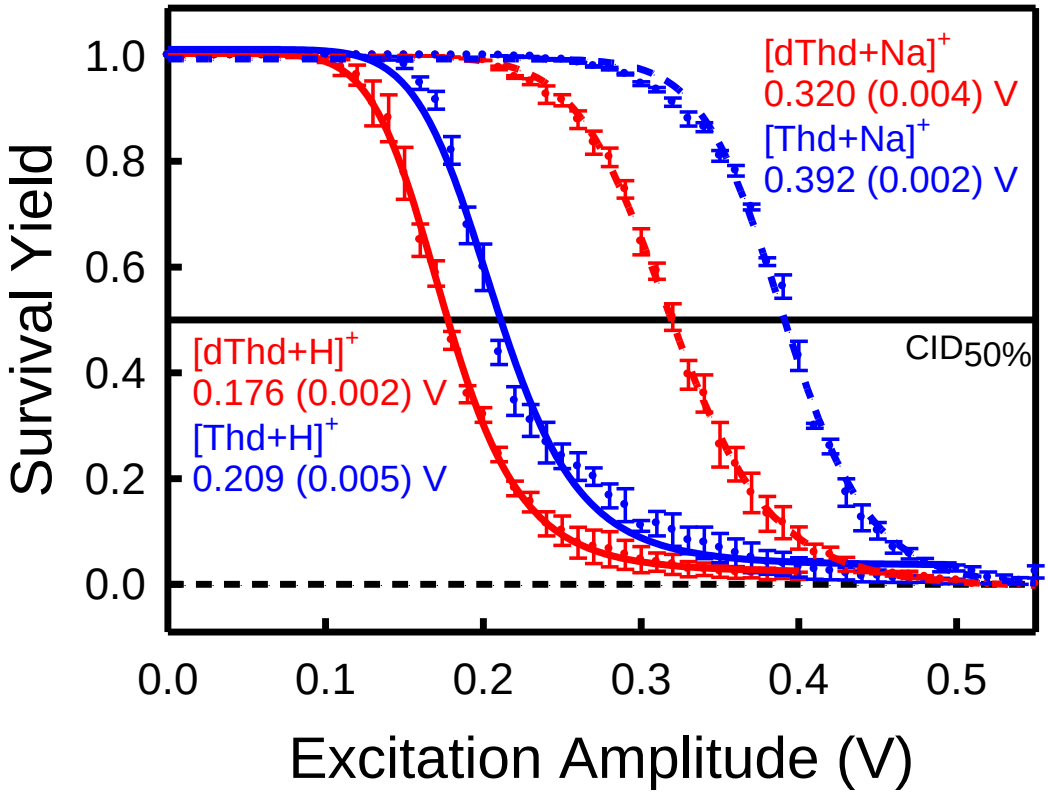

Figure 5.12 Survival yield analyses of protonated and sodium cationized thymine nucleosides and their corresponding $CID_{50\%}$ values. Values (in parentheses) represent the standard deviation for fits to the average of three measurements.

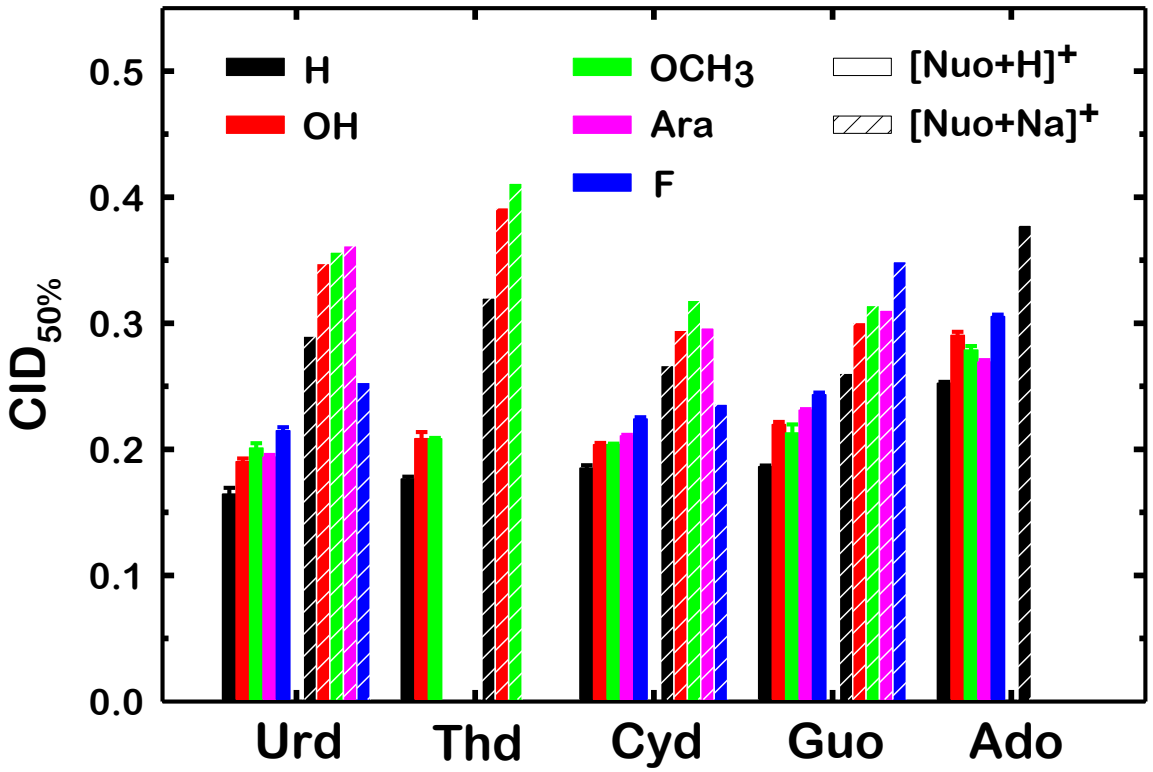

Figure 5.13 $CID_{50\%}$ values for protonated and sodium cationized modified nucleosides. Protonated nucleosides are indicated using solid colors, whereas the sodium cationized nucleosides are in shaded with white cross hatching.

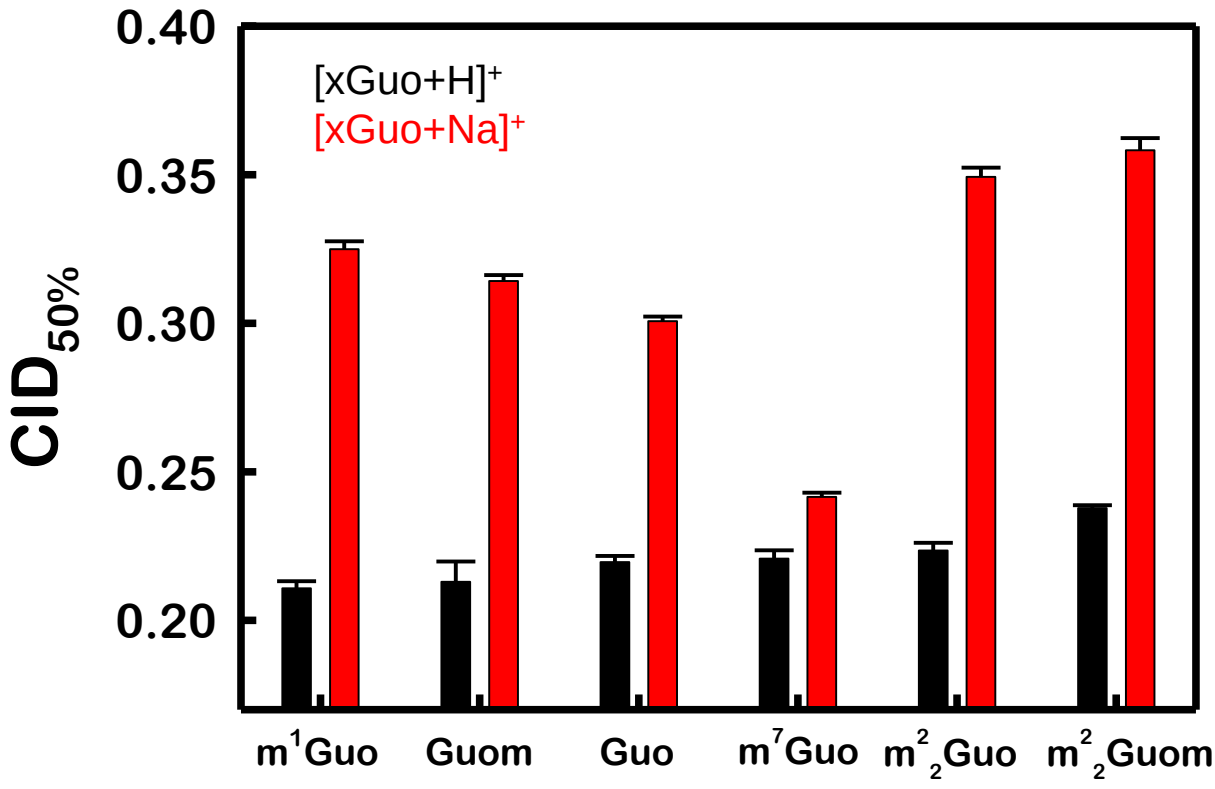

Figure 5.14 The $CID_{50\%}$ values for protonated and sodium cationized methylated guanosines.

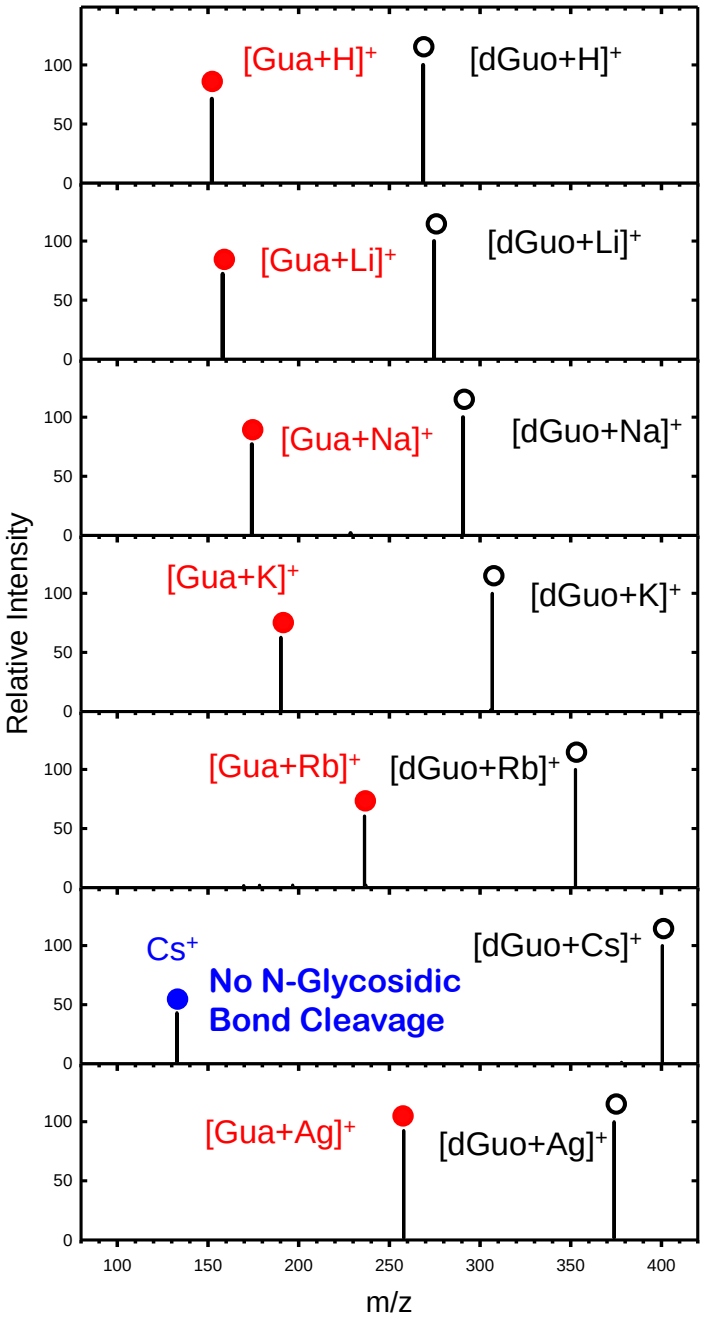

Figure 5.15 CID mass spectra of protonated and metal cationized dGuo at an rf excitation amplitude (rf_{EA}) that produces ~50% dissociation. N-glycosidic bond cleavage and simple noncovalent metal-dGuo bond cleavage are the only CID pathways observed.

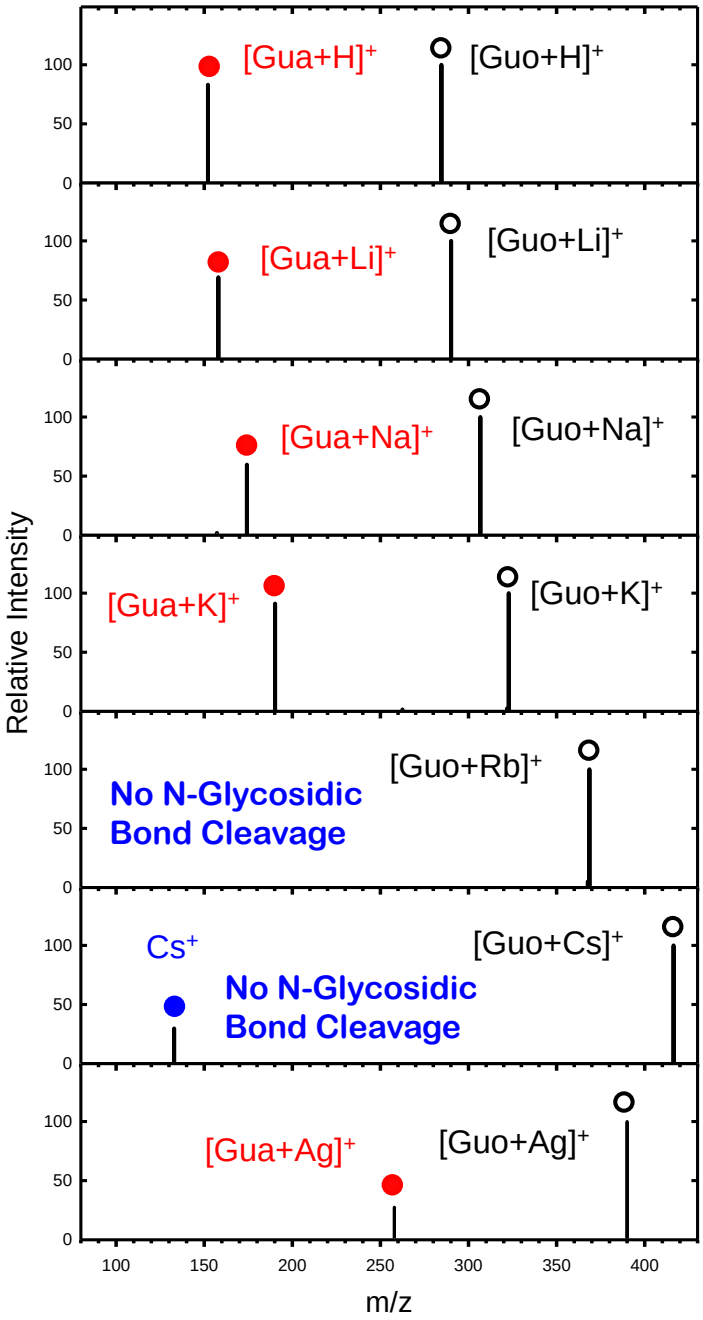

Figure 5.16 CID mass spectra of protonated and metal cationized Guo at an rf excitation amplitude (rf_{EA}) that produces ~50% dissociation. N-glycosidic bond cleavage and simple noncovalent metal-Guo bond cleavage are the only CID pathways observed.

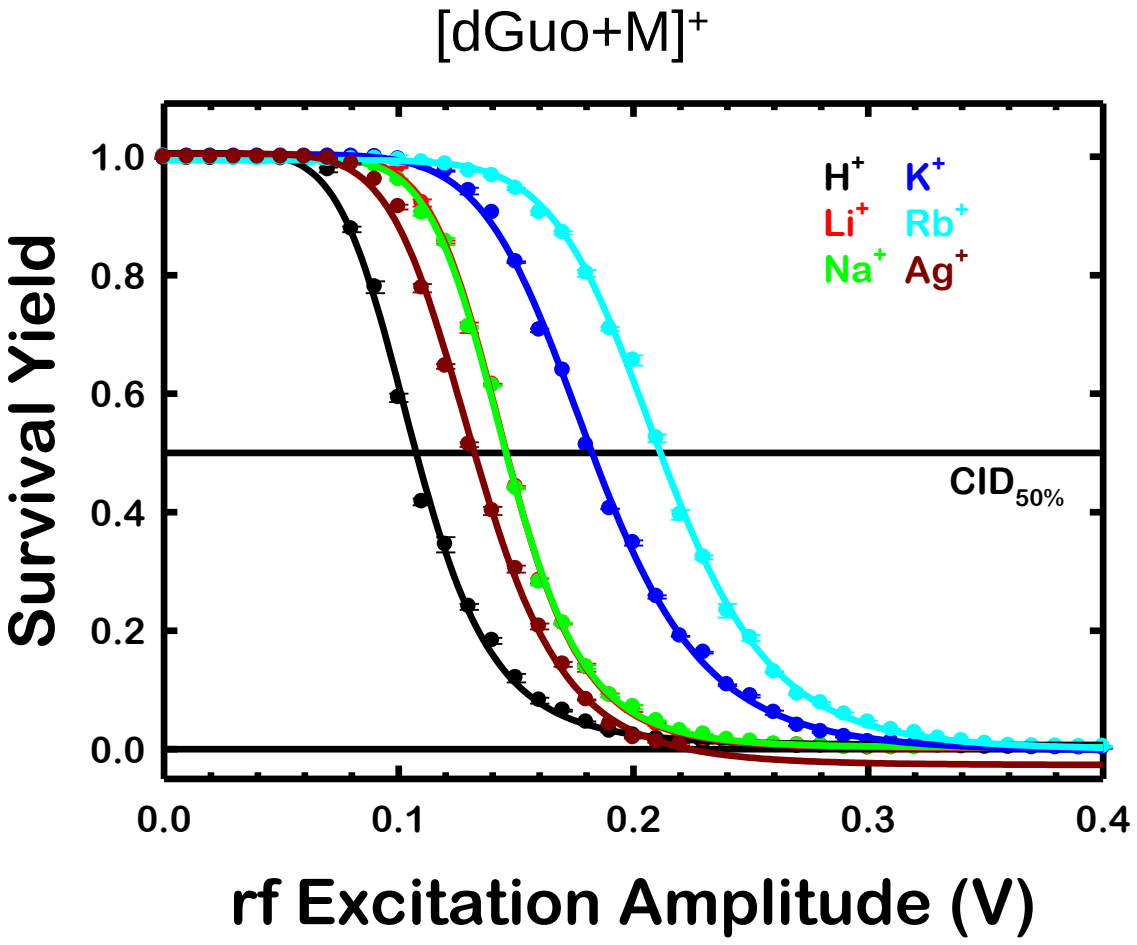

Figure 5.17 Survival yield analyses of protonated and metal cationized dGuo. Error bars represent the standard deviation for fits to the average of three measurements.

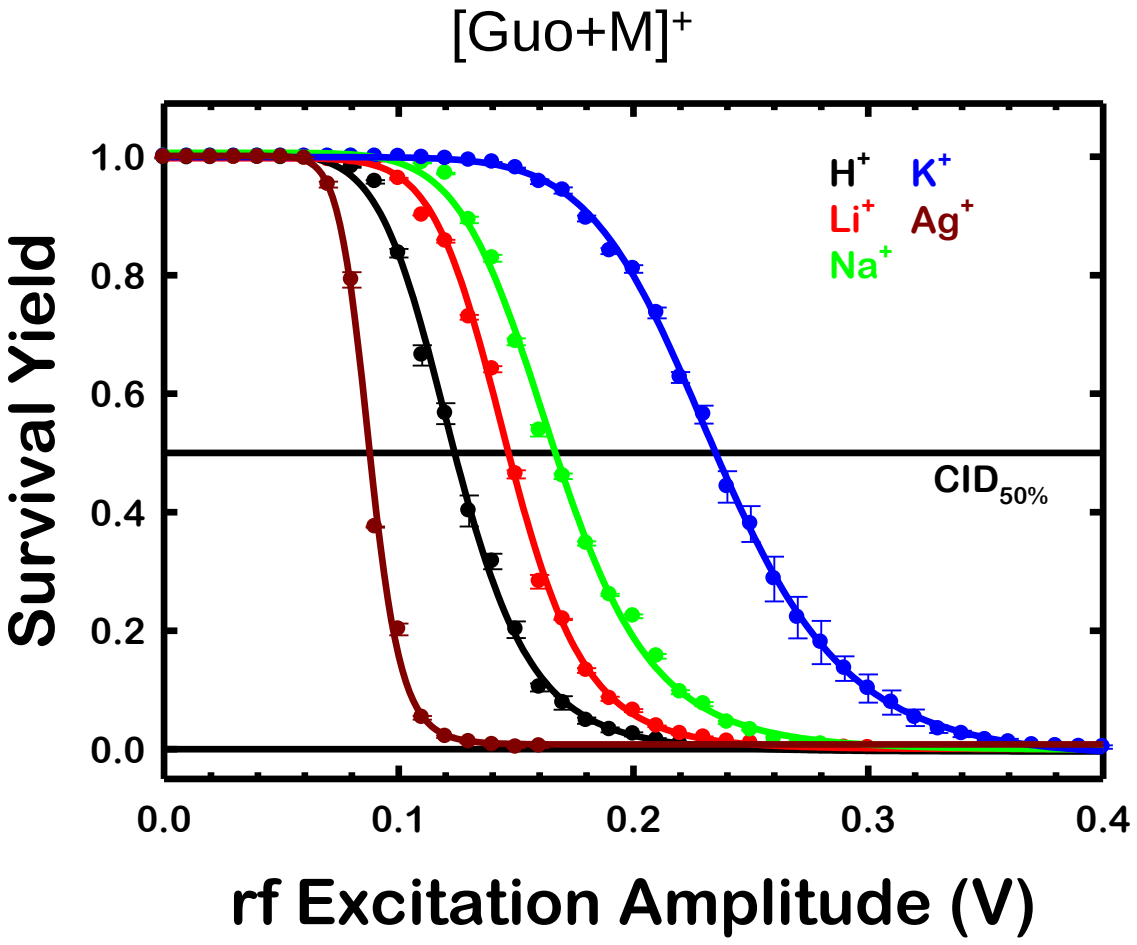

Figure 5.18 Survival yield analyses of protonated and metal cationized Guo. Error bars represent the standard deviation for fits to the average of three measurements.

CHAPTER 6 THEORETICAL RESULTS FOR ADENINE NUCLEOTIDES

6.1 INTRODUCTION

The motivation for studying sodium cation binding to the adenine mononucleotides is introduced in **Chapter 1**. In this chapter, the stable low-energy conformations of the sodium cationized 2'-deoxyadenosine-5'-monophosphate (pdAdo) and adenosine-5'-monophosphate (pAdo), $[pdAdo+Na]^+$ and $[pAdo+Na]^+$, as well as the disodium cationized deprotonated forms of pdAdo and pAdo, $[pdAdo-H+2Na]^+$ and $[pAdo-H+2Na]^+$, are determined and ultimately optimized at the B3LYP/6-311+G(d,p) level of theory. The harmonic vibrational frequencies are also calculated at this same level of theory. Single-point energy calculations are then calculated with an extended basis set, 6-311+G(2d,2p). Additionally, the neutral adenine mononucleotides, pdAdo and pAdo, as well as the sodium cationized deprotonated adenine mononucleotide salts, [pdAdo-H+Na] and [pAdo-H+Na], are also calculated at the same level of theory for comparison. The ground conformers of these sodium cationized forms of adenine mononucleotides are also compared to those of the deprotonated, neutral and protonated adenine mononucleotides to eludicate the effect of the local environment (charge state) on the conformations of these species. The designations of nucleobase orientation and sugar puckering are defined in **Section 1.7**. The computational details are introduced in **Section 2.3**. The structures of pdAdo and pAdo along with the potential Na^+ binding sites are shown in **Figure 2.10**.

6.2 NOMENCLATURE FOR DESCRIBING THE SODIUM CATIONIZED FORMS OF NEUTRAL AND DEPROTONATED ADENINE MONONUCLEOTIDES

The nomenclature employed to describe the stable low-energy conformers of the sodium cationized forms of the neutral and deprotonated adenine mononucleotides is similar to that employed for the sodium cationized DNA and RNA nucleosides. An uppercase letter is used to describe the number of chelation interactions between the sodium cation and adenine mononucleotide (Q for quadridentate, T for tridentate, B for bidentate, and M for monodentate). For the disodium cationized deprotonated adenine mononucleotides, $[pdAdo-H+2Na]^+$ and $[pAdo-H+2Na]^+$, two uppercase letters are used to indicate the number of chelation interactions with the sodium cations and adenine mononucleotide; the more highly chelated cation is designated first. A number follows the uppercase letter(s) and indicates the order of relative Gibbs free energies at 298 K of the conformers found for that mode of Na^+ binding. In parentheses, the atoms bound to the Na^+ cation(s) are given. For the disocium cationized complexes, a comma is used to separate the atoms bound to each Na^+. The oxo and hydroxyl oxygen atoms of the phosphate moiety are indicated as O_X and O_H, respectively.

6.3 STABLE LOW-ENERGY CONFORMERS OF SODIUM CATIONIZED ADENINE MONONUCLEOTIDES

6.3.1 STABLE LOW-ENERGY CONFORMERS OF SODIUM CATIONIZED 2'-DEOXYADENOSINE-5'-MONOPHOSPHATE

The stable low-energy conformers of $[pdAdo+Na]^+$ that are within 20 kJ/mol of the ground conformer along with their relative Gibbs free energies, nucleobase orientations and sugar puckerings are compared in **Figure 6.1**. Among the 18 low-energy conformers found within 20 kJ/mol of the ground conformer, only three modes of Na^+ binding were found, tridentate $T(N3O4'O_X)$, bidentate $B(O_XO_H)$, and bidentate $B(O_XO_X)$. In the ground conformer of $[pdAdo+Na]^+$, the sodium cation binds in a

tridentate fashion to the N3, O4′ and O_X atoms with the adenine nucleobase in a *syn* orientation and C3′-endo ($^3T_2$) sugar puckering. The T1-T4, T8 and T9(N3O4'O_X) conformers differ only in the orientations of the phosphate hydroxyls. Changes in the sugar puckering to C2'-endo ($^2T_1$) as in the T5 and T6(N3O4'O_X) conformers destabilize the complexes by at least 3.2 kJ/mol vs. the ground T1(N3O4'O_X) conformer. The T7(N3O4'O_X) conformer also exhibits C2'-endo sugar puckering, but changes from $^2T_1$ to $^2T_3$. The T11 and T12 (N3O4'O_X) conformers exhibit C1'-exo ($_1T^O$) sugar puckering, and this change in the puckering is even more destabilizing, by at least 10.9 kJ/mol vs. the ground T1(N3O4'O_X) conformer. The T13 and T14(N3O4'O_X) conformers with C2'-exo ($_2T^3$) sugar puckering are even less stable, by at least 16.6 kJ/mol. An additional hydrogen-bonding interaction between the N7 atom of the adenine nucleobase and the phosphate hydroxyl is found in these conformers. An additional hydrogen-bonding interaction between the N3 atom of the adenine nucleobase and a phosphate hydroxyl is found in the T15(N3O4'O_X) conformer, which exhibits C1'-exo ($_1T^2$) sugar puckering and is 19.0 kJ/mol less stable. When one proton is transferred from the phosphate moiety to the N3 atom of adenine, the sodium cation preferentially binds to the negatively charged phosphate group in a bidentate fashion to the oxo and one of the hydroxyl oxygen atoms of the phosphate moiety. The most stable of these zwitterionic phosphate binding conformers, B1(O_XO_H), is 14.1 kJ/mol less favorable than the ground T1(N3O4'O_X) conformer, whereas the most stable B(O_XO_X) conformer, B1(O_XO_X), is 14.3 kJ/mol less stable than the ground conformer. All phosphate binding conformers found here exhibit C1'-exo ($_1T^O$ or $_1T^2$) sugar puckering.

In summary, the ground conformer of $[pdAdo+Na]^+$ exhibits tridentate binding of Na^+ to the N3, O4' and O_X atoms with a *syn* orientation of the adenine nucleobase and C3'-endo ($^3T_2$) sugar puckering. C2'-endo, C2'-exo and C1'-exo sugar puckerings are also found among the low-energy T(N3O4'O_X) conformers. All conformers calculated within 20 kJ/mol prefer a *syn* orientation of the adenine nucleobase. Phosphate binding B(O_XO_H) and B(O_XO_X) conformers are less favorable, with the most stable of these conformers 14.1 and 14.3 kJ/mol less stable than the ground T1(N3O4'O_X) conformer, respectively.

6.3.2 STABLE LOW-ENERGY CONFORMERS OF SODIUM CATIONIZED ADENOSINE-5'-MONOPHOSPHATE

The stable low-energy conformers of $[pAdo+Na]^+$ that are within 20 kJ/mol of the ground conformer along with their relative Gibbs free energies, nucleobase orientations and sugar puckerings are compared in **Figure 6.2**. Among 19 low-energy conformers found within 20 kJ/mol of the ground conformer, 5 modes of Na^+ binding were found, quadridentate Q(N3O4'O5'O_X), tridentate T(N3O4'O_X) and T(O3'O5'O_X), and bidentate B(O_XO_X) and B(O_XO_H). The stable low-energy conformers found for $[pAdo+Na]^+$ are very parallel to those of $[pdAdo+Na]^+$, however, the additional 2'-hydroxyl enables formation of a hydrogen-bonding interaction between the 2'- and 3'-hydroxyls, which is found in all of the low-energy conformers. The T1(N3O4'O_X) conformer with Na^+ binding to the N3, O4' and O_X atoms, a *syn* orientation of the adenine nucleobase, and C3'-endo ($^3T_2$) sugar puckering is also the ground conformer of $[pAdo+Na]^+$. The T1-T3, T7 and T10(N3O4'O_X) conformers differ from the ground conformer only by the orientations of the phosphate hydroxyl. Minor changes in the sugar puckering as found in the T4-T6(N3O4'O_X) conformers to C2'-endo ($^2T_1$) destabilize the complexes by at least 4.4

kJ/mol. The T8, T12, and T14(N3O4'O_X) conformers with C1'-exo ($_1T^O$) sugar puckering are somewhat less stable, by at least 8.4 kJ/mol than the ground T1(N3O4'O_X) conformer. O4'-endo ($^OT_1$) and C2'-exo ($_2T^3$) sugar puckerings are also found among the low-energy T(N3O4'O_X) conformers but are at least 9.8 and 19.4 kJ/mol less stable than the ground conformer, respectively. A unique quadridentate conformer, Q1(N3O4'O5'O_X), is only found for $[pAdo+Na]^+$, but more highly chelated structure is actually 18.4 kJ/mol higher in relative Gibbs free energy than the ground T1(N3O4'O_X) conformer. An additional hydrogen-bonding interaction between hydroxyl substituent of phosphate moiety and the N3 atom of the adenine nucleobase is found in the T14(N3O4'O_X) conformer, whereas an additional hydrogen-bonding interaction between a phosphate hydroxyl substituent and the N7 atom of the adenine nucleobase is found in the T15(N3O4'O_X) conformer. However, these complexes are 16.7 and 19.4 kJ/mol less stable than T1(N3O4'O_X), respectively. Proton transfer from the phosphate group to the N3 atom of the adenine nucleobase is also found for $[pAdo+Na]^+$, where Na^+ again preferentially binds to the negatively charged phosphate moiety. These phosphate binding conformers are at least 8.0 kJ/mol less stable than the ground T1(N3O4'O_X) conformer. Two distinct bidentate phosphate binding modes are again found, however in contrast to pdAdo, a slight preference for B(O_XO_X) over B(O_XO_H) is found. Additional stabilization is again achieved via a hydrogen-bonding interaction between the O_X and N3H atoms. The T1(O3'O5'O_X) conformer, where Na^+ binds to the sugar and phosphate moieties, but not to the nucleobase, is 14.7 kJ/mol less favorable than the ground T1(N3O4'O_X) conformer.

In summary, theory suggests that the ground conformer of $[pAdo+Na]^+$ involves tridentate binding of Na^+ to the N3, O4' and O_X atoms with a *syn* orientation of the adenine nucleobase, and C3'-endo ($^3T_2$) sugar puckering. C2'-endo, C2'-exo, C1'-exo and O4'-endo sugar puckerings are also found among the low-energy T(N3O4'O_X) conformers. A unique quadridentate Q1(N3O4'O5'O_X) conformer is found only for $[pAdo+Na]^+$, but in spite of the additional chelation interaction, this mode of Na^+ binding is less favorable than T(N3O4'O_X). All conformers calculated within 20 kJ/mol prefer a *syn* orientation of the adenine nucleobase. Conformers that involve binding solely to the phosphate moiety, or the phosphate and sugar moieties, are at least 8.0 and 14.1 kJ/mol less stable than the ground T1(N3O4'O_X) conformer, respectively. The 2'-hydroxyl substituent of pAdo does not significantly influence the stable low-energy conformations compared to $[pdAdo+Na]^+$, but does enable an additional hydrogen-bonding interaction between the 2'- and 3'-hydroxyls to stablilize these complexes.

6.4 STABLE LOW-ENERGY CONFORMERS OF DISODIUM CATIONIZED DEPROTONATED ADENINE MONONUCLEOTIDES

6.4.1 STABLE LOW-ENERGY CONFORMERS OF DISODIUM CATIONIZED DEPROTONATED 2'-DEOXYADENOSINE-5'-MONOPHOSPHATE

The stable low-energy conformers of $[pdAdo-H+2Na]^+$ that are within 20 kJ/mol of the ground conformer along with their relative Gibbs free energies, nucleobase orientations, and sugar puckerings are compared in **Figure 6.3**. Among the 16 stable low-energy conformers found within 20 kJ/mol of the ground conformer, 11 unique modes of Na^+ binding were found, including QB(N3O4'O5'O_X,O_XO_X), TT(N3O4'O_X,N7NH_2O_X), QT(N3O4'O5'O_X,N1O_XO_X), QB(N3O4'O5'O_X,O3'O_X), TB(N3O4'O_X,O_XO_H), TT(N3O4'O_X,N7O_XO_X), QT(N3O4'O5'O_X,O3'O_XO_X),

TB(N3O4'O_X,N7O_X), TT(N3O4'O_X,N1$O_X$$O_X$), QB(N3O4'O5'$O_X$,$O_X$$O_H$), and TT(N3O4'$O_X$,O3'O5'$O_X$). In all of these conformers, one sodium cation binds in a tridentate or quadridentate fashion to the adenine nucleobase, sugar and phosphate moieties, whereas the second sodium cation binds in a bidentate or tridentate fashion. When binding of the second Na^+ involves both the adenine nucleobase and phosphate moiety, the structures are highly compact, whereas the conformers that involve only the phosphate moiety, or the phosphate and sugar moieties are somewhat less compact vs. the monosodium cationized counterparts described in **Section 6.3.1**. In the ground conformer of [pdAdo-H+2Na]$^+$, the first Na^+ binds in a quadridentate fashion to the N3, O4′, O5′ and O_X atoms, whereas the second Na^+ binds solely to the phosphate group via chelation interactions with both O_X atoms. In this ground conformer, adenine prefers a *syn* orientation and the sugar moiety is O4'-endo ($^OT_1$) puckered. C2'-endo ($^2T_1$) and C2'-exo ($_2T^3$) sugar puckerings are also found in QB(N3O4'O5'O_X,$O_X$$O_X$) conformers; the change in sugar puckering destabilizes these complexes by 2.6 and 4.6 kJ/mol, respectively. The conformers with the second sodium cation binding to both the phosphate group and the adenine nucleobase, i.e., TT1(N3O4'O_X,N7$NH_2$$O_X$), TT2(N3O4'$O_X$,N7$NH_2$$O_X$), QT1(N3O4'O5'$O_X$,N1$O_X$$O_X$), TT1(N3O4'$O_X$,N7$O_X$$O_X$), TB1(N3O4'$O_X$,N7$O_X$), TB2(N3O4'$O_X$,N7$O_X$), TT1(N3O4'$O_X$,N1$O_X$$O_X$), and TT2(N3O4'$O_X$,N7$O_X$$O_X$) conformers, are at least 3.4 kJ/mol less stable. When the second sodium cation binds only to the phosphate and sugar moieties, i.e., the QB1(N3O4'O5'O_X,O3'O_X), QT1(N3O4'O5'O_X,O3'$O_X$$O_X$), and TT1(N3O4'$O_X$,O3'O5'$O_X$) conformers, the relative Gibbs free energies of these complexes slightly increase, to at least 5.0 kJ/mol. C1'-endo, C2'-endo, C2'-exo, C3'-exo, and O4'-endo sugar puckering

are found in these stable low-energy conformers. The effect of the sugar puckering on the relative Gibbs free energies is clearly less important than that of the Na^+ binding modes.

In summary, theory suggest that the first sodium cation prefers to bind to the adenine nucleobase, sugar moiety and phosphate group in a tridentate or quadridentate fashion. In the ground conformer, the second sodium cation binds solely to the phosphate group. Changes in the sugar puckering produce only a small change in the relative Gibbs free energies.

6.4.2 STABLE LOW-ENERGY CONFORMERS OF DISODIUM CATIONIZED DEPROTONATED ADENOSINE-5'-MONOPHOSPHATE

The stable low-energy conformers of $[pAdo\text{-}H+2Na]^+$ that are within ~20 kJ/mol of the ground conformer along with their relative Gibbs free energies, nucleobase orientations, and sugar puckerings are compared in **Figure 6.4**. Among the 20 stable low-energy conformers found within 21 kJ/mol of the ground conformer, 11 unique modes of Na^+ binding were found, including QB(N3O4'O5'O_X,O3'O_X), QB(N3O4'O5'O_X,$O_X O_X$), TB(N3O4'O_X,$O_X O_H$), BB(N7O_X,O3'O_X), QB(N3O4'$O_X O_H$,$O_X O_X$), TT(N3O4'O_X,N7$NH_2 O_X$), TT(N3O4'O_X,O3'O5'O_X), TB(N3O4'O_X,N7O_X), TT(N3O4'O_X,N7$O_X O_X$), TT(N3O4'O_X,N1$O_X O_X$), and QB(N3O4'$O_X O_X$,$O_X O_H$). In contrast to $[pdAdo\text{-}H+2Na]^+$, theory suggests that the first Na^+ binds in a quadridentate fashion to the N3, O4′, O5′ and O_X atoms of the deprotonated adenine mononucleotide, and the second Na^+ binds to an O_X atom of the phosphate moiety and O3' atom of the sugar moiety. This conformer is similar to the QB1(N3O4'O5'O_X,O3'O_X) conformer of $[pdAdo\text{-}H+2Na]^+$ that is 5.0 kJ/mol less stable than the corresponding ground conformer. The adenine nucleobase prefers a *syn* orientation and the sugar exhibits C4'-exo ($_4T^O$) sugar

puckering. For all stable low-energy conformers, one sodium cation binds in a tridentate or quadridentate fashion to the adenine nucleobase, sugar moiety and phosphate group, except for the BB1(N7O_X,O3'O_X) conformer, where the first sodium cation binds to the adenine nucleobase and phosphate group via the N7 and O_X atoms, and the second sodium cation binds to sugar and phosphate moieties via the O3' and O_X atoms. Conformers with the second sodium cation binding solely to the phosphate moiety, i.e. QB1-QB5(N3O4'O5'O_X,$O_X$$O_X$), TB1-TB2(N3O4'$O_X$,$O_X$$O_H$), QB1(N3O4'$O_X$$O_H$,$O_X$$O_X$), QB1(N3O4'$O_X$$O_X$,$O_X$$O_H$) conformers, are at least 6.7 kJ/mol less stable than the ground conformer. C1'-exo, C2'-exo, C3'-endo, C3'-exo, C4'-exo and O4'-endo sugar puckering are found among these stable low-energy conformers. The effect of the sugar puckering on the relative Gibbs free energies is clearly less important than that of the mode of Na^+ binding. In contrast to $[pdAdo-H+2Na]^+$, the additional 2'-hydroxyl substituent of pAdo often produces significant structural changes and indeed alters the preferred binding mode of the second sodium cation in many of the low-energy conformers.

In summary, theory suggests that the first sodium cation prefers to bind to the adenine nucleobase, sugar moiety and phosphate group in a tridentate or quadridentate fashion. The QB1(N3O4'O5'O_X,O3'O_X) conformer with the second sodium cation binding to phosphate group and sugar moiety is the ground conformer. The effect of the sugar puckering on the relative Gibbs free energies is less important than that of the mode of Na^+ binding, and the 2'-hydroxyl substituent of pAdo changes the preferred binding mode of the second sodium cation in the ground conformer and in many of the other low-energy conformers.

6.5 STABLE LOW-ENERGY CONFORMERS OF NEUTRAL ADENINE MONONUCLEOTIDES

The most stable *syn* and *anti* oriented conformers of pdAdo and pAdo are compared in **Figure 6.5**. The relative Gibbs free energies, nucleobase orientations and sugar puckerings are also shown. 17 and 23 stable low-energy conformers were found for pdAdo and pAdo within 20 kJ/mol of the corresponding ground conformer, respectively. In the ground conformer of pdAdo, a strong hydrogen-bonding interaction between the phosphate hydroxyl substituent and the N3 atom of the adenine nucleobase stabilizes the *syn* orientation of adenine nucleobase. The sugar exhibits C1'-exo ($_1T^2$) sugar puckering. In the most stable *anti* oriented conformer of pdAdo, a strong hydrogen-bonding interaction is found between the 3'-hydroxyl substituent and oxo oxygen atom of the phosphate moiety. The sugar exhibits C3'-endo ($^3T_4$) sugar puckering. This *anti* oriented conformer of pdAdo is 7.3 kJ/mol less stable than the ground *syn* oriented conformer. In contrast to pdAdo, the ground conformer of pAdo exhibits an *anti* orientation of adenine nucleobase and C2'-endo ($^2T_1$) sugar puckering. A strong hydrogen-bonding interaction between the 2'-hydroxyl substituent and the N3 atom of the adenine nucleobase is found to stabilize the *anti* orientation of the adenine nucleobase. The most stable *syn* oriented conformer of pAdo is only 0.5 kJ/mol less stable than the ground conformer. Similar to the ground conformer of pdAdo, a strong hydrogen-bonding interaction between the phosphate hydroxyl substituent and the N3 atom of the adenine nucleobase is also found. The sugar exhibts C1'-exo ($_1T^O$) sugar puckering. Additionlaly, the 2'-hydroxyl substituent of pAdo enables an additional hydrogen-bonding interaction between the 2'- and 3'-hydroxyls.

In summary, the adenine nucleobase of pdAdo prefers *syn* orientation, whereas that of pAdo prefers *anti* orientation. The 2'-hydroxyl substituent of pAdo is able to form

a strong hydrogen-bonding interaction with the N3 atom of adenine nucleobase, such that the *anti* orientation of adenine nucleobase becomes more favorable for pAdo. Additionally, the 2'-hydroxyl substituent of pAdo enables an additional hydrogen-bonding interaction between the 2'- and 3'-hydroxyls, which are found in all stable low-energy conformers of pAdo.

6.6 STABLE LOW-ENERGY CONFORMERS OF NEUTRAL SODIUM CATIONIZED DEPROTONATED ADENINE MONONUCLEOTIDE SALTS

The most stable low-energy conformers of [pdAdo-H+Na] and [pAdo-H+Na] that exhibit a unique binding mode of Na^+ binding and are within 20 kJ/mol of the ground conformer are compared in **Figure 6.6**. The relative Gibbs free energies, nucleobase orientations, and sugar puckerings are also shown. Three unique modes of Na^+ binding were found for both [pdAdo-H+Na] and [pAdo-H+Na] within 20 kJ/mol of the ground conformer, including Q(N3O4'O5'O_X), Q(N3O4'$O_X$$O_X$), and T(N1$O_X$$O_X$). The ground conformers of [pdAd-H+Na] and [pAdo-H+Na] exhibit very similar conformations, where Na^+ binds to the N3, O4', O5' and O_X atoms of deprotonated pdAdo and pAdo with a *syn* orientation of the adenine nucleobase, and C4'-exo ($_4T^O$) sugar puckering. A hydrogen-bonding interaction between the 3'-hydroxyl and O_X atom of phosphate moiety is found in both ground conformers. A hydrogen-bonding interaction between the 2'- and 3'-hydroxyl substituents is also found in [pAdo-H+Na]. When the fourth chelation interaction is with the phosphate oxo oxygen atom, O_X, rather than O5' of the sugar, as in the Q1(N3O4'$O_X$$O_X$) conformers of [pdAdo-H+Na] and [pAdo-H+Na], the complexes are destabilized by 7.6 and 16.8 kJ/mol vs. the corresponding ground conformers, respectively. In both quadridentate binding modes, the adenine nucleobase prefers a *syn* orientation. The Q1(N3O4'$O_X$$O_X$) conformer of [pdAdo-H+Na] exhibits C2'-endo ($^2T_1$)

sugar puckering, whereas that of [pAdo-H+Na] exhibits C3'-endo ($^{3}T_{4}$) sugar puckering. The T1($N1O_XO_X$) conformers of [pdAdo-H+Na] and [pAdo-H+Na] are 12.3 and 18.9 kJ/mol less stable than the corresponding ground conformers, respectively. In these tridentate binding conformers, the adenine nucleobase exhibits an *anti* orientation. The T1($N1O_XO_X$) conformer of [pdAdo-H+Na] exhibits C2'-exo ($_{2}T^{3}$) sugar puckering, whereas that of [pAdo-H+Na] exhibits C3'-exo ($_{3}T^{2}$) sugar puckering. The larger difference in relative Gibbs free energy of the low-energy conformers of [pAdo-H+Na] vs. [pdAdo-H+Na] may result from the additional O2'H•••O3' hydrogen-bonding interaction in the ground conformer of [pAdo-H+Na], which is clearly not possible for [pdAdo-H+Na].

In summary, for the neutral adenine nucleotide salt complexes, [pdAdo-H+Na] and [pAdo-H+Na], theory suggests that the sodium cation prefers to bind to the adenine nucleobase, sugar moiety and phosphate group in a quadridentate fashion. Q1($N3O4'O5'O_X$) conformers with a *syn* orientation and C4'-exo ($_{4}T^{O}$) sugar puckering are the ground conformers of [pdAdo-H+Na] and [pAdo-H+Na]. Sodium cation binding to the N3, O4', and two O_X atoms is less favorable than to N3, O4', O5', and O_X binding mode of the ground conformers. N1 binding conformers with an *anti* orientation of adenine nucleobase are less favorable than the N3 *syn* conformers. The 2'-hydroxyl of pAdo accentuates these preferences.

6.7 INFLUENCE OF CHARGE STATE ON THE GROUND CONFORMATIONS OF ADENINE MONONUCLEOTIDES

6.7.1 DNA ADENINE MONONUCLEOTIDES

The ground conformers of a variety of DNA adenine mononucleotide complexes are compared in **Figure 6.7** including: $[pdAdo-H]^{-}$,[191] pdAdo, [pdAdo-H+Na], $[pdAdo+H]^{+}$,[187] $[pdAdo+Na]^{+}$, and $[pdAdo-H+2Na]^{+}$. For $[pdAdo-H]^{-}$, adenine prefers an

anti orientation and the sugar prefers C3'-endo ($^3T_2$) sugar puckering. A strong hydrogen-bonding interaction is found between the O_X atom of the phosphate moiety and the 3'-hydroxyl substituent. Neutralization of $[pdAdo-H]^-$ by a proton alters the preferred nucleobase orientation via formation of a strong hydrogen-bonding interaction between phosphate hydroxyl hydrogen and N3 atom of the adenine nucleobase to *syn*, and the suger puckering changes to C1'-exo ($_1T^2$). Addition of a second proton to produce $[pdAdo+H]^+$ does not alter the syn orientation of the adenine nucleobase, however it does alter the preferred sugar puckering to C2'-endo ($^2T_1$). The most favorable protonation site of pdAdo is the N3 atom of the adenine nucleobase, such that the *syn* oriented $[pdAdo+H]^+$ is also stabilized by a strong hydrogen-bonding interaction between N3H and O_X atom of phosphate group thus altering the hydrogen bond donor and acceptor atoms. Neutralization of $[pdAdo-H]^-$ by a sodium cation also alters the preferred nucleobase orientation to *syn* and sugar puckering to C4'-exo ($_4T^O$). Unlike a proton, the sodium cation is able to form multiple chelation interactions, such that Na^+ binds to the N3, O4', O5', and O_X atoms of $[pdAdo-H]^-$. Further sodium cationization does not alter the mode of binding of the first sodium cation to $[pdAdo-H]^-$ vs. [pdAdo-H+Na], but does alter the orientation of the phosphate moiety and sugar puckering. The second sodium cation binds to the negatively charged phosphate moiety in the bidentate fashion. The adenine orientation remains *syn*, whereas the sugar puckering changes to O4'-endo ($^OT_1$). $[pdAdo+Na]^+$ can be produced by sodium cationization of pdAdo, or protonation of [pdAdo-H+Na]. The sodium cation binds to the N3, O4, and O_X atoms of pdAdo in the tridentate fashion. The mode of Na^+ binding in $[pdAdo+Na]^+$ is similar to that of [pdAdo-H+Na] and $[pdAdo-H+2Na]^+$ except that

neutrolization of the phosphate moiety by a proton reduces the number of chelation interactions with Na^+ from four to three, such that the O5' atom is no longer involved in the binding, which leads to a change in the rotation of the nucleobase to produce a more compact *syn* conformer and the sugar puckering changes to the more classical C3'-endo ($^3T_2$) puckering. Among all of these DNA adenine mononucleotide complexes, only $[pdAdo-H]^-$ exhibits an *anti* orientation of adenine nucleobase, cationization by either a proton or sodium cation induces base rotation leading to *syn* conformations.

6.7.2 RNA ADENINE MONONUCLEOTIDES

The ground conformers of a variety of RNA adenine mononucleotide complexes are compared in **Figure 6.8** including: $[pAdo-H]^-$,[192] pAdo, [pAdo-H+Na], $[pAdo+H]^+$,[187] $[pAdo+Na]^+$ and $[pAdo-H+2Na]^+$. The main difference between these DNA vs. RNA adenine mononucleotides is that the hydrogen-bonding interaction between 2'- and 3'-hydroxyl substituents is only found in all RNA adenine mononucleotides complexes. The protonated and monosodium cationized forms of the DNA vs. RNA adenine mononucleotide complexes exhibit highly parallel ground conformations, whereas the neutral and disodium cationized forms of the deprotonated mononucleotides exhibit marked differences in their preferred structures. A strong hydrogen-bonding interaction between the phosphate hydroxyl hydrogen and N3 atom of the adenine nucleobase stabilizes the *syn* orientation of the adenine nucleobase of pdAdo, whereas a unique hydrogen-bonding interaction between the 2'-hydroxyl hydrogen and N3 atom of the adenine nucleobase changes the nucleobase orientation to *anti* in pAdo. For the disodium cationized deprotonated adenine mononucleotides, the second sodium cation binds to both O_X atoms of the phosphate moiety in $[pdAdo-H+2Na]^+$, whereas the

second sodium cation binds to one O_X atom of the phosphate moiety and the 3'-hydroxyl substituent in $[pAdo-H+2Na]^+$. Only the deprotonated adenine mononucleotides and neutral pAdo exhibit an *anti* orientation of the nucleobase. Base rotation is facilitated by sodium cationization and/or protonation.

6.8 CONCLUSIONS

Overall, the stable low-energy conformers of the sodium cationized DNA and RNA forms of the adenine mononucleotides are generally highly parallel, suggesting that the additional 2'-hydroxyl substituent in the RNA form of the adenine mononucleotide does not significantly impact the conformations. However, for the disodium cationized deprotonated adenine mononucleotides, the QB1(N3O4'O5'O_X,O_XO_X) conformer is the ground conformer of $[pdAdo-H+2Na]^+$, whereas the QB1(N3O4'O5'O_X,O3'O_X) conformer is the ground conformer of $[pdAdo-H+2Na]^+$. The QB1(N3O4'O5'O_X,O_XO_X) conformer of $[pdAdo-H+2Na]^+$ is only 6.7 kJ/mol less stable than the ground conformer. For the sodium cationized adenine mononucleotides, the sodium cation prefers to bind to the adenine nucleobase, sugar moiety and phosphate group in the tridentate fashion to the N3, O4' and O_X atoms. Comparisons between the sodium cationized and disodium cationized deprotonated adenine mononucleotides suggest that the first Na^+ preferentially binds to adenine nucleobase, sugar moiety and phosphate group in the quadridentate fashion with N3, O4', O5', and O_X atoms The second Na^+ preferentially binds to the negatively charged phosphate group. The effect of the sugar puckering on the relative Gibbs free energies is less important than that of the mode of Na^+ binding. A *syn* orientation of the adenine nucleobase is most favorable for all of the sodium cationized forms of the neutral and

deprotonated adenine mononucleotides. For the DNA adenine mononucleotide, only $[pdAdo-H]^-$ exhibits an *anti* orientation of the adenine nucleobase; base rotation is facilitated by protonation and/or sodium cationization. For the RNA adenine mononucleotides, $[pAdo-H]^-$ and pAdo exhibits an *anti* orientation of adenine nucleobase; base rotation is also facilitated by sodium cationization and/or protonation of pAdo.

6.9 REFERENCES

187. R. R. Wu, C. C. He, L. A. Hamlow, Y.-w. Nei, G. Berden, J. Oomens and M. T. Rodgers, *J. Phys. Chem. B* 2016, **120**, 4616.

191. Y.-w. Nei, N. Hallowita, J. D. Steill, J. Oomens and M. T. Rodgers, *J. Phys. Chem. A* 2013, **117**, 1319.

192. Y.-w. Nei, K. T. Crampton, G. Berden, J. Oomens and M. T. Rodgers, *J. Phys. Chem. A* 2013, **117**, 10634.

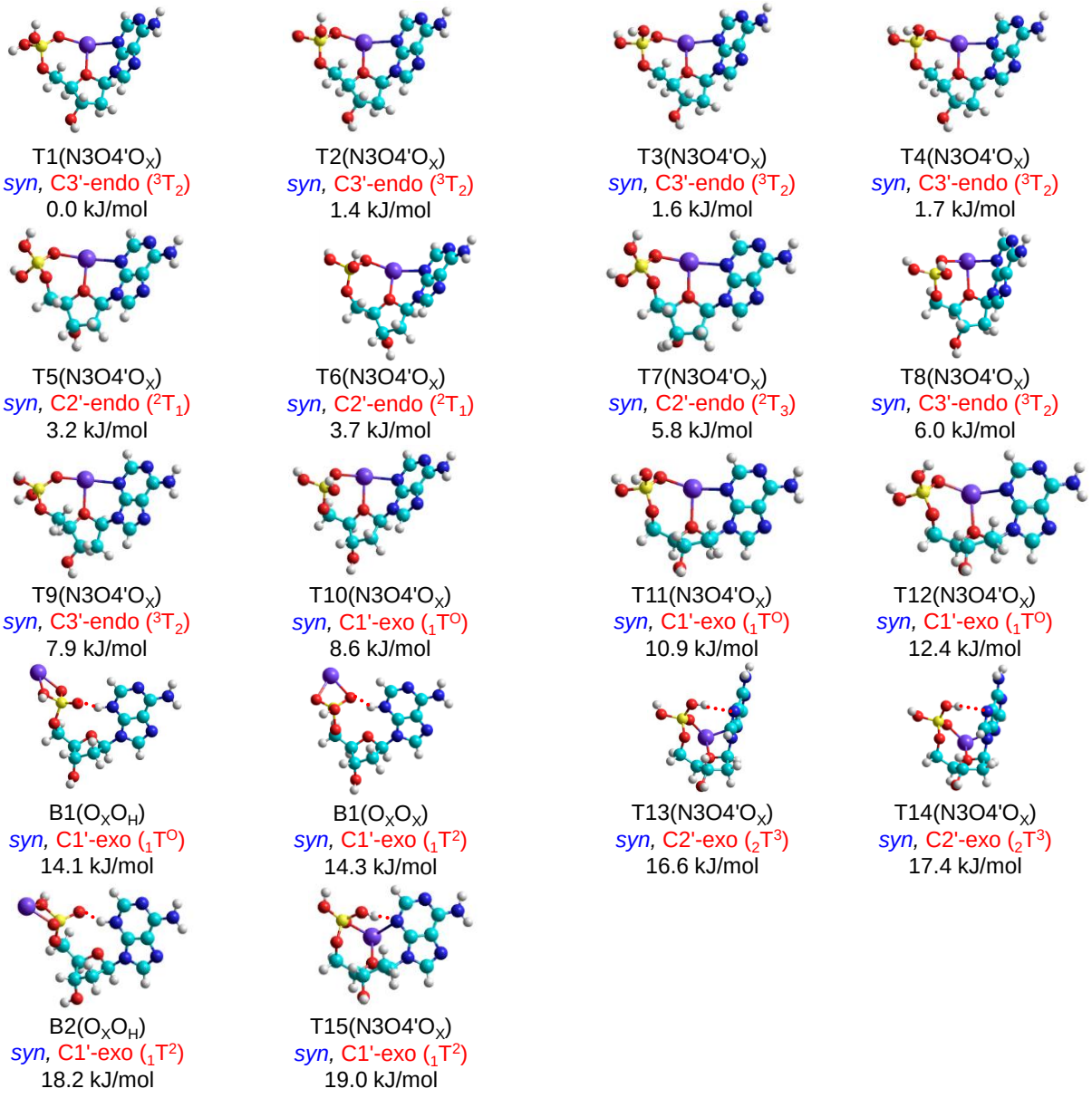

Figure 6.1 Stable low-energy B3LYP/6-311+G(d,p) conformers of [pdAdo+Na]$^+$. The orientations of the adenine nucleobase, sugar puckerings, and the relative 298 K Gibbs free energies at the B3LYP/6-311+G(2d,2p) level of theory are also listed.

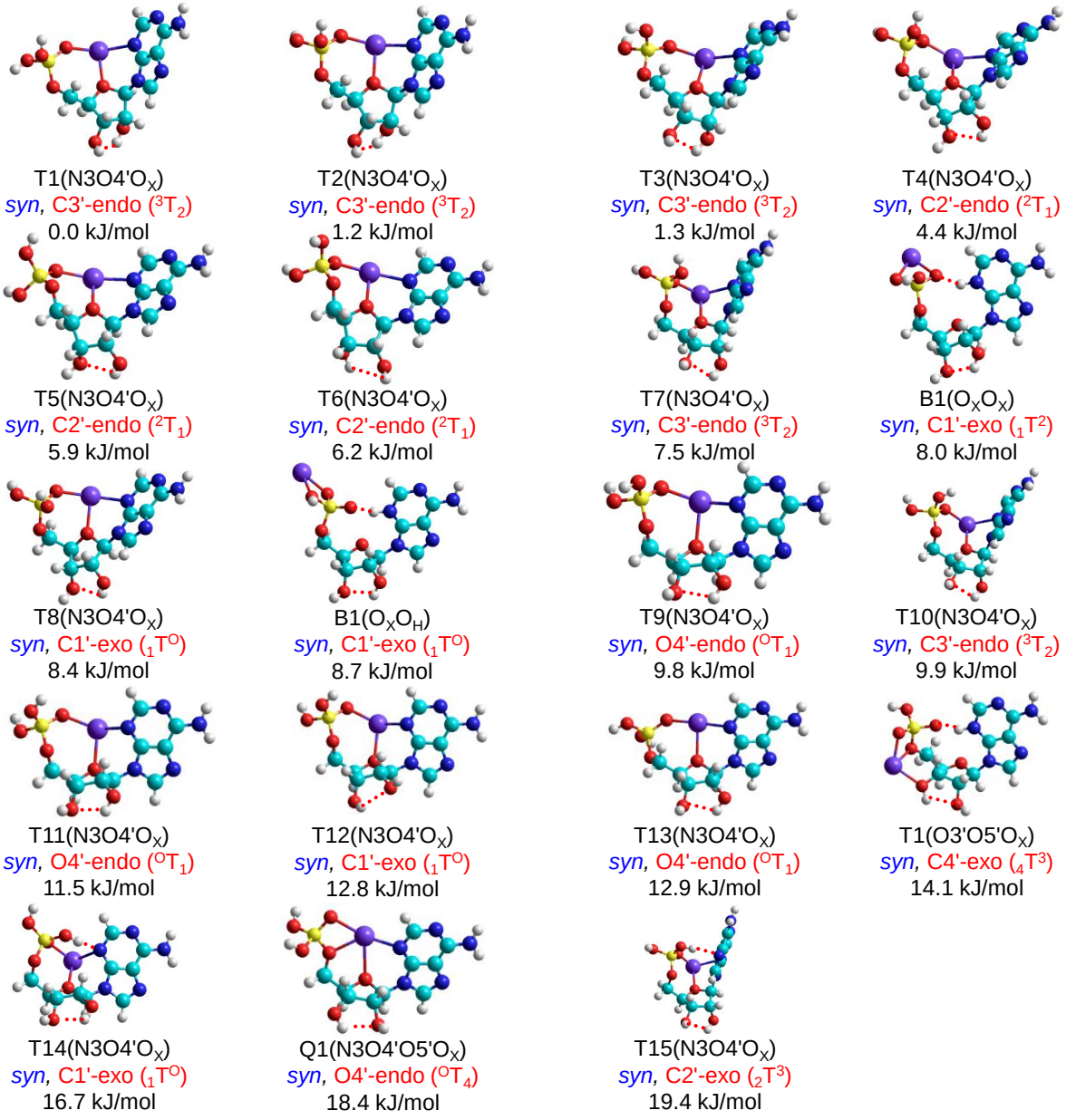

[pAdo+Na]$^+$

Figure 6.2 Stable low-energy B3LYP/6-311+G(d,p) conformers of [pAdo+Na]$^+$. The orientations of the adenine nucleobase, sugar puckerings, and the relative 298 K Gibbs free energies at the B3LYP/6-311+G(2d,2p) level of theory are also listed.

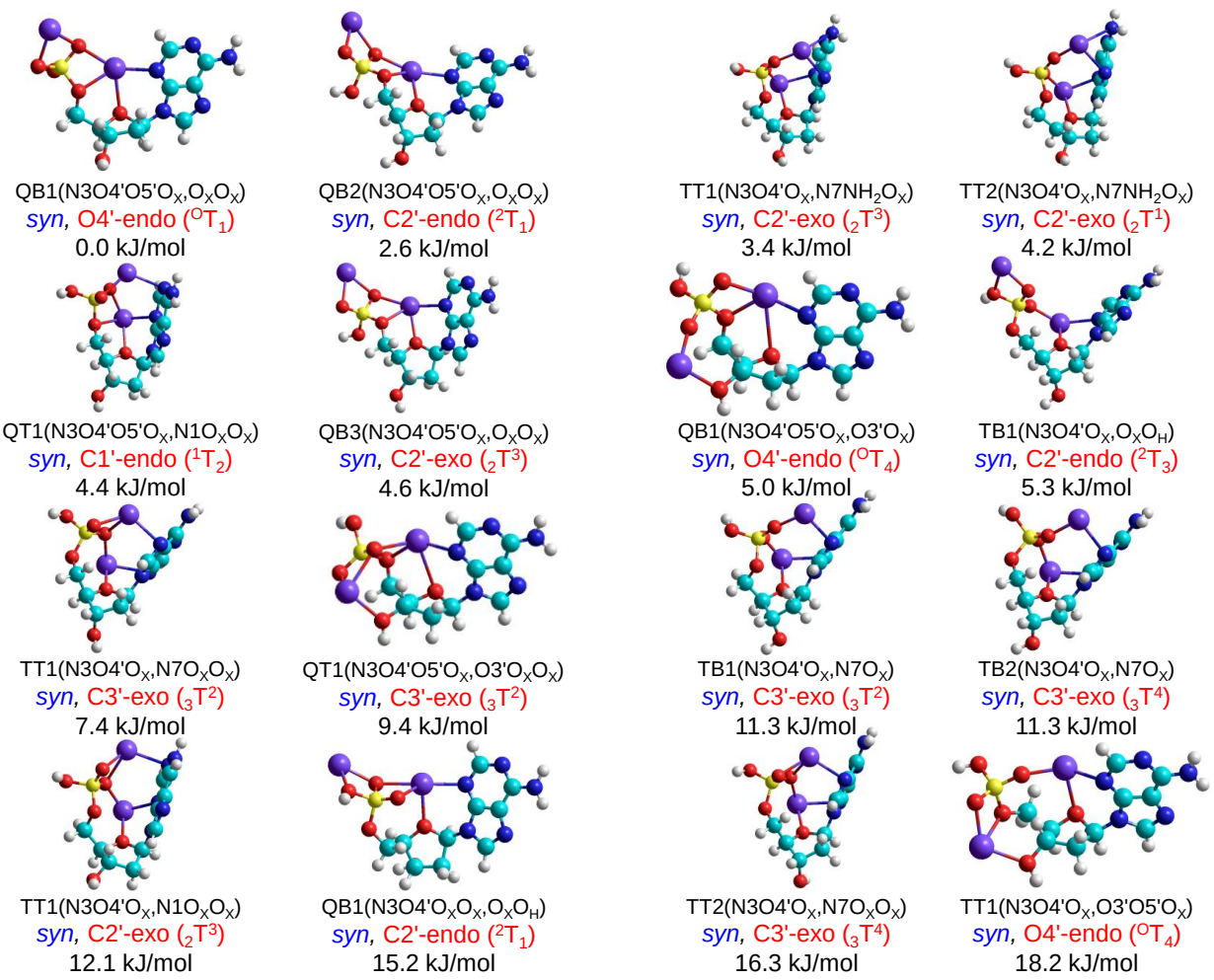

[pdAdo-H+2Na]$^+$

Figure 6.3 Stable low-energy B3LYP/6-311+G(d,p) conformers of [pdAdo-H+2Na]$^+$. The orientations of the adenine nucleobase, sugar puckerings, and the relative 298 K Gibbs free energies at the B3LYP/6-311+G(2d,2p) level of theory are also listed.

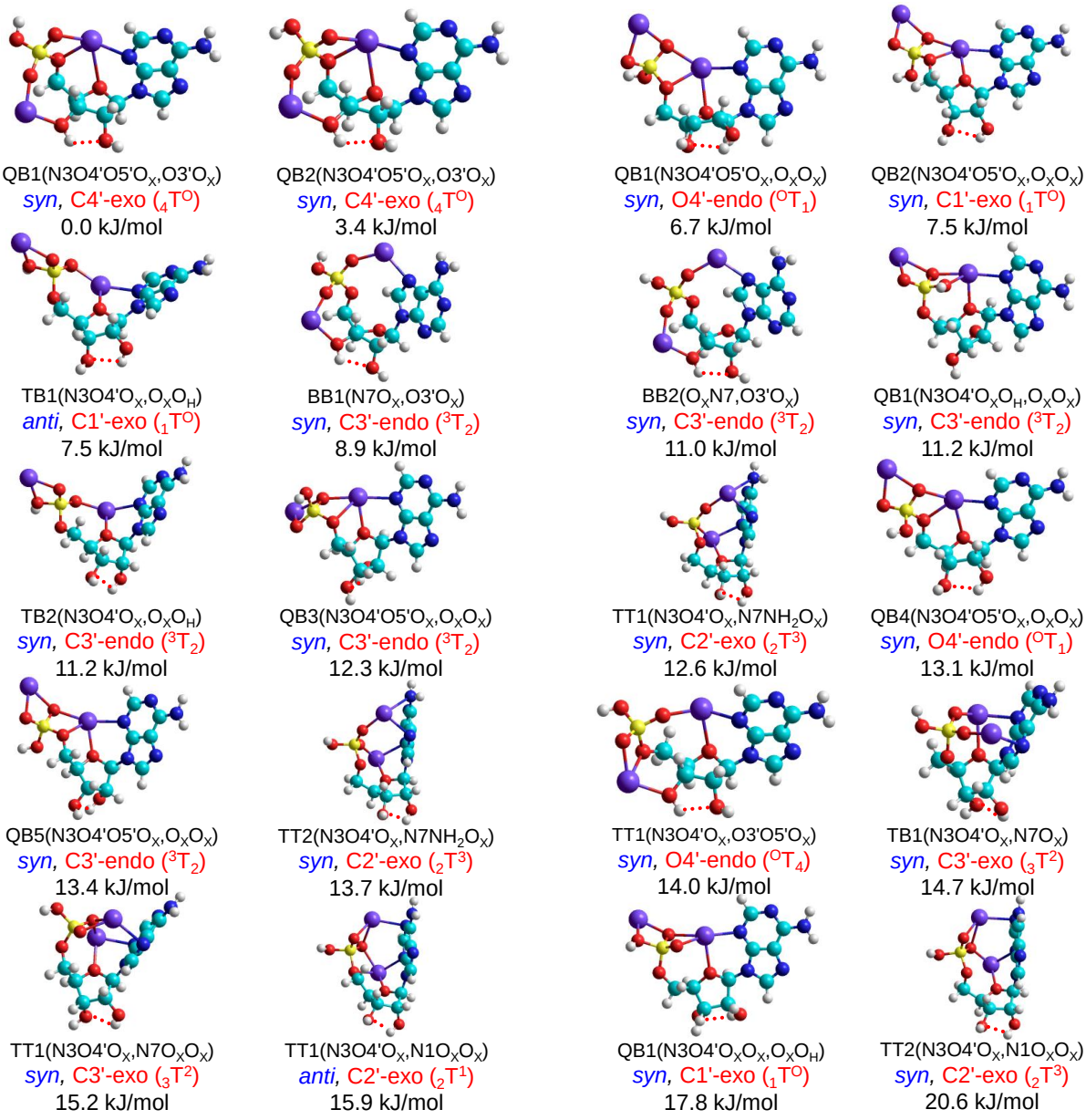

[pAdo-H+2Na]$^+$

Figure 6.4 Stable low-energy B3LYP/6-311+G(d,p) conformers of [pAdo-H+2Na]$^+$. The orientations of the adenine nucleobase, sugar puckerings, and the relative 298 K Gibbs free energies at the B3LYP/6-311+G(2d,2p) level of theory are also listed.

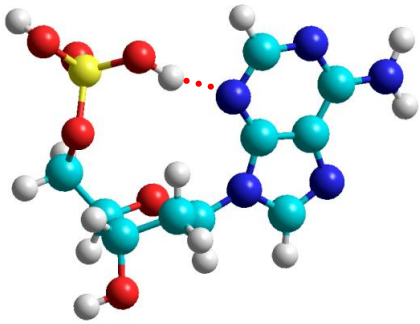

pdAdo
syn, C1'-exo ($_1T^2$)
0.0 kJ/mol

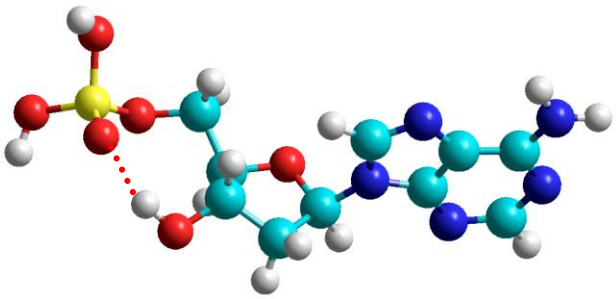

pdAdo
anti, C3'-endo ($^3T_4$)
7.3 kJ/mol

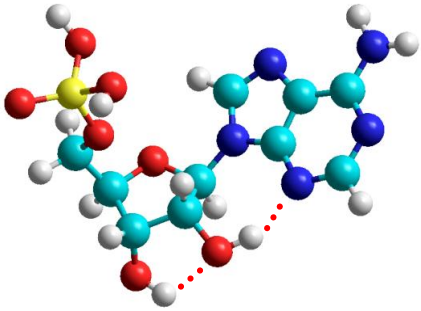

pAdo
anti, C2'-endo ($^2T_1$)
0.0 kJ/mol

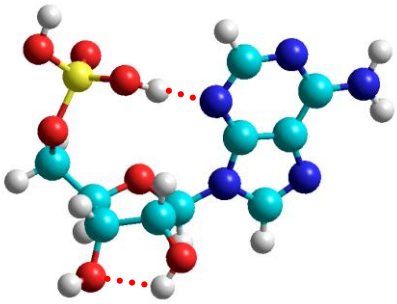

pAdo
syn, C1'-exo ($_1T^O$)
0.5 kJ/mol

Figure 6.5 The most stable B3LYP/6-311+G(d,p) conformers of pdAdo and pAdo with *syn* and *anti* orientation of adenine nucleobase. The orientations of the adenine nucleobase, sugar puckerings, and the relative 298 K Gibbs free energies at the B3LYP/6-311+G(2d,2p) level of theory are also listed.

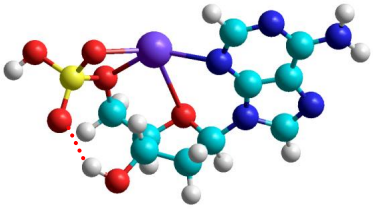

Q1(N3O4'O5'O_X)
syn, C4'-exo ($_4T^O$)
0.0 kJ/mol

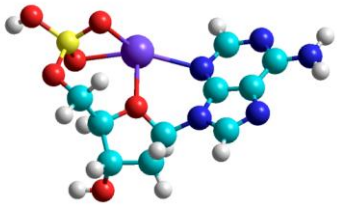

Q1(N3O4'O_XO_X)
syn, C2'-endo ($^2T_1$)
7.6 kJ/mol

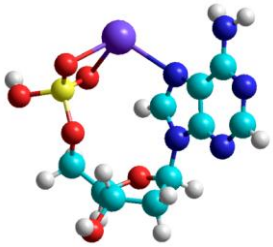

T1(N1O_XO_X)
anti, C2'-exo ($_2T^3$)
12.3 kJ/mol

[pdAdo-H+Na]

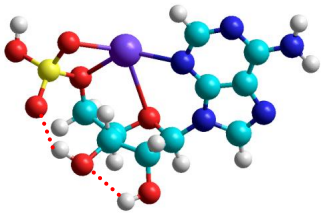

Q1(N3O4'O5'O_X)
syn, C4'-exo ($_4T^O$)
0.0 kJ/mol

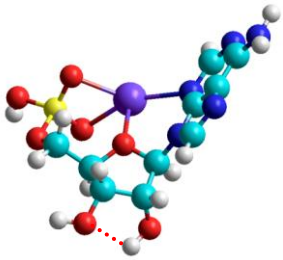

Q1(N3O4'O_XO_X)
syn, C3'-endo ($^3T_4$)
16.8 kJ/mol

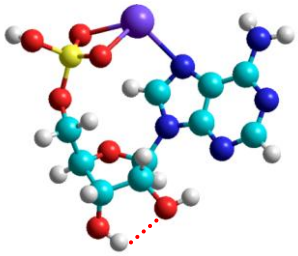

T1(N1O_XO_X)
anti, C3'-exo ($_3T^2$)
18.9 kJ/mol

[pAdo-H+Na]

Figure 6.6 The most stable B3LYP/6-311+G(d,p) conformers of [pdAdo-H+Na] and [pAdo-H+Na] with different binding modes of Na^+ below 20 kJ/mol. The orientations of the adenine nucleobase, sugar puckerings, and the relative 298 K Gibbs free energies at the B3LYP/6-311+G(2d,2p) level of theory are also listed.

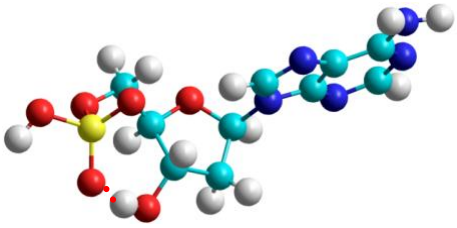

[pdAdo-H]$^-$
anti, C3'-endo ($^3T_2$)

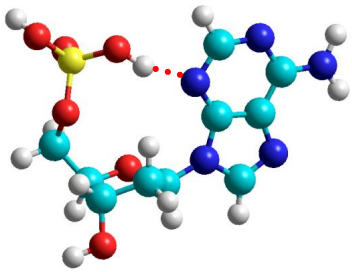

pdAdo
syn, C1'-exo ($_1T^2$)

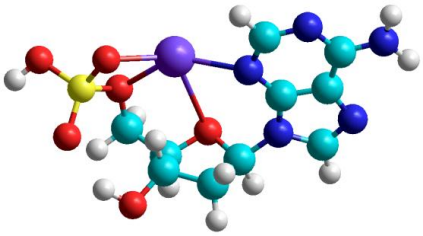

[pdAdo-H+Na]
Q1(N3O4'O5'O_X)
syn, C4'-exo ($_4T^O$)

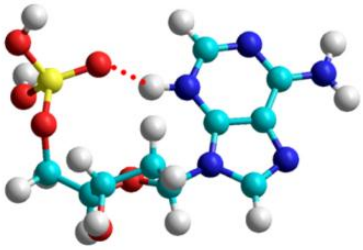

[pdAdo+H]$^+$
N3
syn, C2'-endo ($^2T_1$)

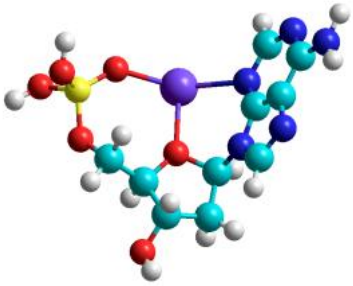

[pdAdo+Na]$^+$
T1(N3O4'O_X)
syn, C3'-endo ($^3T_2$)

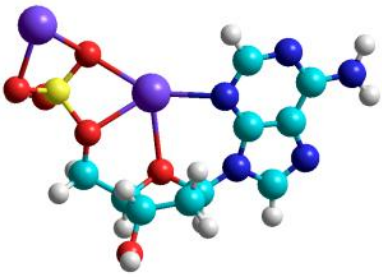

[pdAdo-H+2Na]$^+$
QB1(N3O4'O5'O_X,$O_X$$O_X$)
syn, O4'-endo ($^OT_1$)

Figure 6.7 Ground conformers of a variety of DNA adenine mononucleotide complexes, including [pdAdo-H]$^-$, pdAdo, [pdAdo-H+Na], [pdAdo+H]$^+$, [pdAdo+Na]$^+$, and [pdAdo-H+2Na]$^+$. The orientation of the adenine nucleobase and sugar puckering are also listed.

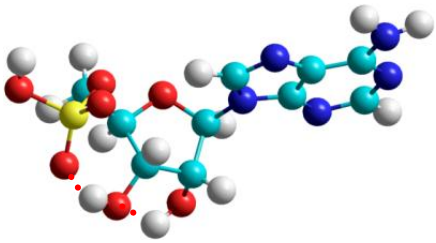

[pAdo-H]$^-$
anti, C3'-endo ($^3T_2$)

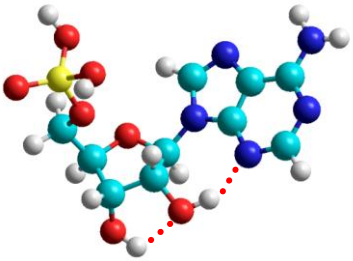

pAdo
anti, C2'-endo ($^2T_1$)

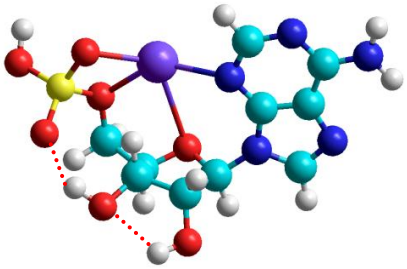

[pAdo-H+Na]
Q1(N3O4'O5'O_X)
syn, C4'-exo ($_4T^O$)

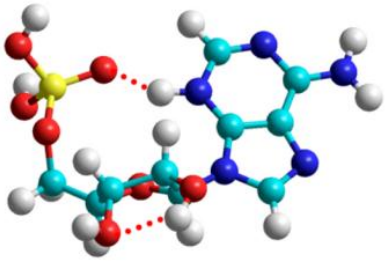

[pAdo+H]$^+$
N3
syn, C2'-endo ($^2T_1$)

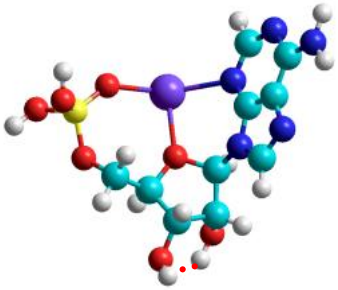

[pAdo+Na]$^+$
T1(N3O4'O_X)
syn, C3'-endo ($^3T_2$)

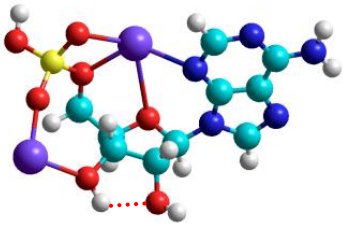

[pAdo-H+2Na]$^+$
QB1(N3O4'O5'O_X,$O_X$$O_X$)
syn, O4'-endo ($^OT_1$)

Figure 6.8 Ground conformers of a variety of RNA adenine mononucleotide complexes, including [pAdo-H]$^-$, pAdo, [pAdo-H+Na], [pAdo+H]$^+$, [pAdo+Na]$^+$, and [pAdo-H+2Na]$^+$. The orientation of the adenine nucleobase and sugar puckering are also listed.

CHAPTER 7 CHARACTERIZATION OF THE STABLE GAS-PHASE CONFORMATIONS OF SODIUM CATIONIZED ADENINE MONONUCLEOTIDES VIA IRMPD ACTION SPECTROSCOPY

7.1 INTRODUCTION

Our motivation for studying the gas-phase conformations of the sodium cationized adenine mononucleotides is discussed in detail in **Chapter 1**. The experimental infrared multiple photon dissociation (IRMPD) spectra of $[pdAdo+Na]^+$, $[pAdo+Na]^+$, $[pdAdo–H+2Na]^+$, and $[pAdo–H+2Na]^+$ in both the IR fingerprint and hydrogen-stretching regions were obtained via the IRMPD action spectroscopy technique introduced in **Section 2.1**. The linear IR spectra of the stable low-energy conformers of these complexes were calculated at B3LYP/6-311+G(d,p) level of theory, as introduced in **Section 2.3**. The experimental IRMPD spectra are compared with the linear IR spectra predicted for these sodium cationized adenine mononucleotides to elucidate the conformations populated in the experiments. Present results are compared to analogous results for the sodium cationized adenine nucleosides discussed in **Section 4.3** to elucidate the effects of the phosphate moiety on the conformations of these nucleic acid building blocks. Present results are also compared to parallel studies of the deprotonated and protonated forms of these adenine mononucleotides to understand the effects of the local environment (charge state) on the conformations of these complexes populated by electrospray ionization (ESI).

7.2 RESULTS OF IRMPD ACTION SPECTROSCOPY EXPERIMENTS

7.2.1 EXPERIMENTAL IRMPD SPECTRA OF SODIUM CATIONIZED ADENINE MONONUCLEOTIDES

The experimental IRMPD spectra of $[pdAdo+Na]^+$ and $[pAdo+Na]^+$ in the IR fingerprint and hydrogen-stretching regions are compared in **Figure 7.1**. The IRMPD

yield of $[pAdo+Na]^+$ is much smaller than that of $[pdAdo+Na]^+$ in the IR fingerprint region. The most intense features differ by a factor of 3.5, whereas the features of minor to moderate intensity differ by a much larger factor, 20. A strong IR absorption at 1640 cm^{-1} is observed for both $[pdAdo+Na]^+$ and $[pAdo+Na]^+$. A moderately intense peak at 1575 cm^{-1} is observed for $[pdAdo+Na]^+$, however, this IR feature is much weaker for $[pAdo+Na]^+$. Several moderately intense IR features at 641, 726, 816, and spanning the region between 1330 and 1442, and 1468 cm^{-1} are apparent in the measured IRMPD spectrum of $[pdAdo+Na]^+$, whereas when these IR features are scaled by a factor of 20 in the measured IRMPD spectrum of $[pAdo+Na]^+$, they are high parallel to that observed in the measured IRMPD spectrum of $[pdAdo+Na]^+$. Two very broad and unresolved IR bands spanning the range from 864 to 1015 cm^{-1}, and from 1015 to 1180 cm^{-1} are observed for both $[pdAdo+Na]^+$ and $[pAdo+Na]^+$. An IR feature at 1280 cm^{-1} with a shoulder to the red is observed for $[pdAdo+Na]^+$, whereas this IR feature for $[pAdo+Na]^+$ is narrower and sharper as the shoulder is much less intense. In the hydrogen-stretching region, two intense IR absorptions are also observed for both $[pdAdo+Na]^+$ and $[pAdo+Na]^+$ at 3440 and 3660 cm^{-1}. A moderate IR band at 3553 cm^{-1} is observed for both $[pdAdo+Na]^+$ and $[pAdo+Na]^+$, whereas a moderate IR band is observed at 3560 cm^{-1} only in the measured IRMPD spectrum of $[pAdo+Na]^+$.

7.2.2 IR PHOTODISSOCIATION PATHWAYS OF SODIUM CATIONIZED ADENINE MONONUCLEOTIDES

The photodissociation pathways observed in the IRMPD action spectroscopy experiments of $[pdAdo+Na]^+$ and $[pAdo+Na]^+$ are summarized in **Reactions 7.1**–**7.5**,

$$[pNuo+Na]^+ + n\,h\nu \rightarrow [Ade+Na]^+ + (pNuo–Ade) \quad (7.1)$$

$$[pNuo+Na]^+ + n\,h\nu \rightarrow [pNuo–Ade+Na]^+ + Ade \quad (7.2)$$

$$[\text{pNuo+Na}]^+ + n\,h\nu \rightarrow [\text{pNuo–Ade–H}_2\text{O+Na}]^+ + \text{Ade} + \text{H}_2\text{O} \quad (7.3)$$

$$[\text{pNuo+Na}]^+ + n\,h\nu \rightarrow [\text{H}_3\text{PO}_4\text{+Na}]^+ + (\text{pNuo–H}_3\text{PO}_4) \quad (7.4)$$

$$[\text{pNuo+Na}]^+ + n\,h\nu \rightarrow [\text{Nuo+Na}]^+ + \text{HPO}_3 \quad (7.5)$$

where pNuo is the adenine mononucleotide. Among these photodissociation pathways, **Reactions 7.1** and **7.2** involve N-glycosidic bond cleavage with Na^+ retained by the adenine nucleobase and sugar moiety, respectively. Both of these reactions are major fragmentation pathways for both $[pdAdo+Na]^+$ and $[pAdo+Na]^+$ in the IR fingerprint and hydrogen-stretching regions. **Reaction 7.3** involves sequential elimination of water from the ionic product of **Reaction 7.2**, and is a moderate fragmentation pathway for both $[pdAdo+Na]^+$ and $[pAdo+Na]^+$ in the IR fingerprint region, but is not observed in the hydrogen-stretching region. **Reactions 7.4** and **7.5** involve phosphate ester bond cleavage with production of $[H_3PO_4+Na]^+$ and elimination of HPO_3, respectively. **Reaction 7.4** is observed in moderate abundance for both complexes in the IR fingerprint region, but is only observed for $[pdAdo+Na]^+$ in the hydrogen-stretching region. **Reaction 7.5** is a major fragmentation pathway for both complexes in the hydrogen-stretching region.

7.2.3 EXPERIMENTAL IRMPD SPECTRA OF DISODIUM CATIONIZED DEPROTONATED ADENINE MONONUCLEOTIDES

The experimental IRMPD spectra of $[pdAdo-H+2Na]^+$ and $[pAdo-H+2Na]^+$ in the IR fingerprint and hydrogen-stretching regions are compared in **Figure 7.1**. In the IR fingerprint region, $[pdAdo-H+2Na]^+$ and $[pAdo-H+2Na]^+$ exhibit very similar behavior with IR features that span almost the entire region. The most intense feature is observed near 1640 cm^{-1} in both spectra. This IR feature is of greater intensity for $[pdAdo-H+2Na]^+$ than $[pAdo-H+2Na]^+$, and is red shifted by ~10 cm^{-1}. An unresolved IR

feature is observed for both complexes as a shoulder to the red of the most intense peak. A moderately intense peak at 1460 cm^{-1} with similar intensity is observed in both spectra. A variety of moderate to weak IR absorptions are observed across the range from 630 to 1440 cm^{-1}, and the intensities of these IR features observed for $[pdAdo\text{-}H+2Na]^+$ are the same or slightly higher than those observed for $[pAdo\text{-}H+2Na]^+$, except for a weak IR feature at ~810 cm^{-1}. The IR feature at 930 cm^{-1} observed for $[pdAdo\text{-}H+2Na]^+$ shifts slightly to 950 cm^{-1} in the experimental IRMPD spectrum of $[pAdo\text{-}H+2Na]^+$. In the hydrogen-stretching region, two intense IR features at 3440 and 3660 cm^{-1} are observed for both $[pdAdo\text{-}H+2Na]^+$ and $[pAdo\text{-}H+2Na]^+$. A very weak IR band at 3553 cm^{-1} is observed for both $[pdAdo\text{-}H+2Na]^+$ and $[pAdo\text{-}H+2Na]^+$, whereas an additional weak IR band at 3590 cm^{-1} is also observed for $[pAdo\text{-}H+2Na]^+$.

7.2.4 IR PHOTODISSOCIATION PATHWAYS OF DISODIUM CATIONIZED DEPROTONATED ADENINE MONONUCLEOTIDES

The photodissociation pathways observed in the IRMPD action spectroscopy experiments of $[pdAdo\text{-}H+2Na]^+$ and $[pAdo\text{-}H+2Na]^+$ are summarized in **Reactions 7.6**–**7.13**.

$$[pNuo\text{-}H+2Na]^+ + n\,h\nu \rightarrow [pNuo\text{-}HPO_3+Na]^+ + NaPO_3 \quad (7.6)$$

$$[pNuo\text{-}H+2Na]^+ + n\,h\nu \rightarrow [PO_3+2Na]^+ + (pNuo\text{-}HPO_3) \quad (7.7)$$

$$[pNuo\text{-}H+2Na]^+ + n\,h\nu \rightarrow [H_2PO_4+2Na]^+ + (pNuo\text{-}H_3PO_4) \quad (7.8)$$

$$[pNuo\text{-}H+2Na]^+ + n\,h\nu \rightarrow [pNuo\text{-}H\text{-}Ade+2Na]^+ + Ade \quad (7.9)$$

$$[pNuo\text{-}H+2Na]^+ + n\,h\nu \rightarrow [Ade+H]^+ + (pNuo\text{-}2H+2Na) \quad (7.10)$$

$$[pNuo\text{-}H+2Na]^+ + n\,h\nu \rightarrow [Ade\text{-}H+2Na]^+ + (pNuo\text{-}Ade) \quad (7.11)$$

$$[pNuo\text{-}H+2Na]^+ + n\,h\nu \rightarrow [Ade+Na]^+ + (pNuo\text{-}H\text{-}Ade+Na) \quad (7.12)$$

$$[pNuo\text{-}H+2Na]^+ + n\,h\nu \rightarrow [pNuo\text{-}H\text{-}Ade\text{-}H_2O+Na]^+ + Ade + H_2O \quad (7.13)$$

$$[\text{pNuo-H+2Na}]^+ + n\,h\nu \rightarrow [\text{pNuo-H-H}_2\text{O+2Na}]^+ + \text{H}_2\text{O} \quad (7.14)$$

Among these photodissociation pathways, **Reactions 7.6**, **7.7**, and **7.8** involve phosphate ester bond cleavage. **Reactions 7.6** and **7.7** were observed for $[\text{pdAdo-H+2Na}]^+$ as the major fragmentation pathways in the IR fingerprint region, and **Reaction 7.7** was observed as a minor fragmentation pathway in the hydrogen-stretching region. In contrast, **Reactions 7.6**, **7.7**, and **7.8** were all minor fragmentation pathways for $[\text{pAdo-H+2Na}]^+$ in the IR fingerprint region. **Reactions 7.9**, **7.10**, **7.11**, and **7.12** involve N-glycosidic bond cleavage. **Reactions 7.9** and **7.10** were observed as minor fragmentation pathways for $[\text{pdAdo-H+2Na}]^+$ in the IR fingerprint region. **Reaction 7.11** was observed as a minor fragmentation pathway for $[\text{pAdo-H+2Na}]^+$ in the IR fingerprint region, whereas **Reactions 7.10** and **7.12** were minor fragmentation pathways in the hydrogen-stretching region. **Reaction 7.13** involves sequential elimination of water from the product of **Reaction 7.9**, or sequential elimination of Ade from the product of **Reaction 7.14**, and it was observed for $[\text{pdAdo-H+2Na}]^+$ as a minor fragmentation pathway in the IR fingerprint region, and the major fragmentation pathway in the hydrogen-stretching region. Elimination of water from disodium cationized deprotonated adenine mononucleotide is summarized in **Reaction 7.14**, and was observed as the major fragmentation pathway for $[\text{pAdo-H+2Na}]^+$ in both the IR fingerprint and hydrogen-stretching regions. The differences in the major photodissociation pathways of $[\text{pdAdo-H+2Na}]^+$ and $[\text{pAdo-H+2Na}]^+$ suggest that 2'-hydroxyl substituent of pAdo stabilizes the phosphate ester bond of the adenine mononucleotide.

7.3 SODIUM CATIONIZED ADENINE MONONUCLEOTIDES

7.3.1 CONFORMERS OF SODIUM CATIONIZED 2'-DEOXYADENOSINE-5'-MONOPHOSPHATE POPULATED BY ESI

The measured IRMPD spectrum and calculated IR spectra of select stable low-energy conformers of $[pdAdo+Na]^+$ are compared in **Figure 7.2**. Overall, the calculated IR spectrum of the ground T1(N3O4'O_X) conformer of $[pdAdo+Na]^+$ shows the best agreement with the measured IRMPD spectrum in the IR fingerprint and hydrogen-stretching regions. T2-T12(N3O4'O_X) conformers, which only differ by the rotation of the hydroxyl substituents of the phosphate and sugar moieties as well as sugar puckering, exhibit highly parallel calculated IR spectra, suggesting that these conformers may also be populated in the experiments, but the higher relative Gibbs free energies of these conformers suggest that these conformers should have lower population than the ground conformer. For the most stable phosphate binding conformer, B1(O_XO_H), the IR features calculated at 1592 and 1644 cm^{-1} slightly shift to the blue compared to the intense peaks observed at 1575 and 1640 cm^{-1} in the experimental IRMPD spectrum. A weak IR feature is found at 1520 cm^{-1} in the calculated IR spectrum, which is not observed in the experimental IRMPD spectrum. These minor spectral differences suggest that this B1(O_XO_H) phosphate binding conformer is either not populated or if present is present in minor abundance in the experiments. The B1(O_XO_X) conformer is only 0.2 kJ/mol less stable than B1(O_XO_H), but the intense IR band predicted at 1162 cm^{-1} is not observed in the measured IRMPD spectrum, indicating that this conformer of $[pdAdo+Na]^+$ is not populated in the experiments. The main difference between the T1(N3O4'O_X) and T13(N3O4'O_X) conformers is that there is an additional hydrogen-π interaction between the phosphate hydroxyl hydrogen and the N7 atom of adenine. The

feature predicted at 3660 cm^{-1} in the calculated IR spectrum of T13(N3O4'O_X) conformer is not observed in the experimental IRMPD spectrum, indicating that this conformer is not an important conformation in the experiments. The T15(N3O4'O_X) conformer has an additional hydrogen-bonding interaction between the phosphate hydroxyl hydrogen and N3 atom of the adenine nucleobase. Interestingly, the calculated IR spectrum of the T15(N3O4'O_X) conformer exhibits reasonably good agreement with the measured IRMPD spectrum. However, the high relative Gibbs free energy suggests that this conformer, if present, is present in much lower population than the ground T1(N3O4'O_X) conformer.

In summary, the ground T1(N3O4'O_X) conformer as well as the low-energy T2-T12(N3O4'O_X) conformers of $[pdAdo+Na]^+$ are populated in the experiments. The sodium cation prefers to bind to the N3 atom of adenine nucleobase, the O4' atom of the sugar moiety and the O_X oxygen atom of phosphate moiety in a tridentate fashion. The B1(O_XO_H) conformer may be present in lower population than the ground conformer as minor shifts in the calculated IR spectrum indicate that it cannot be present in significant abundance. The intense IR band at 1162 cm^{-1} in the calculated IR spectrum predicted for the B1(O_XO_X) conformer suggest that this conformer is not populated in the experiments. Phosphate binding conformers and the T(N3O4'O_X) conformers that possess an additional hydrogen-π interaction between the phosphate hydroxyl and adenine nucleobase are not populated in the experiments. Comparison between the experimental IRMPD and calculated IR spectra of the T15(N3O4'O_X) conformer which has an additional hydrogen bonding interaction between the phosphate hydroxyl hydrogen atom and N3 atom of the adenine nucleobase makes it

hard to eliminate this conformer in the experiments. However, the high relative Gibbs free energy of this conformer suggests that the population of the T15(N3O4'O_X) conformer should be much lower than that of the ground T1(N3O4'O_X) conformer.

7.3.2 CONFORMERS OF SODIUM CATIONIZED ADENOSINE-5'-MONOPHOSPHATE POPULATED BY ESI

The measured IRMPD spectrum and calculated IR spectra of select stable low-energy conformers of $[pAdo+Na]^+$ are compared in **Figure 7.3**. Similar to $[pdAdo+Na]^+$, the calculated IR spectrum of the ground T1(N3O4'O_X) conformer of $[pAdo+Na]^+$, where Na^+ binds to the N3, O4', and O_X atoms of pAdo in a tridentate fashion, exhibits the best agreement with the measured IRMPD spectrum. The T2-T13(N3O4'O_X) conformers, which only differ by rotation of the hydroxyl substituents of the phosphate and sugar moieties as well as sugar puckering, exhibit highly parallel calculated IR spectra, suggesting that these conformers may also be populated in the experiments, but the higher relative Gibbs free energies of these conformers suggest that these conformers should have lower population than the ground conformer. In the calculated IR spectrum predicted for the most stable phosphate binding conformer, B1(O_XO_X), the splitting of the IR feature at 3660 cm^{-1}, the missing IR feature at 3600 cm^{-1}, and the significant shift of the feature at 1163 cm^{-1} indicate that this conformer is not populated in the experiments. The B1(O_XO_H) conformer, which is only 0.7 kJ/mol less stable than B1(O_XO_X) conformer, exhibits parallel IR features in the hydrogen-stretching region as the B1(O_XO_X) conformer, but significant shifts of the IR features at 781 and 1226 cm^{-1} suggest that the B1(O_XO_H) conformer is not present in the experiments. The calculated IR spectrum of the T14(N3O4'O_X) conformer, which has an additional hydrogen-bonding interaction between the phosphate hydroxyl hydrogen atom and the N3 atom of the

adenine nucleobase, does not reproduce the IR feature observed at 3600 cm^{-1}, suggesting that this conformer is not populated in the experiments. Similar to $[pdAdo+Na]^+$, the T15(N3O4'O_X) conformer is not an important conformation in the experiments, as the additional IR feature predicted at 3460 cm^{-1} is not present in the measured IRMPD spectrum.

In summary, the IR spectrum calculated for the ground T1(N3O4'O_X) conformer of $[pAdo+Na]^+$ shows the best agreement with the experimental IRMPD spectrum, indicating that this conformer is dominantly populated in the experiments. The T2-T13(N3O4'O_X) conformers may also be present as they exhibit highly parallel IR spectra. The sodium cation preferentially binds to the N3, O4' and O_X atoms in the tridentate fasion. It can be concluded that phosphate binding conformers of $[pAdo+Na]^+$ are not populated in the experiments as significant mismatches in both the IR fingerprint and hydrogen-stretching regions are found. The T(N3O4'O_X) conformers that possess an additional hydrogen-π interaction and hydrogen-bonding interaction between hydroxyl substituent of the phosphate moiety and the adenine nucleobase are not important conformations in the experiments as the IR features predicted for these conformers do not reproduce the measured IRMPD spectrum in the hydrogen-stretching region.

7.4 DISODIUM CATIONIZED DEPROTONATED ADENINE MONONUCLEOTIDES

7.4.1 CONFORMERS OF DISODIUM CATIONIZED DEPROTONATED 2'-DEOXYADENOSINE-5'-MONOPHOSPHATE POPULATED BY ESI

The measured IRMPD spectrum and calculated IR spectra of select stable low-energy conformers of $[pdAdo-H+2Na]^+$ are compared in **Figure 7.4**. Overall, the IR spectrum calculated for the ground conformer of $[pdAdo-H+2Na]^+$ with the first sodium

cation binding to the N3, O4', O5' and O_X atoms and the second sodium cation binding to the two O_X atoms of phosphate group shows the best agreement with the experimental IRMPD spectrum. Sodium cation binding to the amino substituent significantly shifts the IR bands associated with the C-NH_2 stretch and the NH_2 symmetric and asymmetric stretches, which are not seen in the experimental IRMPD spectrum. Thus, the TT1(N3O4'O_X,N7NH_2O_X) conformer is not populated in the experiments. This observation parallels that found for the sodium cationized adenine nucleosides. The IR spectra predicted for the QB1(N3O4'O5'O_X,O3'O_X) and TT1(N3O4'O_X,O3'O5'O_X) conformers show reasonable agreement with the experimental IRMPD spectrum, indicating that these conformers may be populated in the experiments. However, the relative intensities of the IR features at 3436 and 3644 cm^{-1} do not reproduce the experimental features as well as those calculated for the ground conformer, and the higher relative Gibbs free energies of these conformers also suggest that if present, these conformers are populated in much lower abundance than the ground conformer in the experiments.

In summary, the ground conformer of $[pdAdo–H+2Na]^+$ is dominantly populated in the experiments. The first Na^+ binds to deprotonated pdAdo in the quadridentate fashion via the N3, O4', O5', and O_X atoms, and the second Na^+ binds to the negatively charged phosphate moiety via the two oxo oxygen atoms. Conformers in which Na^+ binds to the NH_2 substituent of the adenine nucleobase can be completely ruled out, due to the significant mismatches between the measured IRMPD and calculated IR spectra. When the second sodium cation binds to the phosphate and sugar moieties, the spectral comparisons suggest that these conformers may be populated. However,

the relative intensities of the IR features at 3436 and 3644 cm^{-1} and the higher Gibbs free energies indicate that if present, these conformers have much lower populations than the ground conformer in the experiments.

7.4.2 CONFORMERS OF DISODIUM CATIONIZED DEPROTONATED ADENOSINE-5'-MONOPHOSPHATE POPULATED BY ESI

The measured IRMPD spectrum and calculated IR spectra of select stable low-energy conformers of $[pAdo-H+2Na]^+$ are compared in **Figure 7.5**. In contrast to that found for $[pdAdo-H+2Na]^+$, the QB1(N3O4'O5'O_X,O3'O_X) conformer with the second sodium cation binding to the phosphate and sugar moieties is the ground conformer of $[pAdo-H+2Na]^+$. However, the splitting of the IR feature at 3660 cm^{-1}, the missing feature at 3600 cm^{-1}, and the significant shift of the feature at 3512 cm^{-1} indicate that the ground conformer is not populated in the experiments. Overall, the IR spectrum calculated for the QB1(N3O4'O5'O_X,O_XO_X) conformer of $[pAdo-H+2Na]^+$, which is similar to the ground conformer of $[pdAdo-H+2Na]^+$, exhibits the best agreement with the measured IRMPD spectrum, indicating that this conformer is dominantly populated in the experiments. Sodium cation binding to the amino substituent significantly shifts the IR bands associated with the C-NH_2 stretch and the NH_2 symmetric and asymmetric stretches, which are not observed in the experimental IRMPD spectrum. Thus, the TT1(N3O4'O_X,N7NH_2O_X) conformer is not populated in the experiments. Similar observations are made in the cases of the disodium cationized deprotonated form of pdAdo and the sodium cationized forms of dAdo and Ado. The IR spectrum calculated for the TT1(N3O4'O_X,O3'O5'O_X) conformer exhibits significant spectral mismatches in the hydrogen-stretching region, indicating that this conformer is not present in the experiments.

In summary, the QB1(N3O4'O5'O_X,O_XO_X) conformer of $[pAdo-H+2Na]^+$, which parallels the ground conformer of $[pAdo-H+2Na]^+$, except for the hydrogen-bonding interaction between the 2'- and 3'-hydroxyls, is dominantly populated in the experiments. The conformers in which Na^+ binds to the amino substituent of the adenine nucleobase are not present in the experiments. The conformers with the second sodium cation binding to the phosphate and sugar moieties are clearly not important contributors in the experiments as significant mismatches in the hydrogen-stretching region are found.

7.5 VIBRATIONAL ASSIGNMENTS FOR SODIUM CATIONIZED ADENINE MONONUCLEOTIDES AND DISODIUM CATIONIZED DEPROTONATED ADENINE MONONUCLEOTIDES

Tables 7.1, 7.2 and 7.3 summarize the vibrational assignments for $[pdAdo+Na]^+$, $[pAdo+Na]^+$, and $[pdAdo-H+2Na]^+$ based on their ground T1(N3O4'O_X) and QB1(N3O4'O5'O_X,O_XO_X) conformers, whereas for $[pAdo-H+2Na]^+$, the vibrational frequencies are assigned based on the dominantly populated QB1(N3O4'O5'O_X,O_XO_X) conformer. **Tables 7.1, 7.2 and 7.3** list the vibrational assignments of the adenine nucleobase, phosphate, and sugar moieties, respectively. The bands in the range from 1300 to 1640 cm^{-1} of the IR fingerprint region are primarily IR active modes associated with the nucleobase, with minor mixed character modes arising from the sugar moiety. The very intense IR feature at 1640 cm^{-1} along with a moderate IR feature to the red is observed for all complexes, and is associated with NH_2 scissoring. The moderate IR bands observed for $[pdAdo+Na]^+$, $[pdAdo-H+2Na]^+$, and $[pAdo-H+2Na]^+$ in the range from 1320 to 1540 cm^{-1} are associated to nucleobase stretches, whereas these IR features in the measured IRMPD spectrum of $[pAdo+Na]^+$ are very weak. IR features in the region from 750 to 1300 cm^{-1} are primarily bending and stretching modes that arise

from the phosphate and sugar moieties with minor mixed character of the nucleobase moiety. The IR absorptions in this range are very parallel for all complexes. The bands in the region extending from 600 to 750 cm^{-1} are mixed character modes involving ring bending and stretching of the sugar and nucleobase moieties, with very minor contributions from the phosphate moiety. The IR features in this region observed for $[pAdo+Na]^+$ are much weaker than those of $[pdAdo+Na]^+$, $[pdAdo-H+2Na]^+$, and $[pAdo-H+2Na]^+$. In the hydrogen-stretching region, the IR absorption at ~3440 cm^{-1} observed for all complexes is associated with the NH_2 symmetric stretch. The weak IR absorption at ~3550 cm^{-1} observed for all complexes is associated with the NH_2 asymmetric stretch. The unique IR band at 3600 cm^{-1} is only observed in the RNA forms of the adenine nucleotide, and is associated with the 2'-hydroxyl stretch. The most intense IR band at ~3660 cm^{-1} observed for all complexes is contributed by the 3'-hydroxyl and phosphate hydroxyl stretches. Overall, the experimental IRMPD spectra of the sodium cationized adenine mononucleotides vs. disodium cationized deprotonated adenine mononucleotides are highly parallel.

7.6 COMPARISONS OF DIFFERENT FORMS OF ADENINE NUCLEOSIDES AND MONONUCLEOTIDES POPULATED BY ESI

Figure 7.6 shows the conformers of the sodium cationized adenine nucleosides and mononucleotides that are dominantly populated in the experiments along with their respective adenine nucleobase orientation and sugar puckering.[147,187,191,192] For the deprotonated adenine mononucleotides, adenine prefers an *anti* orientation and the sugar prefers C3'-endo ($^3T_2$) sugar puckering. A hydrogen-bonding interaction between the 3'-hydroxyl substituent and the phosphate oxo oxygen atom is found in both the deprotonated DNA and RNA adenine mononucleotides. For the protonated adenine

mononucleotides, the most favorable protonation site is the N3 atom of the adenine nucleobase. Adenine prefers a *syn* orientation, and the sugar prefers C2'-endo ($^{2}T_{1}$) puckering. Compared to a proton, the sodium cation prefers to form multiple chelation interactions with multiple atoms, such that Na^{+} binds to the N3 atom of the adenine nucleobase, but also binds to the sugar and phosphate moieties. A strong hydrogen-bonding interaction between the N3-H and O_X atoms stabilizes the *syn* oriented protonated adenine mononucleotides. Among these adenine mononucleotide complexes, only the deprotonated adenine mononucleotides exhibit an *anti* orientation of the adenine nucleobase. Compared to the sodium cationized adenine nucleosides, the phosphate group of the adenine mononucleotides changes the third Na^{+} chelation site from the O5' atom to the O_X atom. The adenine nucleobases of all of the sodium cationized adenine nucleosides and mononucleotides prefer a *syn* orientation. $[dAdo+Na]^{+}$ prefers C2'-endo ($^{2}T_{1}$) sugar puckering, whereas $[Ado+Na]^{+}$ prefers C1'-exo ($_{1}T^{O}$) sugar puckering. Both $[pdAdo+Na]^{+}$ and $[pAdo+Na]^{+}$ exhibit C3'-endo ($^{3}T_{2}$) sugar puckering, and both $[pdAdo-H+2Na]^{+}$ and $[pAdo-H+2Na]^{+}$ exhibit O4'-endo ($^{O}T_{1}$) sugar puckering. Indeed, the phosphate group and sodium cation markedly influence the sugar puckering among these complexes. In all cases, the N3 atom of the adenine nucleobase is the most favorable binding site for Na^{+} to the adenine nucleosides and mononucleotides. Chelation interactions with the sugar or sugar and phosphate moieties stabilize these sodium cationized complexes.

7.7 CONCLUSIONS

The gas-phase conformations of the sodium cationized complexes of the neutral and deprotonated forms of the adenine mononucleotides have been examined in this

chapter via IRMPD action spectroscopy in both the IR fingerprint and hydrogen-stretching regions. Comparison of the measured IRMPD spectra with the calculated IR spectra predicted for the stable low-energy conformations of these species calculated at the B3LYP/6-311+G(d,p) level of theory allows the structures populated in the experiments to be determined. For $[pdAdo+Na]^+$ and $[pAdo+Na]^+$, the ground conformers are dominantly populated in the experiments. The sodium cation prefers to bind to the phosphate group, sugar moiety and adenine nucleobase in the tridentate fashion via the N3, O4' and O_X atoms. Adenine exhibits a *syn* orientation and the sugar exhibits C3'-endo ($^3T_2$) puckering. For $[pdAdo-H+2Na]^+$ and $[pAdo-H+2Na]^+$, the QB1($N3O4'O5'O_X,O_XO_X$) conformers are dominantly populated in the experiments. The first sodium cation binds to the deprotonated adenine mononucleotides in a fashion parallel to that found for the [pdAdo-H+Na] and [pAdo-H+Na] salt complexes, and the second sodium cation binds to the phosphate group via both O_X atoms. Adenine exhibits a *syn* orientation and the sugar exhibits O4'-endo ($^OT_1$) sugar puckering. Compared to the sodium cationized adenine nucleosides, the phosphate group of pdAdo and pAdo changes the third binding interaction of Na^+ from the O5' atom to an O_X atom. Compared to the protonated adenine mononucleotides, the sodium cation binds to the neutral and deprotonated adenine mononucleotides via multiple chelation interactions, whereas the most favorable protonation site of the adenine mononucleotides is the N3 atom of the adenine nucleobase. A strong hydrogen-bonding interaction between the N3-H and O_X atoms stabilizes the *syn* oriented protonated adenine mononucleotides. Among all of the deprotonated, protonated and sodium

cationized forms of the adenine nucleosides and mononucleotides, only deprotonated adenine mononucleotides exhibit an *anti* orientation of the nucleobase.

7.8 REFERENCES

147. Y. Zhu, L. A. Hamlow, C. C. He, S. F. Strobehn, J. K. Lee, J. Gao, G. Berden, J. Oomens and M. T. Rodgers, *J. Phys. Chem. B* 2016, **120**, 8892.

187. R. R. Wu, C. C. He, L. A. Hamlow, Y.-w. Nei, G. Berden, J. Oomens and M. T. Rodgers, *J. Phys. Chem. B* 2016, **120**, 4616.

191. Y.-w. Nei, N. Hallowita, J. D. Steill, J. Oomens and M. T. Rodgers, *J. Phys. Chem. A* 2013, **117**, 1319.

192. Y.-w. Nei, K. T. Crampton, G. Berden, J. Oomens and M. T. Rodgers, *J. Phys. Chem. A* 2013, **117**, 10634.

Table 7.1. Observed band positions (in cm^{-1}) and assignments of the vibrational modes of the adenine nucleobase moiety of the sodiated neutral and disodiated deprotonated forms of 2'-deoxyadenosine-5'-monophosphate and adenosine-5'-monophosphate in the IR fingerprint and hydrogen-stretching regions.

Vibrational Mode				
Nucleobase	$[pdAdo+Na]^{+a}$	$[pAdo+Na]^{+a}$	$[pdAdo-H+2Na]^{+a}$	$[pAdo-H+2Na]^{+a}$
Ring stretch	725	730		
Ring out-of-plane	640, 810	650, 780	640, 795	640, 810
C2–N3–C4 asym.			1335	1345
C5–N7 stretch			1335	1345
C8–N9 stretch				1220
C8–H in plane	1220	1225	1220, 1335,	1220, 1345,
C4=C5 stretch	1575	1580	1375	
C4–N9 stretch			1415	1410
N6–H in plane	1460, 1575	1470, 1580	1460	1470
C2–H in plane	1300, 1380,	1300, 1470	1375, 1415,	1370, 1410,
N7=C8 stretch	1460, 1575	1470, 1580	1460, 1580	1470, 1590
N1=C6 stretch	1460, 1575	1470, 1580	1460, 1580	1470, 1590
N3–C4 stretch	1575	1580	1580	1590
C5–C6 stretch			1580	1590
N1–C2 stretch	1575	1580	1580	1590
C6–N stretch	1640	1640	1630	1640
NH_2 rock	1220	1225		
NH_2 scissoring	1575, 1640	1580, 1640	1580, 1625	1590, 1640
NH_2 sym stretch	3436	3436	3436	3436
NH_2 asym stretch	3552	3552	3554	3554

[a] The assignments of $[pdAdo+Na]^+$, $[pAdo+Na]^+$ and $[pdAdo-H+2Na]^+$ are based on the corresponding ground conformer. The assignments of $[pAdo-H+2Na]^+$ are based on the most populated QB1(N3O4'O5'O_X,$O_X$$O_X$) conformer **.**

Table 7.2. Observed band positions (in cm^{-1}) and assignments of the vibrational modes of the phosphate moiety of the sodiated neutral and disodiated deprotonated forms of 2'-deoxyadenosine-5'-monophosphate and adenosine-5'-monophosphate in the IR fingerprint and hydrogen-stretching regions.

Vibrational Mode				
Phosphate	$[pdAdo+Na]^{+a}$	$[pAdo+Na]^{+a}$	$[pdAdo-H+2Na]^{+a}$	$[pAdo-H+2Na]^{+a}$
P–OC5' stretch	810	780	715	725
P–OH stretch			885	890
HO–P–OH sym.	890	900		
HO–P–OH asym.	925	940		
PO–H in plane	925, 1040	940, 1025	1037	1040
O=P stretch	1270	1270		
O=P=O sym.			1090	1110
O=P=O asym.			1270	1275
P–OH stretch	3436	3436		
Free P–OH	3656	3656	3656	3656

[a] The assignments of $[pdAdo+Na]^+$, $[pAdo+Na]^+$ and $[pdAdo-H+2Na]^+$ are based on the corresponding ground conformer. The assignments of $[pAdo-H+2Na]^+$ are based on the most populated QB1(N3O4'O5'O_X,$O_X$$O_X$) conformer **.**

Table 7.3. Observed band positions (in cm^{-1}) and assignments of the vibrational modes of the sugar moiety of the sodiated neutral and disodiated deprotonated forms of 2'-deoxyadenosine-5'-monophosphate and adenosine-5'-monophosphate in the IR fingerprint and hydrogen-stretching regions.

Vibrational Mode				
Sugar	$[pdAdo+Na]^{+a}$	$[pAdo+Na]^{+a}$	$[pdAdo-H+2Na]^{+a}$	$[pAdo-H+2Na]^{+a}$
Ring stretch	725	730	640	640
O–C1'–C2' out-of-plane bends		825		
C5'H_2 rock			930	945, 1110
C5'H_2 twist	1300	1300		
C5'H_2 wag	1380		1375	1370
C1'–C2' stretch			1037	
C1'–O stretch	925	940		1040
C2'–O stretch		1110		1110
C3'–O stretch	1110		1090	1110
C4'–O–C1' asym. stretch			1037	
C4'–O–C1' sym.			1090	
C4'–O stretch	1060	1065		1110
C5'–O stretch	1060	1065	1120	1120
Hydrogen atoms			1375, 1415	1370, 1410
C1'–H bend	1380			
C1'–H and C2'–H sym. bend		1410		
C3'–H and C2'–H asym. bend	1350			
C1'–H and C4'–H sym. bend		1345		1345
C4'–H bend		1300		1110, 1345
C3'–H bend	1420	1225	1150	
C2'–H bend		1225, 1345		
C2'–H_2 rock			930	
C2'–H_2 twist	1220		1150	
C2'–H_2 wag	1300			
C2'O–H in plane		1345		
C3'O–H in plane	1420	1025, 1225	1037, 1150,	1410
C2'O–H stretch		3600		3600
C3'O–H stretch	3665	3665	3665	3665

[a] The assignments of $[pdAdo+Na]^+$, $[pAdo+Na]^+$ and $[pdAdo-H+2Na]^+$ are based on the corresponding ground conformer. The assignments of $[pAdo-H+2Na]^+$ are based on the most populated QB1(N3O4'O5'O_X,O_XO_X) conformer **.**

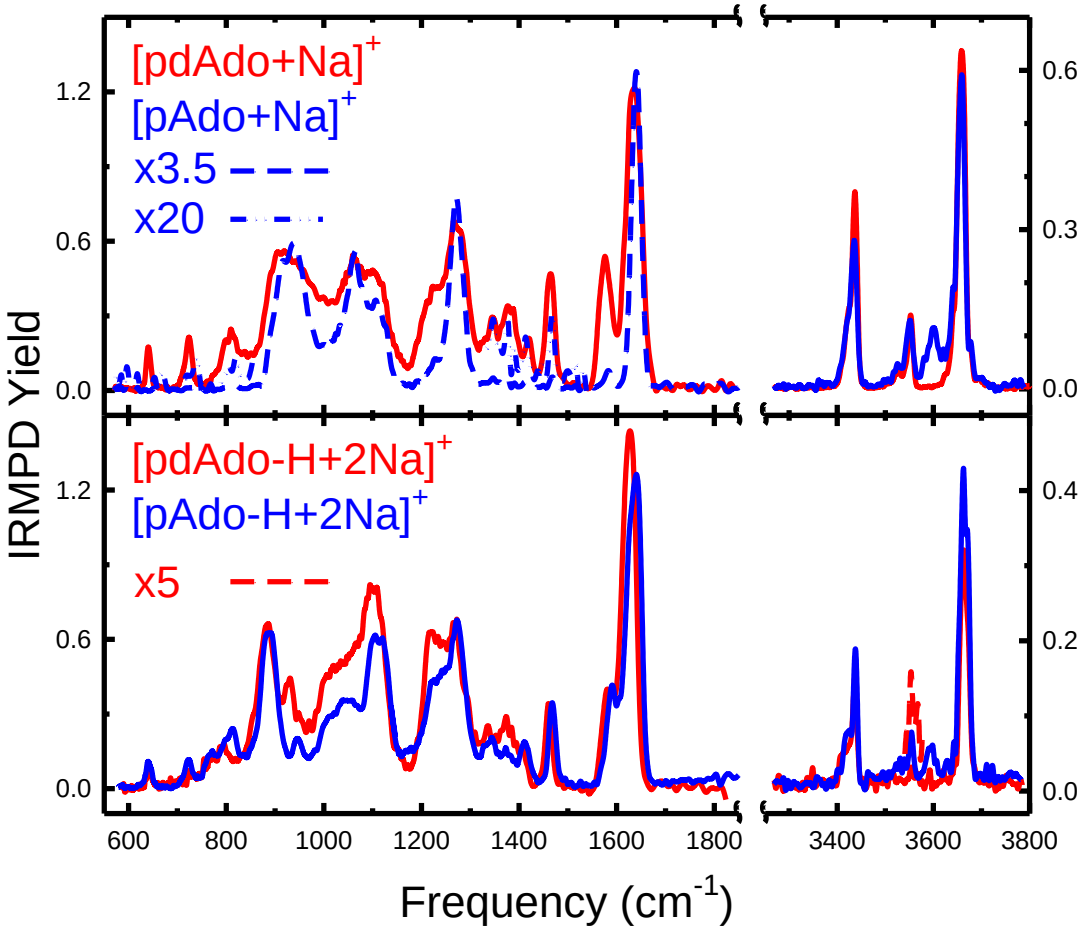

Figure 7.1 Experimental IRMPD action spectra of $[pdAdo+Na]^+$, $[pAdo+Na]^+$, $[pdAdo-H+2Na]^+$, and $[pAdo-H+2Na]^+$ in the IR fingerprint and hydrogen-stretching regions. The IRMPD yields of $[pAdo+Na]^+$ in the IR fingerprint region are scaled by a factor of 3.5 (blue dashed line). The IRMPD yields of $[pAdo+Na]^+$ in the range from 550 to 850 cm^{-1}, and from 1300 to 1550 cm^{-1}, are scaled by a factor of 20 (blue dotted line). The IRMPD yields of $[pdAdo-H+2Na]^+$ in the range from 3540 to 3580 cm^{-1} are scaled by a factor of 5 (red dashed line).

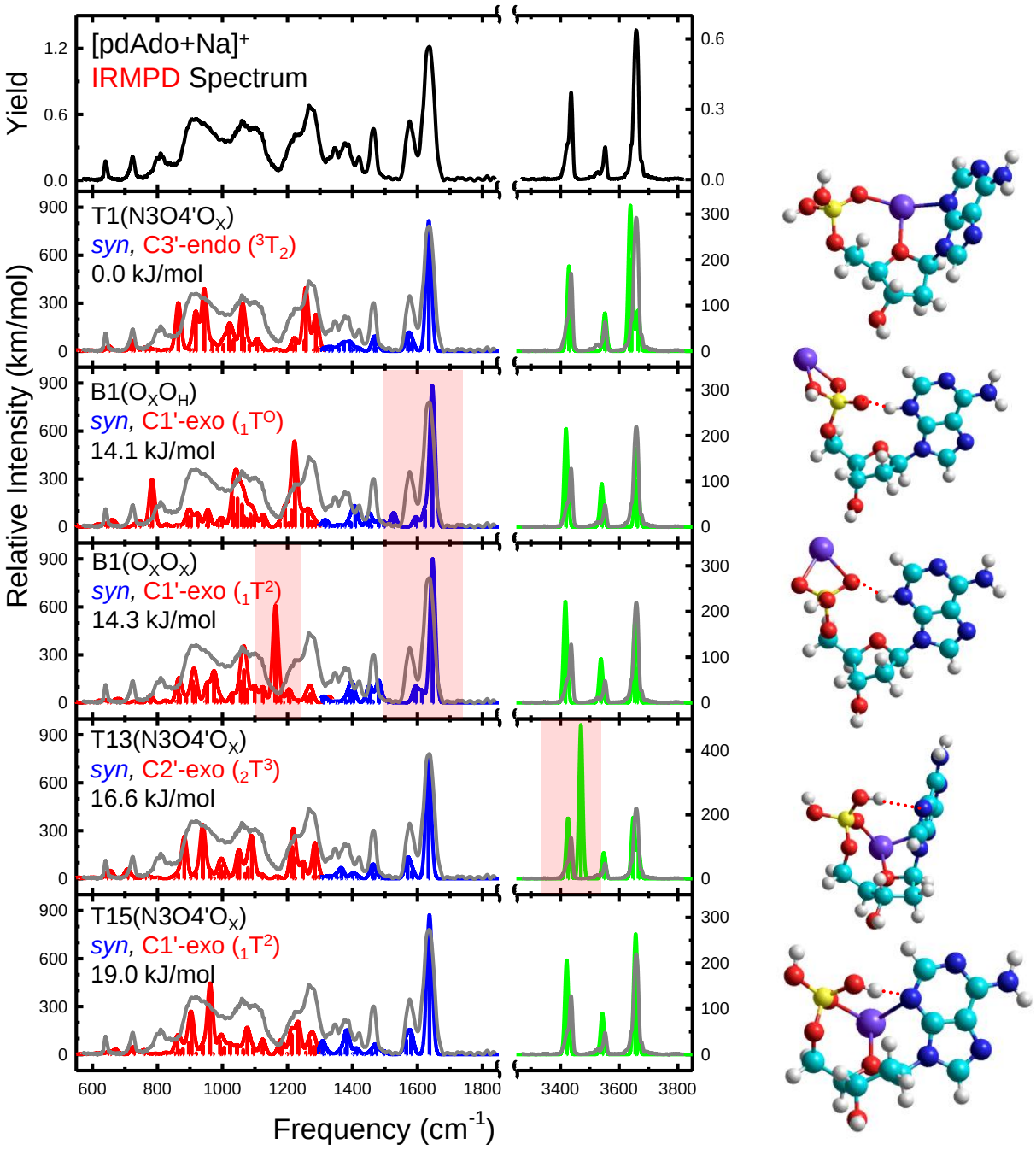

Figure 7.2 Comparison of the experimental IRMPD action spectrum of $[pdAdo+Na]^+$ with the B3LYP/6-311+G(d,p) optimized structures and calculated linear IR spectra for representative low-energy conformers. The nucleobase orientation, sugar puckering, and B3LYP/6-311+G(2d,2p) relative Gibbs free energies at 298 K are also shown.

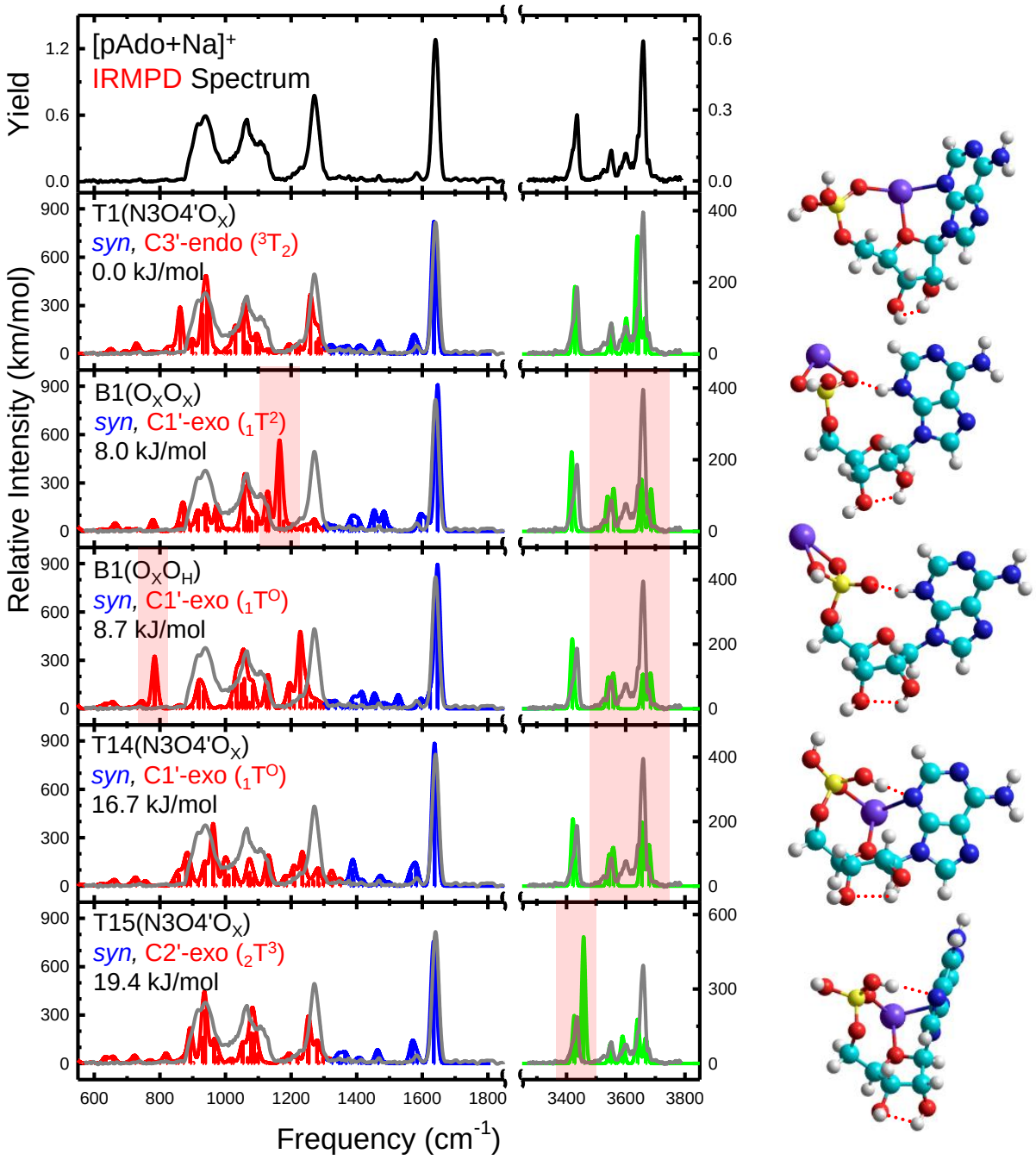

Figure 7.3 Comparison of the experimental IRMPD action spectrum of $[pAdo+Na]^+$ with the B3LYP/6-311+G(d,p) optimized structures and calculated linear IR spectra for representative low-energy conformers. The nucleobase orientation, sugar puckering, and B3LYP/6-311+G(2d,2p) relative Gibbs free energies at 298 K are also shown.

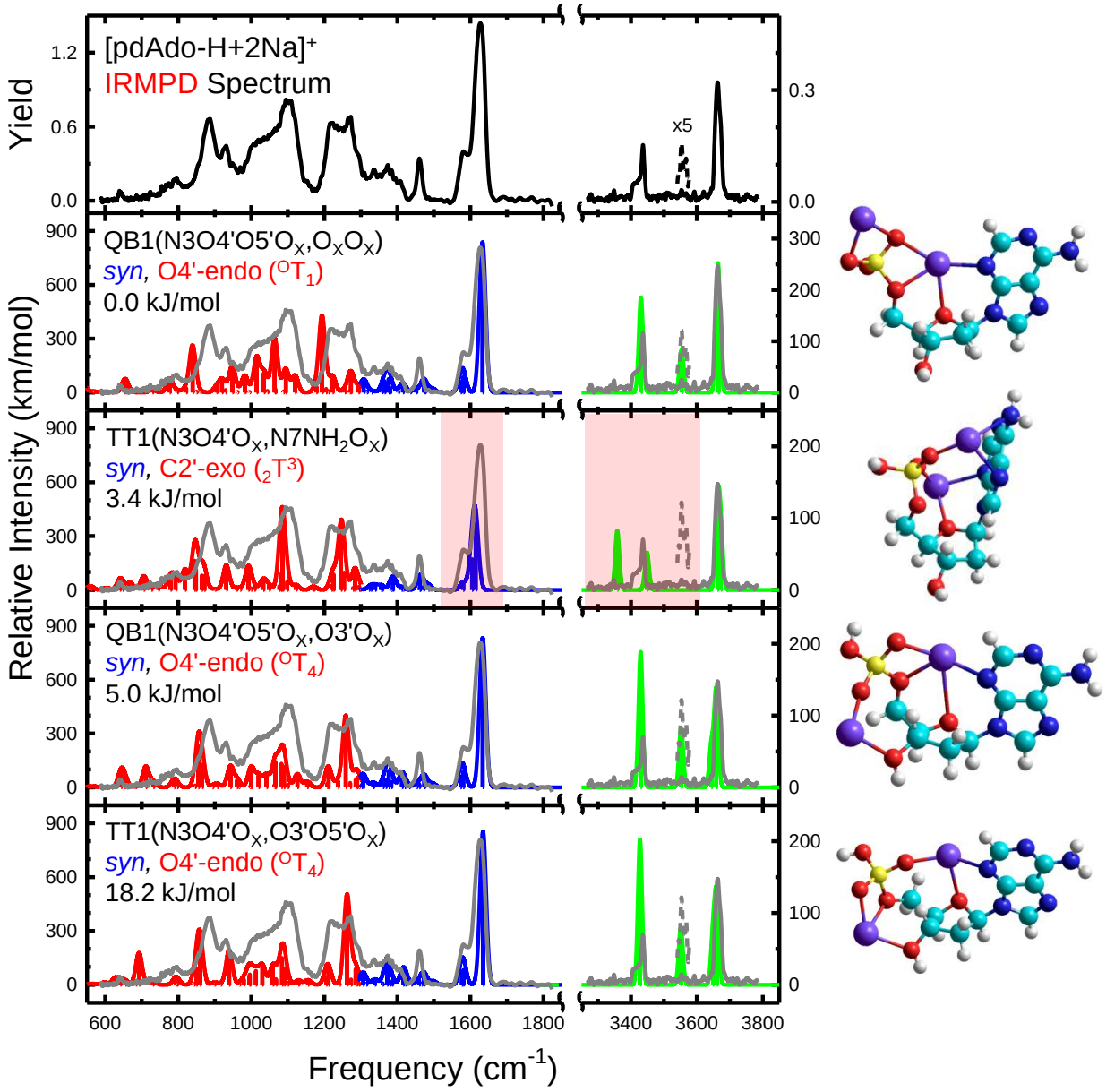

Figure 7.4 Comparison of the experimental IRMPD action spectrum of $[pdAdo-H+2Na]^+$ with the B3LYP/6-311+G(d,p) optimized structures and calculated linear IR spectra for representative low-energy conformers. The nucleobase orientation, sugar puckering, and B3LYP/6-311+G(2d,2p) relative Gibbs free energies at 298 K are also shown.

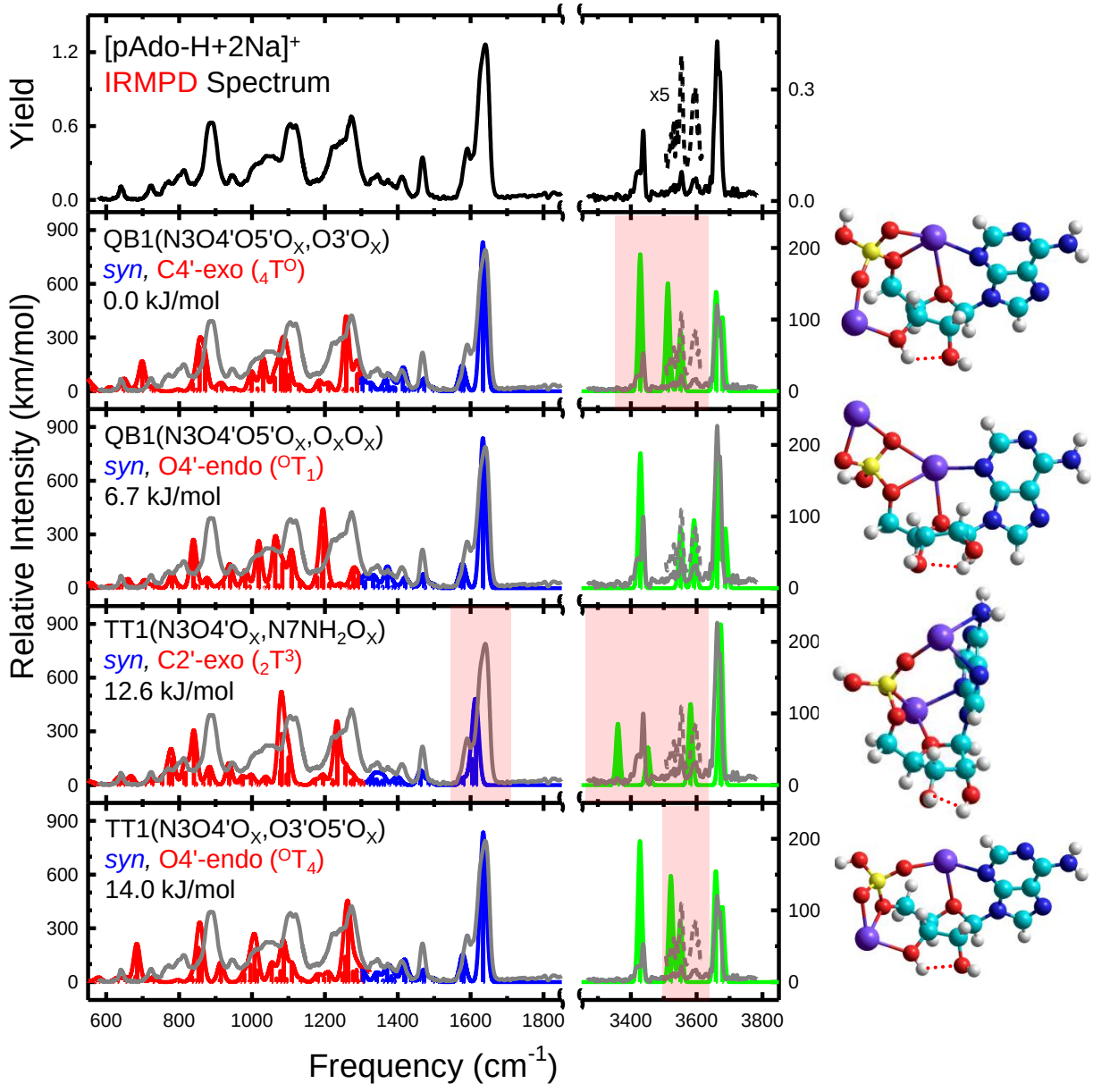

Figure 7.5 Comparison of the experimental IRMPD action spectrum of [pAdo-H+2Na]$^+$ with the B3LYP/6-311+G(d,p) optimized structures and calculated linear IR spectra for representative low-energy conformers. The nucleobase orientation, sugar puckering, and B3LYP/6-311+G(2d,2p) relative Gibbs free energies at 298 K are also shown.

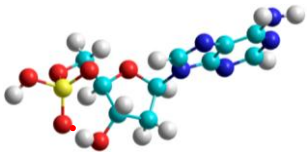

[pdAdo-H]$^-$
AC3_1
anti, C3'-endo ($^3T_2$)

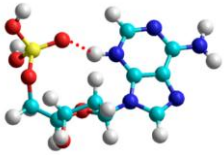

[pdAdo+H]$^+$
N3
syn, C2'-endo ($^2T_1$)

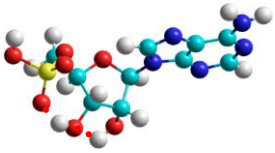

[pAdo-H]$^-$
AC3_1
anti, C3'-endo ($^3T_2$)

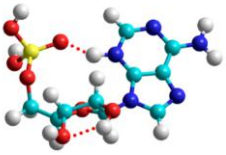

[pAdo+H]$^+$
N3
syn, C2'-endo ($^2T_1$)

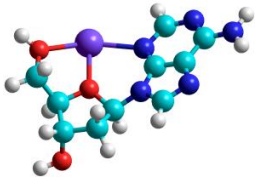

[dAdo+Na]$^+$
T1(N3O4'O5')
syn, C2'-endo ($^2T_1$)

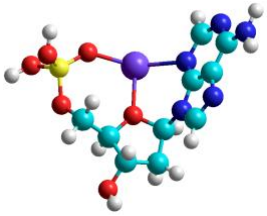

[pdAdo+Na]$^+$
T1(N3O4'O$_X$)
syn, C3'-endo ($^3T_2$)

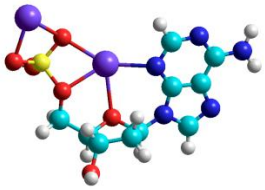

[pdAdo-H+2Na]$^+$
QB1(N3O4'O5'O$_X$,O$_X$O$_X$)
syn, O4'-endo ($^OT_1$)

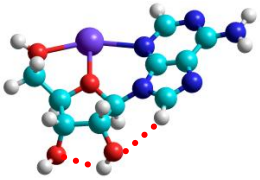

[Ado+Na]$^+$
T1(N3O4'O5')
syn, C1'-exo ($_1T^O$)

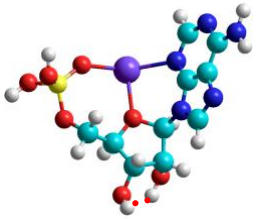

[pAdo+Na]$^+$
T1(N3O4'O$_X$)
syn, C3'-endo ($^3T_2$)

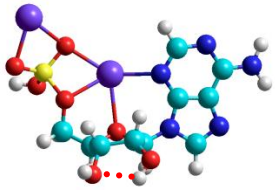

[pAdo-H+2Na]$^+$
QB1(N3O4'O5'O$_X$,O$_X$O$_X$)
syn, O4'-endo ($^OT_1$)

Figure 7.6 Conformers of deprotonated and protonated adenine mononucleotides as well as sodium cationized adenine nucleosides and mononucleotides that are dominantly populated in the experiments. The nucleobase orientation and sugar puckering are also shown.

CHAPTER 8 CONCLUSIONS AND FUTURE WORK

8.1 CONCLUSIONS

In this thesis work, the influence of noncovalent interactions with sodium cations on the conformations and stabilities of the canonical and two modified DNA and RNA nucleosides and the canonical adenine mononucleotides were examined both experimentally and theoretically. Electronic structure calculations are employed to probe the conformational space available to these systems to determine the stable modes of sodium cation binding, and in particular, the preferred modes of sodium cation binding and the factors that lead to stabilization. These calculations also provide predicted infrared spectra for comparison to experiment. Infrared multiple photon dissociation (IRMPD) action spectroscopy experiments were performed to characterize the infrared spectra of these DNA and RNA nucleosides and nucleotides. Comparisons of theory and experimental then enable the structures/conformations of these species experimentally populated to be elucidated, and also enable the measured infrared signatures to be interpreted and assigned. Comparisons among the systems investigated in this thesis and to results for the protonated canonical DNA and RNA nucleosides as well as the protonated and deprotonated forms of the DNA and RNA adenine nucleotides previously investigated then enable the influence of the identity of the nucleobase, the 2'-hydroxyl substituent, and the effects of the local environment (i.e., pH, ionic strength, and in some cases solvation) on the structures and stabilities to be determined.

The stabilities and dissociation behavior of a wide variety of protonated and sodium cationized modified nucleosides are also examined experimentally. Energy-

resolved collision-induced dissociation (ER-CID) experiments were performed to characterize the fragmentation behavior of these systems, which when coupled with survival yield analyses enable to stabilities of these systems to be assessed. The fragmentation pathways observed in the ER-CID experiments often exclusively involve N-glycosidic bond cleavage such that the survival yield analyses provide a direct measure of the relative N-glycosidic bond stabilities of these DNA and RNA nucleosides. Comparisons among these systems thus enable the influence of the identity of the nucleobase, the 2'-hydroxyl substituent, modifications, and the local environment (i.e., pH, ionic strength) on the relative glycosidic bond stabilities of the DNA and RNA nucleosides to be elucidated.

Our motivations for studying these systems are presented in **Chapter 1**, whereas the experimental and theoretical methods employed are discussed in detail including the instrumental set ups employed in this work are presented in **Chapter 2**.

In **Chapter 3**, the results of our electronic structure calculations for the sodium cationized forms of the canonical and two modified DNA and RNA nucleosides (including dAdo, Ado, dCyd, Cyd, Guo, dGuo, dUrd, Urd, dThd, and Thd) are presented and discussed.[147-151] Structures were optimized and harmonic vibrational frequency calculations were performed at the B3LYP/6-311+G(d,p) level of theory, whereas energies were calculated at the B3LYP/6-311+(2d,2p) level of theory. A wide variety of stable structures are found and these structures and their relative stabilities are examined and discussed in detail. For all of the nucleosides examined except the guanine nucleosides, the sodium cation preferentially binds to both the nucleobase and the sugar moiety. In contrast, the sodium cation binds to the guanine nucleosides

exclusively via the nucleobase. The sodium cationized forms of the DNA and RNA nucleosides generally exhibit highly parallel conformations. The 2′-hydroxyl substituent of the RNA nucleosides enables formation of a hydrogen-bonding interaction between the 2'- and 3'-hydroxyl substituents, which is found in all of the sodium cationized RNA nucleosides. However, the 2'-hydroxyl substituent enables unique modes of binding to the RNA pyrimidine nucleosides that are predicted to be relatively low in energy and competitive with the ground conformations.

In **Chapter 4** the results of our IRMPD experiments for the sodium cationized forms of the canonical and two modified DNA and RNA nucleosides (i.e., the same systems computed in **Chapter 3**) are presented and discussed. The measured IRMPD spectra are compared to the IR spectra predicted for the stable structures to elucidate the structures accessed experimentally.[147-151] In general, the relative stabilities of the stable conformations computed are consistent with the experimental measurements in that the conformations populated correspond to the most stable structures found. However, the unique low-energy mode of binding available to the RNA pyrimidine nucleosides (Cyd, Urd, and Thd) is found to be more important in the experiments than theoretically predicted. These seemingly anomalous results are understood by examining the effect of solvation on the relative stabilities of the associated conformations of these species. Theory predicts the stabilities of these conformations of the sodium cationized pyrimidine nucleosides are inverted in aqueous solution and that kinetic trapping of these conformations in the electrospray process occurs.

In **Chapter 5**, the results of our ER-CID experiments and survival yield analyses for the protonated and sodium cationized forms of the canonical and two modified DNA

and RNA nucleosides (i.e., the same systems computed in **Chapters 3** and **4**) are presented and discussed to elucidate the influence of the identity of the nucleobase, the 2′-substituent, and the local environment (i.e., pH and ionic strength) on N-glycosidic bond stability.[147-151] In addition, a wide variety of modified nucleosides are also examined here to determine the effects of these modifications on N-glycosidic bond stability. Many of the modified nucleosides included in this work involve modifications at the 2′-position of the sugar moiety including: naturally occurring O2'-methylated nucleosides (Adom, Guom, Cydm, Urdm, Thdm), synthetically modified 2'-fluoro-substituted nucleosides (Adofl, Cydfl, Guofl, Urdfl) and the arabinose analogs (which involve inversion of the 2′-stereochemistry, araAdo, araGuo, araCyd, araUrd). Several of the modified nucleosides examined in this work involve modifications of the nucleobase, and in particular include a series of methylated guanosines (m^1Guo, m^7Guo, m^2_2Guo and m^2_2Guom). In addition to protons and sodium cations, experiments for the guanine nucleosides were also extended to other cations including: lithium, potassium, cesium and silver to examine the influence of the size and electronic structure of the metal cation on the relative N-glycosidic bond stabilities.

In general, the 2'-hydroxyl substituent of the RNA nucleosides is found to stabilize the N-glycosidic bond compared with their DNA analogues. In all cases, sodium cationization is found to activate the N-glycosidic bond less effectively than protonation. 2'-Fluoro modification stabilizes the N-glycosidic bond compared with the analogous DNA and RNA nucleosides. O2′-Methylation and inversion of the 2′-stereochemistry of the sugar moiety produce only small changes in the N-glycosidic bond stability versus the analogous canonical RNA nucleosides, that are not systematic

(i.e., in some cases a slight weakening of the N-glycosidic bond is found, whereas in other cases these modifications produce a slight strengthening of the N-glycosidic bond.). The survival yield analyses of the protonated and sodium cationized methylated guanosines indicate that the position of the methyl substituent clearly impacts the relative N-glycosidic bond stabilities of these nucleosides. By comparing the $CID_{50\%}$ values of the protonated and metal cationized guanine nucleosides, the effects of local environment on the relative N-glycosidic bond stabilities were also investigated. The order of relative stabilities of alkali metal cationized dGuo and Guo is consistent with the order of increasing size of the alkali metal cation. The binding between the metal cation and the nucleoside become weaker as the size of the alkali metal cation increases.

In **Chapter 6**, the results of our electronic structure calculations for the sodium cationized adenine mononucleotides, $[pdAdo+Na]^+$ and $[pAdo+Na]^+$, and disodium cationized deprotonated adenine mononucleotides, $[pdAdo-H+2Na]^+$ and $[pAdo-H+2Na]^+$, are presented and discussed. Additionally, electronic structure calculations for the neutral adenine mononucleotides, pdAdo and pAdo, and the neutral sodium cationized deprotonated adenine mononucleotide salts, [pdAdo-H+Na] and [pAdo-H+Na], are also discussed for comparisons. Optimization and harmonic frequency calculations were performed at B3LYP/6-311+G(d,p) level of theory, whereas the single-point energy calculations were calculated at B3LYP/6-311+G(2d,2p) level of theory. Overall, theory suggests that these sodium cationized DNA and RNA species exhibit highly parallel ground conformations, except for the disodium cationized deprotonated adenine mononucleotides. For neutral pdAdo and pAdo, pdAdo prefers a *syn* orientation of the adenine nucleobase, whereas pAdo prefers an *anti* orientation of

the adenine nucleobase. For $[pdAdo+Na]^+$ and $[pAdo+Na]^+$, Na^+ binds to the adenine nucleobase, sugar and phosphate moieties in a tridentate fashion. Adenine exhibits a *syn* orientation and the sugar exhibits C3'-endo ($^3T_2$) puckering. For [pdAdo-H+Na] and [pAdo-H+Na], theory suggests that Na^+ binds to the adenine nucleobase, sugar and phosphate moieties in a quadridentate fashion. Adenine exhibits a *syn* orientation and the sugar exhibits C4'-exo ($_4T^O$) puckering. For $[pdAdo-H+2Na]^+$ and $[pAdo-H+2Na]^+$, the first Na^+ binds to the deprotonated adenine mononucleotides in the same fashion as found for the sodium cationized deprotonated adenine mononucleotide salt. The second Na^+ binds solely to the phosphate group in $[pdAdo-H+2Na]^+$, whereas the second Na^+ binds to the sugar and phosphate moieties in $[pAdo-H+2Na]^+$. Adenine exhibits a *syn* orientation in both cases. $[pdAdo-H+2Na]^+$ exhibits O4'-endo ($^OT_1$) sugar puckering, whereas $[pAdo-H+2Na]^+$ exhibits C4'-exo ($_4T^O$) sugar puckering. For the DNA adenine mononucleotides, only $[pdAdo-H]^-$ exhibits an *anti* orientation of adenine nucleobase, such that base rotation is facilitated by protonation and sodium cationization. For the RNA adenine mononucleotides, $[pAdo-H]^-$ and pAdo exhibits an *anti* orientation of the nucleobase, indicating that base rotation is facilitated by sodium cationization and protonation of pAdo.

In **Chapter 7**, the results of our IRMPD experiments for the sodium cationized forms of the canonical DNA and RNA adenine mononucleotides are presented and discussed. The spectral comparisons indicate the conformers of the DNA and RNA forms of these sodium cationized species that are dominantly populated in the experiments are highly parallel. The ground conformers of $[pdAdo+Na]^+$, $[pAdo+Na]^+$, and $[pdAdo-H+2Na]^+$ are the major contributors in the experiments. The stable low-

energy conformer of $[pAdo-H+2Na]^+$, which is similar to the ground conformer of $[pdAdo-H+2Na]^+$, is dominantly populated in the experiments. Comparisons between the sodium cationized adenine nucleosides and mononucleotides indicate that the phosphate group of the adenine mononucleotides changes the mode of Na^+ binding such that the third chelation interaction is altered from the O5' atom to the O_X atom. Compared with previous IRMPD action spectroscopy studies of the protonated and deprotonated forms of the adenine mononucleotides, only the deprotonated adenine mononucleotides exhibit an *anti* orientation of the nucleobase. The most favorable protonation site of the adenine mononucleotides is the N3 atom of the adenine nucleobase. Unlike a proton, the sodium cation prefers multiple chelation interactions with the adenine mononucleotides, such that the sodium cation binds to the adenine nucleobase, sugar and phosphate moieties in either a tridentate or quadridentate fashion.

8.2 FUTURE WORK

The present thesis examines the conformations and energetics of sodium cationized DNA and RNA nucleosides as well as adenine mononucleotides via IRMPD action spectroscopy experiments and complementary electronic structure calculations. The relative stabilities of protonated and metal cationized canonical and modified DNA and RNA nucleosides are also determined via ER-CID experiments and survival yield analyses. These studies could be further expanded to elucidate the structural and energetic effects on the nucleosides and nucleotides. Several potential projects are discussed below:

(1) IRMPD action spectroscopy combined with electronic structure calculations have proven to be a robust approach to study the gas-phase conformations and energetics of nucleosides and nucleotides. The present thesis mainly focuses on the effects of sodium cationization. However, the effects of other metal cations are also of fundamental interest. For example, IRMPD action spectroscopy studies of alkali metal cationized nucleosides and nucleotides using the same techniques could be used to better understanding the effects of the size and electronic structure of metal cations on the gas-phase conformations and energetics of nucleosides and nucleotides. In particular, whether the behavior observed for the sodium cationized RNA pyrimidine nucleosides will also be observed for other alkali metal cationized nucleosides. Preliminary calculations suggest that lithium cationized uridine should exhibit a ground conformation similer to that found for sodium cationized uridine, whereas potassium, rubidium and cesium cationized uridines prefer an *anti* orientation of uracil with the metal cation binding to O2 and O2' atoms. Further calculations and IRMPD action spectroscopy experiments could be performed to confirm these predictions. Additionally, nucleosides and nucleotides binding to a multiply charged metal cation as well as heavy metal cations are also worthwhile to study. For example, magnesium and zinc ions play very important roles in many biological processes.[210,211] Therefore, a series of IRMPD action spectroscopy experiments and theoretical calculations could be pursued to provide insight into the differences in the metal cation-nucleic acid interactions for these and other biologically relevant metal cations.

(2) As introduced in **Section 1.3**, there are over 140 naturally occurring modified nucleosides and a variety of modified nucleosides that have been synthesized for

pharmaceutical and research applications.[212] The present thesis mainly focuses on the relative stability studies of protonated and metal cationized modified nucleosides via ER-CID experiments and survival yield analyses. It would be worthwhile to use IRMPD action spectroscopy combined with electronic structure calculations to elucidate the effects of modifications on the gas-phase conformations and energetics. Our lab has already initiated investigations of several modified nucleosides, including the modified nucleosides discussed in **Chapter 5**, and other modified nucleosides, such as locked nucleic acids and oxidized nucleosides. Our evolving database of information could be expanded by including additional modifications. Therefore, studies of the gas-phase conformations and energetics of these modified nucleosides may provide insight into the effects of these modifications on the structures and chemical properties of these systems.

(3) Survival yield analysis is a robust technique to study the relative stabilities of precursor ions. This project can be expanded by including more modified nucleosides to investigate the effects of modifications on the relative stabilities of nucleosides. This high throughput method can be used as a guide for threshold collision-induced dissociation (TCID) experiments. Even though survival yield analysis is only a semi-quantitative method which is only used to determine relative stabilities, this method can be compared with quantitatively measured accurate thermochemical data from TCID experiments. It would be interesting to determine how linear the correlation between $CID_{50\%}$ values and activation energies of N-glycosidic bond cleavage are, and what factors lead to deviations. Preliminary results show that the $CID_{50\%}$ values of the protonated adenine, guanine and cytosine nucleosides exhibit a highly linear correlation

with the activation energies of these protonated nucleosides determined by TCID experiments, because the only fragmentation pathway observed in the ER-CID experiments involves the N-glycosidic bond cleavage with the proton retained by nucleobase. In order to improve survival yield analysis and enable improved quantitation, it would be worthwhile to build a database of $CID_{50\%}$ values determined by survival yield analyses and activation energies determined by TCID experiments.

8.3 REFERENCES

147. Y. Zhu, L. A. Hamlow, C. C. He, S. F. Strobehn, J. K. Lee, J. Gao, G. Berden, J. Oomens and M. T. Rodgers, *J. Phys. Chem. B* 2016, **120**, 8892.

148. Y. Zhu, L. A. Hamlow, C. C. He, J. K. Lee, J. Gao, G. Berden, J. Oomens and M. T. Rodgers, *J. Phys. Chem. B* 2017, **121**, 4048.

149. Y. Zhu, L. A. Hamlow, C. C. He, H. A. Roy, N. A. Cunningham, M. U. Munshi, G. Berden, J. Oomens and M. T. Rodgers, *Int. J. Mass Spectrom.* 2017, DOI: https://doi.org/10.1016/j.ijms.2017.04.005.

150. Y. Zhu, H. A. Roy, N. A. Cunningham, S. F. Strobehn, J. Gao, M. U. Munshi, G. Berden, J. Oomens and M. T. Rodgers, *Phys. Chem. Chem. Phys.* 2017, **19**, 17637.

151. Y. Zhu, H. A. Roy, N. A. Cunningham, S. F. Strobehn, J. Gao, M. U. Munshi, G. Berden, J. Oomens and M. T. Rodgers, *J. Am. Soc. Mass Spectrom* 2017, **28**, 2437.

210. G. Zubay, *Biochim. Biophys. Acta* 1959, **32**, 233.

211. U. Weser, S. Seeber and P. Warnecke, *Experientia* 1969, **25**, 489.

212. S. Li and C. E. Mason, *Annu. Rev. Genomics Hum. Genet.* 2014, **15**, 127.

REFERENCES

1. O. T. Avery, C. M. MacLeod and M. McCarty, *J. Exp. Med.* 1944, **79**, 137.

2. P. F. Agris, *Nucleic Acids Res.* 2004, **32**, 223.

3. P. F. Agris, *RNA* 2015, **21**, 552.

4. B. X. S. Zhao, I. A. Roundtree and C. He, *Nature Rev. Mol. Cell Biol.* 2017, **18**, 31.

5. M. Duechler, G. Leszczynska, E. Sochacka and B. Nawrot, *Cell. Mol. Life Sci.* 2016, **73**, 3075.

6. L. van Dam, N. Ouwerkerk, A. Brinkmann, J. Raap and M. H. Levitt, *Biophys. J.* 2002, **83**, 2835.

7. A. Rich, A. Nordheim and A. H. J. Wang, *Annu. Rev. Biochem.* 1984, **53**, 791.

8. H. Htun and J. E. Dahlberg, *Science* 1988, **241**, 1791.

9. A. Siddiqui-Jain, C. L. Grand, D. J. Bearss and L. H. Hurley, *Proc. Natl. Acad. Sci. USA* 2002, **99**, 11593.

10. J. Ogawa, S. Takeda, S. X. Xie, H. Hatanaka, T. Ashikari, T. Amachi and S. Shimizu, *Appl. Environ. Microb.* 2001, **67**, 1783.

11. H. Mitsuya, K. J. Weinhold, P. A. Furman, M. H. Stclair, S. N. Lehrman, R. C. Gallo, D. Bolognesi, D. W. Barry and S. Broder, *Proc. Natl. Acad. Sci. USA* 1985, **82**, 7096.

12. C. M. Galmarini, J. R. Mackey and C. Dumontet, *Lancet Oncol.* 2002, **3**, 415.

13. S. K. Mahto and C. S. Chow, *Bioorgan. Med. Chem.* 2008, **16**, 8795.

14. M. Yoshikaw, T. Kato and T. Takenish, *Tetrahedron Lett.* 1967, **50**, 5065.

15. C. C. Richards, *Proc. Natl. Acad. Sci. USA* 1965, **54**, 158.

16. J. A. Fyfe, P. M. Keller, P. A. Furman, R. L. Miller and G. B. Elion, *J. Biol. Chem.* 1978, **253**, 8721.

17. M. L. Lacombe, L. Milon, A. Munier, J. G. Mehus and D. O. Lambeth, *J. Bioenerg. Biomembr.* 2000, **32**, 247.

18. F. Eckstein, *Annu. Rev. Biochem.* 1985, **54**, 367.

19. E. R. Giblett, J. E. Anderson, F. Cohen, B. Pollara and H. J. Meuwissen, *J. Immunol.* 2012, **188**, 936.

20. D. W. Martin and E. W. Gelfand, *Annu. Rev. Biochem.* 1981, **50**, 845.

21. S. Seto, C. J. Carrera, M. Kubota, D. B. Wasson and D. A. Carson, *J. Clin. Invest.* 1985, **75**, 377.

22. B. S. Mitchell, E. Mejias, P. E. Daddona and W. N. Kelley, *Proc. Natl. Acad. Sci. USA* 1978, **75**, 5011.

23. S. Murgia, S. Lampis, P. Zucca, E. Sanjust and M. Monduzzi, *J. Am. Chem. Soc.* 2010, **132**, 16176.

24. O. Adelfinskaya, M. Terrazas, M. Froeyen, P. Marliere, K. Nauwelaerts and P. Herdewijn, *Nucleic Acids Res.* 2007, **35**, 5060.

25. M. Ohmori, K. Ohmori and K. Hasunuma, *Arch. Microbiol.* 1988, **150**, 203.

26. A. Moutinho, P. J. Hussey, A. J. Trewavas and R. Malho, *Proc. Natl. Acad. Sci. USA* 2001, **98**, 10481.

27. H. K. Eltzschig and P. Carmeliet, *N. Engl. J. Med.* 2011, **364**, 656.

28. H. K. Eltzschig, *J. Mol. Med.* 2013, **91**, 141.

29. E. K. Jackson and D. K. Raghvendra, *Annu. Rev. Physiol.* 2004, **66**, 571.

30. E. K. Jackson, *Am. J. Physiol.-Renal Ph.* 2011, **301**, F1160.

31. E. K. Jackson, D. M. Cheng, T. C. Jackson, J. D. Verrier and D. G. Gillespie, *Am. J. Physiol.-Cell Ph.* 2013, **304**, C406.

32. K. S. Lovejoy, R. C. Todd, S. Z. Zhang, M. S. McCormick, J. A. D'Aquino, J. T. Reardon, A. Sancar, K. M. Giacomini and S. J. Lippard, *Proc. Natl. Acad. Sci. USA* 2008, **105**, 8902.

33. T. W. Hambley, *Coordin. Chem. Rev.* 1997, **166**, 181.

34. D. Z. Yang, S. S. G. E. Vanboom, J. Reedijk, J. H. Vanboom and A. H. J. Wang, *Biochemistry-US* 1995, **34**, 12912.

35. A. M. J. Fichtingerschepman, J. L. Vanderveer, J. H. J. Denhartog, P. H. M. Lohman and J. Reedijk, *Biochemistry-US* 1985, **24**, 707.

36. M. Sip, A. Schwartz, F. Vovelle, M. Ptak and M. Leng, *Biochemistry-US* 1992, **31**, 2508.

37. B. Chiavarino, M. E. Crestoni, S. Fornarini, D. Scuderi and J. Y. Salpin, *Inorganic Chemistry* 2015, **54**, 3513.

38. B. Chiavarino, M. E. Crestoni, S. Fornarini, D. Scuderi and J. Y. Salpin, *J. Am. Chem. Soc.* 2013, **135**, 1445.

39. J. Dehand and J. Jordanov, *J. Chem. Soc. Chem. Comm.* 1976, **0**, 598.

40. U. Warnke, C. Rappel, H. Meier, C. Kloft, M. Galanski, C. G. Hartinger, B. K. Keppler and U. Jaehde, *ChemBioChem* 2004, **5**, 1543.

41. N. Farrell, *Platinum-Based Drugs in Cancer Therapy*, Humana Press Inc., New York, **2000**; pp 321-338.

42. E. G. Chapman and V. J. DeRose, *J. Am. Chem. Soc.* 2012, **134**, 256.

43. P. K. Wu, M. Kharatishvili, Y. Qu and N. Farrell, *J. Inorg. Biochem.* 1996, **63**, 9.

44. P. A. Limbach, P. F. Crain and J. A. Mccloskey, *Nucleic Acids Res.* 1994, **22**, 2183.

45. S. Bjelland and E. Seeberg, *Mutat. Res. Fund. Mol. Mech. Mut.* 2003, **531**, 37.

46. C. J. Burrows and J. G. Muller, *Chem. Rev.* 1998, **98**, 1109.

47. H. Wiseman and B. Halliwell, *Biochem. J.* 1996, **313**, 17.

48. M. Masuda, T. Suzuki, M. D. Friesen, J. L. Ravanat, J. Cadet, B. Pignatelli, H. Nishino and H. Ohshima, *J. Biol. Chem.* 2001, **276**, 40486.

49. J. A. Liu, C. J. Petzold, L. E. Ramirez-Arizmendi, J. Perez and H. Kenttamaa, *J. Am. Chem. Soc.* 2005, **127**, 12758.

50. S. Neidle and M. A. Read, *Biopolymers* 2001, **56**, 195.

51. T. Shalaby, G. Fiaschetti, K. Nagasawa, K. Shin-ya, M. Baumgartner and M. Grotzer, *Molecules* 2013, **18**, 12500.

52. S. Lyonnais, C. Hounsou, M. P. Teulade-Fichou, J. Jeusset, E. Le Cam and G. Mirambeau, *Nucleic Acids Res.* 2002, **30**, 5276.

53. C. Perigaud, G. Gosselin and J. L. Imbach, *Bioorg. Med. Chem. Lett.* 1992, **2**, 677.

54. C. Perigaud, G. Gosselin and J. L. Imbach, *Nucleosides Nucleotides Nucleic Acids* 1992, **11**, 903.

55. W. Saenger, *Principles of Nucleic-Acid Structure*, Springer-Verlag, New York, **1984**; pp 20-22.

56. K. Gehring, J. L. Leroy and M. Gueron, *Nature* 1993, **363**, 561.

57. B. Yang and M. T. Rodgers, *J. Am. Chem. Soc.* 2014, **136**, 282.

58. C. Wang, H. Gao, B. L. Gaffney and R. A. Jones, *J. Am. Chem. Soc.* 1991, **113**, 5486.

59. J. L. Leroy, K. Gehring, A. Kettani and M. Gueron, *Biochemistry-US* 1993, **32**, 6019.

60. H. E. Moser and P. B. Dervan, *Science* 1987, **238**, 645.

61. C. Delossantos, M. Rosen and D. Patel, *Biochemistry-US* 1989, **28**, 7282.

62. L. E. Xodo, G. Manzini, F. Quadrifoglio, G. A. Vandermarel and J. H. Vanboom, *Nucleic Acids Res.* 1991, **19**, 5625.

63. S. F. Singleton and P. B. Dervan, *Biochemistry-US* 1992, **31**, 10995.

64. H. A. Day, P. Pavlou and Z. A. E. Waller, *Bioorgan. Med. Chem.* 2014, **22**, 4407.

65. B. Yang and M. T. Rodgers, *J. Am. Soc. Mass Spectrom.* 2015, **26**, 1394.

66. L. S. Ni, M. C. Sung, H. Yu, H. Chokhawala, X. Chen and A. J. Fisher, *Biochemistry-US* 2006, **45**, 2139.

67. J. M. de Muys, H. Gourdeau, N. Nguyen-Ba, D. L. Taylor, P. S. Ahmed, T. Mansour, C. Locas, N. Richard, M. A. Wainberg and R. F. Rando, *Antimicrob. Agents Chemother.* 1999, **43**, 1835.

68. K. Klumpp, G. Kalayanov, H. Ma, S. Le Pogam, V. Leveque, W. R. Jiang, N. Inocencio, A. De Witte, S. Rajyaguru, E. Tai, S. Chanda, M. R. Irwin, C. Sund, A. Winqist, T. Maltseva, S. Eriksson, E. Usova, M. Smith, A. Alker, I. Najera, N. Cammack, J. A. Martin, N. G. Johansson and D. B. Smith, *J. Biol. Chem.* 2008, **283**, 2167.

69. S. B. Kaye, *Br. J. Cancer* 1998, **78**, 1.

70. K. Possinger, *Anti-Cancer Drugs* 1995, **6**, 55.

71. H. E. Krokan, F. Drablos and G. Slupphaug, *Oncogene* 2002, **21**, 8935.

72. R. Shapiro, *Chromosome Damage and Repair*, Plenum Press, New York, **1980**; pp 3-18.

73. H. E. Krokan, R. Standal and G. Slupphaug, *Biochem. J.* 1997, **325**, 1.

74. T. Lindahl, *Nature* 1993, **362**, 709.

75. G. W. Camiener and C. G. Smith, *Biochem. Pharmacol.* 1965, **14**, 1405.

76. T. P. Wang, H. Z. Sable and J. O. Lampen, *J. Biol. Chem.* 1950, **184**, 17.

77. S. S. Brar, M. Watson and M. Diaz, *J. Biol. Chem.* 2004, **279**, 26395.

78. H. M. Shen, S. Ratnam and U. Storb, *Mol. Cell. Biol.* 2005, **25**, 10815.

79. B. K. Tye, P. O. Nyman, I. R. Lehman, S. Hochhauser and B. Weiss, *Proc. Natl. Acad. Sci. USA* 1977, **74**, 154.

80. E. Wist, O. Unhjem and H. Krokan, *Biochim. Biophys. Acta* 1978, **520**, 253.

81. R. K. Singhal, R. Prasad and S. H. Wilson, *J. Biol. Chem.* 1995, **270**, 949.

82. G. Dianov and T. Lindahl, *Curr. Biol.* 1994, **4**, 1069.

83. G. Dianov, A. Price and T. Lindahl, *Mol. Cell. Biol.* 1992, **12**, 1605.

84. H. Kang, K. T. Lee, B. Jung, Y. J. Ko and S. K. Kim, *J. Am. Chem. Soc.* 2002, **124**, 12958.

85. J. Cadet, E. Sage and T. Douki, *Mutat. Res. Fund. Mol. Mech. Mut.* 2005, **571**, 3.

86. S. T. Kim and A. Sancar, *Biochemistry-US* 1991, **30**, 8623.

87. Y. Nosenko, M. Kunitski and B. Brutschy, *J. Phys. Chem. A* 2011, **115**, 9429.

88. S. Nonin and J. L. Leroy, *J. Mol. Biol.* 1996, **261**, 399.

89. T. Ramreddy, M. Kombrabail, G. Krishnamoorthy and B. J. Rao, *J. Phys. Chem. B* 2009, **113**, 6840.

90. A. Zamir, R. W. Holley and M. Marquise, *J. Biol. Chem.* 1965, **240**, 1267.

91. G. R. Bjork and F. C. Neidhardt, *J. Bacteriol.* 1975, **124**, 99.

92. B. C. Chen, S. L. Quinlan and J. G. Reid, *Tetrahedron Lett.* 1995, **36**, 7961.

93. B. C. Chen, S. L. Quinlan, D. R. Stark, J. G. Reid, V. H. Audia, J. G. George, E. Eisenreich, S. P. Brundidge, S. Racha and R. H. Spector, *Tetrahedron Lett.* 1995, **36**, 7957.

94. V. Singh, B. I. Fedeles and J. M. Essigmann, *RNA* 2015, **21**, 1.

95. V. H. Harris, C. L. Smith, W. J. Cummins, A. L. Hamilton, H. Adams, M. Dickman, D. P. Hornby and D. M. Williams, *J. Mol. Biol.* 2003, **326**, 1389.

96. J. D. Watson and F. H. C. Crick, *Nature* 1953, **171**, 964.

97. J. C. Cochrane and S. A. Strobel, *Acc. Chem. Res.* 2008, **41**, 1027.

98. J. C. Cochrane and S. A. Strobel, *RNA* 2008, **14**, 993.

99. J. C. Cochrane, S. V. Lipchock and S. A. Strobel, *Chemistry & Biology* 2007, **14**, 97.

100. C. F. Guerra, F. M. Bickelhaupt, S. Saha and F. Wang, *J. Phys. Chem. A* 2006, **110**, 4012.

101. M. Mons, I. Dimicoli, F. Piuzzi, B. Tardivel and M. Elhanine, *J. Phys. Chem. A* 2002, **106**, 5088.

102. J. L. Alonso, I. Pena, J. C. Lopez and V. Vaquero, *Angew. Chem. Int. Ed.* 2009, **48**, 6141.

103. A. Zhachkina, M. Liu, X. J. Sun, F. S. Amegayibor and J. K. Lee, *J. Org. Chem.* 2009, **74**, 7429.

104. D. L. Barker and R. E. Marsh, *Acta Crystallographica* 1964, **17**, 1581.

105. R. J. Mcclure and B. M. Craven, *Acta Crystallographica Section B-Structural Science* 1973, **B 29**, 1234.

106. E. Nir, M. Muller, L. I. Grace and M. S. de Vries, *Chem. Phys. Lett.* 2002, **355**, 59.

107. M. Szczesniak, K. Szczepaniak, J. S. Kwiatkowski, K. Kubulat and W. B. Person, *J. Am. Chem. Soc.* 1988, **110**, 8319.

108. R. D. Brown, P. D. Godfrey, D. Mcnaughton and A. P. Pierlot, *J. Am. Chem. Soc.* 1989, **111**, 2308.

109. Z. Yang and M. T. Rodgers, *Phys. Chem. Chem. Phys.* 2012, **14**, 4517.

110. B. Yang and M. T. Rodgers, *Phys. Chem. Chem. Phys.* 2014, **16**, 16110.

111. J. S. Kwiatkowski, T. J. Zielinski and R. Rein, *Adv. Quantum Chem.* 1986, **18**, 85.

112. R. Czerminski, B. Lesyng and A. Pohorille, *Int. J. Quantum Chem.* 1979, **16**, 605.

113. I. R. Gould, N. A. Burton, R. J. Hall and I. H. Hillier, *J. MOL. STRUC.-THEOCHEM.* 1995, **331**, 147.

114. H. T. Miles, *Biochim. Biophys. Acta* 1956, **22**, 247.

115. J. P. Kokko, L. Mandell and J. H. Goldstein, *J. Am. Chem. Soc.* 1961, **83**, 2909.

116. J. Y. Salpin, S. Guillaumont, J. Tortajada, L. MacAleese, J. Lemaire and P. Maitre, *ChemPhysChem* 2007, **8**, 2235.

117. Y.-w. Nei, T. E. Akinyemi, J. D. Steill, J. Oomens and M. T. Rodgers, *Int. J. Mass Spectrom.* 2010, **297**, 139.

118. Y.-w. Nei, T. E. Akinyemi, C. M. Kaczan, J. D. Steill, G. Berden, J. Oomens and M. T. Rodgers, *Int. J. Mass Spectrom.* 2011, **308**, 191.

119. R. R. Wu, B. Yang, C. E. Frieler, G. Berden, J. Oomens and M. T. Rodgers, *Phys. Chem. Chem. Phys.* 2015, **17**, 25978.

120. A. O. Alyoubi and R. H. Hilal, *Biophysical Chemistry* 1995, **55**, 231.

121. P. Colarusso, K. Q. Zhang, B. J. Guo and P. F. Bernath, *Chem. Phys. Lett.* 1997, **269**, 39.

122. S. L. Zhang, K. H. Michaelian and G. R. Loppnow, *J. Phys. Chem. A* 1998, **102**, 461.

123. M. T. Rodgers and P. B. Armentrout, *J. Am. Chem. Soc.* 2000, **122**, 8548.

124. M. Kabelac and P. Hobza, *J. Phys. Chem. B* 2006, **110**, 14515.

125. R. R. Wu, B. Yang, C. E. Frieler, G. Berden, J. Oomens and M. T. Rodgers, *J. Am. Soc. Mass Spectrom.* 2016, **27**, 410.

126. W. A. Decatur and M. J. Fournier, *Trends Biochem. Sci.* 2002, **27**, 344.

127. W. A. Cantara, P. F. Crain, J. Rozenski, J. A. McCloskey, K. A. Harris, X. N. Zhang, F. A. P. Vendeix, D. Fabris and P. F. Agris, *Nucleic Acids Res.* 2011, **39**, D195.

128. W. A. Decatur and M. J. Fournier, *J. Biol. Chem.* 2003, **278**, 695.

129. M. A. Machnicka, A. Olchowik, H. Grosjean and J. M. Bujnicki, *RNA Biol.* 2014, **11**, 1619.

130. P. F. Agris, F. A. P. Vendeix and W. D. Graham, *J. Mol. Biol.* 2007, **366**, 1.

131. Y. Motorin and M. Helm, *Biochemistry-US* 2010, **49**, 4934.

132. M. Pastor-Anglada, A. Felipe and F. J. Casado, *Trends Pharmacol. Sci.* 1998, **19**, 424.

133. C. J. McGinn, D. S. Shewach and T. S. Lawrence, *J. Natl. Cancer Inst.* 1996, **88**, 1193.

134. S. Grant, *Adv. Cancer Res.* 1998, **72**, 197.

135. D. L. Nelson and M. M. Cox, *Lehninger Priciples of Biochemistry*, Macmillan Education, Belmont, CA, 6th ed., **2013**; pp 160-161.

136. H. Lodish, A. Berk, S. L. Zipursky, P. Matsudaira, D. Baltimore and J. Darnell, *Molecular Cell Biology*, W. H. Freeman, New York, NY, 4th ed., **2000**; pp 31-63.

137. R. B. Silverman, *The Organic Chemistry of Drug Design and Drug Action*, Elsevier, Amsterdam, The Netherlands, 2nd ed., **2004**; pp 197-198.

138. M. Eisler, *Encyclopedia of Nanoscience and Society*, SAGE Publications, Thousand Oaks, CA, **2010**; pp 839-841.

139. E. Anslyn and D. A. Dougherty, *Modern Physical Organic Chemistry*, University Science, Sausalito, CA, **2004**; pp 207-220.

140. E. C. Constable, *The Metal-Ligand Interaction, in Metals and Ligand Reactivity: An Introduction to the Organic Chemistry of Metal Complexes*, VCH Verlagsgesellschaft mbH: Weinheim, Germany, New, revised and expanded ed., **2005**; pp 46-47.

141. G. Yassaghi, L. Jasikova and J. Roithova, *Int. J. Mass Spectrom.* 2016, **407**, 92.

142. Y. J. Alahmadi, A. Gholami and T. D. Fridgen, *Phys. Chem. Chem. Phys.* 2014, **16**, 26855.

143. M. T. Rodgers and P. B. Armentrout, *Mass Spectrom. Rev.* 2000, **19**, 215.

144. P. B. Armentrout and M. T. Rodgers, *J. Phys. Chem. A* 2000, **104**, 2238.

145. B. S. Fales, N. O. Fujamade, J. Oomens and M. T. Rodgers, *J. Am. Soc. Mass Spectrom.* 2011, **22**, 1862.

146. B. S. Fales, N. O. Fujamade, Y. W. Nei, J. Oomens and M. T. Rodgers, *J. Am. Soc. Mass Spectrom.* 2011, **22**, 81.

147. Y. Zhu, L. A. Hamlow, C. C. He, S. F. Strobehn, J. K. Lee, J. Gao, G. Berden, J. Oomens and M. T. Rodgers, *J. Phys. Chem. B* 2016, **120**, 8892.

148. Y. Zhu, L. A. Hamlow, C. C. He, J. K. Lee, J. Gao, G. Berden, J. Oomens and M. T. Rodgers, *J. Phys. Chem. B* 2017, **121**, 4048.

149. Y. Zhu, L. A. Hamlow, C. C. He, H. A. Roy, N. A. Cunningham, M. U. Munshi, G. Berden, J. Oomens and M. T. Rodgers, *Int. J. Mass Spectrom.* 2017, DOI: https://doi.org/10.1016/j.ijms.2017.04.005.

150. Y. Zhu, H. A. Roy, N. A. Cunningham, S. F. Strobehn, J. Gao, M. U. Munshi, G. Berden, J. Oomens and M. T. Rodgers, *Phys. Chem. Chem. Phys.* 2017, **19**, 17637.

151. Y. Zhu, H. A. Roy, N. A. Cunningham, S. F. Strobehn, J. Gao, M. U. Munshi, G. Berden, J. Oomens and M. T. Rodgers, *J. Am. Soc. Mass Spectrom* 2017, **28**, 2437.

152. N. C. Polfer, J. Oomens and R. C. Dunbar, *ChemPhysChem* 2008, **9**, 579.

153. C. Ruan and M. T. Rodgers, *J. Am. Chem. Soc.* 2004, **126**, 14600.

154. R. Amunugama and M. T. Rodgers, *J. Phys. Chem. A* 2002, **106**, 5529.

155. R. Amunugama and M. T. Rodgers, *J. Phys. Chem. A* 2002, **106**, 9092.

156. R. Amunugama and M. T. Rodgers, *Int. J. Mass Spectrom.* 2003, **227**, 339.

157. R. Amunugama and M. T. Rodgers, *J. Phys. Chem. A* 2002, **106**, 9718.

158. R. Amunugama and M. T. Rodgers, *Int. J. Mass Spectrom.* 2003, **222**, 431.

159. M. T. Rodgers and P. B. Armentrout, *Int. J. Mass Spectrom.* 1999, **185**, 359.

160. R. Amunugama and M. T. Rodgers, *Int. J. Mass Spectrom.* 2000, **195**, 439.

161. Z. Yang and M. T. Rodgers, *J. Am. Chem. Soc.* 2004, **126**, 16217.

162. A. M. Pyle, *J. Biol. Inorg. Chem.* 2002, **7**, 679.

163. G. L. Eichhorn, J. J. Butzow and Y. A. Shin, *J. Biosci.* 1985, **8**, 527.

164. S. Arnott, *Nature* 1984, **312**, 174.

165. R. H. Crabtree, *Science* 1994, **266**, 1591.

166. G. L. Eichhorn, *Coordin. Chem. Rev.* 1993, **128**, 167.

167. D. Sen and W. Gilbert, *Nature* 1988, **334**, 364.

168. W. I. Sundquist and A. Klug, *Nature* 1989, **342**, 825.

169. G. N. Parkinson, M. P. H. Lee and S. Neidle, *Nature* 2002, **417**, 876.

170. S. Burge, G. N. Parkinson, P. Hazel, A. K. Todd and S. Neidle, *Nucleic Acids Res.* 2006, **34**, 5402.

171. S. J. Lippard; and J. M. Berg., *Principles of Bioinorganic Chemistry*, University Science Books, Mill Valley, CA, **1994**; pp 57-69.

172. A. Rich and S. G. Zhang, *Nature Rev. Genet.* 2003, **4**, 566.

173. G. L. Eichhorn and Y. A. Shin, *J. Am. Chem. Soc.* 1968, **90**, 7323.

174. J. T. Stivers and Y. L. Jiang, *Chem. Rev.* 2003, **103**, 2729.

175. P. J. O'Brien, *Chem. Rev.* 2006, **106**, 720.

176. E. M. Moody, J. T. J. Lecomte and P. C. Bevilacqua, *RNA* 2005, **11**, 157.

177. Y. Zheng, Y. Xue and S. G. Yan, *J. Mol. Struc. Theochem* 2008, **860**, 52.

178. G. P. Margison and P. J. Oconnor, *Biochim. Biophys. Acta* 1973, **331**, 349.

179. R. S. Das, M. Samaraweera, M. Morton, J. A. Gascon and A. K. Basu, *Chem. Res. Toxicol* 2012, **25**, 2451.

180. Z. A. Tehrani, A. Fattahi and A. Pourjavadi, *Carbohydr. Res.* 2009, **344**, 771.

181. Z. A. Tehrani, A. Fattahi and A. Pourjavadi, *Journal of Molecular Structure-Theochem* 2009, **913**, 117.

182. R. Rios-Font, J. Bertran, L. Rodriguez-Santiago and M. Sodupe, *J. Phys. Chem. B* 2006, **110**, 5767.

183. C. Altona and M. Sundaralingam, *J. Am. Chem. Soc.* 1972, **94**, 8205.

184. R. R. Wu, B. Yang, G. Berden, J. Oomens and M. T. Rodgers, *J. Phys. Chem. B* 2015, **119**, 2795.

185. R. R. Wu, B. Yang, G. Berden, J. Oomens and M. T. Rodgers, *J. Phys. Chem. B* 2014, **118**, 14774.

186. R. R. Wu, B. Yang, C. E. Frieler, G. Berden, J. Oomens and M. T. Rodgers, *J. Phys. Chem. B* 2015, **119**, 5773.

187. R. R. Wu, C. C. He, L. A. Hamlow, Y.-w. Nei, G. Berden, J. Oomens and M. T. Rodgers, *J. Phys. Chem. B* 2016, **120**, 4616.

188. R. R. Wu, C. C. He, L. A. Hamlow, Y. W. Nei, G. Berden, J. Oomens and M. T. Rodgers, *Phys. Chem. Chem. Phys.* 2016, **18**, 15081.

189. R. R. Wu, L. A. Hamlow, C. C. He, Y. W. Nei, G. Berden, J. Oomens and M. T. Rodgers, *J. Am. Soc. Mass Spectrom.* 2017, **28**, 1638.

190. R. R. Wu, L. A. Hamlow, C. C. He, Y.-w. Nei, G. Berden, J. Oomens and M. T. Rodgers, *Phys. Chem. Chem. Phys.* 2017, DOI: 10.1039/C7CP05521H.

191. Y.-w. Nei, N. Hallowita, J. D. Steill, J. Oomens and M. T. Rodgers, *J. Phys. Chem. A* 2013, **117**, 1319.

192. Y.-w. Nei, K. T. Crampton, G. Berden, J. Oomens and M. T. Rodgers, *J. Phys. Chem. A* 2013, **117**, 10634.

193. R. R. Wu, Y. Chen and M. T. Rodgers, *Phys. Chem. Chem. Phys.* 2016, **18**, 2968.

194. R. R. Wu and M. T. Rodgers, *Phys. Chem. Chem. Phys.* 2016, **18**, 24451.

195. R. R. Wu and M. T. Rodgers, *J. Phys. Chem. B* 2016, **120**, 4803.

196. R. R. Wu and M. T. Rodgers, *Phys. Chem. Chem. Phys.* 2016, **18**, 16021.

197. R. R. Wu and M. T. Rodgers, *J. Am. Soc. Mass Spectrom.* 2017, manuscript in preparation.

198. J. J. Valle, J. R. Eyler, J. Oomens, D. T. Moore, A. F. G. van der Meer, G. von Helden, G. Meijer, C. L. Hendrickson, A. G. Marshall and G. T. Blakney, *Rev. Sci. Instrum.* 2005, **76**, 023103.

199. N. C. Polfer, J. Oomens, D. T. Moore, G. von Helden, G. Meijer and R. C. Dunbar, *J. Am. Chem. Soc.* 2006, **128**, 517.

200. N. C. Polfer and J. Oomens, *Phys. Chem. Chem. Phys.* 2007, **9**, 3804.

201. A. Memboeuf, A. Nasioudis, S. Indelicato, F. Pollreisz, A. Kuki, S. Keki, O. F. van den Brink, K. Vekey and L. Drahos, *Anal. Chem.* 2010, **82**, 2294.

202. F. Derwa, E. Depauw and P. Natalis, *Org. Mass Spectrom.* 1991, **26**, 117.

203. X. H. Guo, M. C. Duursma, P. G. Kistemaker, N. M. M. Nibbering, K. Vekey, L. Drahos and R. M. A. Heeren, *J. Mass Spectrom.* 2003, **38**, 597.

204. A. Memboeuf, L. Jullien, R. Lartia, B. Brasme and Y. Gimbert, *J. Am. Soc. Mass Spectrom.* 2011, **22**, 1744.

205. T. M. Kertesz, L. H. Hall, D. W. Hill and D. F. Grant, *J. Am. Soc. Mass Spectrom.* 2009, **20**, 1759.

206. K. Wolinski, J. F. Hinton, D. S. Wishart, B. D. Sykes, F. M. Richards, A. Pastone, V. Saudek, P. D. Ellis, G. E. Maciel, J. W. McIver Jr., A. C. Blizzard, D. P. Santry, J. A. Pople, N. S. Ostlund, L. Ducasse, J. Hoarau, M. Pesquer, M. Kondo, I. Ando, R. Chujo, A. Nishioka, E. C. Vauthier, S. Odiot, F. Tonnard, J. D. Baker, M. C. Zerner, D. V. Beveridge, W. P. Anderson, T. R. Cundari, R. C. Bingham, M. J. S. Dewar, D. H. Lo, J. Li, P. C. Mello, K. Jug, W. Tihiel, E. G. Zoebisch, E. F. Healy, J. J. P. Stewart, M. Fraser and D. M. Hayes, HyperChem Computational Chemistry Software Package, hypercube, Inc., Gainsville, FL, version 7.0, 2001.

207. M. J. Frisch, G. W. Trucks, H. B. Schlegel, G. E. Scuseria, M. A. Robb, J. R. Cheeseman, G. Scalmani, V. Barone, B. Mennucci, G. A. Petersson, H. Nakatsuji, M. Caricato, X. Li, H. P. Hratchian, A. F. Izmaylov, J. Bloino, G. Zheng, J. L. Sonnenberg, M. Hada, M. Ehara, K. Toyota, R. Fukuda, J. Hasegawa, M. Ishida, T. Nakajima, Y. Honda, O. Kitao, H. Nakai, T. Vreven, J. A. Montgomery Jr., J. E. Peralta, F. Ogliaro, M.

J. Bearpark, J. Heyd, E. N. Brothers, K. N. Kudin, V. N. Staroverov, R. Kobayashi, J. Normand, K. Raghavachari, A. P. Rendell, J. C. Burant, S. S. Iyengar, J. Tomasi, M. Cossi, N. Rega, N. J. Millam, M. Klene, J. E. Knox, J. B. Cross, V. Bakken, C. Adamo, J. Jaramillo, R. Gomperts, R. E. Stratmann, O. Yazyev, A. J. Austin, R. Cammi, C. Pomelli, J. W. Ochterski, R. L. Martin, K. Morokuma, V. G. Zakrzewski, G. A. Voth, P. Salvador, J. J. Dannenberg, S. Dapprich, A. D. Daniels, Ö. Farkas, J. B. Foresman, J. V. Ortiz, J. Cioslowski and D. J. Fox, Gaussian 09, Gaussian, Inc., Wallingford, CT, revision C.01, 2009.

208. M. T. Rodgers, P. B. Armentrout, J. Oomens and J. D. Steill, *J. Phys. Chem. A* 2008, **112**, 2258.

209. C. F. Correia, P. O. Balaj, D. Scuderi, P. Maitre and G. Ohanessian, *J. Am. Chem. Soc.* 2008, **130**, 3359.

210. G. Zubay, *Biochim. Biophys. Acta* 1959, **32**, 233.

211. U. Weser, S. Seeber and P. Warnecke, *Experientia* 1969, **25**, 489.

212. S. Li and C. E. Mason, *Annu. Rev. Genomics Hum. Genet.* 2014, **15**, 127.

ABSTRACT

TANDEM MASS SPECTROMETRY AND COMPUTATIONAL APPROACHES TO ELUCIDATE CONFORMATIONS AND N-GLYCOSIDIC BOND STABILITIES OF DNA AND RNA NUCLEOSIDES AND MONONUCLEOTIDES

by

YANLONG ZHU

May 2018

Advisor: Dr. Mary T. Rodgers

Major: Analytical Chemistry

Degree: Doctor of Philosophy

The influence of noncovalent interactions with sodium cations on the conformations and energetics of ten DNA and RNA nucleosides as well as two adenine mononucleotides were elucidated via infrared multiple photon dissociation (IRMPD) action spectroscopy experiments and complementary electronic structure calculations. Energy-resolved collision-induced dissociation (ER-CID) experiments of protonated and metal cationized DNA and RNA nucleosides were performed using a Bruker amaZon ETD quadrupole ion trap mass spectrometer (QIT MS). By comparing the $CID_{50\%}$ values of these nucleosides, which are the rf excitation amplitudes required for 50% dissociation of the precursor ion, the effects of local environment and modifications on the relative stabilities of the DNA and RNA nucleosides were elucidated. In particular, when the fragmentation pathways observed in the ER-CID experiments solely involve N-glycosidic bond cleavage, the survival yield analyses are directly correlated to the relative N-glycosidic bond stabilities of the DNA and RNA nucleosides.

For eight of the 10 sodium cationized DNA and RNA nucleosides examined in this thesis, the sodium cation preferentially binds to both the nucleobase and sugar moiety. In contrast, the guanine nucleosides bind the sodium cation solely via the guanine nucleobase. Theory suggests that the DNA and RNA forms of sodium cationized nucleosides exhibit highly parallel conformations. However, comparisons between the experimental IRMPD and calculated IR spectra demonstrate that for the pyrimidine nucleosides, stable low-energy bidentate conformers with an *anti* orientation of the nucleobase are dominantly populated in the experiments. This conclusion is confirmed by the relative Gibbs free energies calculated for water adducts of the ground tridentate *syn* oriented conformers and these bidentate *anti* oriented conformers of sodium cationized RNA pyrimidine nucleosides.

In general, the 2'-hydroxyl substituent of the RNA nucleoside stabilizes the N-glycosidic bond compared with their DNA analogues. Sodium cationization activates the N-glycosidic bond less effectively than protonation. The effects of methylation, 2'-fluoro substitution, and 2'-stereochemistry inversion on the N-glycosidic bond stabilities were also investigated via ER-CID experiments and survival yield analysis. The 2'-fluoro substituent significantly stabilizes the N-glycosidic bond compared with the analogous DNA and RNA nucleosides, whereas a 2'-O-methyl substituent produces a similar effect on the N-glycosidic bond stabilities as found for a 2'-hydroxyl substituent. Additionally, changing the stereochemistry of the 2'-hydroxyl substituent has only slight impact on the N-glycosidic bond stabilities. Methylation of different positions clearly impacts the relative N-glycosidic bond stabilities of these nucleosides. By comparing the $CID_{50\%}$ values of protonated and metal cationized guanine nucleosides, the effects of local

environment, i.e. pH and the presence of metal cations, on the relative N-glycosidic bond stabilities were also investigated. The order of relative stabilities of alkali metal cationized dGuo and Guo is consistent with the order of increasing size of the alkali metal. The binding between the metal cation and the nucleoside become weaker as the metal cation becomes larger.

The gas-phase conformations of the sodium cationized complexes of the neutral and deprotonated adenine mononucleotides have been examined in the present work via IRMPD action spectroscopy in both the IR fingerprint and hydrogen-stretching regions. Comparison of the measured IRMPD spectra with the calculated IR spectra of the stable low-energy conformations of these species calculated at the B3LYP/6-311+G(2d,2p)//B3LYP/6-311+G(d,p) level of theory allows the structures populated in the experiments to be determined. Overall, the conformers of the sodium cationized forms of the neutral and deprotonated adenine mononucleotides that are dominantly populated in the experiments are highly parallel. Based on comparisons of the measured IRMPD and computed IR spectra, it is clear that in the dominant conformers of sodium cationized adenine mononucleotides populated, Na^+ binds to the adenine nucleobase, sugar and phosphate moieties in a tridentate fashion, adenine exhibits a *syn* orientation, and the sugars prefer C3'-endo ($^3T_2$) puckering in both cases. In the dominant conformers of the disodium cationized deprotonated adenine mononucleotides populated, the first Na^+ binds to the adenine nucleobase, sugar and phosphate moieties in a quadridentate fashion, the second Na^+ binds solely to the phosphate moiety, adenine exhibits a *syn* orientation, and the sugars prefer O4'-endo ($^OT_1$) puckering in both cases. Present results are compared with those for the sodium

cationized adenine nucleosides as well as the protonated and deprotonated forms of the adenine mononucleotides to elucidate the effects of the phosphate group and charge state on the gas-phase conformations of these nucleic acid building blocks.

AUTOBIOGRAPHICAL STATEMENT

Yanlong Zhu

EDUCATION

Ph. D. Analytical Chemistry.....**August 2011 – December 2017**

Wayne State University, Detroit, MI

Ph.D. Mentor: Professor Mary T. Rodgers

B.S. Chemistry ..... **September 2007 – June 2011**

University of Science and Technology of China, Hefei, Anhui, China

B.S. Mentor: Professor Shuhong Yu

AWARDS AND HONORS–WAYNE STATE UNIVERSITY

- Thomas C. Rumble University Graduate Fellowship, WSU, 2014
- Graduate Student Professional Travel Award, WSU, 2015
- David F. Boltz Analytical Award, WSU, 2017
- American Society for Mass Spectrometry Travel Stipend, 2017
- American Society for Mass Spectrometry 2017 Fall Workshop Student Stipend Award, 2017